DSE Group 11

Ultra-Long Range Business Jet

DID-5 Final Report

Delft University of Technology

TU Delft

STARLING
CORPORATE AIRCRAFT

Ultra-Long Range Business Jet
DID-5 Final Report

by

DSE Group 11

As part of the course:
AE3200 Design Synthesis Exercise
at the Delft University of Technology

J. Borghart (4162293)
F. De Voogt (4193296)
M. Kosec (4275535)
J. Liu (4152085)
S. van Middelaar (4175247)
M. Moussa (4278380)
A. Pandey (4094026)
M. Popescu (4278372)
N. Weij (4209982)
C. van Woensel (4305019)

June 28, 2016

Course coordinators: J. Sinke — Delft University of Technology, Aerospace Material Laboratory
H. Koornneef — Delft University of Technology
A. Alves Vieira — Delft University of Technology

Contents

List of Figures

List of Tables

List of Symbols

A	Aspect ratio	-
a	Acceleration	m/s^2
AR	Aspect ratio	-
b	span	m
b_{eff}	Effective wing span	m
bpr	Bypass ratio	–
$\bar{c}$	Mean aerodynamic chord	m
C	Cost	\$
c	Steady climb rate	m/s
C_D	3D Drag coefficient	-
C_{D_0}	Zero-lift drag coefficient	-
C_{D_y}	Aircraft side drag coefficient	-
C_d	2D Drag coefficient	-
c_j	Fuel Consumption	kg/Ns
C_L	3D Lift coefficient	-
C_l	2D Lift coefficient	-
$C_{l_{max}}$	Maximum 2D Lift coefficient	-
$C_{L_{max}}$	Maximum 3D lift coefficient	-
C_L/C_D	Lift over drag ratio	-
C_m	Coefficient of aerodynamic pitching moment	-
C_{m_α}	Pitching moment derivative	1/rad
C_{n_β}	Directional stability derivative	1/rad
$C_{n_{\delta_R}}$	Rudder control derivative	1/rad
C_p	Pressure coefficient	-
C_{y_β}	Sideslip derivative	1/rad
$C_{y_{\delta_R}}$	Rudder control derivative	1/rad
D	Drag	N
D_P	Mass of pollutant emitted	g
d_c	Diameter of shock absorber	m
d_s	Diameter of strut	m
e	Oswald factor	-
E	Endurance	s
F_{oo}	Rated thrust of engine	N
F_f	Friction force on the ground	N
F_w	Cross-wind force	N
g	Gravitational acceleration	m/s^2
K_{f1}	Ratio of contrition of fuselage to aircraft C_{n_β}	-
K_{f2}	Ratio of contrition of fuselage to aircraft C_{y_β}	-
L	Lift	N
L/D	Lift over Drag ratio	-

L/D_{cr}	Lift over Drag ratio for cruise	-
L/D_{loiter}	Lift over Drag ratio for loiter	-
l/c	Length ratio	-
l_c	Canard moment arm	m
l_m	Distance between c.g. and main gear	m
l_n	Distance between c.g. and nose gear	m
l_c	Winglets moment arm	m
$\dot{m}$	Mass flow	kg/s
m	Mass	kg
M_{ff}	Mission fuel fraction	-
M_{res}	Mission reserve fuel fraction	-
M_{tfo}	Trapped fuel and oil fraction	-
$MTOW$	Maximum Take-Off Weight	kg
MLW	Maximum Landing Weight	kg
n	Load Factor	-
n_{max}	Maximum Load Factor	-
n_s	Number of struts	-
P_m	Static load main strut	N
P_n	Static load nose strut	N
q	Dynamic pressure	Pa
R	Range	m
R	Reynolds number	-
RSN	Regulatory Smoke Number	-
S	Wing surface area	m^2
S_{land}	Landing distance	m
S_c	Canard surface area	m^2
S_v	Winglet surface area	m^2
SFC	Specific Fuel Consumption	kg/Ns
t	Thickness	m
T	Temperature	K
T	Thrust	N
T_{cruise}	Thrust at cruise	N
T_i	Station time	$days$
T_{TO}	Thrust at take-off	N
t/c	Thickness ratio	-
TOP	Take-off Parameter	N/m^2
T/W	Thrust Loading	-
V	Velocity	m/s
V_{cruise}	Cruise speed	m/s
$\bar{V}_c$	Canard volume ratio	-
V_D	Dive speed	m/s

V_S	Stall speed	m/s
V_{TO}	Take-off speed	m/s
V_{mc}	Minimum controllable speed	m/s
$\bar{V}_v$	Winglets volume coefficient	-
W	Weight	kg
W_{crew}	Crew Weight	kg
W_E	Empty Weight	kg
W_F	Fuel Weight	kg
W_{OE}	Operating Empty Weight	kg
W_{PL}	Payload Weight	kg
W_{tfo}	Trapped Fuel and Oil Weight	kg
W_{TO}	Take-off Weight	kg
W/S	Wing Loading	N/m^2
α	Angle of attack	rad
β	Sideslip angle	°
δ_E	Elevator deflection	°
δ_R	Rudder deflection	°
η_v	Dynamic pressure ratio	-
$\ddot{\theta}$	Take-off pitch angular acceleration	deg/s^2
θ_{LOF}	Rotation angle	°
Λ	Sweep angle	rad
π_{oo}	Pressure ratio of engine	-
ρ	Air density	kg/m^3
ρ_{land}	Air density during landing	kg/m^3
ρ_0	Air density at sea level	kg/m^3
σ	Correction factor for air density	-
S_{ref}	Reference area for flap design	-
$S_{flapped}$	Reference area along which flaps have been located	-
τ_e	Elevator effectiveness	-
τ_r	Rudder effectiveness	-
ϕ	Clearance angle	°
ψ	Tip-over angle	°

List of Abbrevations

AA	Average available
AC	Alternating Current
ACARE	Advisory Council for Aeronautics Research in Europe
ACM	Acceptable means of Compliance
AoA	Angle of Attack
APU	Auxiliary Power Unit
ARA-D	Aeronautical Research Association-Dowty
ATI	Adherent Technologies Inc.
CEF	Cost Escalation Factor
CFRP	Carbon Fibre Reinforced Polymer
CO	Carbon monoxide
CROR	Counter Rotating Open Rotor
DC	Direct Current
DFDAU	Digital Flight Data Acquisition Unit
DFDR	Digital Flight Data Recorder
DOC	Direct Operating Cost
DOT	Design Option Tree
EASA	European Aviation Safety Agency
ECS	Environmental Control System
ELV	End of Life vehicles
EMEDS	Electro Mechanical Expulsion Deicing System
EOL	End-of-Life
EPNL	Effective Perceived Noise Levels
FAA	Federal Aviation Administration
FAR	Federal Aviation Regulations
FBG	Fibre Bragg Gratings
FDEP	Flight Data Entry Panel
FEM	Finite Element Method
FML	Fibre Metal Laminate
GA	General Aviation
GAC	Ground Air conditioning Cart
GE	General Electric
HC	Hydrocarbons
HLD	High Lift Devices
HP	High Pressure
HPC	High Pressure Compressor
HPT	High Pressure Turbine
HVAC	Heating, ventilation and Air conditioning
H/W	Hardware
ICAO	International Civil Aviation Organisation
JIT	Just-In-Time
LCC	Life Cycle Cost
LEED	Leadership in Energy and Environmental Design
LEMAC	Leading edge mean aerodynamic chord
LP	Low Pressure
LPC	Low Pressure Compressor
LPT	Low Pressure Turbine
M&A	Manufacturing & Acquisition
MAC	Mean aerodynamic chord
MLW	Maximum Landing Weight
MTTF	Mean Time to Failure
MTTR	Mean Time to Repair
MVF	Metal Volume Fraction
MZFW	Maximum zero fuel weight
NASA	National Aeronautics and Space Administration
NDT	Non Destructive Testing
NO_x	Oxides of Nitrogen
OEW	Operating Empty Weight
OR	Open Rotor
PT	Power Turbine
QA	Quality Assurance
QM	Quality Management
RAMS	Reliability, Availability, Maintainability, Safety
RANS	Reynolds Averaged Navier Stokes
RDTE	Research, Development, Test & Analysis
ROI	Return On Investment
SHM	Structural Health Monitoring
S.M.	Stability margin
S/W	Software
T.B.D	To Be Determined
TO	Take-off
TRL	Technology Readiness Level
URBJ	Ultra-Long Range Business Jet
USD	United States Dollars
VHF	Very High Frequency

Summary

As the world economy is recovering from the economical crisis, the demand for business jets is steadily growing. Corporate jets allow businesses to increase their employee efficiency and open up new markets and possibilities. However, current business jets still lack the range capabilities of commercial airliners. The current market leader is the Gulfstream G650, that flies up to 7,000 nm carrying 8 passengers. For the Spring 2016 Design Synthesis Exercise, ten Aerospace Engineering bachelor students were challenged to design a new corporate jet, capable of flying 8,500 nm carrying 18 passengers. Furthermore the new jet should cruise at Mach 0.8 or higher and demonstrate a takeoff length of less than 2,000 m. The unit price was set at a maximum of 60 million USD.

A market analysis was performed to identify customer needs and to explore the current business jet options. Based on the earlier identified needs, the (sub)requirements were determined. Also, a functional breakdown was performed to distinguish all aircraft subsystems and their functions. Early design parameters were established and by the end of the preliminary design phase, four concepts had been created. The concepts were assessed in a trade-off, during which three concepts were eliminated. The remaining concept was then slightly modified to form the basis for the next design phase.

During the next phase of the design process, the original concept was developed into a detailed final design: the Starling 9000 corporate jet. Its unconventional canard configuration is designed for maximum aerodynamic efficiency; by eliminating the need for a conventional tail, drag is drastically reduced. The fuselage measures 36 meters in length, while the canard spans 12 meters. The backwards swept wing of 136 m^2 has a span of 31 meters and features a computationally optimised aerofoil designed for maximum performance during cruise. The single slotted flaps provide enough lift to ensure a comfortable landing speed of 130 kts. Pitch control is provided by movable canard surfaces while the large, 4 meter winglets account for yaw control. Its propfan engines make use of a BMW-Rolls Royce core, combined with contra-rotating open rotor fan blades. The fuel consumption will be 26% less compared to current turbofan engines. The jet has a maximum takeoff weight of 53,000 kg and an operational empty weight of 27,100 kg, allowing it to depart from most domestic airports. Besides its great performance, the Starling 9000 showcases the largest cabin in its class with a floor width of 2.4 m and a cabin height of 2.0 m. The high-quality finish interior offers passengers unmatched views thanks to the two Fokker SkyView panoramic windows.

Compared to the current market leaders, the Starling 9000 operating cost is estimated at 9,633 $/hr, which is 18% more than its cheapest competitor. In return for its higher operating price however, it will fly up to 39% further carrying 56% more passengers. The Starling 9000 therefore lives up to its expectations, meeting its design requirements and offering tomorrow's corporate travellers superior global access at an affordable price.

Preface

This report is the fourth in a series produced by a group of ten third-year aerospace engineering students at the Delft University of Technology in the Netherlands as part of the AE3200 Design Synthesis Exercise. The course is designed to develop the technical, team-working, systems engineering and organisational abilities of students and concludes with a symposium of the design project on 30^{th} June 2016. Group 11 is thankful for the guidance provided by project tutor Jos Sinke and coaches Ana Alves Vieira and Hemmo Koornneef, from the Aerospace Faculty at the Delft University of Technology. Moreover, the group would also like to thank both internal and external experts that have provided further insight into various unique technical aspects of the project. It is their expert assistance that has helped steer this DSE project to success.

DSE Group 11
Delft, June 2016

Introduction

As global wealth continues to increase, air travel is becoming available to a larger part of the world's population. While most people travel with commercial carriers, the business jet market is rapidly growing as well. According to Bombardier, the size of the worldwide business jet fleet has almost doubled in the last 15 years alone [5]. For companies, business travellers and wealthy individuals, business jets are often favourable in terms of travel time, availability and comfort compared to traditional airlines. However, modern business jets have yet to demonstrate the same range capabilities as their long range commercial competitors.

Currently, the Gulfstream G650ER is the market leader with a maximum range of 7,500 nm for 8 passengers. Competitor Bombardier is aiming to take the lead by developing the Global 8000 (7,900 nm) [50]. On the other hand, the Boeing Business Jet version of the Boeing 777-200LR has a range of over 10,030 nm[1], while the new corporate variant of the Airbus A350 is rumoured to fly even up to 10,800 nm[2]. However, with a maximum takeoff weight of 280 tonnes (A350) and 350 tonnes (B777) and wing spans of 65 meters, these jets can hardly be designated as the average business jet[3].

Clearly there is a large gap in range capability between regular business jets (up to 18 passengers) and their larger commercial counterparts. For customers operating the first type of jets there is currently no alternative available that can fly non-stop between almost any city pair. Refuelling stops lengthen travel times and as we know, time equals money in the world of corporate flying. It is clear that there is a need for a new 18 seater business jet capable of flying ultra-long range. Bombardier expects a need for at least 2,500 large corporate jets capable of flying more than 5,000 nm[5].

For the 2016 Spring Design Synthesis Exercise, group 11 has therefore designed the Starling 9000 corporate jet, capable of flying farther than any current business jet in the same large size category (span of over 25 meters). This Final Report covers the eleven-weeks design process and presents the resulting design.

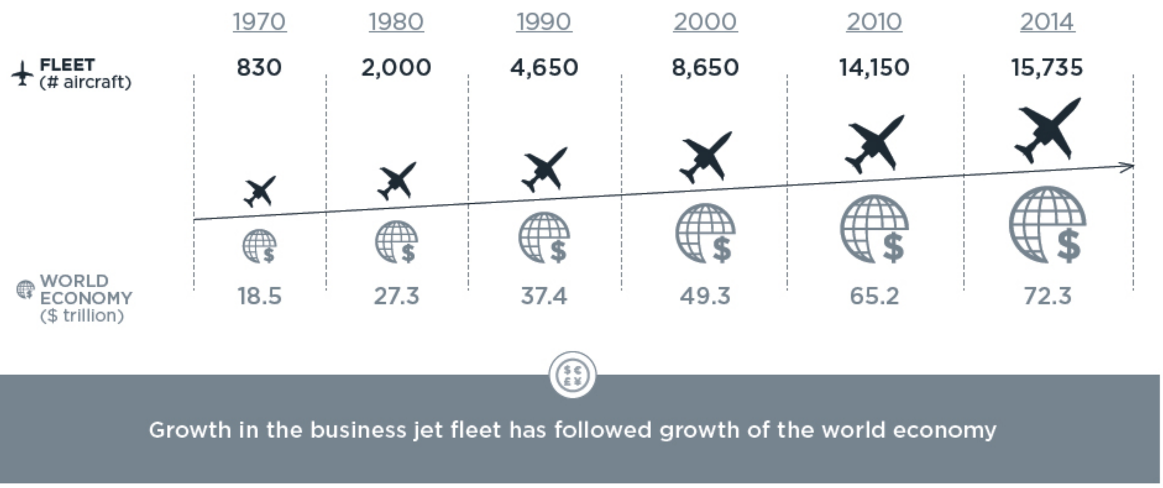

Figure 1: Business jet fleet and worldwide economic growth[5]

[1] URL http://www.boeing.com/commercial/bbj/#/aircraft/bbj-777/characteristics/777-200lr/ [cited May 26 2016]
[2] URL http://www.airbus.com/presscentre/pressreleases/press-release-detail/detail/airbus-launches-acj350-xwb-with-easyfit-outfitting/ [cited May 26 2016]
[3] URL http://www.airbus.com/aircraftfamilies/passengeraircraft/a350xwbfamily/a350-900/specifications/ [cited May 26 2016]

1. Mission

In this chapter the basic outline of the project is presented. The aim is to present the mission type on which the design shall be based. First the stakeholders requirements are defined in Section 1.1. With this covered, the projected market is analysed in order to prove the feasibility of such an aircraft. The chapter is concluded with the project planning.

Need statement: Passengers need to travel at least 8,500nm in a comfortable business class seating layout while cruising at high speed.
Mission statement: DSE group 11 will design an aircraft capable of carrying 18 passengers over a distance of 8,500nm.

1.1 Key Requirements

The design of the aircraft is guided by constant reference to the stakeholder requirements identified in [1]. The key requirements are restated below, while the exhaustive list is provided in Chapter 15.

- Employ a range of 8,500nm
- Carry a total of 18 passengers in a regular business class seating configuration
- Maintain a cruising speed of mach 0.8 or higher
- Be able to take off in less than 2000m
- Total cost of 60 million Dollars when producing in a series of 600 aircraft
- Comply with the latest safety and environmental regulations

1.2 Market Analysis and Forecast

With the global economy steadily recovering from the financial crisis of 2007. The global business jet market has recovered and is showing slight growth. The aim of this section is to provide an overview of the current private business jet market and its projected development in the future. With the growth outlined for the complete market, sales and demand numbers for the larger and further flying business jets will be shown to provide a business case for an ultra-long range capable aircraft.

1.2.1 Global Market Outlook

In 2014 the global business jet market grew by 6.5%, with a total of 722 new deliveries. To estimate the demand for long-range business jet models as a percentage of all business jet, the longest range models from each manufacturer are compared to the total deliveries of that manufacturer in Table 1.1 using statistics from the same source as the global data stated above.

Table 1.1: Size of long-range market relative to total market size

Deliveries/Manufacturer and model	2012		2013		2014	
Bombardier Global 5000/6000	54	30%	62	34%	80	39%
Bombardier total	179		180		204	
Gulfstream G300/G600 series	83	88%	121	84%	117	78%
Gulfstream total	94		144		150	
Embraer Legacy 600/650	17	17%	21	18%	18	15%
Embraer total	99		119		116	
Dassault Falcon 7X/2000LXS	37	56%	46	60%	45	68%
Dassault Falcon Jet total	66		77		66	
Total long-range jet market	**191/438**	**44%**	**250/520**	**48%**	**260/536**	**49%**

In order visualise the data further a graph can be found in Fig. 1.1, here the total sales are plotted against the longest range business jets from the top 3 manufacturers.

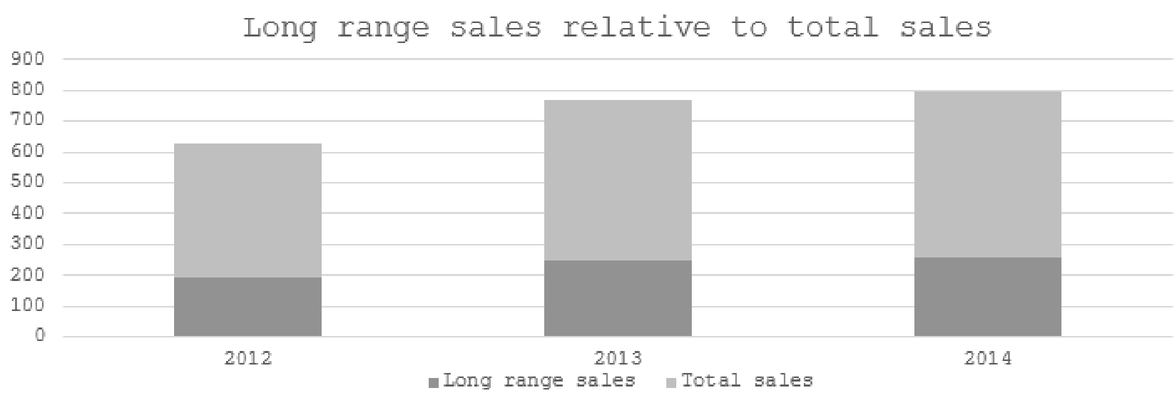

Figure 1.1: Sales share for large, ultra-long range business jets

Table 1.1 indicates the market for long-range business jets to be slightly under 50% of the total business jet deliveries for the 2012, 2013 and 2014 time period. In Addition, the market is seeing the introduction of new aircraft with even longer ranges such as the Bombardier Global 7000/8000 and the Dassault Falcon 8X. A second more optimistic estimate and forecast has been performed by Bombardier. Bombardier takes a similar approach and divides the market into three categories depending on their range: small (2,000 - 3,000nm), medium (3,000 - 5,000nm) and long (> 5,000). The results from this analysis are presented in Table 1.2.

Table 1.2: Revenue and delivery growth in the market for different range categories.

Category	Typical price	Range [nm]	Annual growth rate	Deliveries 2015-24	Revenues 2014-24
Light	$ 9 - 20 M	2,000 - 3,000	2.4%	3,400	$ 39 B
Medium	$ 20 - 42 M	3,100 - 5,000	3.8%	3,100	$ 91 B
Large	$ 50 - 72 M	>5,000	9.6%	2,500	$ 137 B
Total	n.a.	n.a.	3.8%	9,000	$ 267 B

According to this analysis, the ultra-long range business jet market is responsible 51% of the total revenues from business jets. With an average price in between $50 M and $72 M, the sales are worth $137 B. As such, the market share of different companies is readily determined and connected to the expected growth.
The market for business jets is subjected to varying volatility and drivers across the different geopolitical markets. An overview of the expected evolution of each market is obtained from the same source as Table 1.2 and Table 1.3. The long-range jet is intended to span the distance between any two of these geopolitical markets rather than simply allowing movement within a single region or between adjacent regions. This point is further elaborated in Section 1.2.1

Table 1.3: Geopolitical breakdown of market forecast for large (long-range) business jets, with percentage values of market held by long-range jets

Large business jet/Region	Deliveries 2015-2024		Revenues 2014-2024	
North America	700	18%	**$ 39B**	41%
Europe	560	38%	**$ 31B**	62%
Greater China	310	35%	$ 18B	55%
Latin America	210	25%	$ 11B	46%
CIS	130	25%	$ 6B	38%
Middle East	160	40%	$ 9B	60%
Asia Pacific	205	58%	$ 11B	**80%**
South Asia	160	51%	$ 9B	**75%**
Africa	65	24%	$ 3	43%

Going the Extra Mile for Ultra-Long Haul Flights

With the increasing efficiency of jet engines and the development of lighter and stronger materials, it is becoming more attractive to operate and design aircraft for ultra-long haul. Before going into more depth about this re-emerging trend, the different categories for aircraft with respect to distance will be defined:
Short-haul: A short-haul flight is defined as a non-stop flight covering less than 3200 km/2000 nm and taking less than three hours to complete.
Medium-haul: A medium-haul flight is defined as a non-stop flight covering less than 7000 km/3800 nm and taking less than eight hours to complete.
Long-haul: A long-haul flight is defined as a non-stop flight covering less than 12000 km/6500 nm and taking less than thirteen hours to complete.
Ultra long-haul: An ultra long-haul flight is defined as a non-stop flight covering more than 12000 km/6500 nm and taking more than thirteen hours to complete.

From this overview it can be seen that with a required range of 8500 nm (15742 km) the aircraft will be positioned in the ultra long-haul market. The specified range will make it possible to fly non-stop between the worlds most important business hubs as listed in Table 1.4.

Table 1.4: Business hubs reachable with an ultra long-haul range aircraft

City pair	Distance (km/nm)
Los Angeles - Dubai	13420/7246
Singapore - New York	15349/8288
Dallas - Sydney	13804/7454
Hong Kong - Dallas	13072/7058
Auckland - Dubai	14203/7668
Delhi - Mexico-City	14677/7925
Johannesburg - Houston	14509/7834
Moscow - Santiago de Chile	14134/7632

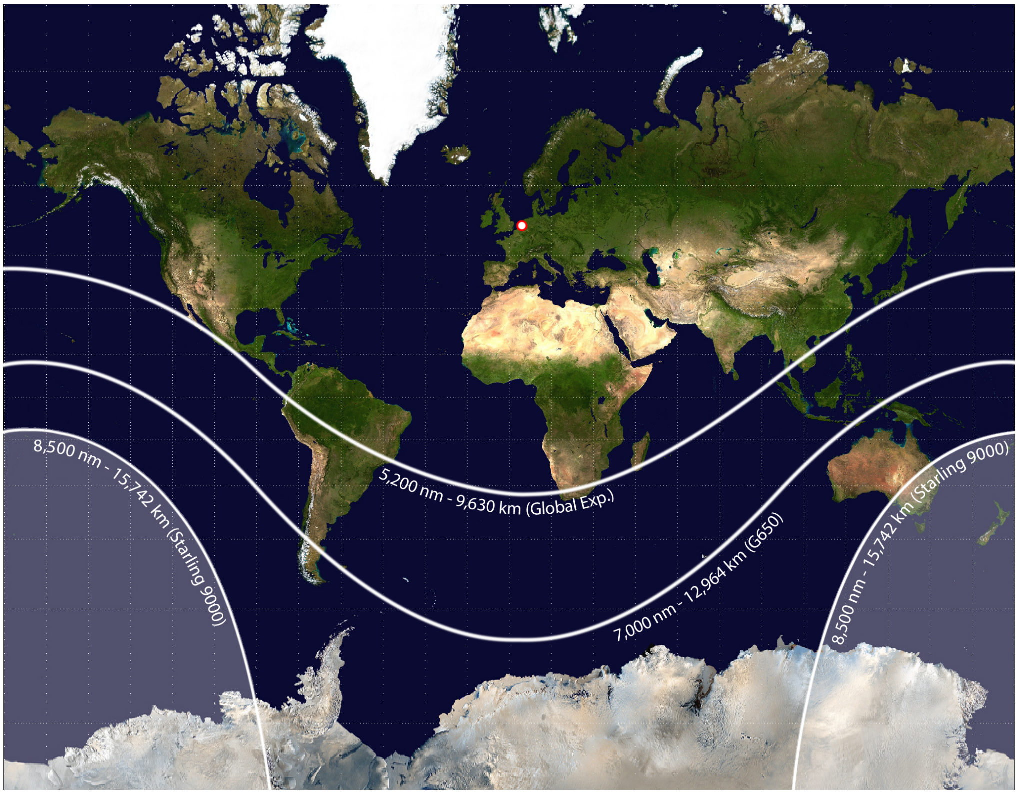

Figure 1.2: Starling 9000 range with 18 passengers, originating from Delft

The added value of these non-stop connections is that the hours on board of the aircraft can be billable and that in case of an overnight flight a proper rest can be enjoyed. Within the sufficient range a refuelling stop has to be made, increasing the travel time and reducing the billable hours.

1.3 Project Planning and Development

The initial design process presented in this report is only the beginning of the full aircraft design. During the initial design, class I and class II estimations are performed as well as basic subsystem design. This report proves the feasibility of the concept and all the advantages that put the Starling 9000 apart from the competition. The actions that need to be performed after the initial design are shown in Fig. 1.3. The actions shown are crucial to the completion of the Starling 9000, earliest in December 2020.
The Gantt chart presents the activities as shown in Fig. 1.3 but on a time-line. This chart represents the necessary time to complete certain tasks. As a living document it serves as an early indicator when the development process is heading for delays. The Fig. 1.4 shows a rough outline of all the steps necessary to get to the finished product. Though the time available is fixed, the chart can be adjusted to the stakeholder needs.

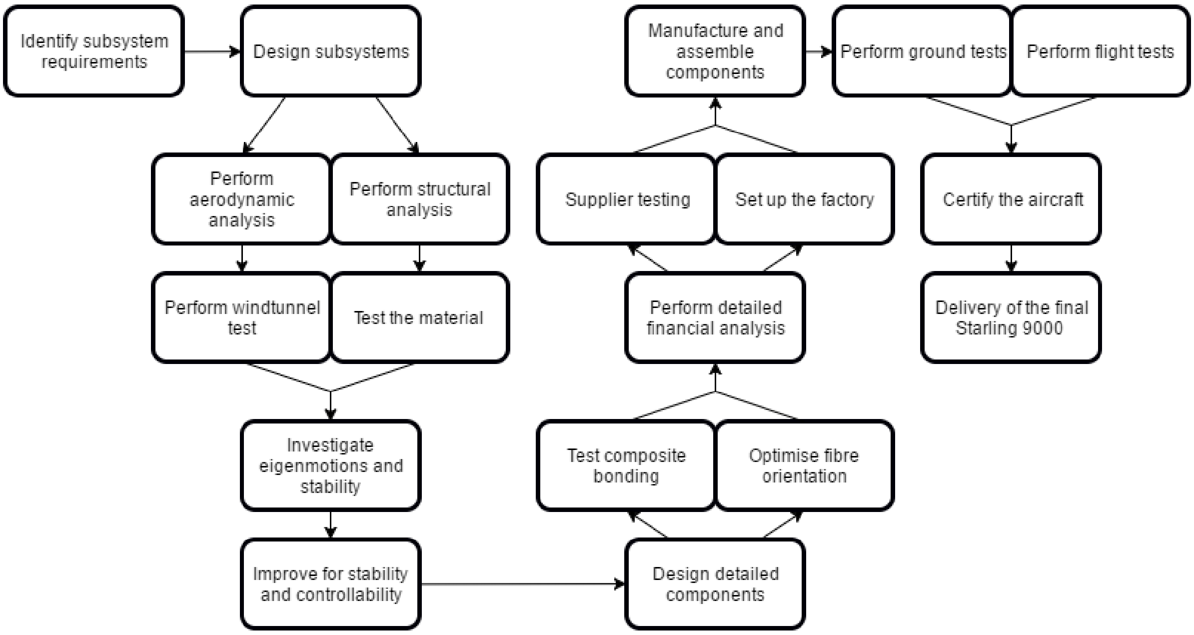

Figure 1.3: The project design and logic diagram presents all the steps and the order in which they are performed

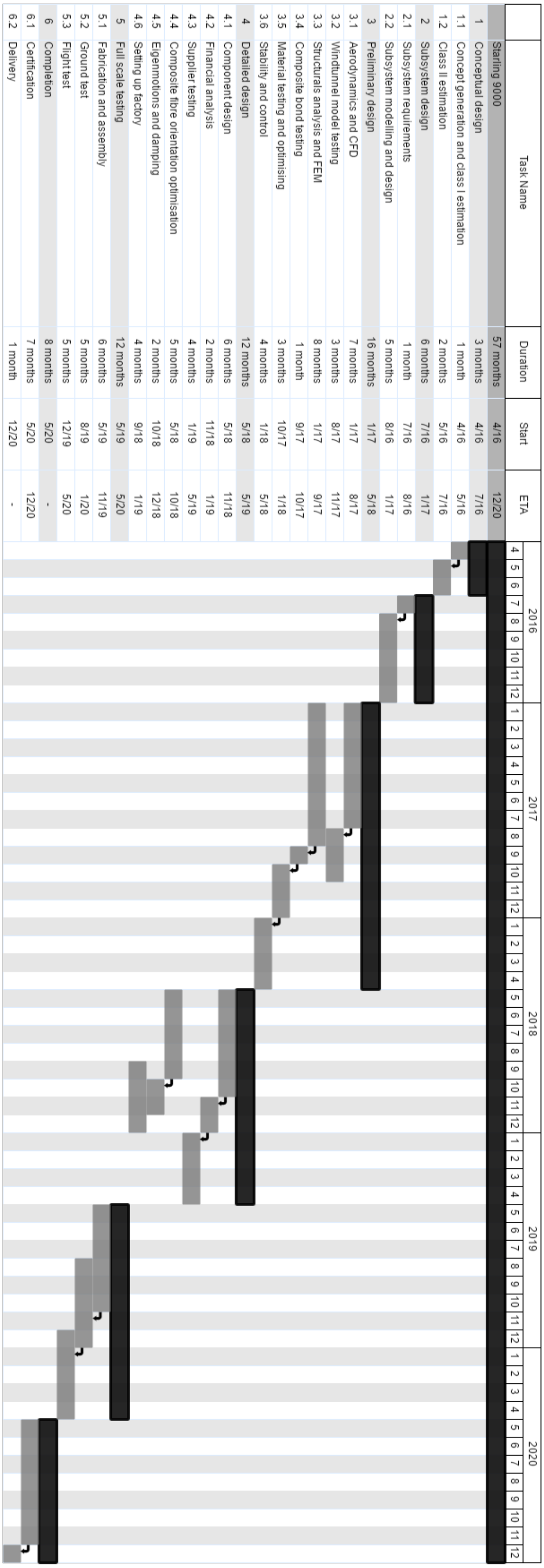

Figure 1.4: The Gantt chart presents the time-line with the activities till entry into service

2. Concepts & Trade-off

The design methodology adopted in the development of the Starling 9000 aircraft is one which puts the needs and requirements of the project stakeholders at the focal point of all decision making. As such, during the first phase of the design project [1] the mission goals and requirements (Section 1.1) were defined in synchrony with key project stakeholders as well as deeper market research. A literature study was performed to identify reference aircraft, analyse the current market and become familiar with the state-of-the-art and future possibilities for engineering solutions. Additionally, a good and convincing design methodology also calls for a structured approach to the design of the system and its components. This enables an enhanced and more easily understood overview for the stakeholders. As a first step in the structuring of the design, the functions and subsystems of the business jet were identified. With the strong basis of knowledge provided by the literature study, and a focused design methodology, the concept generation was initiated.
The initial pool of concepts covered approximately three dozen configurations, featuring different propulsion options and configuration layouts. The concepts were ranked according to stakeholder value and technical feasibility given the delivery time-line [1]. This allowed the majority of concepts to be carefully ruled out. In the end, four concepts made the final selection and are discussed Section 2.1. For these four concepts a trade-off was performed which is summarised in Section 2.2. After the selection of the winning concept through trade-off a sensitivity analysis was initiated to determine the certainty with which the winning concept was preferable over the others. The selected concept was ultimately iterated to remedy some inherent drawbacks in the configuration. The result is shown in Section 2.3.

2.1 Concepts

The four generated concepts can be seen in Fig. 2.1. This section contains a brief explanation of each concept and presents the reader with the main advantages and disadvantages. A more detailed insight on the concept generation is provided in the Mid Term Review [2].

The first concept is a conventional business jet design. Most modern business jets, such as the Gulfstream G650 and the Bombardier Global 7000/8000 have a similar configuration. Typically it features a mid-fuselage, low mounted, backwards swept main wing, and a T-tail. This allows the two turbofan engines to be mounted on behind the cabin on the aft fuselage section. The main advantages include a short landing gear (eliminating the need for an external jetway or airbridge), reduced cabin noise (due to aft engine placement), less chance of foreign object damage to engines (due to engine ground clearance) and a 'clean' wing without engine pods (no airflow disturbance)[18]. Disadvantages include the high cabin vibration levels (due to fuselage-mounted engines), deep stall sensitivity (T-tail design), and limited room for improvement beyond the competition. The latter fact is due to the decades of iterations of the design making further significant performance gains unlikely.

The second concept is radically different as compared to current business jets. It features an aft, forward swept wing and two open rotor engines in the back. It is a tailless design with a canard, as seen on the Beechcraft Starship [1]. Yaw control is provided by rudders incorporated into the super-sized winglets. Main advantages of this design include improved lift efficiency (due to canard instead of horizontal tailplane[18]), a 'clean' wing without engine pods (no airflow disturbance), high fuel efficiency (due to efficient open rotor engines), low cabin noise (due to aft engines) and a short landing gear. Disadvantages include possible stability issues (due to aft centre of gravity, and rudder moment arm), lower cruise speed (due to open rotor engines) and structural difficulty (due to forward swept wings and large winglets).

The third concept is a fairly conventional design with a backwards swept main wing. However, it incorporates several unconventional elements including a pelican tail and open rotor engines. The pelican tail design is comparable to the Northrop YF-23 prototype, or the Antonov An-225 (although this design looks more like an H-tail). The 2050 commercial airliner concept by Airbus also features a pelican tail[2]. Main advantages of the

[1] http://www.scaled.com/projects/starship [cited on 30 May 2016]
[2] http://www.airbus.com/innovation/future-by-airbus/[cited 30 May 2016]

third concept include a high fuel efficiency (due to the open rotor engines), a 'clean' wing without engine pods (no airflow disturbance), reduced cabin noise (due to aft engines) and a short landing gear. Disadvantages include possible stability issues (due to aft centre of gravity), lower cruise speed (due to open rotor engines) and lower engine and control surface efficiency (due to the small tail and engine clearance).

The fourth concept is the unique in its application of a high mounted wing in combination with an anhedral angle. The wing is swept backwards, making the concept similar to many Russian designs such as the Antonov An-148 [3]. It has a V-tail and two turbofan engines podded underneath the wing. Main advantages include the short landing gear, large ground clearance for both wings and engines (allows for unpaved runway operations), a lower structural wing weight (due to wing-mounted engines and high wing design), high manoeuvrability (due to anhedral wing) and easy engine access (useful for maintenance). Disadvantages include severe stability issues (aft centre of gravity) and disturbed airflow over the wing (podded engines underneath).

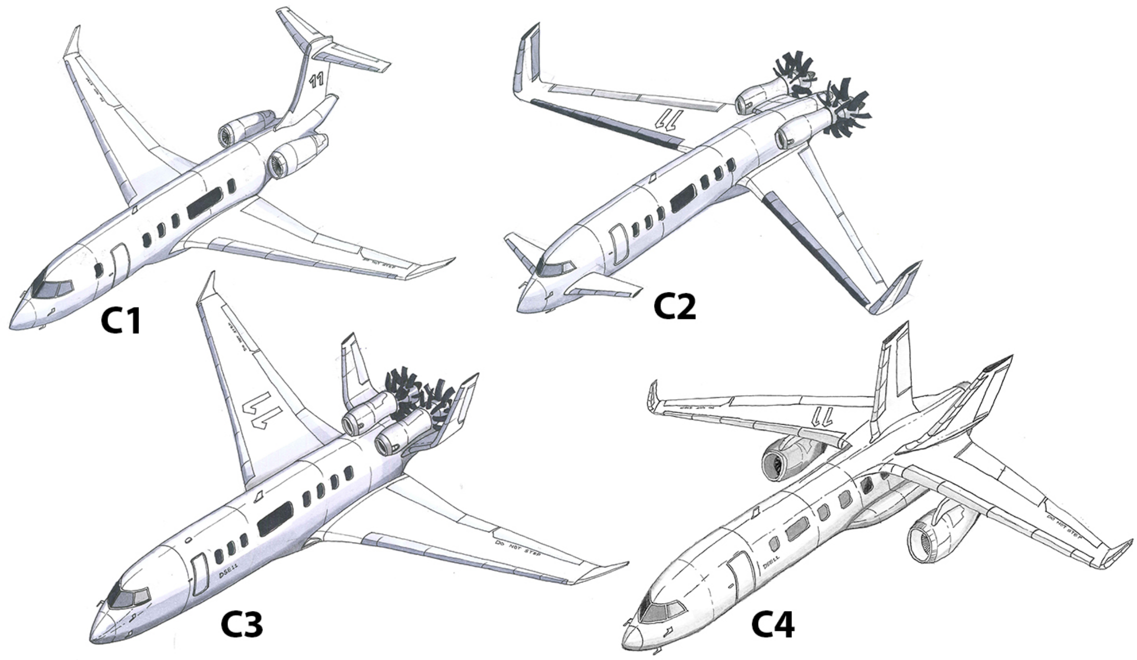

Figure 2.1: The four selected concepts

2.2 Trade-off

Following the selection of the four concepts a trade-off was performed to determine which concept delivers the greatest stakeholder value. This was done both by developing the criteria in the trade-off directly from the requirements, as well as studying the sensitivity of the result of the trade-off with respect to changes in individual grades of the different concepts. A detailed explanation of the trade method and criteria weight determination is covered in the Mid Term Review [2]. Table 2.1 shows the criteria weights and the score assigned to each concept.

[3] http://www.antonov.com/aircraft/passenger-aircraft/an-148 [cited June 4 2016]

Table 2.1: Trade-off scores for the four selected concepts

	Criterion	Weight [%]	Concept 1	Concept 2	Concept 3	Concept 4
1	Range Feasibility	18.6	7	5	4	5
2	Technical Feasibility	9.6	8	5	6	3
3	Stability & Control	10.3	6	7	5	2
4	TO & Landing	11.8	5	6	7	4
5	Safety	13.4	4	8	6	2
6	Sustainability	7.1	5	6	6	3
7	Dimensions	8.9	4	5	6	7
8	Material Choice	5.7	5	4	7	6
9	Timely Delivery	4.2	7	4	5	6
10	Cost	10.4	6	7	7	5
	TOTAL	100.0	5.728	5.906	5.762	4.114

Concepts 1,2, and 3 demonstrated nearly equal value according to the weighing criteria. Nonetheless, Concept 2 did distinguish itself from the competition by a small but not negligible margin. Additionally, as outlined in [2] the innovative nature of the design adds potential for out-performing the competition. It should be noted that some of the trade-off weights can seem counter-intuitive but are supported by qualitative calculations and hours of brainstorming. For instance, it may seem strange that concepts 2 and 3 score lower on range feasibility despite the fact that they use open-rotors engines which are substantially more efficient that the turbofan engine of concept 1. However, aircraft with open rotor propulsion typically fly slower, leading to a lower Brequet equation range [2].
In order to attempt to increase the trade-off margin between the winning concept (concept 2) and concepts 1 and 3, value maximising design iterations on concept 2 were implemented [2]. Details of this refinement of concept 2 are given in Section 2.3.

2.3 Final Concept for Starling 9000

The final concept is shown in Figs. 2.2 and 2.3. Compared to the original second concept, the wing has been swept backward to mitigate the disadvantages of a forward swept wing and further improve stakeholder value. This has made the second concept the best trade-off with a significant margin. The main disadvantage of a forward swept wing is the structural difficulty and the resulting added structural weight. This negatively impacts the fuel efficiency, which poses a threat to the key requirement of reaching the 8,500 nm range. Furthermore the backwards swept wing extends the arm of the rudder and vertical stabiliser as compared to the original design. This allows for smaller winglets (and rudders) to be utilised which is again favourable to the structural complexity and weight of the wing[2]. Moreover, forward swept wings are prone to yaw instability and associated severe Dutch roll problems, making them harder to control. All of these disadvantages have been mitigated by selecting a backwards swept design. The new concept serves as the starting point for the detailed design phases and iterations which are the focus of this report.

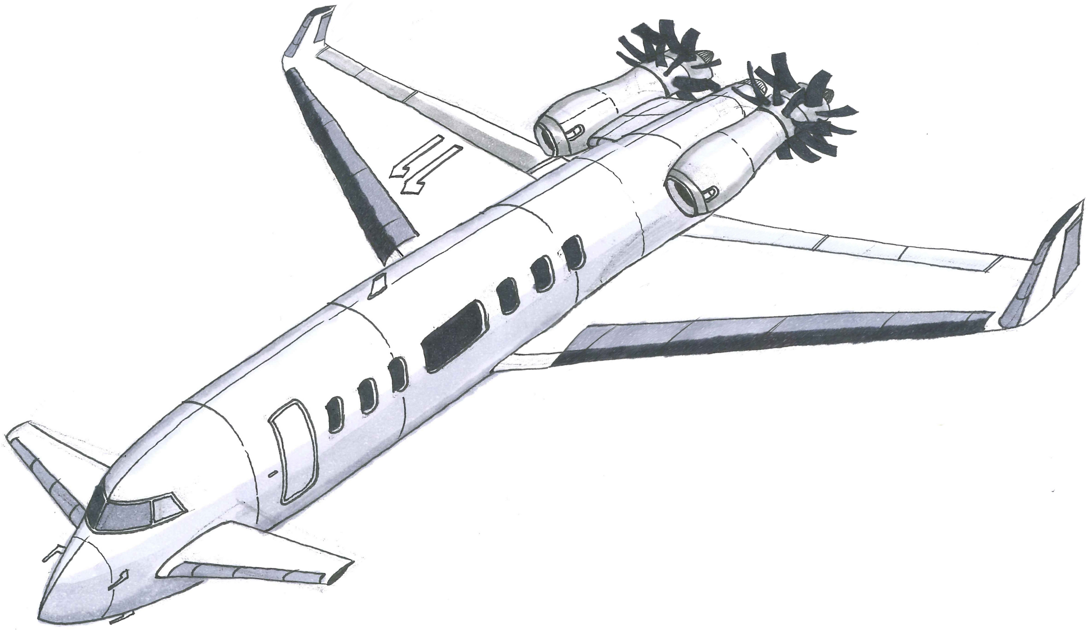

Figure 2.2: The final, modified concept

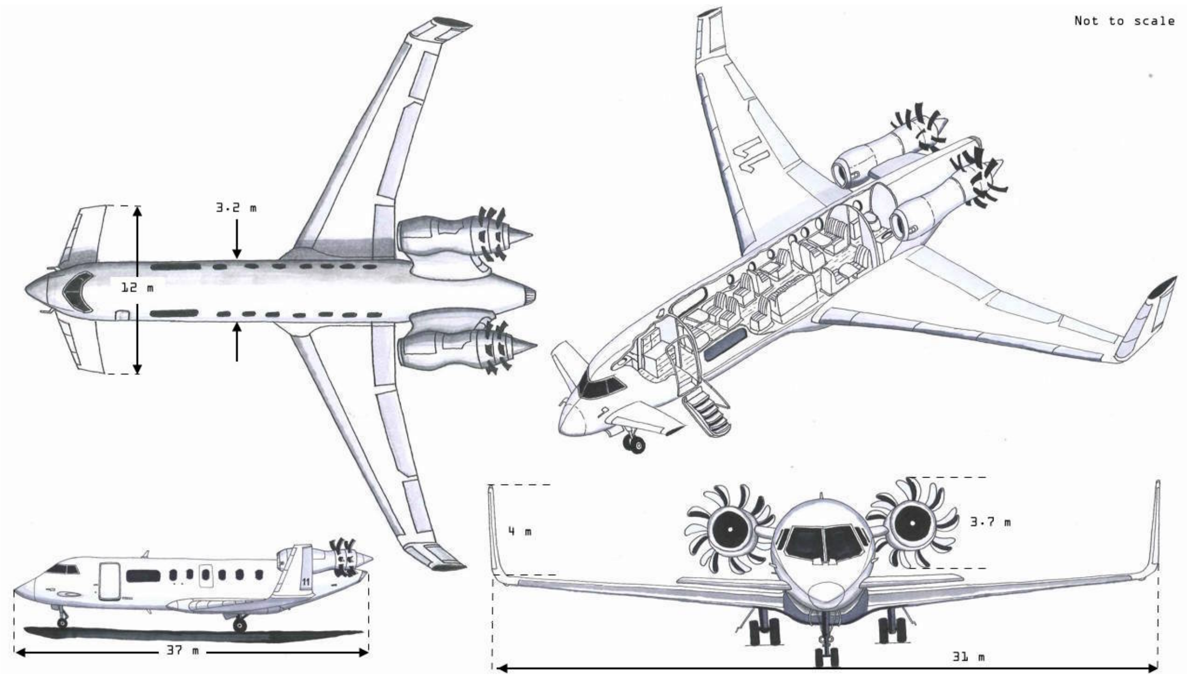

Figure 2.3: Different views of the final concept

3. Cost and Resource Allocation

Proper resource allocation is an important part of every design process. It defines design space and limits it in order to prevent exceeding the design budget. This chapter covers the financial resource allocation. A breakdown of other budgets is discussed in later chapters. The Ultra-long Range Business Jet (URBJ) mission aims at a maximum unit cost of USD 60 million for a series of 600 aircraft [50]. According to Roskam's Airplane Design Part VIII [43] the cost budget for designing an aircraft can roughly be divided into Research, Development, Testing and Evaluation (RDTE) cost, Manufacturing and Acquisition (M&A) cost and Operational cost [43]. The first two categories are discussed in this chapter, while the Operational costs are covered in Chapter 13. The methods provided by Roskam are based on imperial units, resulting in a cost expressed in dollars. All new variables introduced in this chapter are explained below the equation or were already used in previous equations. Values were obtaine from external sources (referenced) or suggested by Roskam.

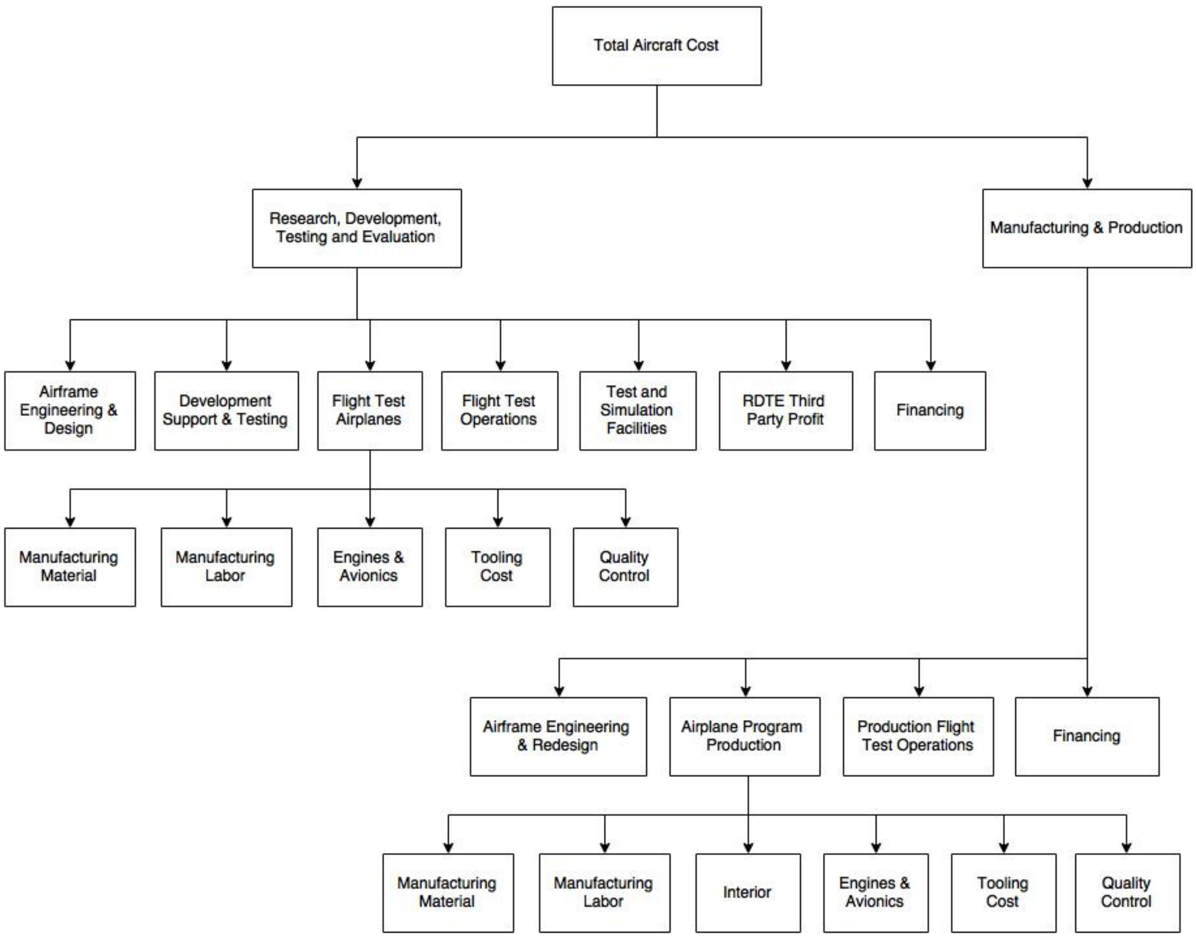

Figure 3.1: Cost breakdown of the new business jet

3.1 Research, Development, Testing and Evaluation Cost

According to Roskam [43], the total RDTE cost is equal to the sum of seven cost categories:

- C_{aed_r} Airframe Engineering and Design Cost
- C_{dst_r} Development Support and Testing Cost
- C_{fta_r} Flight Test Airplanes Cost
- C_{fto_r} Flight Test Operations Cost

- C_{tsf_r} Test and Simulation Facilities Cost
- C_{pro_r} RDTE Profit
- C_{fin_r} Cost to finance RDTE phases

Airframe Engineering and Design

The Airframe Engineering and Design costs covers engineering, design and developmental costs and can be estimated using the following equation:

$$C_{aed_r} = \left(0.0396 \cdot W_{ampr}^{0.791} \cdot V_C^{1.526} \cdot N_{rdte}^{0.183} \cdot F_{diff} \cdot F_{cad}\right) \cdot R_{e_r} = \$278,226,400 \tag{3.1}$$

$$W_{ampr} = log^{-1}(0.1936 + 0.8645(log W_{TO})) = 37,524\ lbs\ (17,020\ kg) \tag{3.2}$$

where:

W_{ampr}	= Aeronautical Manufacturers Planning Report Weight	= 37,524 lbs (17,020 kg)
W_{TO}	= Maximum takeoff weight	= 116,772 lbs (52,967 kg)
V_C	= Cruise speed	= 459 kts (850 km/h)
N_{rdte}	= Number of prototypes	= 3 (1 static, 2 flying)
F_{diff}	= Difficulty judgement factor	= 1.5 (unconventional configuration)
F_{cad}	= Roskam CAD judgement factor	= 0.8 (because of CAD experience)
R_{e_r}	= Engineer hourly rate	= \$100/h

Development Support and Testing

The Development Support and Testing Cost includes windtunnel, structural, propulsion and system testing and can be estimated using:

$$C_{dst_r} = 0.008325 \cdot W_{ampr}^{0.873} \cdot V_C^{1.890} \cdot N_{rdte}^{0.346} \cdot CEF \cdot F_{diff} = \$67,581,819 \tag{3.3}$$

where:

CEF	= Cost Escalation Factor	= 3.5 (estimated for 2016)

Flight Test Airplanes

The Flight Test Airplanes Cost covers the cost for building the static and two flying prototypes of the design. It can be estimated using:

$$C_{fta_r} = C_{(e+a)_r} + C_{man_r} + C_{mat_r} + C_{tool_r} + C_{qc_r} = \$657,298,206 \tag{3.4}$$

where:

$C_{(e+a)_r}$	= Engine and Avionics Cost
C_{man_r}	= Manufacturing Labor Cost
C_{mat_r}	= Manufacturing Material Cost
C_{tool_r}	= Tooling Cost
C_{qc_r}	= Quality Control Cost

The variables from Equation (3.4) can be estimated using the formulas below:

$$C_{(e+a)_r} = N_e \cdot (N_{rdte} - N_{st}) \cdot E_{price} + A_{price} = \$48,000,000 \tag{3.5}$$

$$C_{man_r} = R_{m_r}\left(28.984 \cdot W_{ampr}^{0.740} \cdot V_C^{0.543} \cdot N_{rdte}^{0.524} \cdot F_{diff}\right) = \$261,570,046 \tag{3.6}$$

$$C_{mat_r} = 37.632 \cdot F_{mat} \cdot W_{ampr}^{0.689} \cdot V_C^{0.624} \cdot N_{rdte}^{0.792} \cdot CEF = \$51,064,498 \tag{3.7}$$

$$C_{tool_r} = R_{t_r}\left(4.0127 \cdot W_{ampr}^{0.764} \cdot V_C^{0.899} \cdot N_{rdte}^{0.178} \cdot N_{r_r}^{0.066} \cdot F_{diff}\right) = \$262,659,556 \tag{3.8}$$

$$C_{qc_r} = 0.13 C_{man_r} = \$34,004,106 \tag{3.9}$$

where:

N_e	= Number of engines	= 2
N_{st}	= Number of static prototypes	= 1
E_{price}	= Engine price	= \$10,000,000 [1]
A_{price}	= Avionics price	= \$8,000,000
R_{m_r}	= Manufacturing labor hourly rate	= \$50/h
F_{mat}	= Correction factor based on material choice	= 2.5 (mainly composite)
R_{r_r}	= Tooling labor hourly rate	= \$50/h
N_{r_r}	= RDTE Production Rate (units/month)	= 0.33 (typical rate [43])

Flight Test Operations

The Flight Test Operations cost covers flight testing of the prototypes and associated simulator activities. It can be approximated using:

$$C_{fto_r} = 0.001244 \cdot W_{ampr}^{1.160} \cdot V_C^{1.371} \cdot (N_{rdte} - N_{st})^{1.281} \cdot CEF \cdot F_{diff} \cdot F_{obs} = \$14,326,791 \tag{3.10}$$

where:

F_{obs} = Factor for 'stealthy' military aircraft = 1.0 (for commercial aircraft)

Test and Simulation Facilities

The Test and Simulation Facilities costs include the construction of dedicated test and simulation facilities, such as hardware and software test setups. The cost is highly dependent on the facilities already available to the manufacturer. For example, a new Airbus type might not require any additional facilities compared to previous model testing, while a new manufacturer might have no facilities available beforehand at all. Roughly the cost can be estimated using:

$$C_{tsf_r} = C_{RDTE} \cdot F_{tsf} \tag{3.11}$$

where:

C_{RDTE}	= Total RDTE cost	
F_{tsf}	= Facilities judgement factor	= 0.20 (new facilities, unconventional configuration)

Research, Development, Testing and Evaluation Profit

The profit made by other shareholders during the RDTE phases (due to joined or shared research for example) can be estimated using:

$$C_{pro_r} = C_{RDTE} \cdot F_{pro_r} \tag{3.12}$$

where:

F_{pro_r} = Profit factor = 0.1

Financing Research, Development, Testing and Evaluation

Often manufacturers (especially those new on the market) will have to borrow money in order to start aircraft development. The costs for financing such development highly depend on interest rates and the financial situation of the manufacturer. However, a rough approximation can be made using:

$$C_{fin_r} = C_{RDTE} \cdot F_{fin_r} \tag{3.13}$$

where:

F_{fin_r} = Interest judgement factor = 0.2

Total Research, Development, Testing and Evaluating Cost

The final sum for Research, Development, Testing and Evaluation cost then becomes:

$$C_{RDTE} = C_{aed_r} + C_{dst_r} + C_{fta_r} + C_{fto_r} + C_{tsf_r} + C_{pro_r} + C_{fin_r} \tag{3.14}$$

[1] URL http://www.public.navy.mil/navsafecen/Documents/aviation/maintenance/2015_eng_cost_msg.docx[cited June 14 2016]

$$C_{RDTE} = \$278,226,400 + \$67,581,819 + \$657,298,206 + \$14,326,791 + 0.2C_{RDTE} + 0.1C_{RDTE} + 0.2C_{RDTE} \quad (3.15)$$

$$C_{RDTE} = \$2,034,866,432 \quad (3.16)$$

This value can be validated by comparing it to the developmental costs of competing aircraft. For example, the development of the Gulfstream G650 (2009) is assumed to have cost 1.2 billion USD. The Bombardier Global Express (1996) is estimated at 0.8 billion USD. Bombardiers Global 7000/8000 model, currently under development, are estimated to cost 1.4 billon USD [20]. Since the Starling jet is not an iteration of a previous concept, the development costs were expected to be higher than for the aircraft models above. The development cost calculated above therefore seems to be a realistic estimate.

3.2 Manufacturing & Acquiring Cost

According to Roskam, the acquiring cost of an aircraft equals the manufacturing cost plus the profit made by the manufacturer [43]. In order to estimate the manufacturing cost, the following equation is used:

$$C_{MAN} = C_{aed_m} + C_{apc_m} + C_{fto_m} + C_{fin_m} \quad (3.17)$$

where:

C_{MAN}	= Total Manufacturing Cost
C_{aed_m}	= Airframe Engineering and Design Cost
C_{apc_m}	= Airplane Program Production Cost
C_{fto_m}	= Production Flight Test Operations Cost
C_{fin_m}	= Cost to finance manufacturing phase

Airframe Engineering and Design

The Airframe Engineering and Design Cost comprises engineering design work necessitated by problems uncovered during the RDTE phase, but also customer specific design studies. It also includes the release and maintenance of technical drawings and specifications, as well as RAMS assessments of the aircraft. It can be estimated using:

$$C_{aed_m} = R_{e_r}\left(0.0396 \cdot W_{ampr}^{0.791} \cdot V_C^{1.526} \cdot N_{program}^{0.183} \cdot F_{diff} \cdot F_{cad}\right) - C_{aed_r} = \$456,090,100 \quad (3.18)$$

where:

$N_{program}$	= Number of aircraft to be produced (including prototypes)	= 603

Airplane Program Production

The Airplane Program Production consists of engine and avionics acquiring costs, interior costs, manufacturing labor and material costs, tooling costs and finally quality control costs. It is slightly different from the airplane production costs during the RDTE phase and can be approximated using:

$$C_{apc_m} = C_{(e+a)_m} + C_{int_m} + C_{man_m} + C_{mat_m} + C_{tool_m} + C_{qc_m} = \$25,311,482,020 \quad (3.19)$$

where:

$C_{(e+a)_m}$	= Engine and Avionics Cost
C_{int_m}	= Interior cost
C_{man_m}	= Manufacturing Labor Cost
C_{mat_m}	= Manufacturing Material Cost
C_{tool_m}	= Tooling Cost
C_{qc_m}	= Quality Control Cost

The variables above are calculated below:

$$C_{e+a_m} = N_m \cdot (N_e \cdot E_{price} + A_{price}) = \$16,800,000,000 \quad (3.20)$$

$$C_{int_m} = F_{int} \cdot N_{pax} \cdot N_m \cdot CEF/CEF_{1990} = \$37,800,000 \quad (3.21)$$

$$C_{man_m} = R_{m_r}\left(28.984 \cdot W_{ampr}^{0.740} \cdot V_C^{0.543} \cdot N_{program}^{0.524} \cdot F_{diff}\right) - C_{man_r} = \$4,047,403,710 \tag{3.22}$$

$$C_{mat_m} = 37.632 \cdot F_{mat} \cdot W_{ampr}^{0.689} \cdot V_C^{0.624} \cdot N_{program}^{0.792} \cdot CEF - C_{mat_r} = \$3,354,980,240 \tag{3.23}$$

$$C_{tool_m} = R_{t_r}\left(4.0127 \cdot W_{ampr}^{0.764} \cdot V_C^{0.899} \cdot N_{program}^{0.178} \cdot N_{r_m}^{0.066} \cdot F_{diff}\right) - C_{tool_r} = \$545,081,584 \tag{3.24}$$

$$C_{qc_m} = 0.13 C_{man_m} = \$526,162,482 \tag{3.25}$$

where:

N_m	= Number of production aircraft	= 600
F_{int}	= Interior cost factor	= \$3,000/pax for business jets
N_{pax}	= Number of passengers	= 18
CEF_{1990}	= Cost Escalation Factor for 1990	= 3.0
N_{r_m}	= Production Rate (units/month)	= 5

Production Flight Test Operations

The Production Flight Test Operations cost covers operational costs of the airplane during pre-delivery test flying. It can be estimated using:

$$C_{fto_m} = N_m \cdot C_{ops/hr} \cdot t_{pft} \cdot F_{ftoh} = \$196,400,000 \tag{3.26}$$

where:

$C_{ops/hr}$	= Airplane operating cost per hour	= \$8,183
t_{pft}	= Number of flight test hours per aircraft before delivery	= 10 hrs (suggested by Roskam)
F_{ftoh}	= Overhead factor associated with production flight test activities	= 4.0

For now, the operational cost per hour is derived from the Direct Operating Costs (DOC) of multiple comparable aircraft. The Gulfstream G550 (\$8,640/hr) and Bombardier Global Express (\$8,045/hr) and Dassault Falcon 7X (\$7,865/hr) are assumed to have approximately the same operational cost[2]. The average hourly operational cost then becomes \$8,183/hr. Chapter 13 presents a more detailed estimation of operational costs.

Financing the Manufacturing Phase

Similar to the RDTE phase, manufacturers (especially those new on the market) will often have to borrow money in order to start aircraft development. The costs for financing such development highly depend on interest rates and the financial situation of the manufacturer. However, a rough approximation can be made using:

$$C_{fin_m} = C_{MAN} \cdot F_{fin_r} \tag{3.27}$$

Total Manufacturing & Acquiring Cost

The final calculation for Manufacturing & Acquiring Cost then becomes:

$$C_{MAN} = \$456,090,100 + \$25,311,482,020 + \$196,400,000 + 0.2 C_{MAN} \tag{3.28}$$

$$C_{MAN} = \$32,454,897,650 \tag{3.29}$$

$$C_{MAN_{unit}} = \$54,091,496 \tag{3.30}$$

The proposed unit price for the new business jet is 60 million USD, which would lead to a profit of:

$$C_{PROFIT} = C_{REV} - C_{MAN} = N_m \cdot P_{unit} - C_{MAN} = \$3,545,102,350 \tag{3.31}$$

[2]URL http://www.forbes.com/sites/davidewalt/2013/02/13/thirty-amazing-facts-about-private-jets/#42f4bb872730[cited June 1 2016]

or:

$$C_{PROFIT_{unit}} = \$5,908,503 = 9,85\% \tag{3.32}$$

where:

C_{PROFIT}	= Total profit	
C_{REV}	= Total revenue	
P_{unit}	= Unit price	= 60 million USD

According to Roskam, profit rates of 10% are not uncommon in the aerospace field. This indicates that the profit rate calculated above is a realistic estimation.

3.3 Return on Investment Analysis (ROI)

Fig. 3.2 shows the RDTE costs, production costs, sales and resulting profit against time. The break-even point is expected in 2027, 7 years after the production initiation, and after the delivery of 385 aircraft. While a constant production rate of 5 aircraft per month was assumed in the Mid Term Report [2], a variable rate has been assumed in this report in order to obtain a more accurate and conservative estimate of the return on investment. The new variable rate accounts for the learning effect is meant to account for the learning effect inhere in production ramp-up. Specifically, as factory workers gain experience and kinks in the supply chain are ironed out, the delivery interval naturally decreases. To model this behaviour a power-law learning curve has been implemented. The latter is characterised by a factor of 0.85 decrease in unit cost over the production series of 600 aircraft [3]. As a result of the modelling of the learning effect, the revenues and total cost graphs in Fig. 3.2 become slightly non-linear, and the break-even point shifts farther into the future in comparison to a linear curve with the assumption of a constant production rate.

The learning effect directly relates the serial number of the aircraft to its unit cost. It does not, however, directly link to the production time of the unit. To establish this connection, the conservative assumption is made that the decrease in unit cost through the series is due to purely the reduction of labour costs. As these are proportional to the production time of each aircraft they allow the unit cost to be related to unit production time. It should be noted that not the entire decrease in cost is, in fact, due to the reduction in spending on labour. Costs are also reduced as less material is wasted (rework, or scrap due to bad quality), or optimisation and better negotiations across the supply chain. However, by assuming that these contributions are negligible in comparison to the variation in labour costs a conservative estimate for the break-even point is obtained. As such, there is a high likelihood that the Starling 9000 programme will reach its break even point by the time computed in this analysis, or sooner.

The cost of unit 'i' (C_i) is given by the first relation in Equation (3.33), where for a production series of 600 aircraft and a learning factor of 0.85, 'b' is given by the second relation.

$$C_i = C_0 \cdot i^b \qquad\qquad b = log(0.85) \cdot log\left(\frac{1}{600}\right) \tag{3.33}$$

In order to balance the learning curve such that the average unit cost for 600 aircraft remains \$54,091,496, as estimated above, the cost of the first unit produced (C_0) should be calculated as in Equation (3.34). The cost of the final unit is then simply defined through Equation (3.33).

$$C_0 = 600 \cdot \$54,091,496 \cdot \left(\sum_{i=0}^{600} i \cdot b\right)^{-1} = \$62,032,000 \qquad\qquad C_{600} = \$52,727,000 \tag{3.34}$$

From the total cost of each aircraft obtained through Equation (3.34) and knowing that the labour cost represents 14,2% of the total aircraft cost, the labour cost may be determined. Next, the learning curve is balanced such that the average time per each of the 5 manufacturing stations is 15 days. The minimum station time (ΔT_i) for each aircraft serial number is then given by Equation (3.35). Finally, because all production stations must move forward simultaneously, the production interval at any given moment is driven by the aircraft with the lowest serial number i.e. slowest aircraft. This discrete correction is applied through a Python script.

$$\Delta T_i = \frac{C_i - (1 - 0.142) \cdot \$54,091,496}{0.142 \cdot \$54,091,496} \cdot 15 days \tag{3.35}$$

[3] URL http://fas.org/news/reference/calc/learn.htm[cited June 16 2016]

As a result of the balancing of the learning curve, both the total production time and total production cost remain the same as the initial estimates. It should be noted that the negative effect of interest rates on the increased rate of spending on the initial aircraft is not accounted for in this analysis. However, the effect can be considered minor in comparison to the assumption that labour rates dominate the time-dependent cost component. As such, the total profit for the series of 600 Starling 9000 aircraft remains unchanged with respect to the initial estimate using a constant production rate.

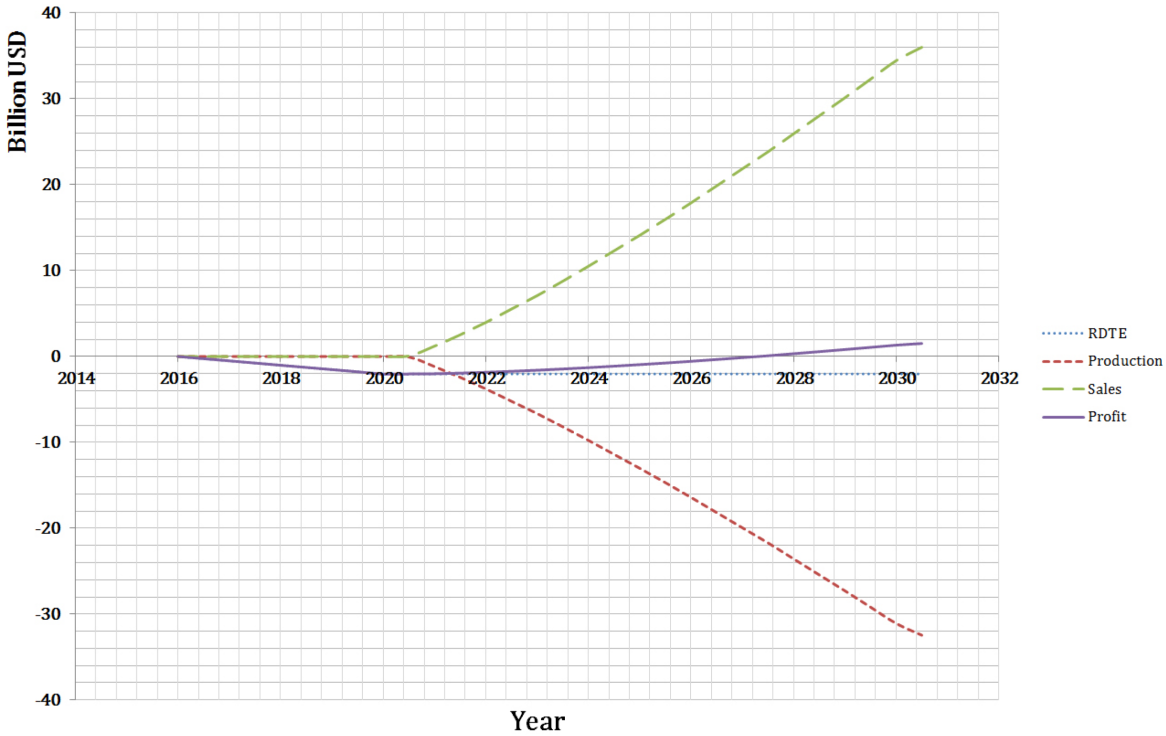

Figure 3.2: Return on Investment

In summary, the first aircraft is expected to take 183 days to deliver (unit cost 62.0 million USD), while the final one will take only 79 days (unit cost 52.7 million USD). The first aircraft is the only aircraft manufactured which costs exceeding the sales price. The additional labour time and production inexperience eat through the 9.56% profit margin. However, starting with aircraft No. 2, the production of Starling 9000 aircraft becomes profitable. Additionally, it should be acknowledged that the list price of the aircraft is subject to change throughout the production series. As such, stating a higher price for the first deliveries is a possible way to to compensate for the decrease in profitability at the start of production.

4. Risk & Sensitivity

For the design of business jet, several estimations and assumptions are necessary, some of these are impossible to be very accurate and have a level of uncertainty. These uncertainties imply that there are risks involved. It is important to identify these risks at an early stage, before they become a serious problem. With proper risk management, these risks can be mitigated or at least can be accounted for. This section will take this under consideration. Technical risk assessment is the procedure which is defined as; "what is the likelihood that a system when constructed meets the performance requirements set? And if a shortfall in performance is expected, what will be the impact on the system and where are changes needed?" [23].

4.1 Risk Identification

The first step in addressing potential risks is identifying them all separately. There is a distinction between internal and external risks. The internal risks will rise out of the development itself and can thus be influenced by the development itself. Foreseeing a problem in the planning phase will reduce further problems like delayed development. External risks are much harder to influence, these external risks should be dealt early, preferably before the development. Table 4.1 gives an overview of the risks but not the likelihood nor the impact.

Table 4.1: Internal and external risks

Internal risk	High RDTE costs
	Too long RDTE time
	Late break-even point
	Weight over budget
	High ownership costs
	Unfeasible initial concept
	Structural difficulty
	Not meeting range requirements
	Not meeting stability requirements
	Not meeting speed requirements
	Concept requires heavy modification
External risk	Not meeting noise and emissions regulations
	High number of potential competitors
	Changing economics
	Lack of suitable engines
	Program financing
	Rising fuel prices
	Decreased demand for large business jets
	Low interest for new design
	Lack of reference material
	High production cost
	Certification difficulty

4.2 Risk Map

The risks are judged on a combination of two factors, namely the likelihood and the impact of the risk. The likelihood represents the probability that the event will take place and the impact is the severity of the consequences in case the event happens. Every risk will be separately analysed for likelihood and impact as shown in Table 4.2. The scale is defined as 1 (highly unlikely) to 4 (very likely) for likelihood and 1 (very little impact) to 4 (very high impact) for impact. The risks which have a combination of a high impact and a high probability of happening, are the ones that require the most attention. For most risks it is possible to reduce the impact or the probability of occurrence. Below are the identified risks discussed with possible solutions to reduce each risk.

Table 4.2: Risk assessment and Mitigation Strategies

	Risk	Likelihood	Impact
A	High RDTE costs	3	2
B	Long RDTE time	3	1
C	Late break even point	3	1
D	High ownership cost	2	3
E	Unfeasible initial concept	1	4
F	Structural difficulty	3	3
G	Not meeting range requirements	2	3
H	Not meeting stability requirements	1	2
I	Not meeting speed requirements	2	2
J	Concept requires heavy modification	1	3
K	Weight over budget	2	4
L	Not meeting noise and emissions requirements	1	3
M	High number of potential competitors	2	3
N	Changing economics	1	2
O	Lack of suitable engines	2	3
P	Program financing	2	2
Q	Rising fuel prices	3	2
R	Decreased demand for large business jets	1	3
S	Low interest for new design	2	2
T	Lack of reference material	4	3
U	High production cost	4	2
V	Certification difficulty	2	4

High RDTE costs
For most concepts the RDTE costs will be relatively high because of the new unconventional design. These high costs are as predicted and fit in the financial budget.

Long RDTE design
The unconventional design will highly likely lead to a long RDTE period, good planning should still keep the aircraft completion on track. Delays in aircraft development are not unusual, but need to be kept to a minimum. If there is delay, the customer should be kept up to date about the delivery date.

Late break even point
Both high RDTE costs and long RDTE time can lead to a delayed break even point, this can be solved by producing more aircraft or producing aircraft faster if there is still a demand for the aircraft after the delay.

High ownership cost
The aircraft is newly developed and will have a high initial purchase price, but low running costs because of low fuel consumption. Material choices will have a big influence on both initial price and maintenance costs. A too high ownership cost will make the jet less attractive for businesses and private owners.

Unfeasible initial concept
Out of multiple concepts, four were selected because of their potential to succesfully carry out the mission. Preliminary analysis with basic aeronautical engineering tools allow to asses the concepts based on estimated specifications. Out of the possible configurations the best trade-off is chosen to maximise the probability of satisfying the base requirements. In case a problem in the chosen configuration is critically underestimated, a different concept should be selected or at least big changes will be required.

Structural difficulty
One of the main sources of structural difficulty on top of the standard load scenarios is the addition of the big windows, which will probably add weight to the aircraft due to the required structural reinforcements. Furthermore most concepts have unconventional configurations, such as a V-tail or winglet rudders, which

introduce complex structural designs. Minor optimisations in the configuration can lead to reduced forces and thus less structural difficulty.

Not meeting range requirements
Most concepts generated are driven by the long range requirements. The main cause of not satisfying these requirements will be exceeding design budgets for example weight, fuel or aerodynamic efficiency or the lack of appropriate materials and subsystems. As this is the main objective, other requirements might have to be compromised to achieve the 8500 nm range.

Not meeting stability requirements
The concepts will be designed to be statically longitudinal stable. Some concepts allow to be designed dynamically stable as well. When it is not possible to have a dynamically stable configuration this is solved with an electronic flight control computer.

Not meeting speed requirements
The final cruise speed will be determined by multiple factors to achieve the optimal trade off. This trade-off will favour the most important requirements and limits. In case of reduced cruise speed, the reduction will only be minor and subordinate to the other improvements.

Concept requires heavy modification
If the chosen concept proves to be unfeasible, then major changes will be needed. At that point the critical areas of change will be clearly defined and these changes will require new preliminary estimates. This course of actions will take a lot of time. Careful selection of concepts and diligent iterations will drastically reduce the need for a concept overhaul.

Weight over budget
First estimates for the MTOW are the guideline to see what is realistic. Contingencies are put in place to stay within feasible limits. If these limits are monitored and appropriate trade-offs are made to stay within those limits, the chance of going over the weight budget is very small. The weight estimate was based on the range and thus deviation will be detrimental to the primary requirements.

Not meeting noise and emissions requirements
When the business jet is ready for delivery, different noise and emissions regulations will be put in place. Not complying with those regulations would reduce the effectiveness of the business jet because of operational limitations. The noise is produced by the airframe and the engines on the aircraft. The emissions are produced by the engines. Aircraft configuration will have an influence on drag and therefore the required thrust, but only slightly. The engine manufactures will be required to produce the engines that are possible to comply with latest regulations. The concept will need to be provided with state of the art engines for fuel efficiency reasons and this will help the emissions regulations.

High number of potential competitors
The fact that the long range business jets are a niche market makes two competitors already a lot. With the global 8000 already announced there is not much room left for more competitors. This puts more pressure on getting to market soon.

Changing economics
Changes in economics would influence the sales numbers of an ultra long range business jet. If due to negative changes in economics the sales go down, it forms a risk for the sale of the aircraft. Providing more advantages than only extended range over other business jets will help to negate this risk.

Lack of suitable engines
Though open rotor engines provide major environmental and fuel efficiency advantages, the noise and appearance hold back the development and implementation. The turbofans have a higher fuel consumption but produce less noise, therefore they have the preference of the industry and continue to be improved with every generation. If the concept requirements demand a minimum engine fuel efficiency that can not be met and there are no alternatives, than the range will be reduced.

Program financing
The development of a new aircraft is a risky investment, many investors will not be enthusiastic to spend money on an unproven design. If the predetermined budget is not superseded outside investments will not be required.

Rising fuel prices
Fuel prices are very likely to rise, but this influence can be felt in any mode of transportation working on fossil fuels. The reduced fuel consumption of the chosen concept mitigates the effect of increasing fuel prices.

Decreased demand for large business jets
With the globalisation of business and high profile business people that need to travel across the world, the concept will fulfil specific long range requirements. As mentioned before, other aspects can help to solidify the position of the concept as the best option on the market.

Low interest for new design
A radical design is likely to draw attention, but it can not be predicted how the aircraft will be perceived by the potential costumers. The appeal of the aircraft or lack of interest for a new configuration individually could be detrimental to the aircraft sales. Good managerial and sales skills, performance characteristics, sales price and operating cost have a high influence on the success of the aircraft.

Lack of reference designs
Conventional designs own the advantage of being mainly iterations of proven design and thus having a lot of reference material available providing good estimates and speeding up the development process. The new designs can hardly be based on previous designs and thus need more development time. This is a big drawback but still could be a carefully considered choice. Proper planning of the development and having contingencies appropriate for the specific configuration will prevent the development program from running stuck.

High production cost
In order to meet the high performance requirements it is necessary to use state of the art materials, sub-systems and designs. All these contribute to the high production cost. This is incorporated in the financial analysis and will be reflected in the final unit cost.

Certification difficulty
Unproven designs require more testing to guarantee safety. Changes to the original concept may be necessary to meet regulations, which will be detrimental to the performance of the aircraft that profiles it within the market. Designing the aircraft to be certifiable is as important as achieving the base requirements.

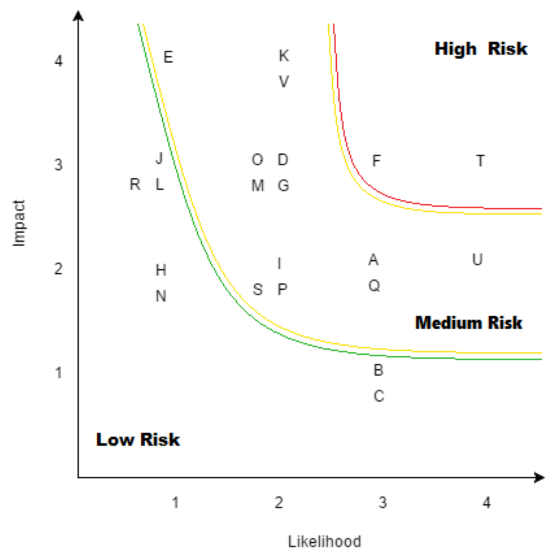

Figure 4.1: Riskmap

4.3 Risk Mitigation

To reduce threats to the aircraft, the most significant risks are to be mitigated by decreasing the likelihood and/or the impact of the risk. This applies to both risks which present threats to the Starling 9000 program and those which present opportunities. Risk mitigation is comprised of several different strategies, which are discussed in the sections below. As depicted in the risk map above, Fig. 4.1, prior to mitigation the chosen concept has several high risks. The handling and abatement of these risks are also discussed below.

4.3.1 Risk Management

Through risk mitigation, strategies are taken to reduce risk by either decreasing the likelihood or the impact of the risk. Several mitigation strategies exist that are used as handling methods when significant risks are experienced[1]:

1. **Risk Acceptance**
Risk acceptance does not reduce the risk, however may be applied when the cost of other risk mitigation strategies is larger than the cost of the risk itself. This strategy is mainly used for lower risks and not for high risks, as these risks cannot be accepted (ignored).

2. **Risk Avoidance**
The risk avoidance strategy is opposite to the risk acceptance as it strives to avoid any exposure to risk. Risk avoidance can be achieved by actions and schedule adjustments needed to avoid, hence reduce risk, and therefore improve performance of the project and its design as well[2]. Risk avoidance is usually the most expensive strategy.

3. **Risk Limitation**
Risk limitation strategy limits exposure by applying a combination of risk acceptance and risk avoidance. The distribution will depend on the risk in question. Risk limitation would for example be accepting that certain parts may fail (e.g. bolts or rivets) and avoiding would be to use safety factors in the number of parts to use.

4. **Risk Transference**
Risk transference is the reassigning accountability or responsibility of a certain risk to a another organisation or third party. Risk transference is usually used for risks that are not involved in specialised or core competency of the aircraft manufacturer. It may therefore also leave extra resources that can be used to focus on other areas of risk. Some disadvantages of risk transference however are that it results in dependencies and decrease in control over the risk.

4.3.2 High Risk Mitigation

According to the risk map in Fig. 4.1 there are two high risks at the moment. The risk of 'structural difficulty' and the risk of 'lack of reference designs.' The most suitable risk strategy regarding the risk of structural difficulty is 'Risk Limitation.' Due to the implementation of non-conventional elements to the design, such as the panoramic windows and winglet rudders, there will always be the risk of structural difficulty, due to the required structural reinforcements. The risk will be limited by optimisations in the configurations resulting in reduced forces and loads, therefore lowering the likelihood of the structural failure. One of the optimisations is the position of the window. Instead of locating it above the wing, an area of the fuselage with high loads, it will be moved to an area with lower loads. The design of the winglets include optimisations as well. A change in wing position is analysed regarding the moment arm of the rudder and the force acting on it, resulting in a change in required surface area of the winglet.

For the risk 'lack of reference designs' the mitigation strategy is 'Risk Limitation' as well. The risk can not be accepted or transferred due to the high level of the risk and the risk cannot be avoided due to the unconventional design choices and their lack of previous designs. The main consequence due to this risk is the increase of development time and the time needed for certification. To limit the risk proper planning of the development is needed and contingencies, such as safety margins and verification and validation of used methods, are used to account for uncertainties during the design.

[1] URL http://www.mha-it.com/2013/05/four-types-of-risk-mitigation/[cited 14 June 2016]
[2] URL https://www.mitre.org/publications/systems-engineering-guide/acquisition-systems-engineering/risk-management/risk-mitigation-planning-implementation-and-progress-monitoring[cited 14 June 2016]

Next to the high risks there are also medium risks. These risk do not need immediate mitigation, but should be monitored closely. At the moment the likelihood or the impact of the risks are relatively low. However, they could increase during development or operation, resulting in an unexpected high risk. If the risks are monitored and a change is noticed, mitigation strategies can be used before the risk become to high.

4.4 Sensitivity Analysis

The determination of the design sensitivities is necessary as the conceptual design methods are based on first-order and statistical estimates. The sensitivities allow contingencies to be build for the different parameters. The sensitivity of the take-off weight with respect to different parameters will be discussed in this section. This is done to find out which of the parameters will drive the design and how a change in these parameters will affect the take-off weight. Firstly the general analytical method of how to find the the sensitivity of take-off weight with respect to a general parameter is described in Section 4.4.1. After the general method is established the sensitivity of the take-off weight to range, endurance, speed, lift-to-drag and empty weight are found. Afterwards, the range sensitivity metric is found in Section 4.4.7. The sensitivities results are all summarised in Section 4.4.8.

It should be noted that the main requirement in this design exercise is not the MTOW but rather the mission range. The two are, however, intricately interrelated. Defining MTOW sensitivities is viewed as preferable because weight may readily be budgeted among different design teams. On the other hand, range is more intangible and not a direct property of the structural or other sub-system being designed. This makes it inconvenient to budget among sub-systems and design team. The effect of a change in MTOW on range may implicitly be determined given that the sensitivity of the MTOW to range is known.

4.4.1 Analytical MTOW Sensitivity Method

A general analytical method for computing the sensitivity of W_{TO} with respect to some parameter y can be obtained by partial differentiation of Equation (4.1) with respect to y [40].

$$log_{10}(W_{TO}) = A + Blog_{10}(CW_{TO} - D) \tag{4.1}$$

Since the regression constants A and B only vary with the type of aircraft, their partial derivatives are both zero. This therefore results into Equation (4.2) [40].

$$\frac{\partial W_{TO}}{\partial y} = \frac{B(W_{TO})^2 \cdot \partial C/\partial y - BW_{TO} \cdot \partial D/\partial y}{C(1-B)W_{TO} - D} \tag{4.2}$$

Parameter y can now be any of the previously mentioned parameters, such as range and endurance, speed, lift-to-drag and empty weight which will be treated in the following sections. If parameter y is not the payload, using equation for design parameter D, Equation (4.2) can be simplified to Equation (4.3) and the partial derivative of C can be found from its definition and is seen in Equation (4.4) [40].

$$\frac{\partial W_{TO}}{\partial y} = \frac{B(W_{TO})^2 \cdot \partial C/\partial y}{C(1-B)W_{TO} - D} \tag{4.3}$$

$$\frac{\partial C}{\partial y} = (1 + M_{res})\frac{\partial M_{ff}}{\partial y} \tag{4.4}$$

Where $\frac{\partial M_{ff}}{\partial y}$ is determined in the Preliminary Weight Estimates (Mid Term Review [2]) using Roskam and the factor F can be defined in Equation (4.6) [40].

$$\frac{\partial M_{ff}}{\partial y} = M_{ff}(W_i/W_{i+1})\frac{\partial W_{i+1}}{\partial W_i} \tag{4.5}$$

$$F = -\frac{B(W_{TO})^2 \cdot (1 + M_{res})M_{ff}}{C(1-B)W_{TO} - D} \tag{4.6}$$

Where the weight fraction is determined from the Breguet's equations. The Breguet equation are in two different forms, range and endurance and can be generalised for jet engines to Equation (4.7) and Equation (4.8). The difference between range and endurance depends on the weight ratio in the different phases.

$$\bar{R} = Rc_j(VL/D)^{-1} \tag{4.7}$$

$$\bar{E} = Ec_j(L/D)^{-1} \tag{4.8}$$

From Roskam [40] it follows that the sensitivity of W_{TO} with respect to a general parameter y can be written, for the case involving ratio W_i/W_{i+1} dependent on range, as in Equation (4.9), and, in case it is dependent on endurance, as in Equation (4.10)

$$\frac{\partial W_{TO}}{\partial y} = F\frac{\partial \bar{R}}{\partial y} \tag{4.9}$$

$$\frac{\partial W_{TO}}{\partial y} = F\frac{\partial \bar{E}}{\partial y} \tag{4.10}$$

Having determined the general sensitivity of W_{TO} with respect to any y expression, to find the sensitivity with respect to range and endurance, speed, lift-to-drag, specific fuel consumption and empty weight, their partials are found by changing y and differentiating Equation (4.7) and Equation (4.8) with respect to R, E, V, L/D, C_j or W_E. The required input data are gathered from the Preliminary Weight Estimates chapter (midterm review report) and the all the sensitivities are

4.4.2 Sensitivity to Range and Endurance

Differentiating Equation (4.7) (range) and Equation (4.8) (endurance) with respect to R and E for jet aircraft, Equation (4.11) and Equation (4.12) are found, respectively. The L/D for cruise is used in the range case, and the L/D for loiter is used in the endurance case (this is the case for all the upcoming sensitivities). The values from the preliminary weight estimation are used in the following equations.

$$\frac{\partial \bar{R}}{\partial R} = c_j(VL/D)^{-1} \tag{4.11}$$

$$\frac{\partial \bar{E}}{\partial E} = c_j(L/D)^{-1} \tag{4.12}$$

Substituting the solutions of Equation (4.11) and Equation (4.12) into Equations (4.9) and (4.10) respectively, the sensitivity of W_{TO} to range and to endurance can be found. These sensitivities stay constant with varying range or endurance.

4.4.3 Sensitivity to Speed

Differentiating Equation (4.7) (range) with respect to V for jet aircraft, Equation (4.13) is found. The endurance case is not used because it is independent of speed so the sensitivity to W_{TO} is zero.

$$\frac{\partial \bar{R}}{\partial V} = -Rc_j(V^2L/D)^{-1} \tag{4.13}$$

Substituting the solution of Equation (4.13) into Equation (4.9), the sensitivity of W_{TO} to velocity is found. From the relation it can been seen that the higher the velocity of the aircraft, the lower the sensitivity of W_{TO} will be to a change in velocity.

4.4.4 Sensitivity to Lift-to-Drag

Differentiating Equation (4.7) (range) and Equation (4.8) (endurance) with respect to L/D for jet aircraft, results into Equation (4.14) and Equation (4.15) respectifully.

$$\frac{\partial \bar{R}}{\partial (L/D)} = -Rc_j(V(L/D)^2)^{-1} \tag{4.14}$$

$$\frac{\partial \bar{E}}{\partial (L/D)} = -Ec_j(L/D)^{-2} \tag{4.15}$$

Substituting the solutions of Equation (4.14) and Equation (4.15) into Equation (4.9) and Equation (4.10) respectively, the sensitivity of W_{TO} to L/D for the range and endurance cases are is determined. From this, as well as from literature, it can be seen that for a range dominated aircraft a change in L/D has a major affect on the W_{TO} [40]. As can be seen from the relation, the higher the L/D the less the sensitivity of W_{TO} with respect to L/D will change.

4.4.5 Sensitivity to Specific Fuel Consumption

Differentiating Equation (4.7) (range) and Equation (4.8) (endurance) with respect to c_j for jet aircraft, results into Equation (4.16) and Equation (4.16), respectively.

$$\frac{\partial \bar{R}}{\partial R} = R(VL/D)^{-1} \tag{4.16}$$

$$\frac{\partial \bar{E}}{\partial E} = E(L/D)^{-1} \tag{4.17}$$

Substituting the solutions of Equation (4.16) and Equation (4.17) into Equation (4.9) and Equation (4.10) respectively, the sensitivity of W_{TO} to c_j for the range and endurance case are found. From results which will be mentioned at the end of this section it might seem that W_{TO} is extremely sensitive to a change in C_j, however C_j is in the order of 10^{-5}, meaning that changing the fuel consumption by 1 unit will be unrealistically high regarding typical fuel consumption values, causing the W_{TO} to increase drastically as well. A feasible change in fuel consumption is insignificant with respect to the W_{TO} sensitivity. Therefore the sensitivity remains constant with varying C_j.

4.4.6 Sensitivity to Empty Weight

Equation (4.1) can be rearranged for the W_{TO}, as can be seen in Equation (4.18).

$$log_{10} W_{TO} = A + B log_{10} W_E \tag{4.18}$$

Taking the the partial derivative of W_{TO} with respect to W_E in Equation (4.18), the sensitivity can be expressed as shown in Equation (4.19) [40].

$$\frac{\partial W_{TO}}{\partial W_E} = \frac{B W_{TO}}{invlog_{10}\big((log_{10} W_{TO} - A)/B\big)} \tag{4.19}$$

Using the values for A, B and W_{TO} , the sensitivity $\frac{\partial W_{TO}}{\partial W_E}$ can be determined. The sensitivities remains constant with varying W_E.

4.4.7 Range Sensitivity Metric

For the trade-off procedure a qualitative metric to evaluate risk of the range decreasing below requirements is desired. This metric is intended to evaluate how severely and adverse event (weight increase, performance decrease) in the design process will affect the aircraft's range. The Chain rule of calculus may be suited to determine the sensitivity of range to a change in parameter 'y':

$$\frac{\partial R}{\partial y} = \left(\frac{\partial R}{\partial W_{TO}}\right) \cdot \left(\frac{\partial W_{TO}}{\partial y}\right) \tag{4.20}$$

The range risk metric to be used is the total derivative of the range i.e. the gradient with respect to the following vector of variables 'Y' (endurance, speed, $(L/D)_{cruise}$, SFC, empty weight). This metric is normalised such that it represents the effect of each 'y' variable changing by 1%. Additionally, to represent an adverse design change, all contributions are negative. The final range risk metric is given by Equation (4.21):

$$-\vec{Y} \cdot \left|\nabla_{\vec{Y}} R\right| \cdot 1\% = -\sum_{i=0}^{i<5} y_i \cdot \left|\frac{\partial R}{\partial y_i}\right| \cdot 1\% \tag{4.21}$$

The units of the metric are $[nm/1\%]$ or in words: the number of nautical miles the range is decreased for a 1% change in all design parameters (a negative value is expected). This method incorporates the endurance phase of the mission (the fuel for endurance translates into weight which has to be carried through the cruise phase) into the range risk . For this reason it is an improvement on the Roskam method presented throughout Section 4.4 which treats endurance and range entirely separately. Thus, the values in the 'Y' vector for Equation (4.21) all correspond to the range case except for the endurance value which corresponds to the endurance case.

4.4.8 Sensitivity Summary for Concepts

Using the input data of the aircraft together with the values of A,B, C and D from the midterm review report, the sensitivities of the different parameters can be found and are summarised in Table 4.3.

Table 4.3: Sensitivities for the range case of the parameters for the aircraft (inputs given in italic)

Parameter	**Concept 2**
V	*221.3*
SFC	$12.8 \cdot 10^{-6}$
L/D (cruise)	*18.69*
L/D (loiter)	*21.58*
M_{ff}	*0.5783*
M_{res}	*0.055*
W_{TO}	*63600 kg*
Sensitivity to Range [kg/m]	$\frac{\partial W_{TO}}{\partial R} = 0.0047$
Sensitivity to Endurance [kg/s]	$\frac{\partial W_{TO}}{\partial E}$ =0.8983
Sensitivity to Speed [kg/m/s]	$\frac{\partial W_{TO}}{\partial V}$ = -333.38
Sensitivity to Lift-to-Drag [kg]	$\frac{\partial W_{TO}}{\partial L/D}$ = -3947
Sensitivity to SFC [kg· Ns]	$\frac{\partial W_{TO}}{\partial c_j}$ = 5.76E9
Sensitivity to Empty Weight [kg/kg]	$\frac{\partial W_{TO}}{\partial W_E}$ = 1.9074
Range Sensitivity Metric [nm/l %]	$-\vec{Y} \cdot \left|\nabla_{\vec{Y}} R\right| \cdot 1\%$ = -204.94

4.5 RAMS Assessment

In the design of critical combinations and complex integrations of large engineering systems, their engineering integrity needs to be determined [52]. Engineering integrity consists of reliability, availability, maintainability and safety (RAMS) of the system functions and their related equipment. The following section will present a brief description of each of these design criteria.

4.5.1 Reliability

Reliability can be seen as the probability of successful operation of the system with minimum risk of loss or disaster of system failure for a stated time interval. This does not mean that redundant parts may not fail. Such parts can fail and be repaired without operational interruption at system level [8]. This can be generally analysed by evaluation of the most critical component of the aircraft. This could include creep lifetime and bending fatigue performance analysis. This will give a good approximation of the aircraft reliability. Generally, a numerical statement of reliability is used (e.g. R = 0.9) which range from 0 to 1. A survey [3] conducted on 2000 business jets in the US showed that the reliability of these jets was 0.9. The survey especially focused on the average maintenance dispatch reliability which will be presented in Section 4.5.3.

4.5.2 Availability

Availability of the system is directly related to the logistics. It is generally expressed by the ratio of delivered to expected service. Higher availability means the customer can expect to receive the aircraft quicker from the manufacturer and/or maintenance department. Designing for availability requires an evaluation of the consequences of unsuccessful operation, and the critical requirements necessary to restore the operation to design expectations [52]. Another important aspect is reducing the amount of involved suppliers. This would primarily decrease the risk of supply delays and hence, increase the availability. Evaluation of this kind

[3]URL https://www.conklindd.com/t-measuringreliabilityandavailability.aspx[cited 20 May 2016]

is often difficult, as logistic support and human factors should be considered in addition to reliability and maintainability. For a given system, the average availability (AA) is given by [8]:

$$AA = \frac{MTTF}{(MTTF + MTTR)} \tag{4.22}$$

where:
MTTF is mean time to failure
MTTR is mean time to repair

4.5.3 Maintainability

Maintainability is the aspect of maintenance that takes downtime of the aircraft into account. Designing for this criteria requires analysis of the accessibility and 'repairability' of the aircraft and its sub-systems. Maintenance is divided into 'preventive maintenance', carried out at predetermined intervals to reduce wear out failures, and 'corrective maintenance', carried out after failure detection [8]. Aim of preventive maintenance is also to detect hidden failure which is the failure of redundant systems. Hence, maintainability is a characteristic of the system, which is expressed as a probability that a preventive maintenance will be carried out within a stated time interval. The overview for the preventive maintenance cycle has been shown in Fig. 4.2. Maintainability has to be incorporated into the system during the design and development phase by realising a maintenance concept. The same survey mentioned in Section 4.5.1 indicated the maintenance dispatch reliability of 99.6 %. To achieve this, the operators reported that each aircraft spent an average of 25.2 days per year down for maintenance. This equates to 5.75 days per 100 flight hours.

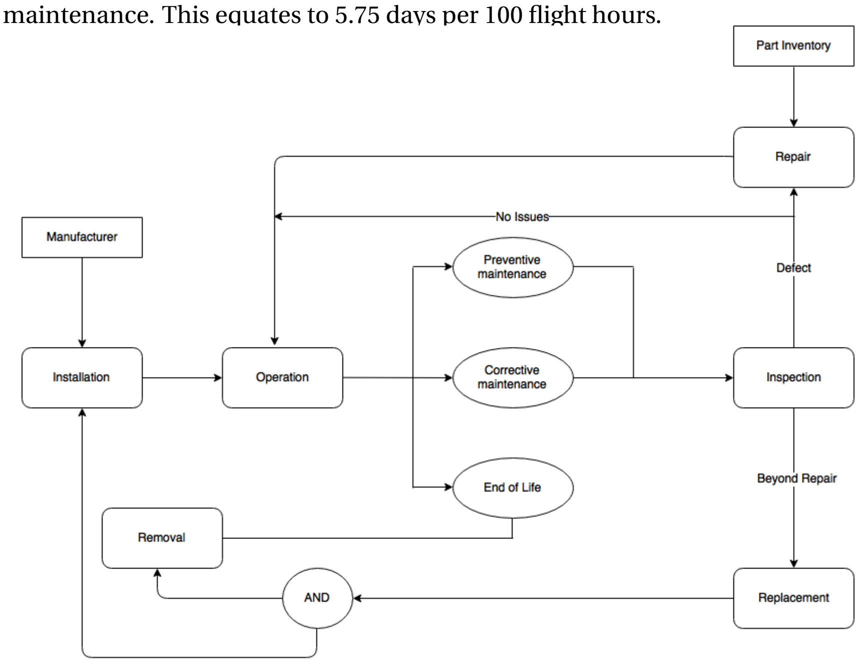

Figure 4.2: Maintenance cycle of the business jet

4.5.4 Safety

Safety is the condition in which the system will not cause injury to the any person, nor significant material damage or other unacceptable consequences during its use [8]. Safety is generally evaluated considering two scenarios: Safety when the system functions and is operated correctly and safety when the system, or a part of it, has failed. The first part is concerned with accident prevention while the second is that of technical safety. A distinction between technical safety and reliability is necessary. While safety assurance examines measures which allow the item to be brought into a safe state in the case of failure (fail-safe behaviour), reliability assurance deals with measures for minimising the total number of failures [8]. Also, for technical safety, external environmental factors like human errors, catastrophes, sabotage, etc. carry great significance. However, increasing in safety can reduce reliability.

5. Aircraft Systems & Functions

Any aircraft is a complex design consisting of many different subsystems. This chapter identifies the functions of a business jet and presents subsystem designs, including for example the cabin interior and landing gear.

5.1 Functional Breakdown

The different functions of the Starling 9000 business jet are shown in Fig. 5.1. Fig. 5.2 shows the functional flow diagram of a normal operation cycle.

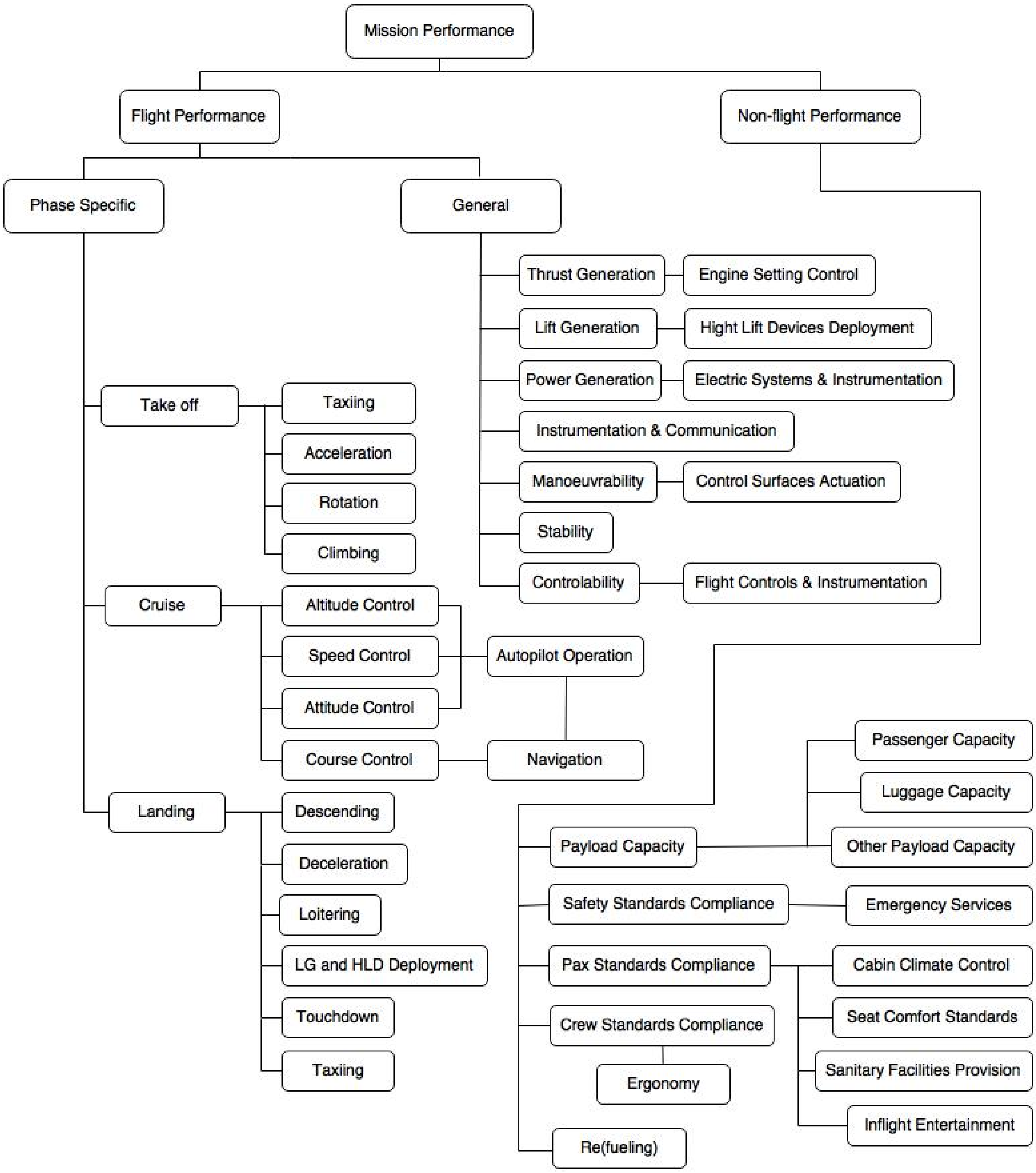

Figure 5.1: Functional breakdown structure

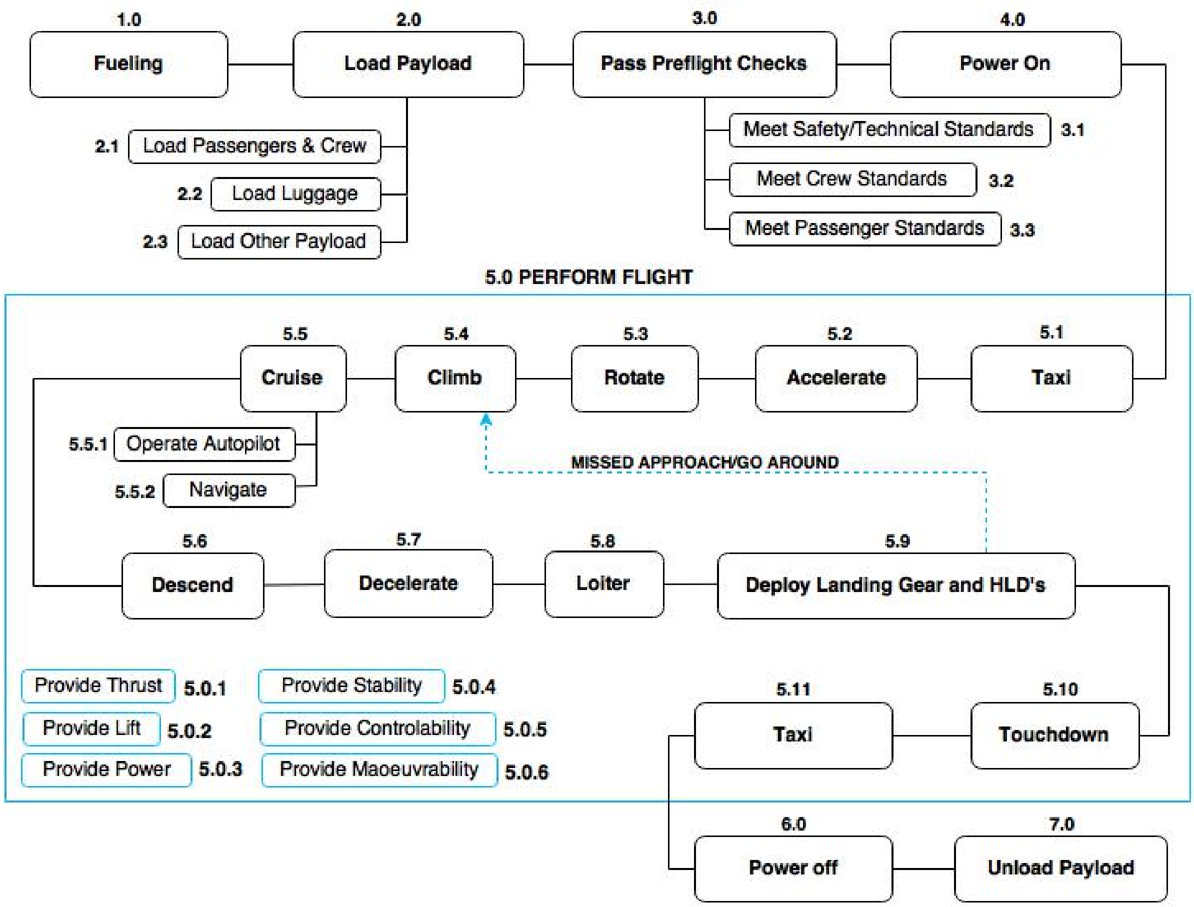

Figure 5.2: Functional flow diagram

5.2 Interior Configuration

The Starling 9000's interior design will be a symbol of sustainable luxury. Besides sustainability, cabin makes the stakeholder value the top priority during the design process. The two primary requirements that apply to cabin are URBJ-OPR-BCL-01 that requires the cabin to have a standard business class interior and URBJ-OPR-RNG-01, that constrains the cabin to hold 18 passengers. This section discusses and illustrates the cabin configuration, the rationale behind the choices and the sustainability that plays a big part on what the Starling 9000 makes use of for the interior design.

Starling 9000 strives to set a benchmark for sustainability when it comes to interior design and material choice. Today, with the enrichment of people's awareness on environmental problems and the demand of environmentally friendly fabric, natural fibres have received a great deal of attention [55]. The Starling 9000 makes use of environmentally friendly composites with a customisable blend of natural fibres [1] (e.g. hemp).The main reason to use natural fibre is because they are carbon neutral: they absorb the same amount of carbon dioxide they produce. Importantly, at the end of their life cycle, they are 100% biodegradable. In Starling 9000, they will provide important applications such as interior wall panels, hard panels for the seats, furnishings and several other trim options.

[1] http://www.naturalfibersforautomotive.com/[cited June 16 2016]

Figure 5.3: Starling 9000 business jet floor plan as per the requirement

As can be seen from Fig. 5.3, the cabin layout is designed to hold 18 passengers as per the requirement. It is divided into multiple sections which gives large freedom for customisation and tailoring the cabin to any configuration. For example, compartment B, which is in a conference configuration supporting multimedia amenities, could be easily modified into a dining area if there is the need. This makes the layout very adaptable which is always desirable to all kinds of operators and private owners. It can also be observed that the layout includes aft-facing seats. This feature is approved within the Cabin Safety section of the FAA regulations [2]. This configuration allows for more social setting in the cabin along with more safety to the passenger [51]. This is due to the fact that the passengers have more surface area in contact and support for the neck and head during an impact. Figs. 5.4 to 5.7 show more comprehensive overviews of the cabin *(some cabin walls have been removed for clarity)*.

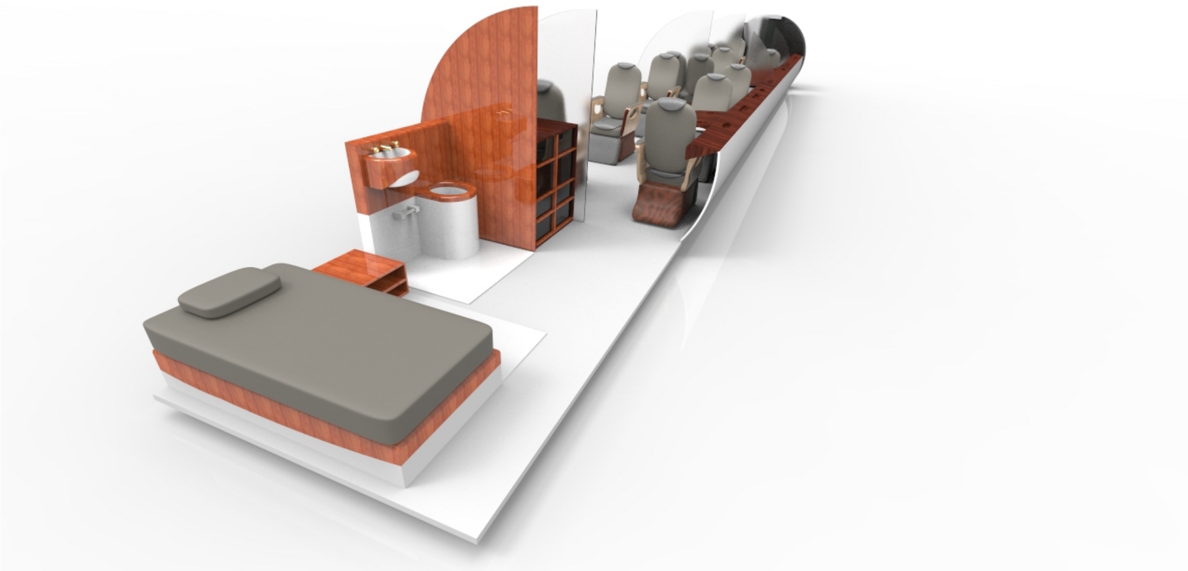

Figure 5.4: Starling 9000 business jet cabin configuration as seen from the front

[2] http://fsims.faa.gov/WDocs/8900.1/V03%20Tech%20Admin/Chapter%2033/03_033_006.htm[cited June 21 2016]

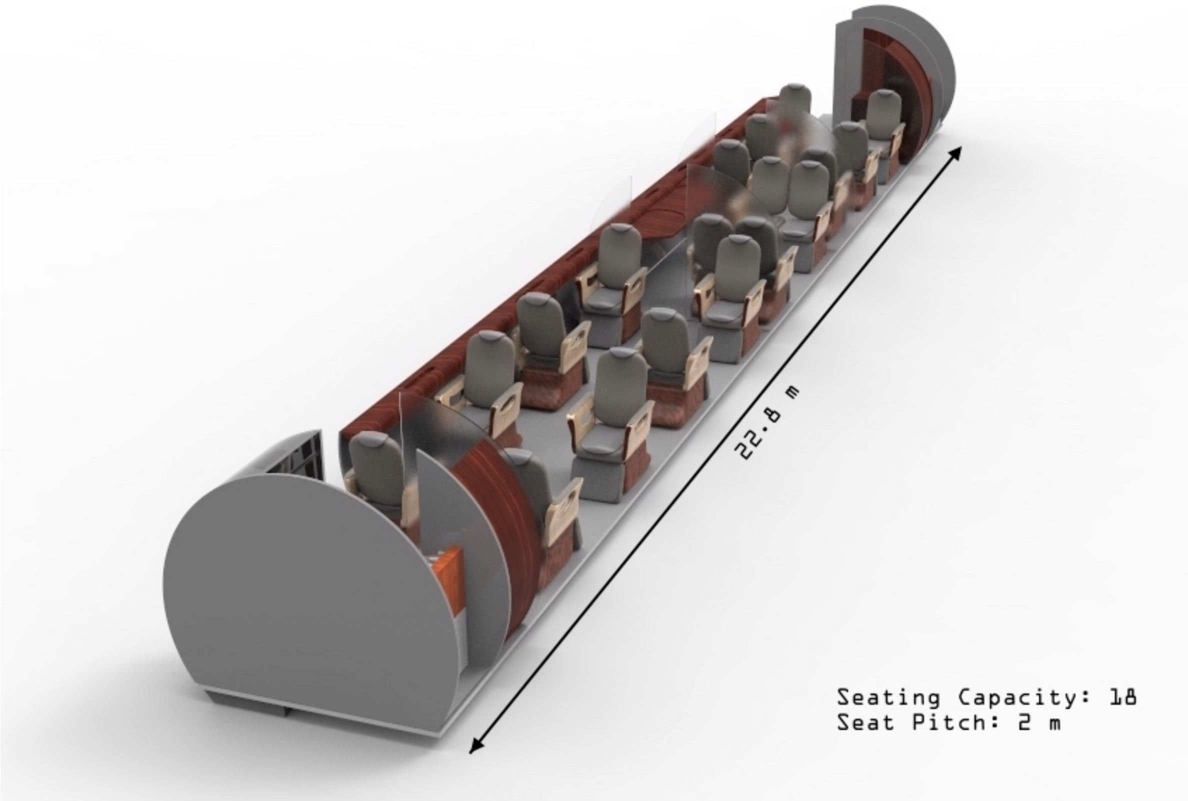

Figure 5.5: Starling 9000 business jet cabin with 18 seat configuration as seen from the rear

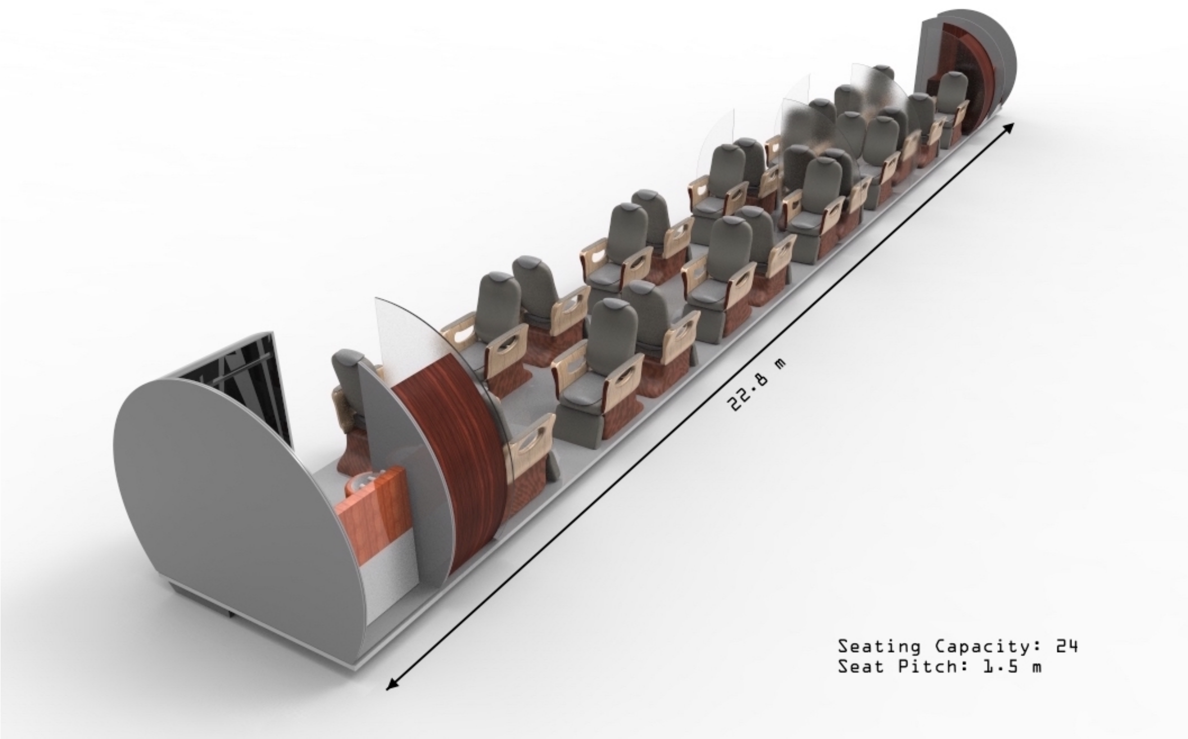

Figure 5.6: Starling 9000 business jet cabin with 24 seat configuration as seen from the rear

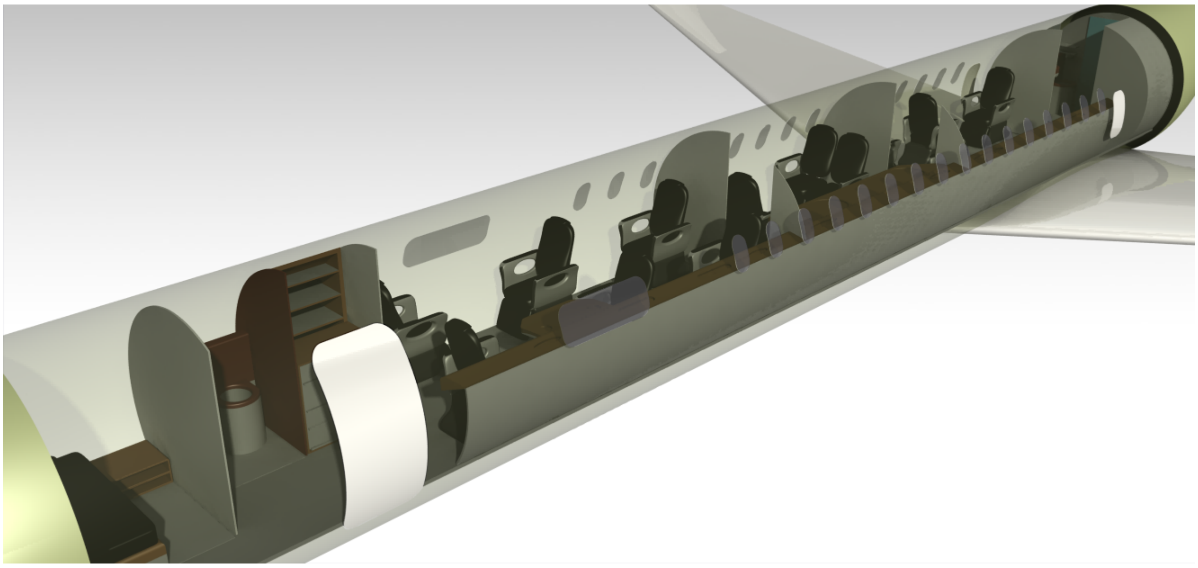

Figure 5.7: Starling 9000 business jet fuselage-cabin interaction

Currently, there are no regulations for decommissioning aircraft in safe and environmentally responsible conditions and the existing End of Life vehicles (ELV) are not aircraft specific. Nevertheless, the Starling 9000 interior aims to comply with the European Directive 2000/53 [3], stating that 85-95% of the components will be recycled, reused or recovered. Using ustainable materials like natural fibres will greatly help towards reaching that figure.

5.3 Detailed Systems Layout

The following sections will discuss about different systems of the aircraft.

5.3.1 Fuel System

The fuel system helps the crew to pump fuel to the propulsion system and the APU. To enable the crew to manage the complex fuel system with multiple tanks and engines requires each wing to have its own electric boost pump, and each engine to have its own mechanical pump. Being able to operate all of these separately allows the crew to feed fuel to the engine from the opposite side of the respective engine, cross-feed, in case of single-engine operation. Furthermore, to balance the asymmetric weight, flow valves and pumps are used to feed both engines from one tank and also to transfer fuel between tanks. Finally, to avoid water condensation or the fuel to solidify at low temperatures of cruising altitude, fuel tanks have thermometers and heating systems installed into them. These all have been illustrated in Fig. 5.8.
The volume of the fuel tanks, determined from the CATIA model, is equal to 38.8 m^3. This volume is reduced by 4% due to the volume taken by the structure and systems and another 5% needs to be left empty to account for fuel expansion [53]. The resulting volume of the fuel tanks is equal to 35.3 m^3. The required fuel volume is determined from the fuel weight, which is equal to 23300 kg. Using Jet A1 fuel, with a density[4] of 0.81 kg/m^3, results in a required volume equal to 29 m^3. This allows to reduce the centre wing tank size. Also, it can be moved away from the bottom side of the fuselage to avoid the risk of rupture of the fuel tank in case of belly landing scenario. It can be concluded that there is enough fuel volume available in the wing and that there is even space available for other systems, such as landing gear or high lift devices.

5.3.2 De-icing and Anti-icing

The Starling 9000 de-icing design is equipped with ice detection system and is triggered automatically once the ice is detected. First, an electro-thermal strip heats the wing's leading edge to just above freezing, melting the ice. This system heats the leading edge enough to evaporate moisture on contact, preventing it from escaping and refreezing elsewhere as runback ice.

[3] http://ec.europa.eu/environment/life/project/Projects/index.cfm?fuseaction=home.showFile&rep=file&fil=ACADEMY_PAMELA.pdf [cited June 16 2016]
[4] URL http://www.experimentalaircraft.info/homebuilt-aircraft/aviation-fuel-jet.php [cited June 17 2016]

The deicing component of the system includes two sets of elliptical-shaped coils of which one set is at the aerofoil's upper portion and one at the lower. The coils are installed behind the heated strip, between the aircraft skin and a rigid housing which forms the Electro-Mechanical Expulsion Deicing Systems (EMEDS) actuator [5]. An electrical current is sent through one set of coils at a time, and as the current loops through the coil, it flows in one direction and then the opposite, inducing a magnetic field. The upper and lower portions of the coil then repel, changing the coil from an elliptical shape to a more circular one. The shape change, in turn, causes the coil to flex the aircraft skin and break the ice's grip. Jolted with electrical energy pulses that last .0005 second, the coils deliver impact accelerations of over 10,000 Gs to the aerofoil skin once a minute, shedding ice as thin as 0.2 cm [61]. Despite the high G-load, the impact amplitude, the amount of movement of the aircraft skin, is only about 0.6 mm and metal fatigue is not a problem [61]. The system has been shown in Fig. 5.8.

5.3.3 Hydraulic System Lay-out

Hydraulic systems are used on aircraft to move and actuate landing gear, flaps and brakes along with other flight control surfaces. To achieve the necessary redundancy and reliability, the system may consist of several subsystems [6]. Each subsystem has a power generating device (pump) reservoir, accumulator, heat exchanger, filtering system, etc. They combine the advantages of light weight, ease of installation and inspection, and minimum maintenance requirements. Hydraulic operations are also very efficient, with only negligible loss due to fluid friction. Some of the major hydraulic actuator layout is shown below in Fig. 5.8.

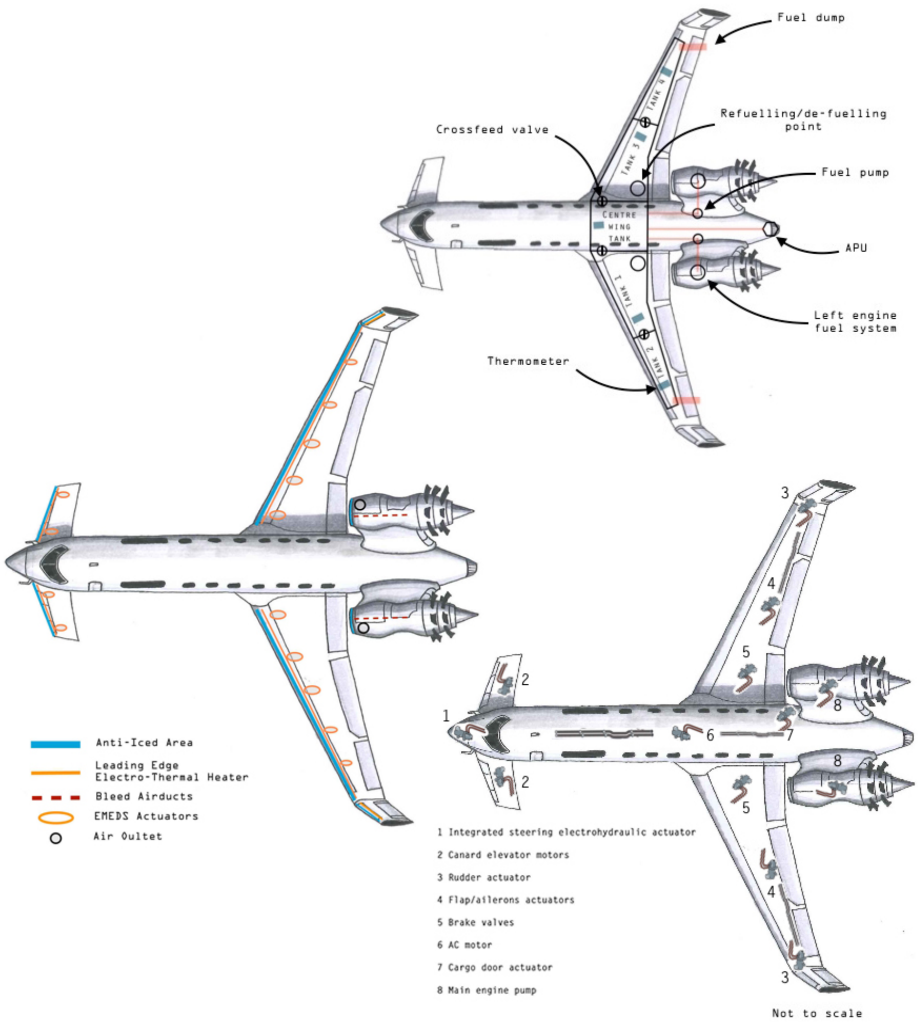

Figure 5.8: Fuel system, de-icing system and hydraulic system

[5] http://www.coxandco.com/files/pdf/AIAA-2007-0692.pdf [cited June 24 2016]

[6] http://www.faa.gov/regulations_policies/handbooks_manuals/aircraft/amt_airframe_handbook/media/ama_ch12.pdf [cited June 10 2016]

5.3.4 Environment Control

At a cruising altitude of 40,000 feet, the outside air temperature is between –50 and –60 degree Celcius and the pressure is 0.3 atm to 0.2 atm. These conditions are much too low for passenger safety and comfort, and must be raised inside the cabin to a comfortable level [7]. Hot high-pressure air bled from the engine is cooled by ram air in a heat exchanger which reduces the pressure. A compressor is required to again pressurize the air to reach the desirable pressure but at a high temperature. The hot air is cooled again in the main heat exchanger to the required temperature and a suitable pressure. Finally, the cool air mixes with the filtered return air from the cabin to deliver a comfortable aircraft climate. The environmental control system (ECS) then distributes air from the mixing manifold to the cabin to remove heat in cabin air produced by passengers, crew and equipment, and to maintain a pressure in the cabin similar to that at around 6,000 feet above sea level [7]. Fig. 5.9 illustrates this when the aircraft is on the ground and the air-conditioning cart (GAC) system feeds outside air into the aircraft.

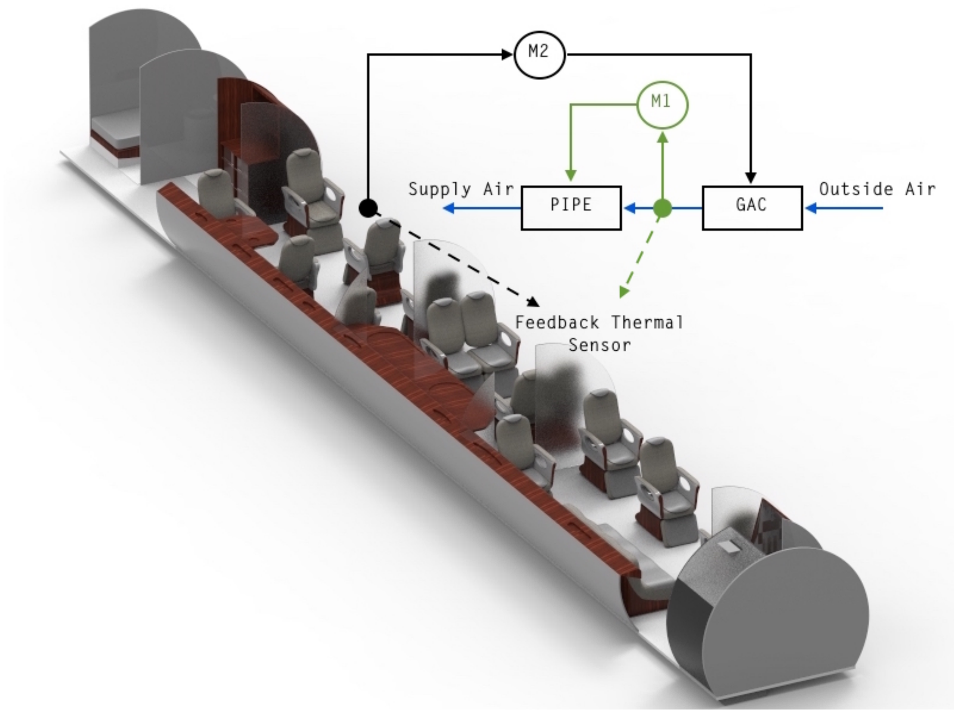

Figure 5.9: Process diagram of airflow from the external environment into the cabin through the Ground Air Conditioning system. M1 and M2 represent the locations of two different temperature controllers

5.4 Electrical Block Diagram

The electrical block diagram, Fig. 5.10, presents the current path from the source to various appliances. In this analysis three different sources have been considered. AC generators consist of two power generators connected to the engines and an additional one connected to the APU. From a ground source, either AC or DC current can be obtained through the external power connection. The two DC generators represent the aircraft's batteries. DC current can be also obtained from the main AC bus via a transformer rectifier unit, and can be further classified into 28V DC and 115V DC.

5.5 Data Handling Block Diagram

Fig. 5.11 illustrates the data handling of the aircraft by showing what and how data flows through the system. At the core of the of the data handling process lies the "Digital Flight Data Acquisition Unit" (DFDAU) that acts as the processor of the aircraft, through which all the data that is gathered from the different subsystems and components enters. The data that is gathered by the DFDAU is then continuously fed to the black box or "Digital Flight Data Recorded" (DFDR) Which records all the flight data in a continuous loop where it can

[7] http://www.ansys.com/About-ANSYS/Advantage-Magazine/Volume-X-Issue-1-2016/climate-control-gets-elevated [cited June 10 2016]

store up to 25 hours of data. Apart from the DFDR, the control panel, accelerometer, "Flight Data Entry Panel" (FDEP), printer and engine control are also connected to the DFDAU.

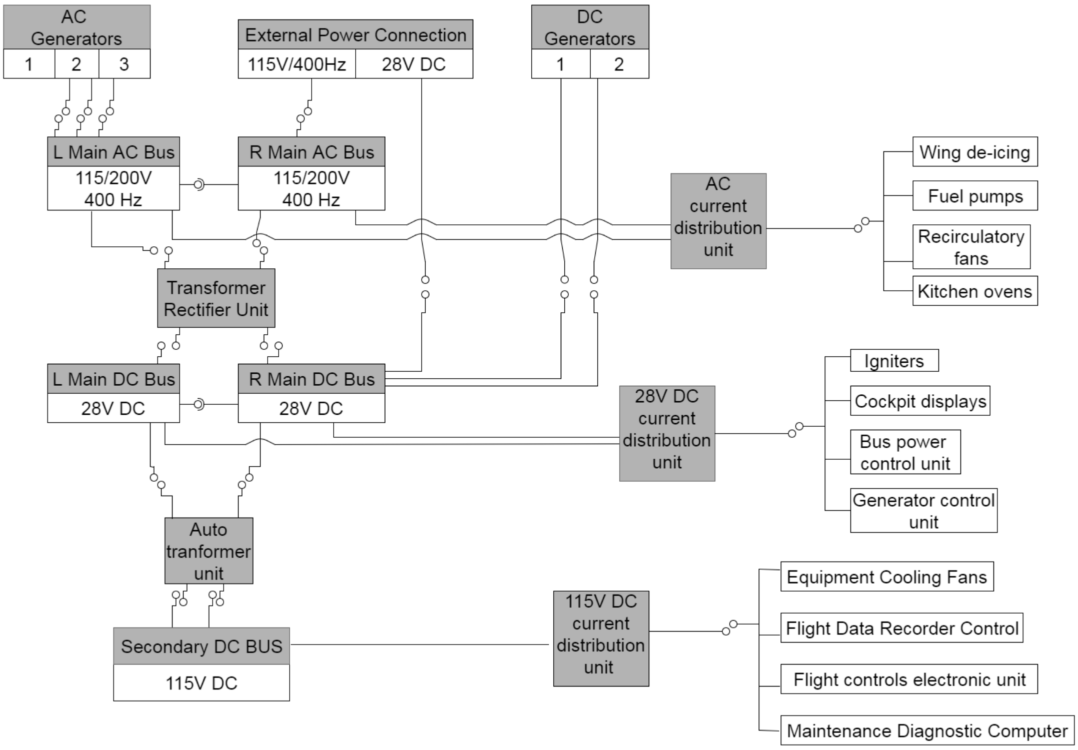

Figure 5.10: Electrical block diagram

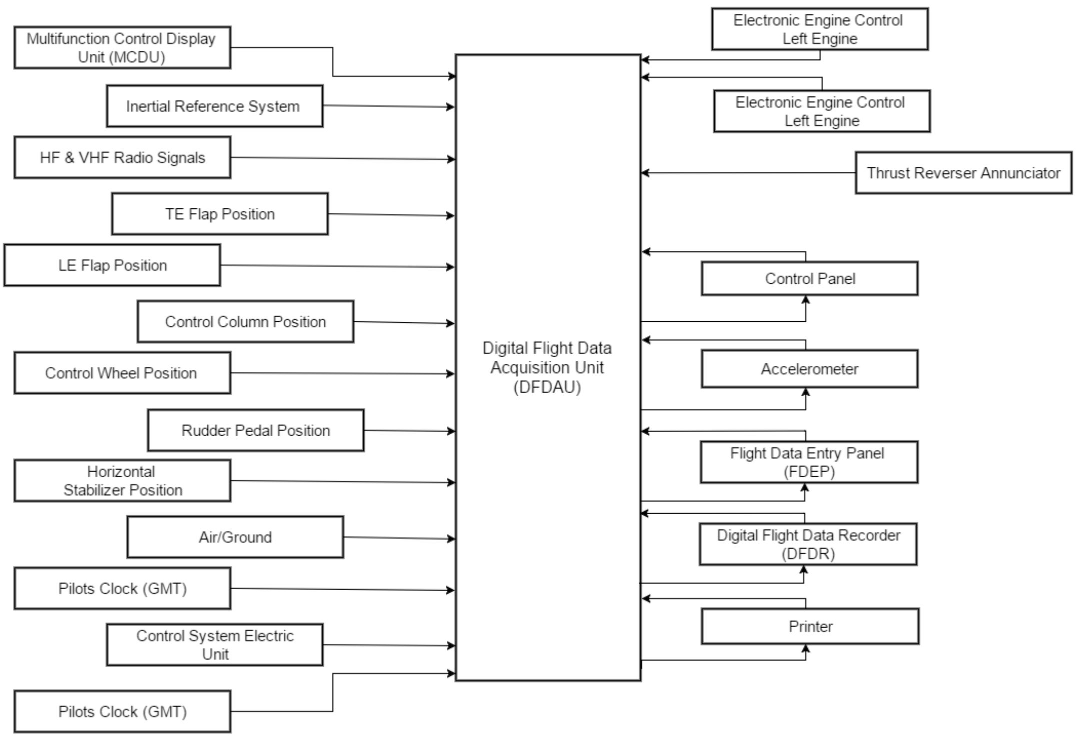

Figure 5.11: Data handling block diagram

5.6 H/W, S/W Block Diagrams

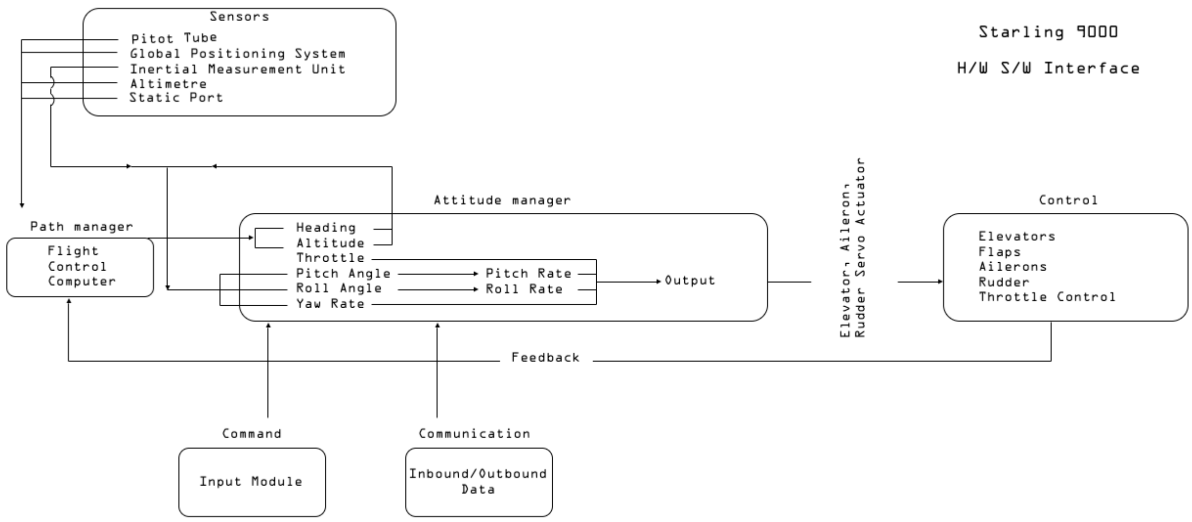

Figure 5.12: Hardware software block diagram

5.7 Landing Gear

This section covers the landing gear configuration, sizing, tire selection and relevant subsystems of the landing gear. The main subsystems that will be discussed are the retraction mechanism, shock absorber and brakes.

5.7.1 Landing gear Configuration

Previously it was determined that based on the DOT feasibility reasoning and the cruise speed requirement (URBJ-MCH-01) of the aircraft, it is obvious that the only possible choice is to opt for a retractable gear to avoid the unacceptably high drag penalty [2].
It was also found that for the configuration selection the most viable option for almost all business jet aircraft is the conventional (tricycle) configuration. This is mainly based on the considerations made on the ease of ground manoeuvring, ground looping behaviour and the cabin level [2].

The identified geometric criteria which need to be considered in deciding the disposition of the landing gear struts are:

1. Tip-over criteria
2. Ground clearance

1. Tip-over Criteria: This criteria is further divided into longitudinal and lateral criteria [41].

- Longitudinal Tip-over criterion: The main landing gear must be behind the aft centre of gravity location. Fig. 5.13 shows the angle relation (15°) between the aft c.g. and the main gear.
- Lateral Tip-over criterion: The lateral tip-over is dictated by the tip-over angle ψ in Fig. 5.13 which is generally limited by 55 °.

2. Ground Clearance Criteria Fig. 5.14[41] summarises the relevant angles required for both the lateral and longitudinal ground clearance criteria. It can be seen that for longitudinal criterion, the angle θ should be larger than 15° which is the approximate rotation angle (θ_{LOF}). For the lateral criterion, it can be seen that the clearance angle ϕ, which is the angle between the ground and the engine, measured from the main landing gear, should be greater than 5°.

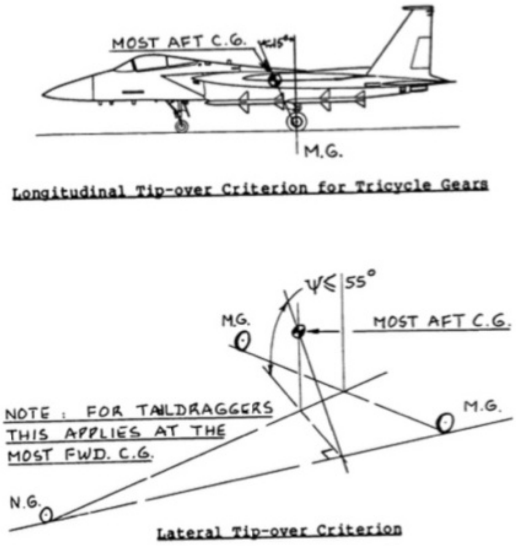

Figure 5.13: Lateral and longitudinal tip-over criterion for conventional configuration

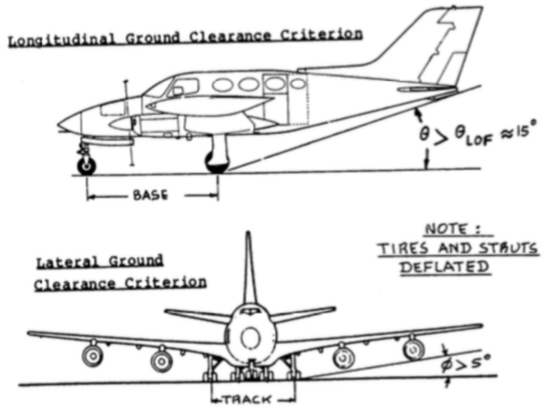

Figure 5.14: Lateral and longitudinal ground clearance criterion for conventional configuration

It was determined that for the chosen design the main landing gear will be retracted inside the fuselage (fairing) and wing due to its potential large size (similiar to most business jets), and from the Mid-term review [2] it was determined that the centre of gravity is placed between minimum 19.7m and maximum 22.7m from the nose. The main landing gear is placed at 26.6 m (must be behind the c.g.), because assuming a 1.8 m ground clearance to the c.g. location, ensures the 15 °longitudinal tip-over criteria is met. The nose landing gear is placed at 3.7 m from the nose [2]. Secondly the position of the main landing gear with respect to the main central axis needs to be determined, as can be seen in Fig. 5.15.

Setting the main landing gear height to 1.3 meter (wheel and strut) from ground to hinge point, the lateral position, L, on the wing can be determined as shown in Fig. 5.15. To comply with the lateral tip-over criteria (ψ< 55°), it can be determined from the geometry of the aircraft in Fig. 5.13 and the positions of the landing gears that the distance from the centre line to the landing gear should be at least 1.81 m. This is slightly more than the radius of the fuselage of 1.6 m. Since the landing gear height is set at 1.3 m, this space needs to be accounted for inside the wing and fuselage as well. Therefore the landing gear is desired to be placed as close to the root as possible since the most available space inside the wing is located here. The wheel will take up the most horizontal space when looking at Fig. 5.15, therefore it will be placed closest at the root, making the landing gear fold inward after take-off. The folded location of the main landing gear is therefore the minimum location required of 1.81m and a margin of 20 cm (about 10% of the necessary length) to account for landing gear retraction systems. Therefore the lateral position of the main landing gear connection to the wing will be positioned at L=2.0 m, from the center line (Fig. 5.15).

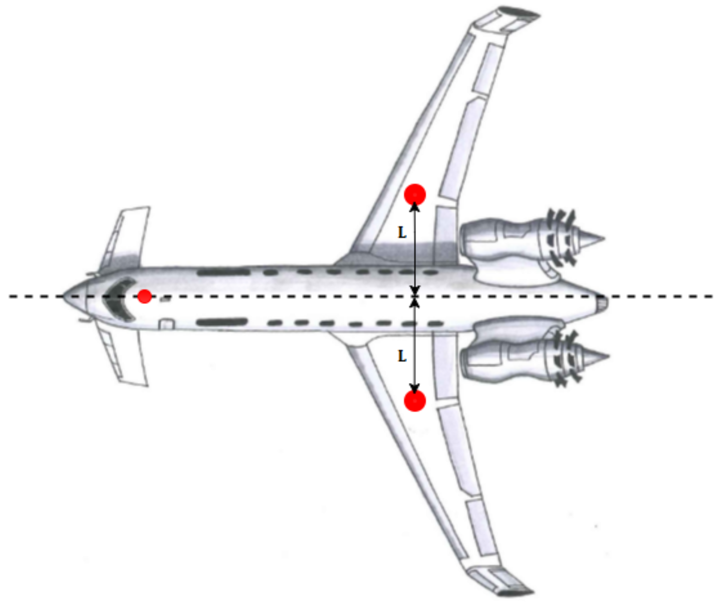

Figure 5.15: Schematic illustration of lateral position of the main landing gears

5.7.2 Landing gear sizing

The static loads of the landing gears struts can be determined from Fig. 5.16 [41]. From this, Equation (5.1) and Equation (5.2) are found and can be used to determine the static load per strut.

$$P_n = \frac{W_{TO} \cdot l_m}{l_m + l_n} \tag{5.1}$$

$$P_m = \frac{W_{TO} \cdot l_n}{n_s \cdot (l_m + l_n)} \tag{5.2}$$

Where l_m is the distance from the minimum c.g. to the main gear, l_n is the distance from the maximum c.g. to the nose gear and n_s is the number of main landing gear. From [2] l_m and l_n were found to be 3.9 m and 15.99 m respectively, n_s is equal to 2 and W_{TO} is 52967.6 kg. Therefore using Equation (5.1) and Equation (5.2) , P_n and P_m are found to be 101,885 N and 208,864 N respectively.

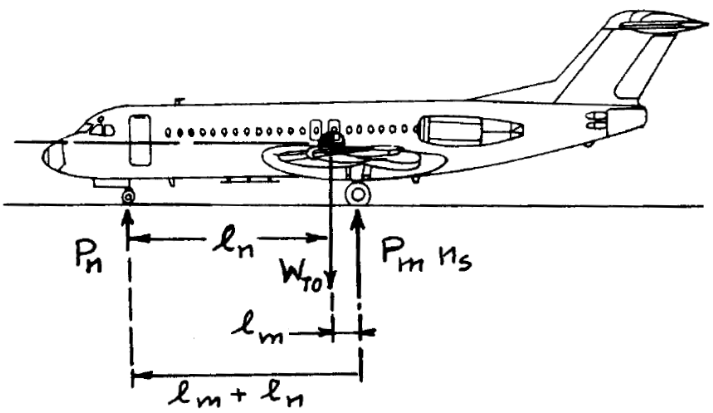

Figure 5.16: Geometry for static load calculation for tricycle landing gears

5.7.3 Landing Gear Tires

After the static load is computed, the number of tires to be used is decided, which are influenced by several aspects. The load per tire and the associated bearing strength are the main aspects that determine the

number of tires. Also a safety margin should be taken into account in case of a tire blow-out.
Using the typical landing gear data for aircraft with comparable W_{TO}, both the number of tires and tire size can be decided [41]. For a take-off weight of approximately 50,000 kg, dual wheel attachment is the most suited for business jets and approximation based on Roskam [41] for the tires sizes and pressures are outlined in Table 5.1. These estimated parameters are used as a reference when selecting the specific tires for the aircraft, with a focus on whether the indicated pressure is met. For tire selection pressures are frequently expressed by the "ply rating system", which are also indicated in the Table 5.1.

Table 5.1: Number of wheel and tire estimates sizes for typical nose and main gears

	Nose	Main
Number	2	2X2
Size [cmXcm]	60X20	101X35
Pressure [bar]	7.5	11.7
Ply rating [-]	14	20

Table 5.2: The parameters of the tires for the nose and main landing gear

	Nose	Main
Part number	266F43-2	382K03-3
Size [cmXcm]	66X17	97X31
Ply rating [-]	14 0	20
Maximum airspeed [m/s]	93.9	93.9
Weight [kg] [a]	14.1	39.5
Cost per tire [USD] [b]	1282.58	2743.50

[a] URL http://www.aircraftspruce.eu/ [cited May 31 2016]
[b] URL http://www.aircraftspruce.eu/ [cited May 31 2016]

The current most widely used landing gear tire in business jets is the Flight Eagle tire by Goodyear Tire [8]. Many sizes and corresponding pressures exist for this tire and therefore the appropriate size and corresponding pressure need to be selected for the nose and main landing gear.
To meet the specified pressures, the selected landing gear tires are the Flight Eagle 382K03-3 for the main landing gear that are used on the Bombardier Global 5000, 6000 and Express. For the nose landing gear the Flight Eagle 266F43-2 will be used, which is also used on the Dassault Falcon 20, 200 and 50. The properties are summarised in Table 5.2. The total tire weight and cost are therefore 93,1 kg and 6770 USD respectively.

5.7.4 Landing Gear Retraction

As was mentioned previously, the landing gear is retracted from the wing in lateral direction into the fuselage and wing as this is the most common jet retraction mechanism. The retraction mechanism is illustrated in Fig. 5.17 [9].
The retraction system components and main landing gear are arranged similarly to the illustration shown at the end of this section in Fig. 5.21 [3] . As can be seen from the figure, the extension and retraction of the landing gear is carried out by the different actuators (downlock and uplock) which are supplied by hydraulic fluid under pressure and with support from the respected spring bungee, reaction link and downlock. The retraction is driven by torque shaft powered by the main gear box which are also connected to the torsion link at the tire. The loads are supported by the main shock strut and the drag strut.

The nose landing gear has a retraction mechanism that works similarly to the main landing gear using scaled down retraction system components because it carries significantly less load than the main landing gear and retracts in the longitudinal direction instead of the lateral. The nose landing gear retracts inside the fuselage after take-off.

5.7.5 Shock Absorption

The main landing gear strut that is shown at the end of this section in Fig. 5.21 will not only supports the aircraft during taxing, but also acts as a shock absorber for the impact during landing. The shock impact can be absorbed through two different methods. Either the shock energy is transversed throughout the airframe at a different rate and time followed by the single strong impact pulse and/or the shock impact is absorbed by converting the energy into heat [3].

[8] URL https://www.goodyearaviation.com/tires/tire-line-details.html?search=all&sortorder=20 [cited May 31 2016]
[9] URL https://www.rose-hulman.edu/~adams1/courses/em121/project.html [cited May 31 2016]

The shock absorber (shock strut) that is shown in Fig. 5.21, which will be used in the main landing gear is illustrated in more detail in Fig. 5.18 [3]. An oleo-pneumatic shock absorber will be used since it has one of the highest efficiencies among the available shock absorbers. It is assumed that the entire touch-down kinetic energy is absorbed by the main landing gear [42].

As the tires touches the ground, the shock strut begins the compression stroke. As the aircraft further touches down, the shock strut will further compressed and the bottom cylinder/piston is then forced up into the top cylinder. As a consequence, the metering pin is moved upward through the orifice. The pin controls the rate at which the hydraulic fluid flows from the bottom to the top cylinder chamber at all the points during the compression stroke. Through this way the largest amount of heat energy is dissipated through the walls of the strut. At the end of this downward stroke, the air that was compressed in the top cylinder is than further compressed which limits the compression stroke of the shock strut with minimum impact. Finally the strut recoils and levels off to the load experienced during taxing [3].

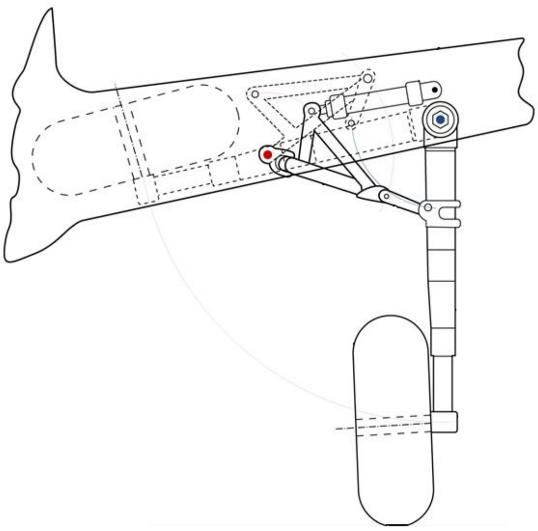

Figure 5.17: Schematic retraction mechanism main landing gear

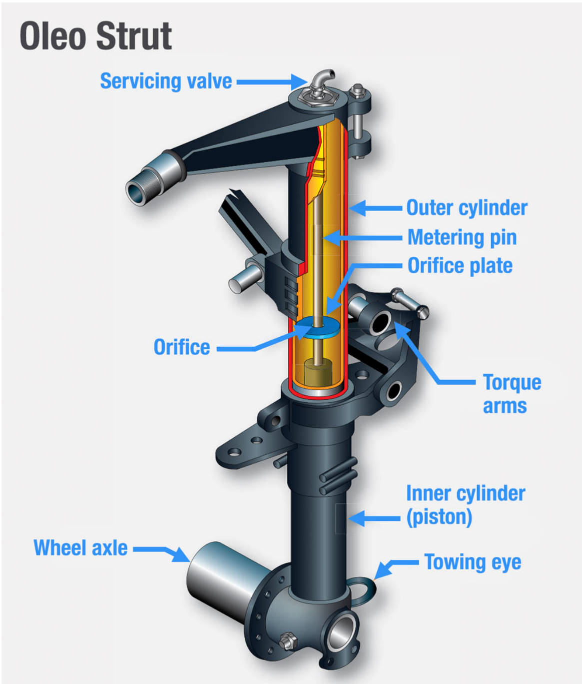

Figure 5.18: Shock absorber strut components

The diameter of the shock absorber (strut) can be estimeted using Equation (5.3) [42].

$$d_s = 0.041 + 0.0025(P_m)^{1/2}[m] \tag{5.3}$$

From Equation (5.3) the shock absorber diameter is estimated to be around 0.21 m.

5.7.6 Brakes

The landing gear brakes together with the wing spoilers are mainly used to bring the aircraft to a still during landing or rejected take-off runs. The most used brake system in the landing gear are breaking disks due to their high thermal energy dissipation capability. The landing gear brakes manufacturer that will create the brakes is Messier-Bugatti-Dowty (Safran group) which is one of market leaders in landing and braking systems. Safran groups have created the brakes for the Global family 5000/6000/7000/8000 and the Boeing Business Jet. The breaks that are appropriate for the specified W_{TO} and landing speed of the aircraft will be a carbon brake disc which is said to have a proven high endurance, and therefore reduction in maintenance costs and also has a reduction in weight compared to metallic brakes.[10] The braking system is show in Fig. 5.19[10] and a schematic drawing in Fig. 5.20 [10].

[10]URLhttp://www.safranmbd.com/wheels-and-brakes/products/boeing-business-jet-brake[cited on 2 June 2016]

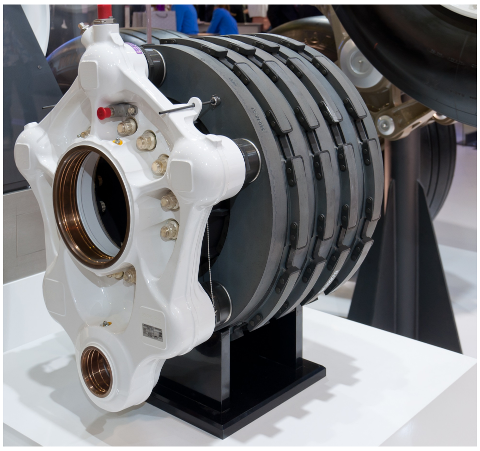

Figure 5.19: Messier-Bugatti-Dowty (Safran group) Carbon disk braking system

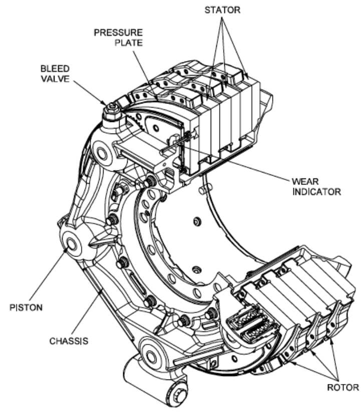

Figure 5.20: Schematic drawing of the braking system components

5.7.7 Summary of Parameters

The parameters of the landing gear parameters that are determined in this section are summarised in Table 5.3. The weight of landing gears are estimated from the weight fractions to the W_{TO} from [2] are used. The values indicated in the table for main landing gear are specified for one of the landing gears.

Table 5.3: Summary of landing gear parameters

	Nose	Main
Number	2	2X2
Size [cmXcm]	66X17	97X31
Ply rating [-]	14	20
Load per landing gear [N]	101885	208864
Landing gear length [m]	1.3	1.3
Strut Length [m]	0.97	0.82
Longitudinal Position [m]	3.7	26.6
Lateral Position [m]	0	2.0
Strut Diameter Main [m]	-	0.21
Maximum airspeed [m/s]	93.9	93.9
Weight per tire [kg]	14.1	39.5
Cost per tire [Dollar]	1282.58	2743.50
Weight [kg]	250	1320

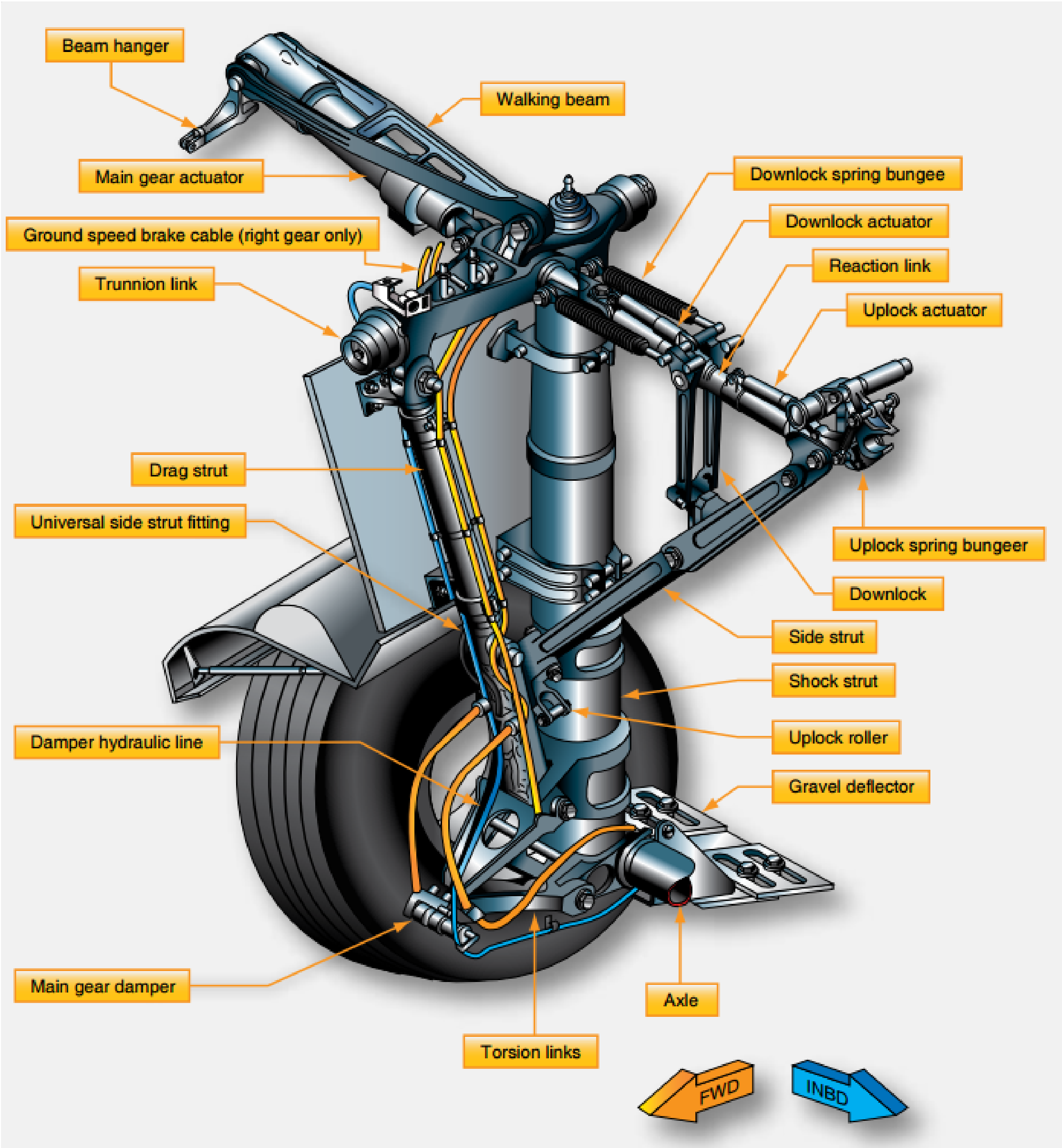

Figure 5.21: Main landing gear (right) system and components

6. Propulsion

Cost of fuel and concern for aviation's environmental impact has led to a renaissance of fuel efficient engines [44]. One of the most interesting developments at the moment is the open rotor engine. This chapter discusses the open rotor as the propulsion system chosen for the design of the business jet. The engine type is discussed in Section 6.1. The resulting engine characteristics are described in Section 6.2, fuselage integration is discussed in Section 6.3 and impact analysis is described in Section 6.4.

6.1 Engine Type

Open rotor engine is chosen for the propulsion of the aircraft. It consists of two counter rotating propellers combined with a turbojet core, referred to as counter rotating open rotor (CROR). It is shown in Fig. 6.1. The CROR engine is chosen because of its reduction in fuel consumption compared to modern turbofan engines. The open rotating propellers virtually increase the bypass ratio of the engine therefore increasing the propulsive efficiency. A second counter rotating row removes the spin from the air downstream of the first row, resulting in a more direct thrust[1]. In general the CROR engines are 26% more fuel efficient than modern turbofan engines [44], leading to a decrease in emissions. However there are some downsides to the CROR engine, such as the noise generated by the propeller blades and the loss of protection from removing the nacelle.

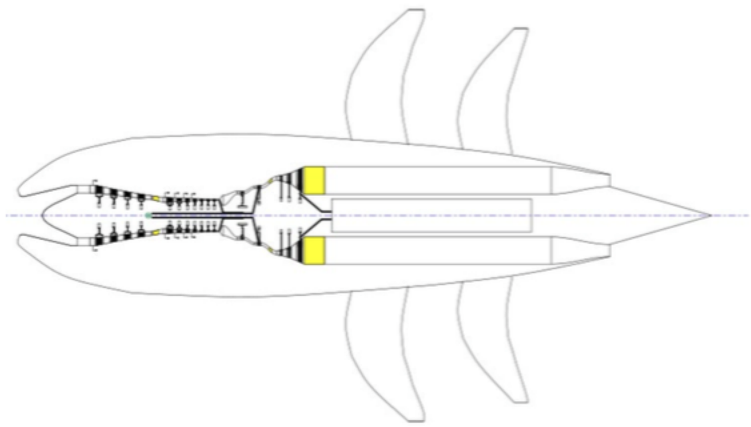

Figure 6.1: Cross section of open rotor engine [13]

The core of the CROR engine will be the BMW-Rolls Royce BR710-C4-11 engine. The BR710C4-11 is a two shaft turbofan engine with a bypass ratio of 4.2, which entered service in 1997[2]. The rated thrust of the engine is equal to 68.42 kN[2]. Using the core of the engine and by adapting it to a CROR engine, the core and the rotors generate thrust, which increases the thrust of the engine to the required level. It also decreases the fuel burn per kN, which leads to lower emissions.

6.2 Engine Characteristics

As mentioned above, the BR710C4-11 is used as the engine core. Combining this core with the CROR configuration results in updated engine characteristics. These engine characteristics, such as the performance, dimensions, noise generation and emissions are discussed in the following sections.

[1]URL http://www.rolls-royce.com/about/our-technology/research/research-programmes[cited May 26 2016]
[2]URL http://www.rolls-royce.com/products-and-services/civil-aerospace/products/small-aircraft-engines[cited June 1 2016]

6.2.1 Engine Performance

Propellers are usually restricted to low velocities, however previously performed tests show that open rotors are not restricted to low flight speeds. From a full scale open rotor test with Gen1A+B blades (Fig. 6.3), conducted by the FAA, it was concluded that the propeller net efficiency remains at an acceptable value up until a Mach number of 0.8, as can be seen in Fig. 6.2. The graph shows the propeller efficiency as a function of the Mach number. After a Mach number of 0.8 the efficiency starts to drop. From this it is concluded that a cruise Mach number of 0.78 is optimum [44] and a cruise Mach number of 0.8 is still acceptable for open rotor aircraft. However, a cruise speed Mach number of 0.78 increases the flight duration slightly compared to a Mach number of 0.8, which is not preferred. Therefore 0.8 Mach is used as the cruise speed in the design of the business jet.

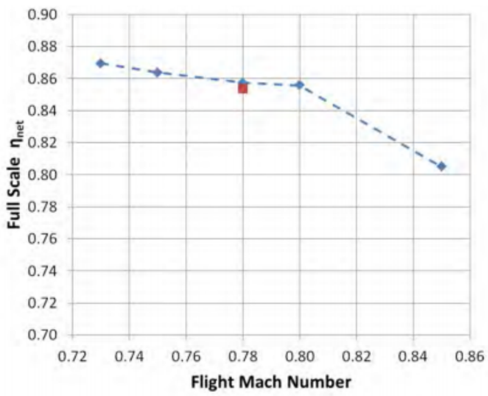

Figure 6.2: Propeller efficiency as a function of Mach number [44]

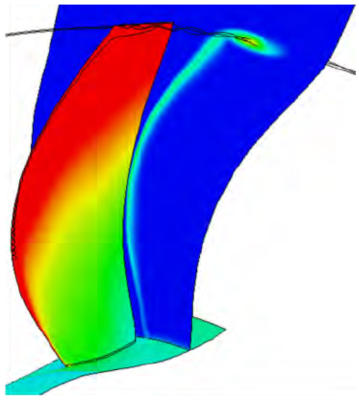

Figure 6.3: Take-off condition CFD results for Gen1A design [44]

An important parameter, next to the cruise speed, is the fuel consumption. The specific fuel consumption of an engine determines the amount of fuel used by engine. As the fuel consumption has a considerable influence on the required fuel weight and therefore the take-off weight, it has to be determined. As mentioned above, the fuel consumption of an open rotor engine is 26% lower than modern turbofan engines. The specific fuel consumption of the BR710C4-11 engine is equal to 17.1 μg/Ns. A 26% reduction leads to a specific fuel consumption of the open rotor equal to 12.6 μg/Ns.

The engines are designed based on the thrust they need to provide. The maximum thrust required during take-off is equal to 148.3 kN. The design of the business jet uses two engines, Therefore the required thrust per engine is equal to 74.15 kN. During the engine selection it is assumed that part of the thrust delivered by the engine core and part of the thrust is delivered by the open rotors. To determine the thrust distribution, Equation (6.1) is used. To calculate the mass flows, the dimensions of the engine and Equation (6.2) are used.

$$T = T_{fan} + T_{core} = \dot{m}_f(V_f - V_0) + (\dot{m}_c + \dot{m}_{fuel})V_j - \dot{m}_c V_0 \tag{6.1}$$

$$1.\ \dot{m} = \dot{m}_c + \dot{m}_f \qquad 2.\ bpr = \frac{\dot{m}_f}{\dot{m}_c} \tag{6.2}$$

From the mass flow ($\dot{m}$) and the bypass ratio of the original engine the mass flow of the core ($\dot{m}_c$) is determined. Using the required thrust per engine and selected engine dimensions the mass flow of the rotors ($\dot{m}_f$) and the jet exhaust velocity (V_j) are determined. From these parameters the thrust required from the engine core and the thrust required from the open rotors are determined and are equal to 38.0 kN and 36.1 kN, respectively. The same procedure can be done for the original engine to determine the core thrust and fan thrust. This results in a core thrust and fan thrust equal to 65.7 kN and 2.8 kN, respectively. As can be seen, the thrust of the CROR core is lower than the original, because of the power loss to the rotors. However the total thrust and the efficiency of the CROR engine are increased.

6.2.2 Preliminary engine stages computations

The selected engine core has a rated shaft horse power of 10000 hp (7.46 MW). As opposed to the original case where the turbine is used to drive the compressor, in the modified version the turbine shall provide power to both the compressor and the open rotors. In order to gain an insight into the engines performance characteristics that were derived in Section 6.2.1, a preliminary cycle analysis is performed for the take off configuration. Parameters from critical stations are presented in Table 6.1.

Table 6.1: Engine stages parameters

Station number and location	**Parameter**	**Value**
2. First Compressor inlet	Temperature (K)	288.0
	Pressure (Pa)	$9.63 \cdot 10^4$
	Compressor Pressure ratio (-)	24
3. Last compressor exit	Temperature (K)	789.3
	Pressure (Pa)	$2.31 \cdot 10^6$
	Work done in compressor (W)	$18.99 \cdot 10^6$
4. Combustor exit	Temperature (K)	1520.0
	Pressure (Pa)	$2.22 \cdot 10^6$
5. Low pressure turbine exit	Temperature (K)	912.7
	Pressure (Pa)	$2.01 \cdot 10^5$
	Work done in turbine (W)	$27.03 \cdot 10^6$
8. Nozzle throat	Temperature (K)	783.5
	Pressure (Pa)	$1.05 \cdot 10^5$
	Jet velocity (m/s)	546.9

The results indicate a power of 27 MW provided by the turbine, out of which 19 MW shall be directed to the compressor and the remaining to the counter rotating propellers. Based on this numbers, the gearbox design will be selected in Section 6.2.4.

6.2.3 Preliminary Rotor Design

In order to better understand the noise profile and overall performance of the open rotor system, a preliminary design has been attempted using Mark Drela's "xrotor" program [3].

This design routine is, however, limited to design of un-raked and un-swept rotors. As such, designing blades with variable sweep along their span is not possible. However, through a brief modification of the source code, a rotor can be designed with a constant rake angle. Specifically, the rotor is designed for the take-off condition where the thrust is highest. Since the shape of the open rotors found in literature is driven mostly by the need to reduce transonic wave drag in cruise condition, this proposed preliminary rotor designed for take-off thrust and speed does not resemble an open rotor's shape. However, this preliminary design is nonetheless useful for obtaining low speed noise and performance figures.

The design of an open rotor system itself is an iterative process due to the fact that the engine features two counter-rotating rotors. Firstly, the front rotor is designed in unobstructed freestream for a prescribed thrust value, hub radius, blade radius, and rotational frequency. Then, the aft rotor is designed inside the slipstream of this front rotor, and typically has a different thrust setting and blade radius, but maintains the same rotational frequency. The front rotor is then redesigned using the upstream induced velocity profile caused by the aft rotor. The slipstream created by this new iteration of the front rotor is subsequently used to redesign the aft rotor. This design process may be iterated manually and converges rapidly in just a few iterations. The overall objective of the design routine in xrotor is to create a spanwise chord and twist distribution which minimises the induced loss of the rotor. The flow model used in the analysis is a discrete vortex wake approach which is well suited for the analysis of swept and raked rotor blades.

The imposition of the slipstream of the front on the aft rotor and vice-versa has to be handled manually in the manner suggested in the xrotor design guidleines for counter-rotating assemblies [4]. Specifically, the slipstream of the front rotor is assumed to induce both a radial and an axial velocity on the aft rotor, while the front rotor only experiences an axial velocity component due to the presence of the slipstream of the aft rotor.

[3] http://web.mit.edu/drela/Public/web/xrotor/ [cited May 30 2016]
[4] http://web.mit.edu/drela/Public/web/xrotor/xrotor_doc.txt [cited May 31 2016]

6.2.4 Geared Open Rotor Architecture

Early designs of the open rotor engine assumed a direct drive architecture with a counter rotating power turbine. However, the direct drive configuration makes it necessary for the turbine and propellers to rotate at the same speeds [13]. The propellers designed for open rotor engines are large in diameter and are constrained by tip speed resulting in lower rotational speed. This makes the core design larger with more stages to extract enough power from the core [13]. This will ultimately yield a heavier engine. Alternatively, an engine with a gearbox allows the propeller and turbine to be designed for different rotational speeds. The turbine can be designed to provide equivalent power at a higher rotation speed with a smaller diameter and few additional stages. This design leads to a lighter counter rotating turbine. Fig. 6.4 outlines a general architecture of an open rotor engine with a gearbox implemented into the design. In this configuration, there are two spools composing the gas generator: the low pressure (LP) spool composed of a compressor (LPC) and turbine (LPT) and the high pressure (HP) spool composed of a compressor (HPC) and turbine (HPT). Downstream of the gas generator is a power turbine (PT) which drives the counter-rotating propellers through a gearbox.

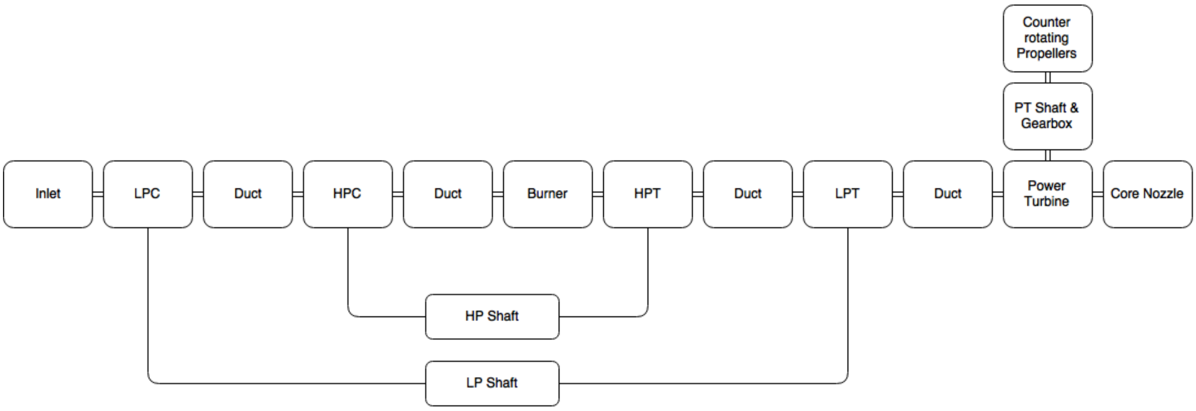

Figure 6.4: Illustration of open rotor engine architecture

6.2.5 Reverse Thrust Performance

Studies have indicated that engines designed with variable-pitch fans for reverse thrust are superior to those with fixed pitch fans and conventional reversers. The advantage of using variable pitch is the elimination of heavy, high maintenance and thrust reversal hardware and the added benefit of improved thrust response time [27]. One of the potential problems in operation of variable pitch fans is difficulty in establishing reverse thrust at certain reverse blade angles. This problem is aggravated when reversing with forward velocity. However, operational techniques during forward-to-reverse transients, such as blade angle overshoot, have been shown to be effective in reducing the time to establish reverse thrust [38, 46]. NASA research showed reverse thrust was established at the onset of fan rotation for a blade angles of $-91°$ to $-101°$. At the blade angle of $-86°$, the rotor appeared to be in stalled, unstarted condition [27]. At rotor speeds up to 79% of design, thrust peaked at a blade angle of $-93.6°$. As the blade angle was held constant, reverse thrust increased almost linearly with increasing fan speed and began to level off above 80%. During the test, the 27,088 N reverse thrust goal was attained with the fixed 30° exlet. This is about 37% of the forward thrust required per engine by the Starling business jet.

6.2.6 Emissions

Emissions of an aircraft depend significantly on its performance. With regard to aircraft emissions there are two different types of emissions which are taken into account. The types of emission are smoke and gaseous emissions. Gaseous emissions are again subdivided into unburned hydrocarbons (HC), carbon monoxide (CO) and oxides of nitrogen (NO_x) [29].

The smoke emission of an aircraft is regulated by a Regulatory Smoke Number (RSN). The RSN should not exceed the number given by Equation (6.3) or a value of 50, whichever is lower [29]. The equation is defined by F_{oo}, the rated thrust of the engine.

$$RSN = 83.6 \cdot F_{oo}^{-0.274} \tag{6.3}$$

The gaseous emissions are subdivided into different types, which have different regulatory levels. The regulatory levels for the gaseous emissions of the hydrocarbons and the carbon monoxides are constant and are equal to 19.6 g/kN and 118 g/kN, respectively. The regulatory level for the NO_x emissions is given by Equation (6.4) [29]. The equation is defined by the reference pressure ratio, π_{oo}.

$$D_p/F_{oo} = 32 + 1.6\pi_{oo} \tag{6.4}$$

The emission data of the engine used for the core is gathered using the ICAO Aircraft Engine Emissions Databank [5]. The emissions of the entire CROR engine follow from improvements in performance with respect to the baseline engine, leading to improvements in emissions as well [44]. Due to the reduced fuel burn of 26%, the engine emissions are also reduced by 26% [44]. The resulting emissions are given in Table 6.2.

Table 6.2: Emission regulation levels and emissions of the engine

Emissions	RSN [-]	HC [g/kN]	CO [g/kN]	NO_x [g/kN]
Regulations	26.26	19.6	118	73.12
BR710C4-11	14.34	4.36	64.37	41.41
CROR engine	10.61	3.23	47.63	30.64

The emission values stated above can be reduced even more by further advancements on the engine. Using an advanced lean combustor, resulting in lower fuel consumption, will lead to an emission reduction of up to 80% [25]. This will assist in reaching compliant the future regulations set by ACARE of a carbon dioxide emission reduction of 50% per passenger kilometre and an 80% nitrogen oxide emission reduction[6].

6.3 Fuselage Integration

The engines are placed at the rear of the fuselage in a push-configuration. They are connected to the fuselage with horizontally installed pylons. The pylons are used to create a certain distance between the rotor blades and the fuselage, to ensure a free rotation. The engines are mounted at the top half of the fuselage to ensure sufficient ground clearance between the rotors and the ground. The aft fuselage mounted push-configuration is preferred for the lower interior noise levels and because there is no effect on the wing by the engine exhaust airflow [25].

6.4 Impact Analysis

Certification of CROR engines is an important issue that needs to be addressed as they do not include containment structure. The following section will propose various safety systems. These includes design of impact shield that would protect the business jet passengers and critical systems from a released blade that could impact the fuselage, blade design that resists bird strike damages and dorsal shield to keep the debris from cross-engine impact.

6.4.1 Bird strikes & Ingestion

A total of 30 airliners and business jets have been destroyed by bird strikes since 1912 to 1995 [56]. The engine regulator representatives stipulated that given there is no containment casing for the open rotor, the open rotor blades must be subjected to a 3.6 kg single large bird, irrespective of the open rotor inlet area. The equivalent for a propeller is a 1.8 kg bird. But recognising the difficulty of performing successful bird tests due to low solidity (gaps between open rotor blades), Acceptable means of Compliance (ACM) introduces the option to demonstrate compliance through a combination of rig testing and validated analysis [14]. The modern blades have a polyurethane foam core, sandwiched between carbon fibre spars, with composite reinforced skins. A thin strip of metal protects the leading edge from foreign object damage. This has been illustrated in Fig. 6.5.

[5]URL https://www.easa.europa.eu/document-library/icao-aircraft-engine-emissions-databank[cited May 31 2016]
[6]URL http://www.cleansky.eu/content/homepage/aviation-environment[cited May 31 2016]

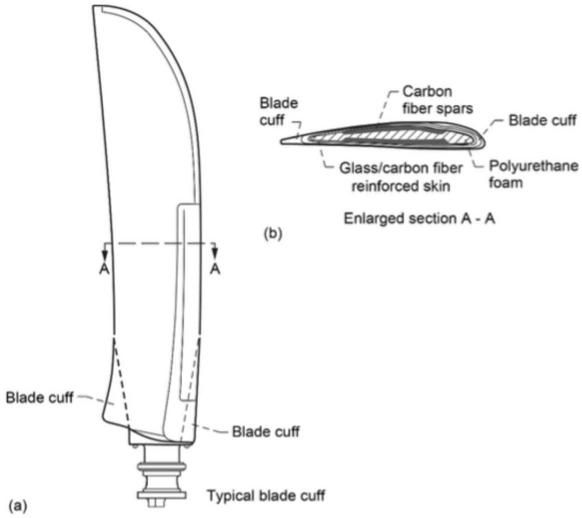

Figure 6.5: Typical composite blade. (a) Full blade. (b) Cross section

6.4.2 Cross-engine Debris

To preclude catastrophic effects for direct engine-to-engine trajectories over the top of the fuselage would require installing a dorsal shield on top of the fuselage [14]. The practicality of that solution largely depends on the size of the shield, positioning of the engines and the axial position on the fuselage. The exposure to direct engine-to-engine trajectories would be minimised depending on other design and performance considerations, by positioning the engines in such a way that it gains the maximum shielding from the fuselage. The reinforcement strategy of the fuselage has been outlined in the next section.
The front view of the Starling in Fig. 2.3 shows that most of the engine is shielded by the fuselage. However, there is a need for a dorsal shield as there is still some exposure for the debris impact in case of a blade-off scenario. This is tackled by a high performance composite shield which is lightweight and has high operational temperature range. This ensures the shielding can be carried out even if the trajectories are at elevated temperature. HicTac [7] project addresses polymeric composite material for demanding high temperature applications. They can withstand substantially higher temperature than traditional epoxy composites [16]. The project was successful in development of composites capable of withstanding temperature over 360 degree Celsius. The overview of the installation and sizing for the dorsal shield has been illustrated in Fig. 6.6 (not to scale). The two dotted lines make sure both the blades and the core are safe in the event of a blade-off.

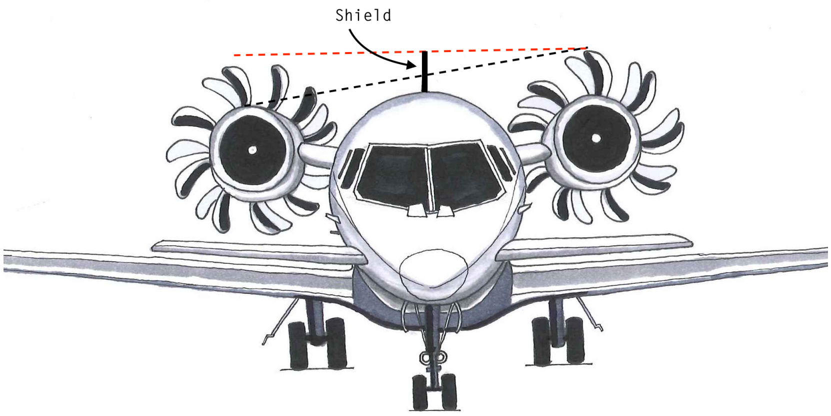

Figure 6.6: Cross engine debris trajectory path range and the dorsal shield installation (not to scale)

[7] URL http://cordis.europa.eu/project/rcn/109261_en.html [cited May 27 2016]

6.4.3 Occupant & critical system risk

The threat to individual occupants arises either from penetration of the cabin or from deflection of the cabin structure [14]. Similarly, critical systems need to be protected from the debris in the event of a blade-off. There are safety requirements that stipulates that crew members and critical systems should not be within the 10° margin (5° front & 5° aft) from the propeller spin axis. Fig. 6.7 (not to scale) shows that no individual are within these bounds. Also, the wing position is considered to make sure that the rudder does not intersect with the debris trajectory. The fuselage section that intersects the debris trajectory will need to be reinforced to make sure there are no important components (e.g. auxiliary power unit) compromised.

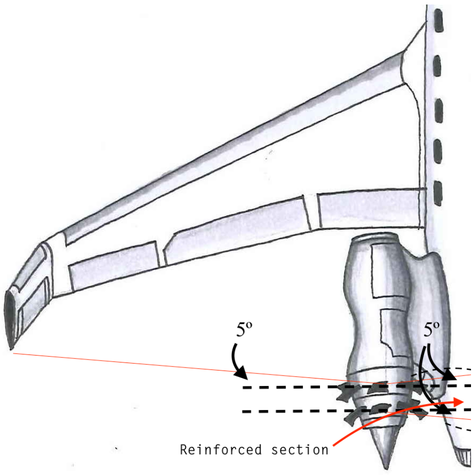

Figure 6.7: Safety angle requirement for individual and critical system from blade-off scenario

The design concept for the shielding is a floating panel that will not be subject to the flexure of the primary aircraft structure. By isolating the panel from the fuselage structure, the panel is not exposed to those additional stresses and strains and can be made of a lighter weight material than a structural shielding panel [13]. The test conducted on 2014 by NASA on a 2.4 m long panel for impact of single rotor engine blades were made of 24 layers of triaxially-braided carbon fibre prepeg resulting in a thickness of 14 mm. The open rotor blade-off test rig setup is shown in Fig. 6.8. A 6.8 kg blade was projected with a velocity of 162 m/s which resulted in a 1.1 m long vertical tear and 0.3 m horizontal tear that did not penetrate the full thickness but only delaminated the panel. Though the results from this test satisfy the requirements, there is a need for the thickness to be optimised. Thus, the reinforcement for the Starling business jet fuselage section will implement Fibre Metal Laminate composed of several thin layers of aluminium interspersed with layers of prepreg, bonded together with a matrix, such as epoxy. This is represented by the equation below [60]:

$$MVF = \frac{\sum t_{aluminium}}{t_{FML}} \tag{6.5}$$

The term MVF represents metal volume fraction and is defined as the ratio of the sum of the thicknesses of all aluminium layers over the total thickness of the fibre-metal laminate. Experiments performed on [0°/90°] crossply orientation with laminate thickness of 4.4 mm with MVF of 0.4 showed the most resistance to the projectile (140 m/s) among the other specimen used [60]. Thus, modifying this floating panel by incorporating aluminium into the laminate significantly reduces the thickness and saving the weight which is crucial to the design.

Figure 6.8: The open rotor blade-off test rig setup

6.5 Development Timeline

In order to successfully deliver the first aircraft by the year 2020, the present technology readiness level (TRL) of the open rotor (OR) engines must be investigated. Under the current CleanSky program [8], Rolls Royce and Snecma are each currently designing open rotor engines (SAGE1 and SAGE2). After performing tests on a 1:5 model scale of SAGE2 in 2013 corresponding to TRL 6, full size prototype tests are scheduled for the end of 2016 [9]. According to CS-E [10] (EASA certification specifications for engines), there is a series of tests that must be performed in case of engine certification. These include ingestion of foreign matter, vibration tests, endurance tests and engine control system failures. The time needed for the open rotor technology to reach maturity cannot be precisely defined since it depends on the manufacturer's desire to introduce the new technology on the market. Considering the present TRL of open rotors together with the objectives of the CleanSky program, it is assumed that the open rotor engines shall be available by the start of the year 2020, a period that also corresponds to the first aircraft delivery. Fig. 6.9 presents the development timeline for the SAGE2 open rotor engine.

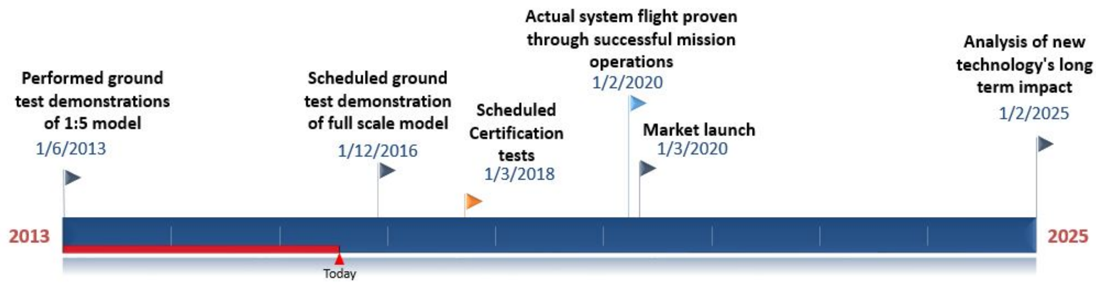

Figure 6.9: Development timeline SAGE2 2013-2025

[8]http://www.rolls-royce.com/about/our-technology/research/research-programmes/clean-sky-jti.aspx [cited June 14 2016]
[9]http://www.safran-group.com/media/20140102_open-rotor-engine-tomorrow-test-bench [cited June 13 2016]
[10]https://www.easa.europa.eu/document-library/certification-specifications/cs-e-amendment-4 [cited June 15 2016]

7. Aerodynamics

The detailed aerodynamic analysis in this Final Report serves to assure the stakeholders of the fundamental feasibility of the aerodynamic design choices unique to this aircraft. Specifically, it is critical to demonstrate that an aerofoil can be selected which delivers the necessary performance, while also enabling adequate fuel storage and integration of high-lift devices. The successful completion of the 8500 nm mission depends on the aerodynamic efficiency of the aircraft. Internal to the design group, the aerodynamic analysis must also interface strongly with the structural design and the stability and control departments.

7.1 Aerofoil Selection Refinement

In order to achieve the desired improvement in cruise drag reduction as stipulated in [2], the traditional aerofoil selection procedure has been substituted with a computational optimisation procedure using the unstructured SU2 solver. This is jointly developed by teams around the world including, primarily, by teams at Stanford University, Delft University of Technology, and Imperial College London [1]. A detailed outline of the capabilities of the SU2 suit is available in [31]. In this instance however, SU2 was chosen due to its powerful, and easy to use adjoint flow solver which enables the sensitivity of the aerofoil performance to be evaluated with respect to a large set of geometric design variables. The primary objective of the optimisation is to aid in achieving the desired reduction in cruise C_{D0} of 9,4% compared to traditional business jets. This advancement falls in the realm of "new technology" [2], meaning that a design based purely on state-of-the-art aerofoils is unlikely to yield the desired performance improvement. Thus, aerofoil optimisation is necessary. The cruise phase of the flight is the most fuel and performance critical segment of the mission. As such, SU2 will be used to design the aerofoil to produce the best performance during cruise. The off-design point performance of the aerofoil is to be evaluated using XFOIL for low, incompressible Mach numbers (i.e. during final approach). On the other hand, the validation and verification procedure of the aerofoil analysis in Section 7.1.2 shows XFOIL to be unable to accurately capture the performance of the aerofoil at transonic Mach numbers and angles of attack for which shocks occur on the upper surface. However, due to the prohibitive computational expense of the Reynolds Averaged Navier Stokes (RANS) flow solutions, the drag and lift polars of the aerofoil cannot be evaluated using SU2 for a considerable set of operational points. In addition to the computational costs, different operational points may also require individually adapted meshes to capture flow separation and turbulent wakes of the aerofoil. The generation of new meshes is highly time consuming, and future development of the aircraft should incorporate automated routines for mesh refinement.

As this is not a feasible option during the current design stage, the performance polars have been created with XFOIL for a reference Mach number of 0. For a small range of angles of attack, the RANS solution using SU2 is also given for the 2D cruise Mach number of 0.721. The optimisation has been carried out using the unstructured SU2 solver, with a continuous adjoint evaluation of the gradient of the design objective with respect to the 38 design variables distributed along the upper and lower surface of the aerofoil mesh as shown in Fig. 7.1. The definition and placement of the design variables in SU2 is achieved through the configuration file by specifying the chord-wise position of the variable and whether it is located on the top or bottom surface. It is this simple procedure for defining the deformation variables that is appealing about using SU2 for optimisation of the aerofoil. Furthermore, the design variable type is such that any deformation of the surface is always smooth.

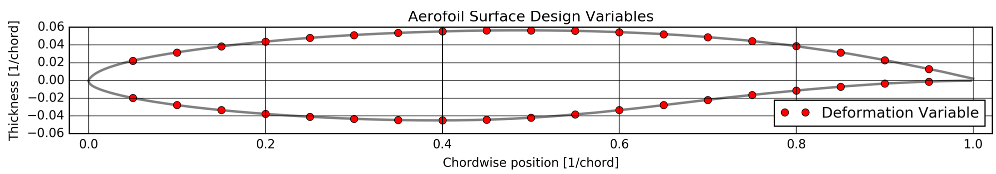

Figure 7.1: The distribution of design variables over the original aerofoil surface

[1] URL http://su2.stanford.edu/develop.html [cited June 24 2016]

To assure stakeholders of the validity of the obtained results, it is necessary to verify the numerical computations and estimate the discretisation error. This typically requires convergence studies on progressively refined meshes. However, due to the limited computational resources these could not be performed in a reasonable amount of time. Rather, the mesh used was one that has previously been tested for convergence and grid independence by the SU2 developers [31][2]. Therefore, the starting point for the optimisation is the RAE-2822 transonic aerofoil also shown in Fig. 7.1. An additional incentive for using this aerofoil is the availability of validation and verification data from NASA [31]. Thus enabling quality assurance of the design and analysis process.

The optimisation objectives and simulation input parameters are shown in Table 7.1 along with the minimum performance constraints as identified in accordance with the stakeholder requirements in [2]. The minimisation of the aerofoil drag coefficient is critical to minimising the overall friction drag on the aircraft. The thickness of the aerofoil is restricted to no smaller than 12% for two reasons: to ensure sufficient internal fuel volume (11% minimum), and to help reduce the structural weight of the aircraft. The thickness of the aerofoil directly affects the second moments of area of the wing-box cross section thus reducing the effective material area needed to carry a particular bending moment. Moreover, the lighter wing structure leads to an implicit drag reduction effect. A lighter wing means that the overall structural weight of the aircraft is also decreased such that less lift is required, thus the wing size can be decreased which implicitly reduces friction drag. The snowballing (self-reinforcing) of this implicit drag reduction mechanism is expected to exceed the purely computational drag reduction achieved through the optimisation of the aerofoil. Lastly, the lifting coefficient of the aerofoil has previously been pre-specified in[2]. This design C_l also corresponds to an aerodynamic efficiency which is the minimum necessary in order to complete the mission given the current state-of-the-art fuel consumption performance.

Table 7.1: Simulation input parameters and optimisation objectives

Parameter	**Type**	**Value**
C_l [N/N]	Constraint	= 0.5
Thickness [m/m]	Constraint	>0.12
Drag [N/N]	Objective	T.B.D.
Reynolds number (based on MAC)	Start of cruise	24’682’000
Mach number 2D	Start of cruise	0.721
Freestream Temperature [K]	Start of cruise	217
Dynamic Viscosity [kg/m/s]	Start of cruise	0.0000142
Freestream Density [kg/m^3]	Start of cruise	0.302
Freestream Pressure [Pa]z	Start of cruise	18780
Flight Velocity [m/s]	Start of cruise	236

An initial attempt at optimising the aerofoil geometry was attempted using the compressible Euler equations. However, these are not able to capture viscous effects and were found to lead to a non-smooth geometry with several potential separation points. In the wake of this result RANS equations were used instead. The Spalart–Allmaras turbulence model was selected, due to it being computationally economical. The optimisation was run for 130 iterations over the course of 4 days on 48 type-g cores of the TU Delft HPC12 cluster. Although it is recommended to further refine the aerofoil design through additional iterations, the set of 130 iterations performed in this report are sufficient to demonstrate the potential of the technique.

Table 7.2 compares the geometric properties of the new optimised aerofoil with the original RAE-2822 and the Whitcomb aerofoil as selected in [2]. The optimised aerofoil is the thickest and is therefore expected to lead to the lightest wing. The thickness position is also moved forward with respect to the original aerofoil, meaning that the average thickness of the wing box cross section is increased as is visible in Fig. 7.2. The figure also shows the chord line and mean camber line of the new aerofoil. Additionally, a visual comparison between the original aerofoil and the optimised version is shown by Fig. 7.3. The area between outline of the original and the optimised aerofoil demonstrates that the latter is thicker in the front and thinner in the back than the starting point RAE-2822 aerofoil. Furthermore, the 1.6% difference in the maximum thickness between

[2] URL https://github.com/su2code/SU2/wiki/Optimal-Shape-Design-of-a-Transonic-aerofoil [cited on June 8 2016]

the original and optimised aerofoil is an understatement of the overall improvement in the structural weight of the wing. Firstly, because the moments of inertia are proportional to the square of the increase in thickness, this leading to an effective 3.3% imrpovement in cross-sectional bending performance. And secondly, because of the implicit drag reduction mechanism described above. The quantification of this effect on the drag performance is a priortiy item for future design work on the Starling 9000. Specifically, this requires at least model for the iteration between all major components of the aircraft weight, as well as the reduction in engine thrust needed to power the lighter aircraft.

Table 7.2: Thickness and camber properties for the three considered aerofoils

Parameter	Whitcomb	Original (RAE-2822)	Optimised
Max thickness value [1/chord]	0.110	0.121	0.123
Location max thickness [1/chord]	0.350	0.379	0.367
Max camber value [1/chord]	0.024	0.013	0.014
Location max camber [1/chord]	0.825	0.757	0.755

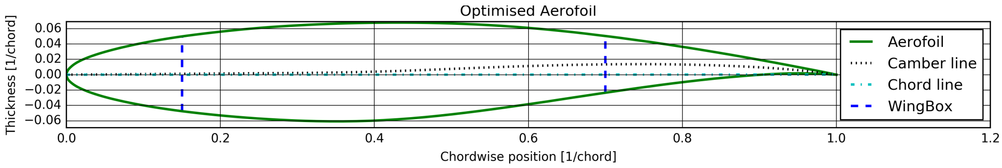

Figure 7.2: Optimized aerofoil geometry and wing box location

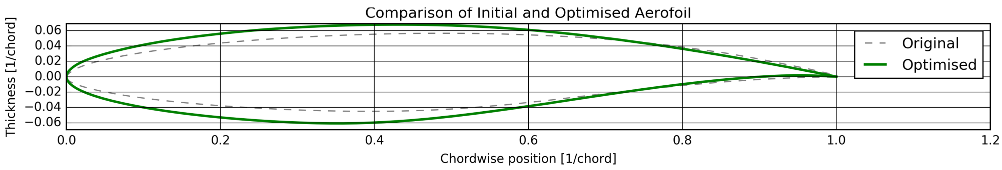

Figure 7.3: Comparison between optimised and original aerofoil Outlines

7.1.1 Aerodynamic Characteristics

The key consideration in the design and optimisation of the aerofoil is determining whether the performance offered is sufficient to enable mission success i.e. provide the required lift at a high enough aerodynamic efficiency. It is important to appreciate that while the drag coefficient reduction due to the optimisation is limited, the implicit drag reduction (outlined above) and improvement in fuel consumption, due to the increased thickness of the aerofoil is much more considerable.

Fig. 7.4 shows the pressure distribution over the aerofoil at the design angle of attack of approximately 1.5 degrees AoA, and at a much higher angle of attack of 4.5 degrees (right). Analysis of the figure shows that at the design Mach number and C_l, the aerofoil does not have shock waves on the top surface (Fig. 7.4, left). This allows the thickness of the aerofoil to be increased without causing drag divergence. At higher angles of attack, however, considerable shocks do occur on the aerofoil as shown in the right of Fig. 7.4. The presence of shock waves fundamentally undermines the applicability of analysis tools such as XFOIL which account for compressibility effects with correction factors (e.g. Prandtl-Glauert) rather than flow mechanics. An additional reason to consider the performance of the aerofoil at high angles of attack is that outboard sections of the wing operate at a higher angle of attack than the inboard sections. This is due to the inboard sections causing an up-wash flow on the outboard sections. The wing twist is typically selected such that the tip is twisted downwards and its angle of attack is reduced such that it operates closer to the design AoA. Furthermore, by increasing the thickness of the inboard aerofoil, the outboard aerofoil can be made thinner while still meeting the wing fuel volume requirements. A thinner outboard section would experience reduced transonic shocks and could therefore operate at a higher angle of attack. Such considerations are critical to the refinement of the 3D wing design to be performed at a later stage.

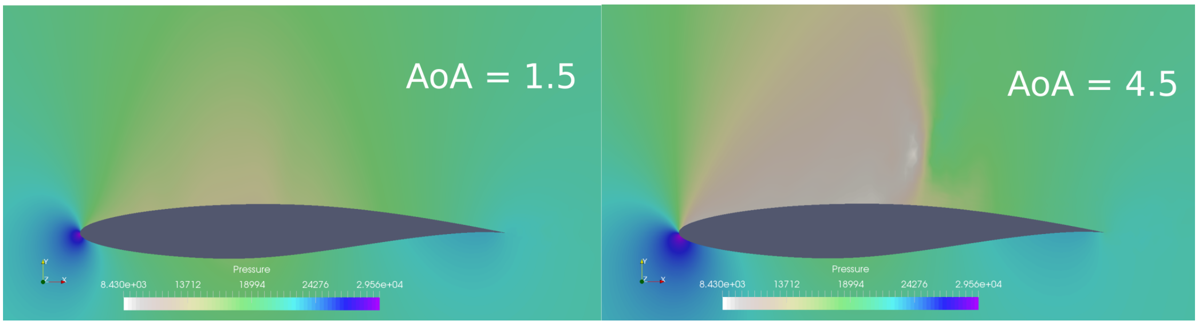

Figure 7.4: (Left) Aerofoil at approximately design cruise condition, (Right) Aerofoil at High AoA During Cruise

Nonetheless, XFOIL may be used for low, incompressible Mach numbers, and be complimented with transonic data gathered using SU2. The pertinent performance parameters are shown in Table 7.3, and the combined XFOIL and SU2 performance polars are given in Fig. 7.5. It should be noted that transonic solutions could only be obtained for angles of attack between -3 and 4 degrees. Beyond these limits, the mesh not converge due to insufficient refinment being present to caputre the flow separation phenomena. The upper left plot in the figure demonstrates that the transonic $C_{l\alpha}$ curve is considerably steeper than its incompressible XFOIL counterpart. This higher gradient has a negative effect on the gust loading. Furthermore, both the original RAE-2822 aerofoil and the optimised version have maximum lift performance inferior to the Whitcomb aerofoil (WC in graph) wich had been the slected aerofoil in the earlier design iterations [2]. The plot on the upper-right demonstrates the divergence of the drag coefficient due to the formation of shocks on the upper surface. Specifically, at an AoA of ≈ 3 deg suddenly increases very quickly although the C_L vs. α plot in the top left does not indicate a stall. This phenomenon corresponds to the drag divergence Mach number being reached for that particular angle of attack. Congruently, this limits the maximum angle of attack at which outboard sections of the wing may operate without significantly impacting the performance of the aircrat.

The middle left graph of Fig. 7.5 indicates the aerodynamic performance of the aerofoil i.e. the C_L vs. C_D obtained for a given geometry. The SU2 results are the most relevant here since the aerodynamic efficiency is critical for transonic cruise and thus the incompressible XFOIL results are highly unrepresentative (as argued in Section 7.1.2). Since the aerofoil has been designed to produce a certain C_L, a better demonstration of its performance is the graphs in the bottom left and the bottom right Fig. 7.5. In these plots, a clear maximum in aerodynamic efficiency is present just above the design C_L of 0.5, and at an AoA of approximatelly 2 degrees. Beyond this optimum point, transonic shocks lead to drag divergence and a consequent decrease in aerodynamic efficiency. As a starting point for further aerodynamic design of the geomtric twist of the 3D wing, it should be ensured that all spanwise sections operatate between ≈ 1.2 and 2.8 degrees AoA. If a shock free configuration cannot be achived with geometric twist alone, aerodynamic twist may be applied such that outboard section aerofoils have a lower thickness ratio. Furthermore, the optimised and original aerofoil nearly overlap in terms of the aerodynamic efficiency. Thus aerodynamic testing would be required to establish wherther ≈ 1 to 2 % improvement manifsests itself in reality as well. Nonetheless, since the optimized aerofoil is substantially thicker than the original, it is expected that the implicit drag reduction will not be insignificant.

Lastly, the graph in the middle right of Fig. 7.5 shows the effect on the pitching moment of the aerofoil as a result of the increase in Mach number between the incompressible XFOIL solution and transonic SU2. Specifically, the pitch-down behaviour of the aerofoil is re-enforced. This is primarily due to the front suction peak (see Fig. 7.6) on the aerofoil being smoothed out at M=0.721, while the lower surface remains largely unaltered.

Table 7.3: Aerofoil aerodynamic 2D characteristics from XFOIL

Parameter	Whitcomb	Original (RAE-2822)	Optimised
$C_{l-\alpha}$	6.36	6.15	6.06
$C_{d-\alpha}$	0.031	0.030	0.037
C_{lmax}	2.47	1.93	1.94
$(\frac{C_l}{C_d})_{opt}$	160.75	138.85	138.26

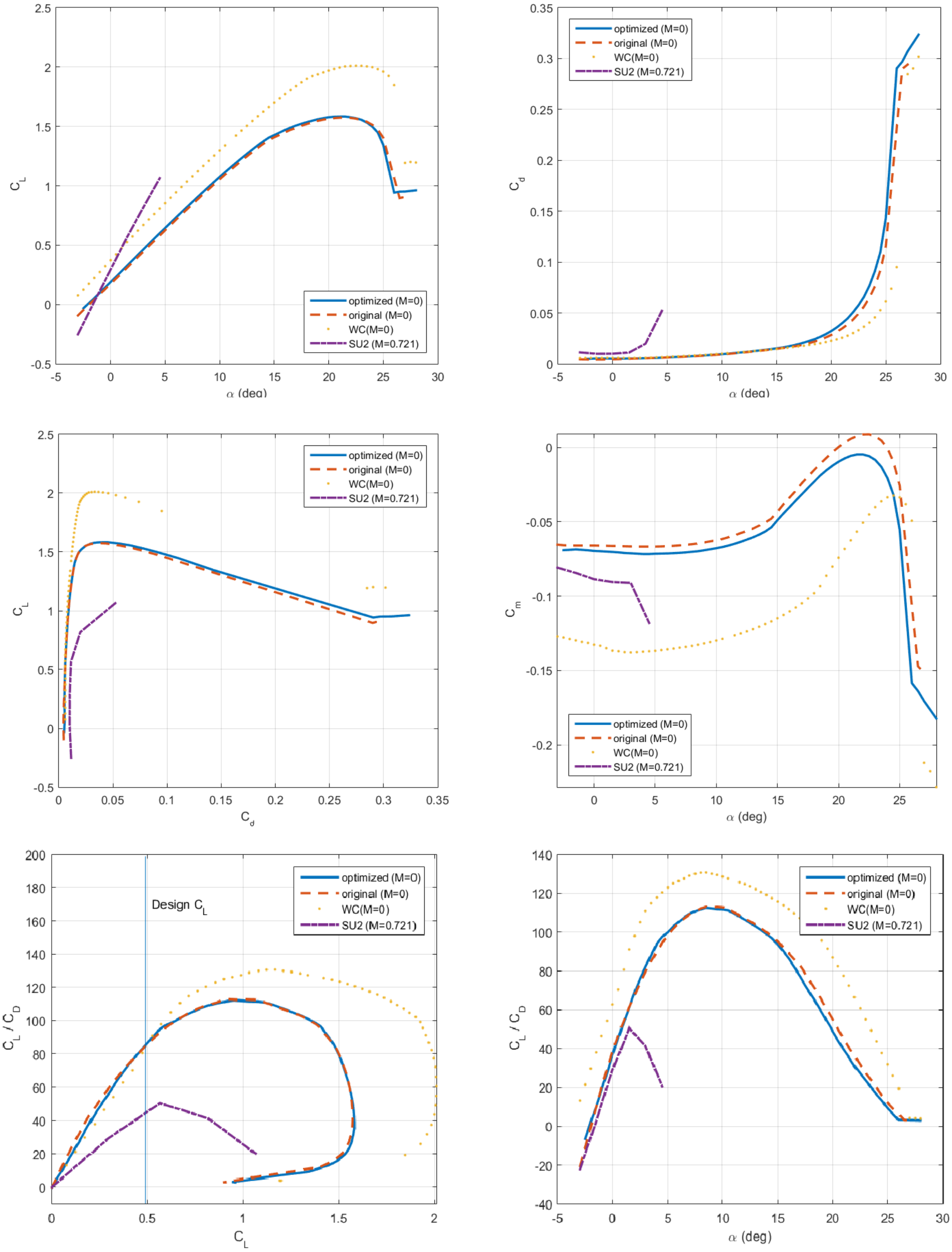

Figure 7.5: C_l - α, C_d - α, C_l - C_d, C_m - α,C_L/C_D - C_L ,C_L/C_D - α plots for the optimised, original, whitcomb (old) and SU2 aerofoils

To further demonstrate that XFOIL is an inappropriate analysis tool for the design 2D Mach number of 0.721, the pressure coefficient has been plotted over the aerofoil surface in Fig. 7.6. The figure shows that XFOIL predicts a peak in pressure at the leading edge that does not occur in the RANS flow solutions obtained using SU2. Additionally, Fig. 7.6 shows the presence of a supersonic flow region on the top surface of the aerofoil.

Specifically, this is the region where the C_p is above the sonic C_p line. This, however, does not immediately have a negative impact on the drag performance of the aerofoil as Fig. 7.6 also shows that a shock wave is not present and therefore wave drag is minimal. In other words, the aerofoil operates above the critical Mach number but below the drag divergence Mach number. This demonstrates to stakeholders that the aerofoil under a wing sweep of 25.6° is capable of meeting the Mach number of 0.8 stated in the requirements in [2].

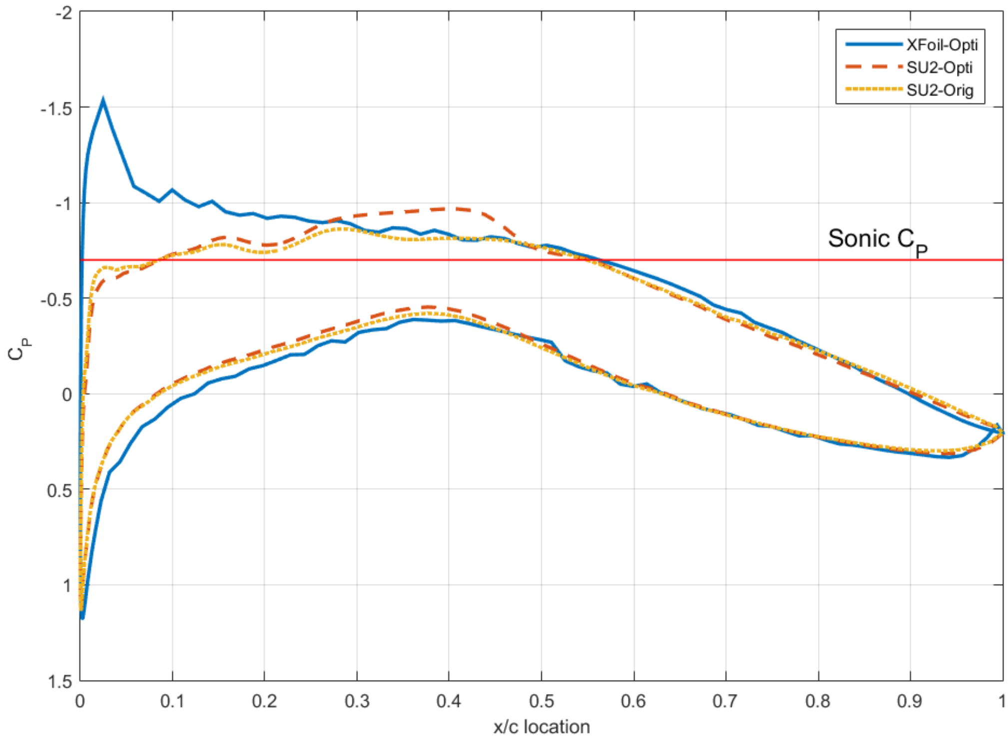

Figure 7.6: C_p plot for optimised and original aerofoil

7.1.2 Verification and Validation of Aerofoil Analysis Tools

The RAE-2822 aerofoil is frequently used as the baseline for verification and validation of 2D transonic flows [31]. The verification of results obtained in this report using the SU2 solver is possible by comparison against the computational results from XFOIL, and NPARC[3]. NPARC is a research code that has been under development at NASA's Glenn Research laboratory since 1993. Its inclusion in the verification process of the SU2 (2013) results allows an estimate to be established of the extent to which computational tools for transonic flows have improved over the last 20 or so years. Similarly, the development of XFOIL also took place during the 1990s by Mark Drela at MIT[4]. As a further validation step, the SU2 results shall be compared against experimental data from AGARD [34] (corrected for wind-tunnel wall effects). The validation test case is based on the the RAE-2822 aerofoil. This aerofoil was used as a starting point for the aerofoil optimisation in Section 7.1 especially due to the presence of high-quality validation data. As such, it is the test case with the closest geometric and computational mesh similarity to the optimised aerofoil that will ultimately be used for the design. The flow conditions of the validation case are listed in Table 7.4.

[3] URL http://www.grc.nasa.gov/WWW/wind/valid/raetaf/raetaf01/raetaf01.html [cited June 9 2016]
[4] URL http://web.mit.edu/drela/Public/web/xfoil/ [cited 27 June 2016]

Table 7.4: Validation case flow and geometry properties

Parameter	**Value**
Aerofoil	RAE-2822
M_∞	0.729
R_c (Reynolds number)	6.5E6
T_∞ [K]	273.15
α	2.31°

The midterm review stated improvements in aerodynamic performance could be achieved due to the increase in both computational resources as well as the accuracy of analysis tools and the efficient adjoint optimisation tools, such as SU2. For instance it was anticipated that the overall aircraft C_{D0} could be decreased by 9%, while also improving the efficient cruise Mach number by 6% [2]. The latter advancement is certainly identifiable with the recently designed Gulfstream 650ER being the fastest business jet with a maximum Mach number of 0.93 [5]. The increase in Mach number and decrease of transonic wave drag go hand-in-hand. By increasing the maximum Mach number, the wave drag for lower Mach numbers is congruently decreased, i.e. the drag divergence Mach number is increased as well. In this sense, the accurate localisation and magnitude prediction of shocks on the top surface of a transonic aerofoil is critical to meeting the stakeholder expectations for drag reduction, speed improvement and fuel efficiency. The baseline performance estimates from the Midterm Review were defined using reference data provided by Roskam [40] and published between 1985 to 2000. This corresponds to the era of greatest activity in the development of NPARC and XFOIL. This establishes a firm link between the baseline drag estimates used in the initial conceptual design and the computational technology level of the time. In other words, the performance numbers stated by Roskam correspond to what was achievable with the computational tools available in the day. The newer codes are expected to be more accurate and thus allow more efficient and reliable designs to be realised.

Fig. 7.7 encouragingly shows that SU2 is indeed considerably better than NPARC at predicting the location of the shock on the top surface. The agreement with experimental data from [34] is excellent and shows the shock to be located at about 0.54c, while the NPARC code estimates the shock to occur at 0.5c. Moreover, SU2 shows good agreement with the experimental data over the entire chord length of the top and bottom surfaces. The maximum deviation in C_p occurs just behind the shock-wave on the top surface.

[5] URL http://www.gulfstream.com/aircraft/gulfstream-g650[cited on June 9 2016]

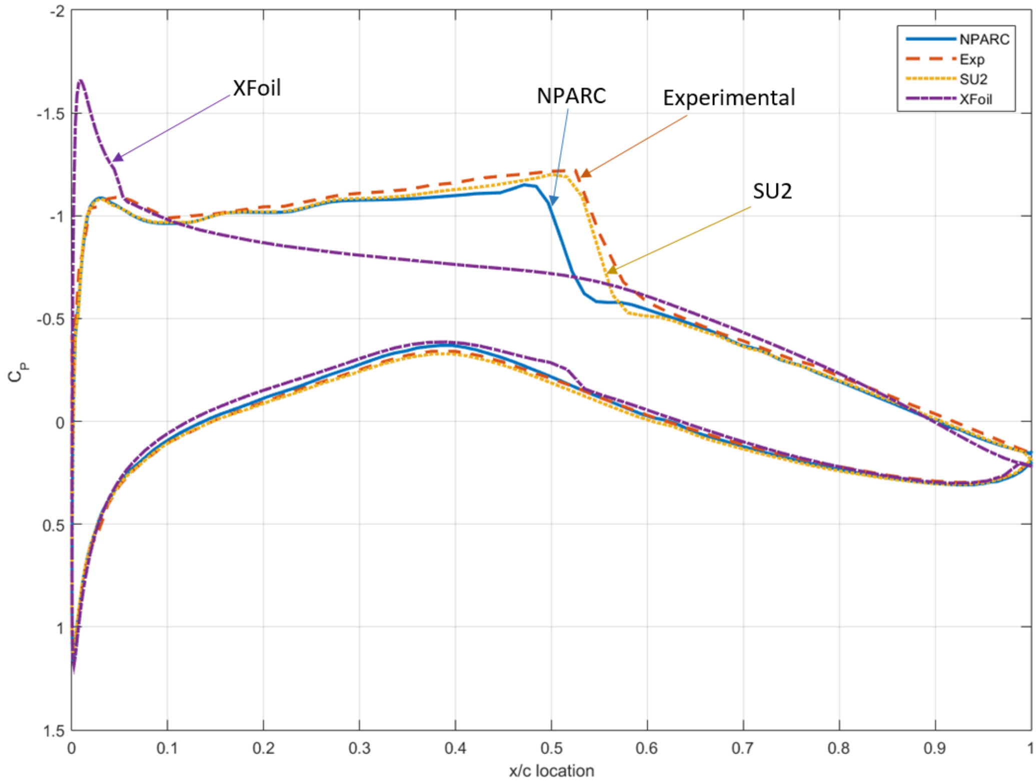

Figure 7.7: C_p plot for verification of aerodynamic tools

Conceptual design projects frequently make use of tools such as XFOIL (for 2D flows) and XFLR5 (for 3D cases). Indeed, these tools were used in the Midterm Review design of this aircraft as well. However, as Fig. 7.7 shows, these are not appropriate for the analysis of flows where the free-stream Mach number exceeds 0.7 and an angle of attack of a few degrees. The discrepancy between the C_p predicted by XFOIL and the experimental values is considerable. Particularly on the top surface, XFOIL is not able to capture the shock behaviour and leads to a large suction peak at the leading edge.

For this reason it is not recommended to continue with the use of XFOIL for the future development of the aircraft and analysis of the cruise performance. Rather, the SU2 suite should be used as the primary analysis and aerodynamic optimisation tool due to its proven accuracy in transonic flow simulation. At lower Mach numbers (approach and take-off), XFOIL and other potential flow solvers may still prove useful due to their enviable speed and efficiency.

Despite the fact that the above validation/verification case already strongly suggests the trustworthiness of SU2 as an analysis tool, the flow filed should nonetheless be validated with a comprehensive test campaign in a transonic wind tunnel. In particular, extra attention should be paid to the performance at higher angles of attack where transition and turbulence effects become more dominant and the appropriateness of the SA viscosity model may diminish. What is more, computational estimation of drag is only accurate to within a few percent and should be given additional attention as the error margin is of the same order of magnitude as the desired drag reduction of 9% [2].

Finally, the validation of the aerofoil itself against stakeholder requirements must be conducted. This includes a comprehensive analysis of the effect on fuel volume, structural weight, landing gear, flaps, and winglet integration. The off-design point performance of the aerofoil must also be considered through analysis and multi-point optimisation. Validation of the design by flight and aerodynamic testing is possible for the three dimensional wing but is not as applicable to the 2D aerofoil. Nonetheless, it is recommended to perform further 3D RANS analysis of the wing so as to avoid the high expenses of physically testing a wing design. A first order validation of the performance of the aerofoil is presented in Section 7.2 below.

7.2 Validation of Mission Success

This section fullfils the essential purpose of assuring the stakeholders that the optimised aerofoil is capable of fulfilling the mission requirements. In particular the aerofoil performance is considered with regards to three categories: cruise performance (L/D), stall performance ($C_{l_{max}}$), and stability and control ($C_{L-\alpha}$). The optimised aerofoil was extended into the full 3D wing geometry in XFLR5. The winglets and canard were also added to the model with their respective aerofoils . Aerodynamic data was collected for the angle of attack range where XFLR5 was found to converge, specifically between -3 and 8 degrees AoA. The results are plotted in Fig. 7.8. To effectively validate that the aerofoil is suitable for the mission, the aerodynamic performance of the aerofoil is compared to the requirements as calculated in [2]. The 3D $C_{L-\alpha}$ and ($\frac{C_L}{C_D}$) are retrieved from the 3D XFLR5 anlysis, while the $C_{L_{max}}$ of the 3D configuration is converted from the the 2D C_{l-max} as obtained using XFOIL. The conversion is carried out using Equation (7.1) and is necessary as XFLR5 did not converge up to the stall point of the wing but only up to 8 degrees. The compliance of the aerofoil with requirements is outlined in Table 7.5.

$$C_L = C_l \cdot cos^2 \Lambda \tag{7.1}$$

Table 7.5: Aerofoil compliance with mission performance requirements

Parameter	**Optimised Aerofoil**	**Required**	Passed
$C_{L-\alpha}$	4.92	5.12	✓/X
C_{Lmax}	1.58	1.58	✓
$(\frac{C_L}{C_D})$	24.1	17.6	✓

The $C_{L-\alpha}$ required is marginally met as a value of 5.12 or higher is desired for stability of a canard aircraft. The achieved value of 4.92 does not have a significant negative impact and is further beneficial for reducing the maximum gust load factor. Because of the small margin between the requirements and the achieved value, the requirement is treated as met. The $C_{L-maxclean}$ and optimum cruise L/D are required to be at least 1.58 and 17.6, respectively [2]. From Table 7.5 the max $C_{L-clean}$ and optimum cruise L/D were found to be 1.58 and 24.16 respectively and therefore meet the requirements for aerodynamic performance. Future designs should account for the increased drag due to the engines and the fuselage in order to better estimate the aerodynamic efficiency and its compliance with requirements.

From Fig. 7.5 it can be seen the optimised aerofoil achieves the highest L/D for the corresponding design C_L and preforms better than the Whitcomb for lower C_L's, which correspond to angles of attack lower than about 5 degree. Since the aircraft will fly bellow an angle of attack of 5 degree during cruise, the optimised aerofoil performs better than the Whitcomb during cruise in terms of L/D. To validate whether the mission will succeed and the 8500 nm objective is met, the Breguet range equation, Equation (7.2), is applied for the L/D of the design C_L. From the Breguet equation the complete wing-canard configuration by is able to achieve a range of 11688 nm for the appropriate cruise weight and specific fuel consumption. Therefore the optimised aerofoil allows the aircraft to comfortably achieve the mission range. However, future design iterations should consider a transonic evaluation of the cruise aerodynamic efficiency rather than using XFLR5. It expected that this will lead to a reduction between the achieved and the required 3D aerodynamic performance.

$$R = \frac{V \cdot L}{c_j \cdot D \cdot g} ln \frac{W_i}{W_f} \tag{7.2}$$

7.2.1 3D Aerofoil Aerodynamics

In order to aid the development of a structural design of the aircraft, the span-wise distribution of the forces on the wing should be known as well as possible. The aerodynamic performance of the wing-canard configuration is outlined in three complimentary figures in this section. Fig. 7.8 illustrates the 3D aerodynamic polars of the wing. In particular, the most important graph is the C_L/C_D vs. C_L graph in the bottom left which demonstrates that the the efficiency of the wing remains relatively constant for a range of C_L values from 0.35 to 0.65. This 'flat' efficiency curve is desirable as it shows that the aircraft can operate efficiently at a large number of operational points different from the cruise design point of a C_L of 0.394. Furthermore, the polar in the bottom right demonstrates the highest efficiency to be 24.1, achieved at 5 degrees AoA. This value is useful for the design of the incidence of the wing with respect to fuselage such that the drag of the fuselage is reduced during the cruise flight. As a preliminary value, a root incidence of -3 degrees is chosen. This is also necessary to achieve longitudinal trim with the canard configuration according to XFLR5 results. The the C_L vs. α graph shows that the angle of attack corresponding to the design C_L of 0.394 is equal to approximately 4 degrees AoA. Lastly, the C_D vs. α curve in the top right shows that at the design angle of attack, the aeroplane operates to the right of the minimum of the drag polar. This is a necessary requirement for speed stability of the Starling 9000.

Fig. 7.9 shows the C_p distribution over the wing and winglets as calculated using XFLR5.In addition to helping visualise the span-wise and chord-wise lift distributions, the C_p plot also shows a preliminary interference effect between the winglet and the wing. A point of interest is the extremely low C_p on the bottom of the trailing edge of the winglet. This anomalous result leads to an unrealistic lift distribution over the winglet. As such, the lift distribution should be analysed using a more comprehensive tool such as SU2. Additionally, the wiglets should be redesigned such that the sharp corner at the bottom of the trailing edge of the winglet is chamfered at an angle larger than 90°. A similar solution seems to have been applied on the Beech Starship [6]

Fig. 7.10 gives (from top to bottom) the lift, shear, and moment distributions generated from XFLR5. The sign of the shear and the moment loading is indicated using the standard notation, such that the sign of the moment curve reflects the curvature experienced by the deformed structure. Additionally, the loading diagrams cannot be considered valid within the fuselage due to the fact that load is alleviated in that particular region. Congruently, the moment diagrams in Fig. 7.10 present an upper bound on the moment loading at the root of the wing. The winglet lift, shear, and moment diagrams have been excluded due to the unrealistic pressure distribution at the bottom trailing edge of the winglet as mentioned above. Additionally, the loading on the winglet is ultimately also carried by the wing and should be added to the wing's shear, and moment diagrams.

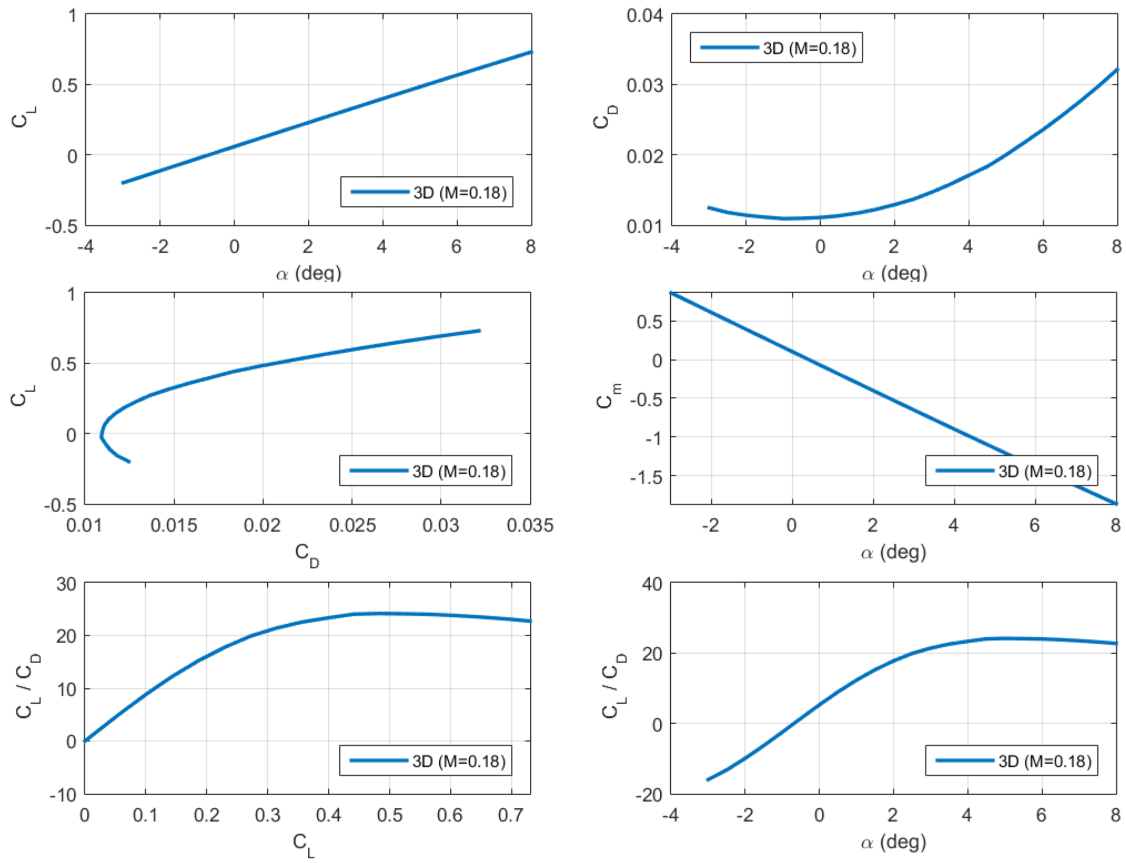

Figure 7.8: 3D aerodynamic plots (XFLR5)

[6]URL http://www.scaled.com/projects/starship[cited June 27 2016]

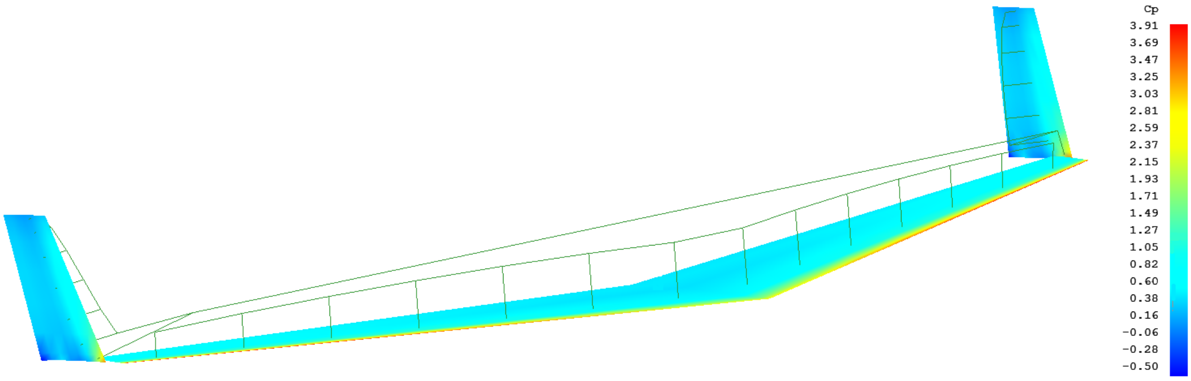

Figure 7.9: Lift and C_p distribution computed with XFLR5

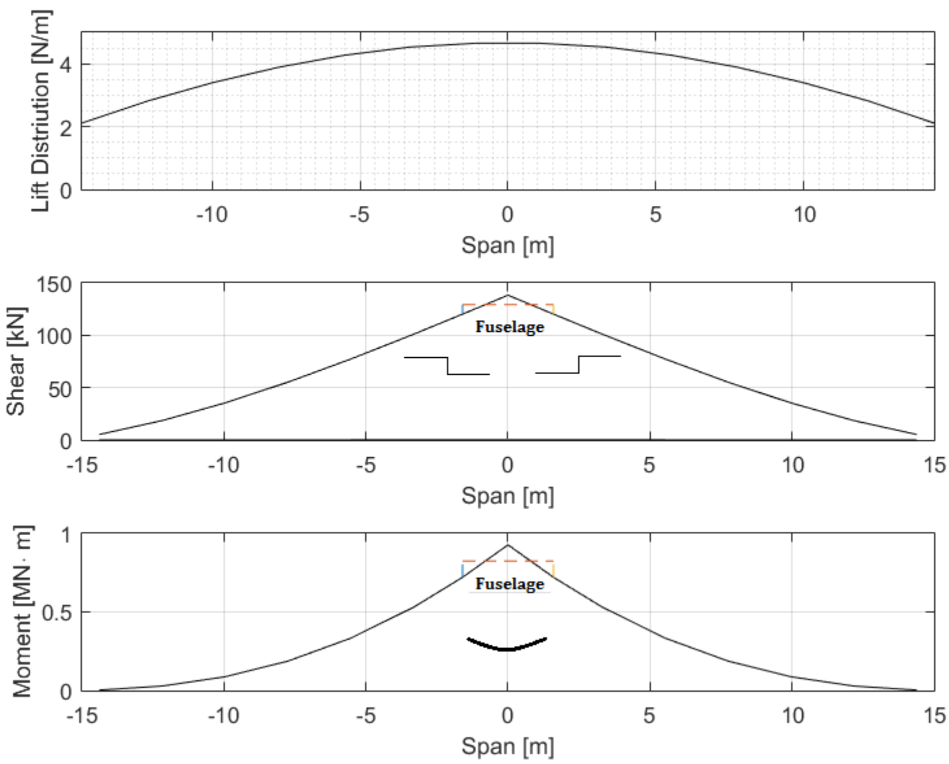

Figure 7.10: 3D span wise lift, Shear and Moment distribution (n=1)

7.3 Preliminary Rotor Aerofoil Selection

Since open rotor engines are not yet widely used in aircraft design, aerofoils available for the blades are very limited. Additionally, the aerofoils on open-rotors may vary significantly over the span of the blade and be the result of a 3D optimisation rather than the extrusion of a single 2D profile. The aerofoil that was selected for the rotor blades is the Aeronautical Research Association-Dowty Rotol (ARA-D) 10% thick aerofoil depicted in Fig. 7.11 [7]. The thick version of the aerofoil was selected to give the rotor additional structural strength. Using XFOIL, the ARA-D10 aerofoil was analysed to obtain its geometric properties which are shown in Table 7.6.

[7] URL http://m-selig.ae.illinois.edu/ads/coord/arad10.dat [cited June 25 2016]

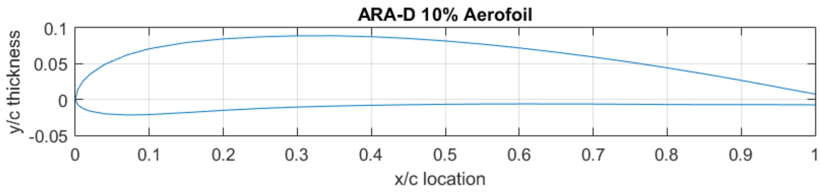

Figure 7.11: Rotor blade aerofoil

Table 7.6: Rotor blade aerofoil properties calculated with XFOIL

Parameter	**Value**
Maximum thickness value [t/c]	0.100
Maximum thickness location [1/c]	0.250
Maximum camber value [t/c]	0.040
Maximum camber location [t/c]	0.350

7.4 Winglet Aerofoil Selection

In order to select a suitable winglet aerofoil, several structural and aerodynamic characteristics need to be accounted for.

First it should be noted that the extra lift created by the winglet generates a bending moment in the same direction as the lift distribution on the wing. Thus the loading on the wing is increase with respect to a plain wing. Consequently a re-enforced (and thus heavier) wing structure is required. This is not desirable since the role of the winglet is to reduce fuel consumption by decreasing the strength of the tip vortexes and the induced drag. Reinforcing the wing structure would increase the weight, thus counteracting the winglet's main purpose. Frequently, the weight increase out-weights the benefits of the drag reduction benefits of the winglet [59]. This can be mitigated by giving the winglet a 'toe-out' inclination [59]. This allows the lift on the winglet to act as a forward pointing (thrust) force. This is possible as the wing vortex changes the local flow direction.

Secondly the conditions at which boundary layer separation occurs differ for the wing and the winglet. The winglet is influenced heavily by the flow over the wing such that it has a tendency to stall prematurely [54]. A typical design practice is to ensure the wing and the winglet flow separate at the same angle of attack, whereby the aerofoil separates due to the strength of the wing-tip vortex and the blanketing from the wing turbulence. An aerofoil with a slightly higher camber than that of the main wing has been chosen [59] to allow.

Thirdly, since the aerofoil is located at the tip of the wing where supersonic speeds can be locally reached, shock waves will form resulting in wave drag. The point at which they occur can be adjusted through the winglet's thickness ratio, which also affects the stall characteristics and lift over drag ratio. During cruise flight, when low angles of attack are encountered, the thickness value has limited effect on the lift characteristics but greatly affects drag. On the other hand, at large angles of attack a thicker aerofoil is preferred as its lift over drag slope is less steep than that of a thinner one, resulting in improved stall characteristics [54]. Since the major part of the flight is the cruise phase, the aerofoil's thickness must be kept to a minimum while also meeting the required airworthiness stall criteria and structural thickness.

The chosen winglet aerofoil which meets all of the above criteria is the NASA/Langley LS(1)-0413 [8], depicted in Fig. 7.12 with properties tabulated in Table 7.7. Further iteration of the design of the aerofoil of the winglet should be performed in future development. Particularly, to establish an effective structural interconnection between the wing and the winglet while keeping the magnitude of transonic shocks to a minimum.

[8] URL http://m-selig.ae.illinois.edu/ads/coord/ls413mod.dat [cited June 26 2016]

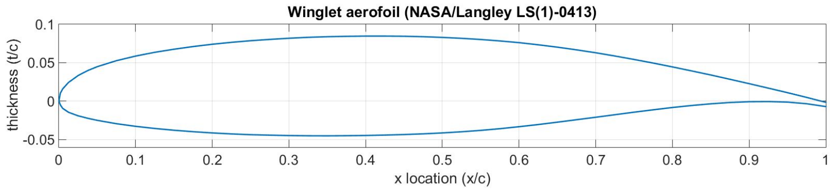

Figure 7.12: Winglet aerofoil geometry

Table 7.7: Winglet aerofoil specifications calculated with XFOIL

Parameter	Value
Maximum thickness value [t/c]	0.129
Maximum thickness location [1/c]	0.376
Maximum camber value [t/c]	0.023
Maximum camber location [1/c]	0.674

7.5 High-Lift Devices

The High-Lift Devices or HLD are responsible for the increase in lift necessary for the aircraft to fly at the low speeds required for take-off and landing. During the cruise the wing design should aim for low drag, implying little camber and a high wing loading. In landing this is reversed, the wing should have a high camber, lots of lift and a low wing-loading. Commonly the HLD are located at the leading and/or trailing edges of the wing and sometimes the canard as well. The lift force for a clean wing depends on the wing reference area, S_{ref}, this area is defined as the complete trapezoidal area including the area where the wing intersects with the fuselage. The dynamic pressure of the free stream air is denoted with q as defined in Equation (7.3).

$$q = \frac{1}{2}\rho V^2 \qquad L = q S_{ref} C_L \tag{7.3}$$

Throughout the entire design cycle, the performance of the wing is one of the most difficult and critical values to estimate. Even with extensive profile testing inside calibrated wind tunnels it is still difficult to predict the lift generated by the 2D profile when used for a finite wing. However, extensive wind tunnel testing of aerofoils and wings has allowed relationships to be defined that allow an aerofoil's 2D performance to be approximately transformed to the performance of a 3D constructed using the same aerofoil. In particular, the efficiency of the 2D aerofoil is decreased considerably due to the high pressure air escaping from the underside of the aerofoil and flowing to the low pressure upper side of the wing. This phenomena is referred to as wingtip vortexes and occurs at the open end of a lifting surface, an example can be seen in Fig. 7.13.

Figure 7.13: Vortexes originating from the HLD on a 737 aircraft

A second factor reducing the lift when transitioning from 2D to 3D is caused by the sweep angle. The sweep is used to delay the formation of shock waves and associated drag. At the lower speeds of approach and take-off, the sweep still has an effect on the 3D C_L of the wing. Combining these factors results into a transformation from 2D to 3D flow results in Equation (7.4) [37].

$$C_{L_{max}} = 0.9 C_{l_{max}} cos(\Lambda) \tag{7.4}$$

The lift coefficient or $C_{l_{max}}$ for the aerofoil developed equals 1.95 (from Section 7.1.1). Applying Equation (7.4) and $\Lambda = 25.6°$ results in a $C_{L_{max}}$ of 1.58 for the clean wing. From the requirements in [2] it follows that the $C_{L_{max}}$ required for take-off and landing should be at least 2.1. As previously mentioned, the end of a lifting surface creates vortexes and thus reduces the lift. For the HLD in the preliminary design it is sufficient to add 0.1 to the 3D case [37] to compensate for the lift loss, see Table 7.8.

Table 7.8: $C_{l_{max}}$ and $C_{L_{max}}$ values for the aircraft, $C_{L_{landing}}$ includes 0.1 margin

	Clean	Landing
$C_{l_{max}}$	1.9498	2.7105
$C_{L_{max}}$	1.5826	2.2

High lift devices can be found on the leading edge of the aerofoil, in this cases referred to as slats. High lift devices located on the back of the wing are referred to as flaps. According to Table 7.8 the required $\Delta C_{L_{max}}$ that needs to be generated by all high lift systems combined is 0.62

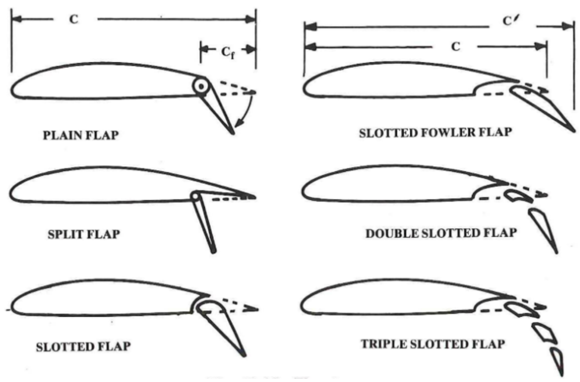

Figure 7.14: Different flap types [37]

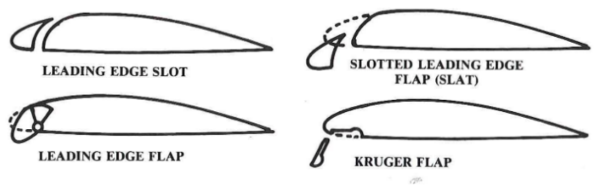

Figure 7.15: Overview of leading edge high-lift devices [37]

In Fig. 7.14 the different flaps types have been illustrated, the associated gain $\Delta C_{L_{max}}$ for each of the different flap types can be found in Table 7.9.

Table 7.9: $\Delta C_{L_{max}}$ increment for the different flap/slat types [37]

High-lift device	$\Delta C_{l_{max}}$
Flaps	
Plain and split	0.9
Slotted	1.3
Fowler	1.3 c'/c
Double slotted	1.6 c'/c
Triple slotted	1.9 c'/c
Leading edge devices	
Fixed slot	0.2
Leading edge flap	0.3
Kruger flap	0.3
Slat	0.4 c'/c

Using Equation (7.5) the Table 7.10 can be generated. From this table it can be seen how large the flapped area of the wing should be in order to achieve the required $\Delta C_{L_{max}}$. In Fig. 7.16 the flapped area with respect to the total wing planform can be seen. From this it can be seen that the flapped area for the leading edge differs from the flapped area for the trailing edge devices. Where the leading edge devices, when present, can span the complete leading edge of the wing, the trailing edge flaps has to share the available edge with low- and high speed ailerons, resulting in a smaller flapped area.

$$\frac{\Delta C_{L_{max}} S_{ref}}{\Delta C_{l_{max}} cos(\Lambda)} = S_{flapped} \tag{7.5}$$

Table 7.10: Required flapped area for the different c'/c ratio's

Flaps	$\Delta C_{L_{max}}$	S_{flaps} (m^2)	$\Delta C_{L_{max}}$	S_{flaps} (m^2)	$\Delta C_{L_{max}}$	S_{flaps} (m^2)
c'/c	1.1		1.2		1.3	
Plain & Split	0.9	95.4	0.9	95.4	0.9	95.4
Slotted	1.3	66.0	1.3	66.0	1.3	66.0
Fowler	1.43	60.0	1.56	55.0	1.69	50.8
Double Slotted	1.76	48.8	1.92	44.7	2.08	41.3
Triple Slotted	2.09	41.1	2.28	37.6	2.47	34.8

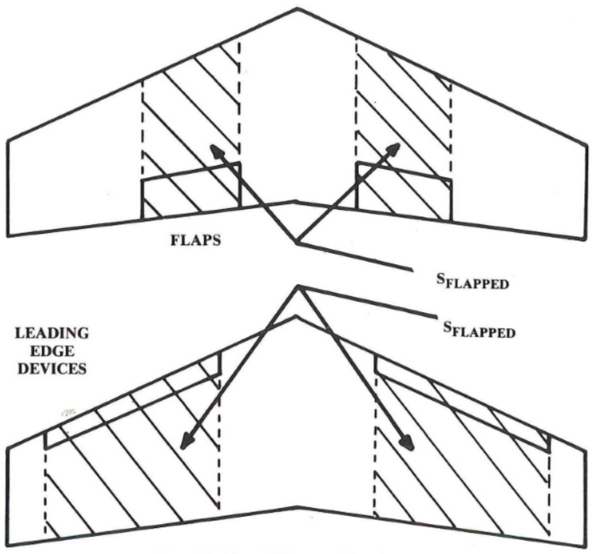

Figure 7.16: Flapped area with respect to the total wing planform area [37]

7.5.1 Leading edge high-lift devices

From Table 7.9 and using the fact that the entire leading edge of the wing can be utilised for leading edge HLD, one can see that the maximum contribution of the slats to the total required $\Delta C_{L_{max}}$ equals about 15 – 25%. From a structural stand point the leading edge HLD increase the complexity as indicated in Fig. 7.15, which shows the different leading-edge slat designs traditionally used on transport aircraft. According to this picture, all but one design (the fixed leading edge slot) involve moving parts on the leading edge of the aerofoil. This creates complications for the deicing systems and adds structural weight where mounting points for attachment to the main wing have to be incorporated. The increase in lift these slats produce can be found in the lower part of Table 7.9. The working principle for the different types is identical, they aim to increase the camber of the aerofoil by extending the front leading edge downward. In most aircraft, the leading edge HLD are present to delay airflow separation on the top surface of the wing at high angles of attack. This helps extend the lift curve to higher angles of attack and also increases the efficiency of the trailing edge HLD [37]. For the canard configuration of the Starling 9000 both the horizontal wing and the canard generate lift. In comparison, a horizontal stabiliser in a conventional configuration generates a negative lift. As a result, the high lift devices on the canard need to generate less lift than in a comparable conventional configuration aircraft. This allows the leading-edge HLDs to be eliminated from the design, thus reducing the weight and complexity of the main wing. More importantly, the absence of the HLD on the leading edge substantially reduces the aircraft noise of the aircraft. During the landing phase, noise due to slats is the second largest component of total airframe noise [7], while a deployed landing gear produces the most noise of any component. Reducing airframe noise is critical to meeting noise targets for 2020, given the fact that the Starling 9000 uses open-rotor engines.

7.5.2 Trailing edge high-lift devices

By omitting the leading edge HLD, the trailing edge has to accommodate all the HLD required to achieve the $\Delta C_{L_{max}}$ of 0.62. For this, a trade-off between surface area and complexity has to be made. As can be seen from Table 7.10, increasing the amount of slots on the HLD raises the $\Delta C_{L_{max}}$ for the system, however a larger area for the flaps results in less complex HLD and thus a lighter wing. The design for the trailing edge has been done conducted in close cooperation with the control and stability team designing and sizing the ailerons in Section 9.1.2. Once the aileron sizing was complete, the span-wise locations and thus the area left for the HLD is simply that not taken-up by the ailerons. Based on this, the HLD system with the best trade-off between complexity and $\Delta C_{L_{max}}$ for the Starling 9000 is the single slotted Fowler flap.

8. Aircraft Mission Performance

The performance of the aircraft must satisfy both the customer needs as well as the certification requirements. In order to make sure the design satisfies all stakeholders, different performance aspects are analysed. These include the payload-range diagram, the flight envelope, the aircraft weight and balance and the mission profile.

8.1 Payload Range Diagram

The choice of an aircraft is predicated upon the requirements of the mission. The main requirement of this business jet is to haul 18 passengers over a range of more than 8,500 nautical miles (15,742 km). One method employed to assess the design involves the evaluation of its payload and range performance. To represent the available trade-off between payload and range, a payload range diagram is constructed.

The payload range diagram showing the design choice of the business jet is depicted in Fig. 8.2. The region inside of the boundary represents feasible combinations of payload and range missions. The maximum number of passengers were decided based on the requirement of ensuring to maximise the comfort of the passengers with enough seat pitch to lie down and adequate space to hold a business meeting or enjoying on board time with the families. When fitting more people in the cabin, seat pitch have to be reduced. By reducing the seat pitch that was designed for 18 passengers to 1.5 m, which is common for business class in airliners, the number of seats could be increased to 24 while retaining the comfort and pleasure to travel by Starling 9000. Thus the maximum payload weight is 2900kg with 24 passengers and 5 crew members including their luggage. When the aircraft is carrying maximum payload its capacity is limited by its maximum zero fuel weight(MZFW), which is the sum of operational empty weight(OEW) and the payload. At point A the aircraft is at maximum payload with no fuel on board. Along point A to B, it indicates the maximum payload range. Fuel is added so the range of 8215 nautical miles can be flown. Point B represents the maximum range the aircraft can fly with maximum payload. At this point the fuel tanks are not full, which explains that in order to increase the range beyond this point fuel should be increased. And it will be at the expense of payload. From point B to C payload is traded for fuel to attain greater range, which can be achieved by mainly reducing the number of passengers. At Point C the maximum fuel volume capacity has been reached. This point represents the maximum range with full fuel tanks where a reasonable payload can be carried. Calculations for the range at point B and C follows the process from the course Aerospace Design and Systems Engineering Elements I [36]. The Equation (8.1) shows the expression for the range calculation. In this equation, the method for the estimates of fuel fraction $\frac{W_4}{W_5}$ during different flight phases is the same in [2]. The weight balance at point B is defined in Equation (8.2). At point C, the weight is shown in Equation (8.3). Those two equations are used for calculating the weight of fuel. Starting from point C, more fuel are carried and the amount of payload limited by fuel. It can be seen from the diagram the last part is very steep. The maximum range of 9286 nautical miles is achieved theoretically at the operational empty weight (OEW). The formula for weight and balance at this point is Equation (8.4). In Fig. 8.1, it summarises the payload range characteristics for the business jet including the weight estimations.

$$R = \left(\frac{V}{g \cdot c_j}\right) \cdot \left(\frac{L}{D}\right) \cdot ln\left(\frac{W_4}{W_5}\right) \tag{8.1}$$

$$W_{TO}(max) = W_{OE} + W_{PL}(max) + W_F \tag{8.2}$$

$$W_{TO}(max) = W_{OE} + W_{PL} + W_F(max) \tag{8.3}$$

$$W_{TO}(max) = W_{OE} + W_f(max) \tag{8.4}$$

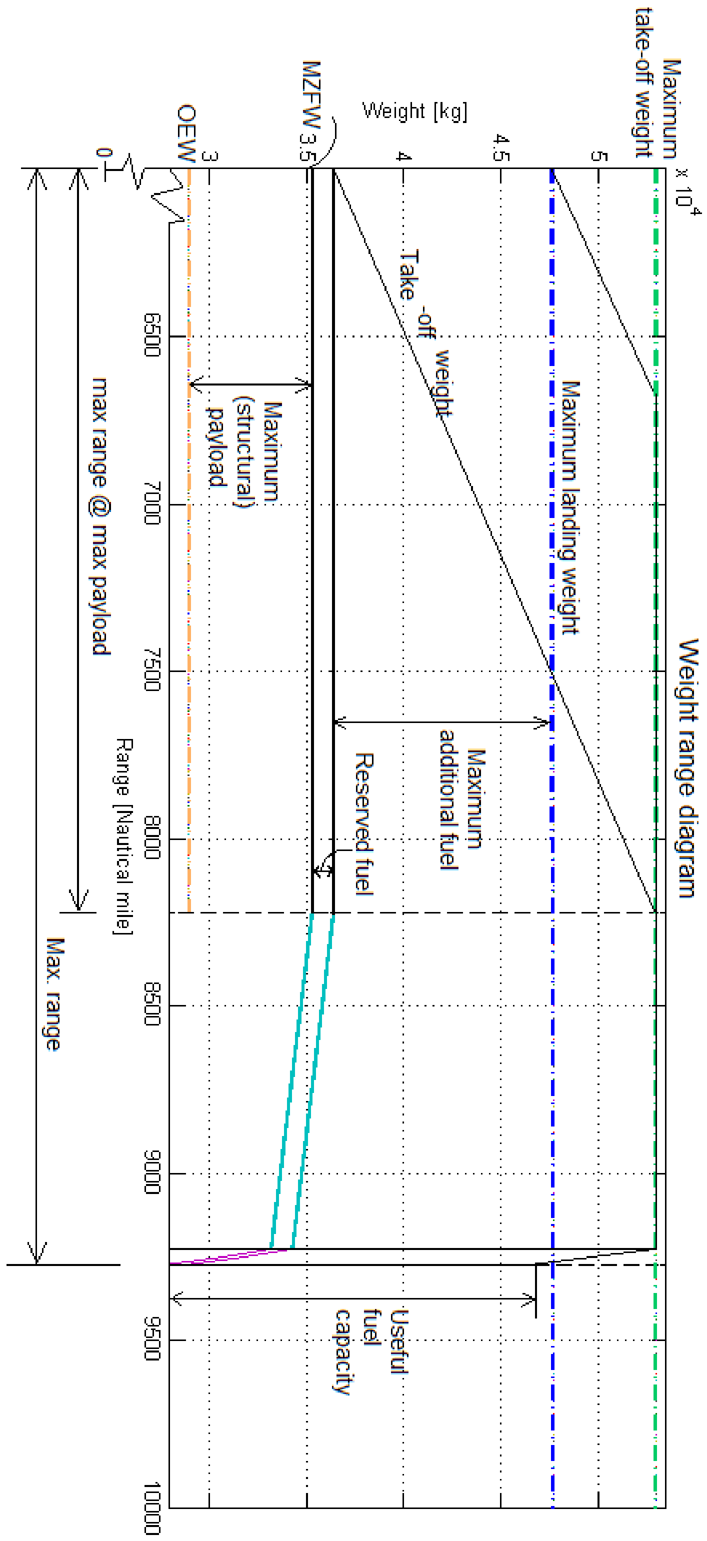

Figure 8.1: Payload range diagram with weight estimations

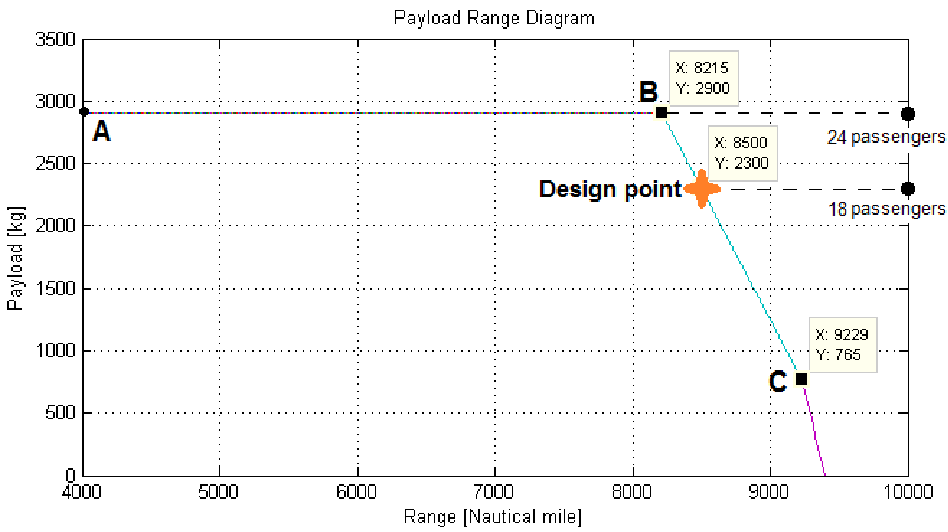

Figure 8.2: Weight range diagram

8.2 Mission Profile

For the purposes of weight estimation and performance analysis, the design mission of the Starling 9000 is broken down into discrete segments. An overview showing the 13 different flight phases is provided in Fig. 8.3. For a nominal mission the different phases are: engine start-up, taxi, take-off, climb, cruise, descent and landing. Non-nominal mission phases include: holding patterns (loitering) and missed approach procedures. Both the nominal mission as well as the reserves have been treated during the design of the Starling 9000 in order to ensure it complies with all applicable fuel and range contingency regulations. Specifically, the non-nominal segments account for deviations from the original flight plan resulting in holding patterns and diversions to an alternate airport. Such manoeuvres may, for instance, become necessary as a result of severely adverse weather or airport closure due to emergency.

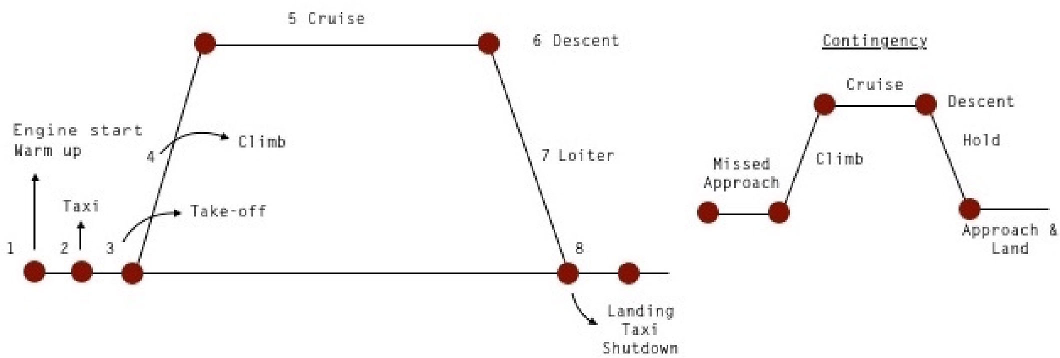

Figure 8.3: Design mission profile of Starling 9000 business jet aircraft

Cruise is the most fuel intensive and challenging in terms of fuel performance. During cruise the trip fuel is being continuously consumed. The Starling 9000 becomes lighter every minute of cruise. Consequently, to maintain the lift-to-weight balance throughout cruise flight, the lift force must also decrease in proportion to the weight. The canonical form of the lift-weight relation for cruise is given by Equation (8.5).

$$W(t) = \frac{1}{2}\rho(t) \cdot V^2 \cdot S \cdot C_L \tag{8.5}$$

The above relation also indicates which variables shall be held constant throughout the entire cruise phase and which shall be allowed to vary with time in order to balance the left- and right-hand sides of Equa-

tion (8.5). The choice has been made to vary density by increasing the flight altitude throughout the flight. The decision to hold other parameters constant is explained as follows. The surface area of the wing is not variable as this would require devices such as extension flaps and slats to be employed during cruise. The velocity of the aircraft should remain equal to Mach 0.8 through cruise to ensure the lowest possible flight time. Since the Starling 9000 flies in the tropopause, the Mach number of 0.8 corresponds to a speed of 236 m/s throughout the entire range of cruise altitudes. As the Starling 9000 is aerodynamically optimised for a certain C_L this is held constant at the optimum value.
The altitude gain is visualised in Fig. 8.4. Overall, the cruise altitude is increased by 2788 m between the beginning and the end of the cruise. Fig. 8.4 also shows that the cruise phase of the flight takes approximately 18.5 flight hours for the design range of 8500 nm.

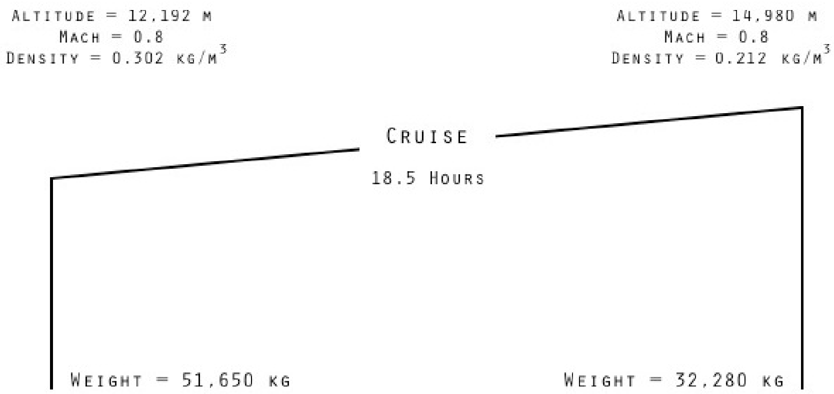

Figure 8.4: Important parameters at the start and the end of the cruise

8.3 V-n Diagram

The V-n diagram, also referred to as the flight envelope, presents the permissible combinations of speeds and load factors. To account for both manoeuvring and gust loadings, two separate diagrams are produced followed by compiling them together in order to identify the critical conditions.

Manoeuvre loading

First the load factors during manoeuvres at different speeds are analysed in order to analyse the flight performance. Based on equilibrium conditions Equation (8.6) is used as a starting point in the derivation of the load factor: Equation (8.7). The load factor is a function of density, thus different load diagrams are associated with various altitudes.

$$L = W = n \cdot m \cdot g = C_L \frac{1}{2} \rho V^2 S \tag{8.6}$$

$$n = \frac{C_L \cdot \rho \cdot V^2 \cdot S}{2 \cdot m \cdot g} \tag{8.7}$$

Based on Equation (8.7), the stall speeds can be obtained by setting the load factor equal to 1 resulting in Equation (8.8). Depending on the setting of the high lift devices, different stall speeds can be defined including the clean stall speed V_S, the landing stall speed V_{S_0} and the take-off stall speed V_{S_1}.

$$V_S = \sqrt{\frac{2 \cdot n \cdot m \cdot g}{\rho \cdot S \cdot C_{L,max}}} \tag{8.8}$$

The corner speed, also referred to as the manoeuvring speed V_A, is the lowest speed associated with the highest positive load factor. It is calculated in Equation (8.9) as a function of the maximum permissible load factor which can be obtained from CS25 specifications as being equal to 2.5 [4].

$$V_A = \sqrt{n_{max}} \cdot V_S \tag{8.9}$$

The flaps design speed, V_F, represents the maximum speed achievable with the flaps fully extended and is calculated according to CS25 certifications as the minimum of either $1.8 \cdot V_{S_0}$ or $1.6 \cdot V_{S_1}$.

The cruise speed is calculated using Equation (8.10), based on the desire to travel at a Mach number of 0.8.

$$V_C = M\sqrt{\gamma \cdot R \cdot T} \tag{8.10}$$

The dive speed, V_D, represents the maximum permissible speed of the aircraft. This speed is generally achieved only during certification testing, and is calculated using Equation (8.11) as given by CS 25 requirements [4]. Equation (8.11) can be further simplified , leading to Equation (8.12) [58].

$$\frac{V_C}{M_C} \leqslant 0.8\frac{V_D}{M_D} \tag{8.11}$$

$$V_D \leqslant \frac{V_C}{0.8} \tag{8.12}$$

Having gathered all the needed data, it must be noticed that different loading diagrams can be constructed for different altitudes. The manoeuvre loading diagram for 10000 ft (3048 m) is part of the complete flight envelope and is depicted in Fig. 8.5.

Gust loading

The gust loading diagram shows the permissible combinations of speed and load factors, based on three key velocities. These are V_B (design speed for maximum gust intensity), V_C (cruise speed) and V_D (dive speed). The derivation starts by analysing the effect of the gust on the aircraft, which comes in the form of an increase in the angle of attack, which in turn leads to an increase in lift. The equilibrium state corresponds to a load factor of 1. After the gust disturbance, the load factor changes by Δn, as shown in Equation (8.13).

$$n = 1 + \Delta n = 1 + \frac{\Delta L}{W} = 1 + \frac{\rho \cdot V \cdot C_{L_\alpha} \cdot V_{gust}}{2 \cdot \frac{W}{S}} \tag{8.13}$$

The highest gust load factors occur while the aircraft is flying at minimum flying weight [32]. The variable V_{gust} can be expressed as a product of the load alleviation factor, K, and a statistical gust velocity, $\hat{V}_{gust}$, which is specified in the CS 25 requirements [4].

$$V_{gust} = K \cdot \hat{V}_{gust} \tag{8.14}$$

The load alleviation factor, K, for the subsonic case is obtained using Equation (8.15) [1]. It depends on the equivalent mass ratio, μ, calculated using Equation (8.16).

$$K = \frac{0.88 \cdot \mu}{5.3 + \mu} \tag{8.15}$$

$$\mu = \frac{2 \cdot \frac{W}{S}}{\rho \cdot g \cdot \bar{c} \cdot C_{L_\alpha}} \tag{8.16}$$

Compared to the manoeuvre loading diagram where CS25 regulations specify minimum and maximum load factors, for the gust loading the limits come in the form of statistical gust velocities, $\hat{V}_{gust}$. These are dependant on altitude and flight condition, reaching peak constant values in the 0-20000 ft regime. These values are 66 f/s (20.1 m/s) for high angle of attack case, 50 f/s (15.2 m/s) for cruise condition and 25 f/s (7.6 m/s) for dive condition. Another key point associated with the gust loading envelope is the design speed for maximum gust intensity, denoted as V_B. An aircraft flying below V_B may stall in case of experiencing a gust. Equation (8.17) presents a first estimate of V_B based on the stall speed and the maximum gust load factor at cruise, n_c.

$$V_B = V_S \cdot \sqrt{n_C} \tag{8.17}$$

Similar to the manoeuvring diagram, the gust loading depends on several factors including altitude. An altitude of 10000 feet (3048 m) is chosen as it corresponds to the critical statistical gust velocities specified by CS-25 requirements. The corresponding gust loading diagram at this altitude is depicted in Fig. 8.5, being part of the overall flight envelope.

Flight envelope

Accounting for both manoeuvre and gust loading, the complete flight envelope at 10000 ft (3048 m) can be obtained by superposition. At different flight speeds the limiting load factor is given by either gust or manoeuvre loading, thus in Fig. 8.5 both the gust and manoeuvring diagrams are presented. Having identified the critical load factor, the design load factor can be obtained from Equation (8.18).

[1] URL http://adg.stanford.edu/aa241/structures/vn.html [cited June 03 2016]

$$n_{design} = 1.5 \cdot n_{max} \tag{8.18}$$

From Fig. 8.5 it is observed that both the minimum and maximum load factors occur during gust loading. The minimum load factor is -1.1 and the maximum is 3.1. This results in a minimum design load factor of -1.65 and a maximum design load factor of 4.65. This flight envelope is applicable for an altitude of 3048 m, chosen due to the statistical gust velocities that reach critical values.

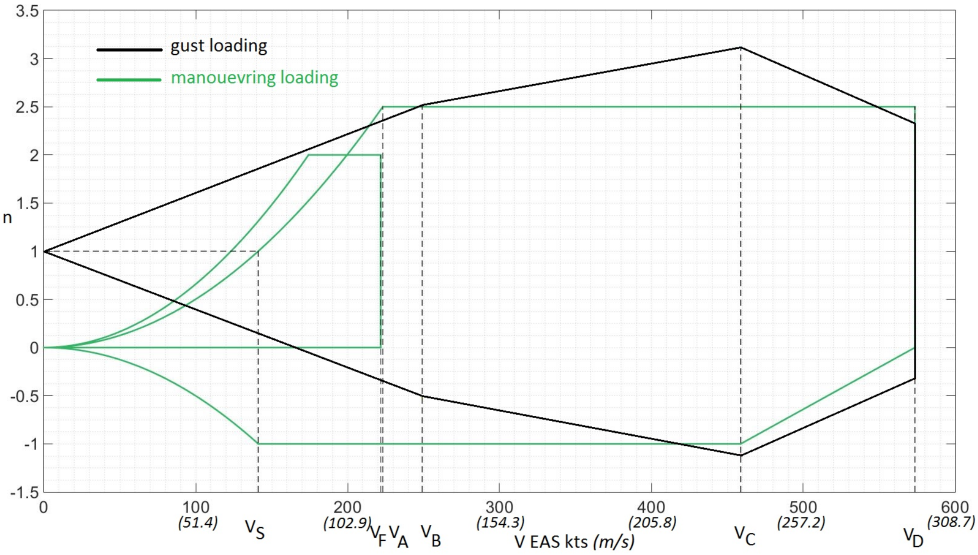

Figure 8.5: Manoeuvre loading diagram for 10000 ft (3048m)

8.4 Aircraft Weight and Balance

After the class I weight estimation done in the Midterm Review [2] a class II weight estimation is done. The Class II weight estimation method used for the estimation is the method provided by Torenbeek [57]. Using this method the weight and the centre of gravity location of the aircraft is estimated. To estimate the weight of the aircraft, the empty weight of the aircraft is divided in main components as mentioned by Torenbeek. The empty weight includes the weight of the wing, the canard, the fuselage, the winglets, the engines, the nacelles, the surface control system, the landing gear and the fixed equipment. These weight components are again arranged into a wing group, containing the wing, the winglets, the main landing gear and the surface control system. And a fuselage group, containing the fuselage, the canard, the fixed equipment, the engines, the nacelles and the nose landing gear. The weight of the components and the centre of gravity location of the component measured from the nose of the aircraft are depicted in Table 8.1.

Table 8.1: Component weights and c.g. location

Aircraft main components		**Component weights**		**C.g. measured from**	
Main group	**Component**	**Weight [kg]**	**% of MTOW**	**Nose [m]**	
Wing group	Wing	7730	15	25	
	Winglets	585	1	31	
	Surface Control	695	1	28	
	Main Gear	1320	2	27	
Fuselage group	Fuselage	11055	21	15	
	Canard	545	1	3	
	Nose gear	250	0.5	4	
	Nacelle	390	1	33	
	Engine	3265	6	33	
	Equipment	1255	2	6	
Total weight		**27100**		**Overall aircraft c.g.**	**21**

Next to the estimation of the weight of the aircraft, the balance of the aircraft is analysed regarding the centre of gravity range during operation. While the centre of gravity of the empty aircraft is fixed, the centre of gravity can change during operation due to variations in fuel and payload.
To show the loading and unloading effect of the payload and fuel on the c.g. range of the aircraft, loading diagrams are made. These loading diagrams show the c.g. positions versus the total mass of the aircraft. The loading diagrams are made for three different longitudinal wing positions: the actual position, a 10% more aft wing position and a 10% less aft wing position. The different wing positions are used to show how the centre of gravity range changes with the longitudinal wing position. The loading diagrams are depicted by Figs. 8.6 to 8.8. For the computation of the loading diagrams the number of passengers at maximum payload is used and it is assumed that the luggage c.g. location is the same as the c.g. location of the passenger. For the loading it is assumed the crew is loaded first, followed by the passengers and the fuel. To determine the individual c.g. locations of the passengers, the internal layout regarding maximum payload is used.
From loading diagrams one can see that the largest contribution to the c.g. shift is caused by the loading of the fuel. This is because the payload weight and crew weight are relatively small compared to fuel weight.

The minimum and maximum centre of gravity positions resulting from the loading diagrams above are used to determine the c.g. range. First 2% is added to or subtracted of the maximum and minimum values, respectively, to account for in-flight variations. Then these values are plotted against the longitudinal positions of the wing. The c.g. range is depicted in Fig. 8.9. The front and aft centre of gravity position needs to comply with stability and controllability characteristics of the aircraft. This is discussed in Chapter 9.

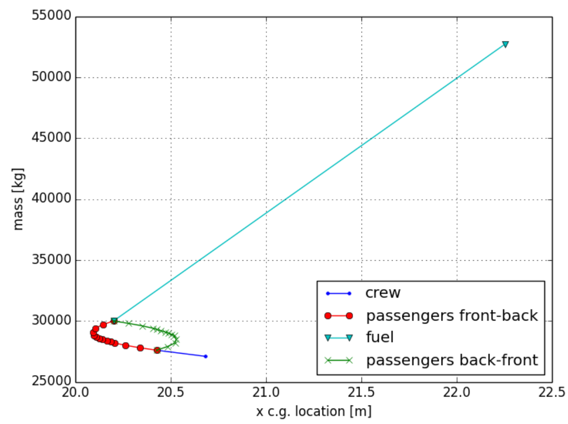

Figure 8.6: Loading diagram with actual wing position

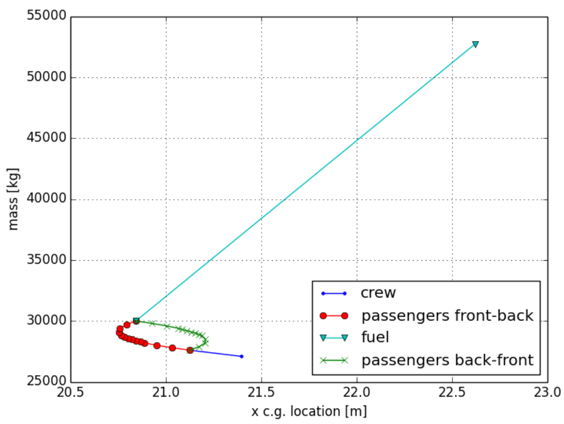

Figure 8.7: Loading diagram with 10% more aft wing position

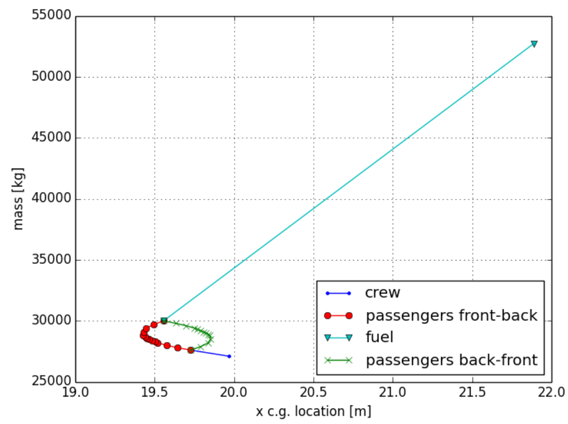

Figure 8.8: Loading diagram with 10% less aft wing position

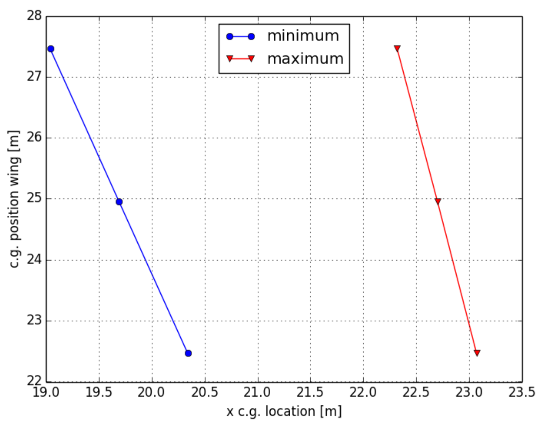

Figure 8.9: Centre of gravity range versus wing longitudinal position

9. Stability & Control

Stability and controllability are two of the most fundamental prerequisites for safe flight. The Starling 9000 will be designed for a favourable balance between the aircraft's inherent stability and controllability. These properties are critical if the aircraft is to appeal to pilots, reduce training hours, and provide a smooth ride for premium passengers. Since the Starling 9000 features an unconventional empennage configuration it is further important to consider stability and controllability of the business jet early in the design process. This chapter addresses the design of the canard and winglets as well as the rudder and elevator control surfaces. First, the empennage is sized on the basis of static stability in Section 9.1. This is followed by the dynamic stability evaluation covering the lateral and longitudinal stability modes of the aircraft and an evaluation of the dependence of the stability performance on the angle of attack.

9.1 Static Stability

During normal flight operations the aircraft will be subjected to forces which cause it to deviate from its steady straight symmetric flightpath. These forces may either come as disturbances from the environment (such as gusts), or as control inputs from the pilot. The Starling 9000 is required to respond to instantaneous disturbances by returning to a stable flight condition following the disturbance. On the other hand the aircraft is required to respond as crisply as possible to control forces. The ailerons located on the main wing of the Starling 9000 are used to control the rolling moment, the elevators on the canard are used to control the pitching moment, and the rudders installed on the winglets are used to control the yawing moment. In this section, the sizing of the canard and winglets, as well as the positioning of the wing are decided based on considerations of both stability and controllability. Subsequently, the rudder, aileron, and elevator control surfaces are designed.

9.1.1 Canard Design

To have a controllable aircraft the canard surface shall stall at a lower aircraft angle of attack than the main wing [18]. Since the canard provides positive lift in most phases of the flight, a canard stall may lead to a sudden pitch down moment. This behaviour may be used to enhance the stall characteristics of the Starling 9000 such that the canard always stalls before (at a lower angle of attack) the main wing. To ensure this, while also maintaining favourable stall recovery control, an aerofoil with a low lift curve slope is used on the canard of the Starling 9000. Fundamentally, this corresponds to an aerofoil with a larger thickness ratio than that of the main wing. Additionally, the canard incidence angle is set higher than the that of the wing. The Wortmann FX 75-141 [1] aerofoil is depicted in Fig. 9.1 and was used on the Aceair Aeriks 200. This aerofoil is presented here as a preliminary choice for the canard of the Starling 9000 due to its history of use as a canard aerofoil. Additionally, it has the required thickness and lift slope characteristic as outline above. The key geometric properties of the aerofoil are summarised in Table 9.1. Finally, and perhaps most importantly, the aerofoil features a smooth rather than an abrupt stall. This prevents the nose of the aircraft from dipping too quickly during stall. This choice of canard aerofoil is not final and should be subject to further iterations later in the design process. However, for the evaluation of dynamic stability derivatives using XFLR5 and DATCOM this preliminary selection of aerofoil is necessary.

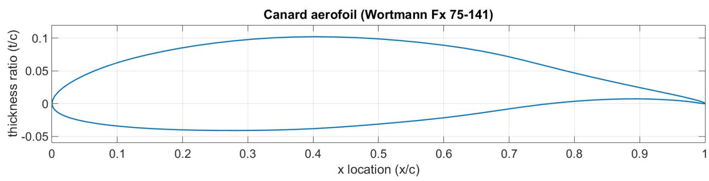

Figure 9.1: Canard aerofoil geometry

[1] URL http://m-selig.ae.illinois.edu/ads/coord_database.html [cited 7 June 2016]

Table 9.1: Canard aerofoil specifications

Parameter	**Value**
Maximum thickness value [t/c]	0.141
Maximum thickness location [1/c]	0.371
Maximum camber value [t/c]	0.034
Maximum camber location [1/c]	0.533

Having selected the canard aerofoil, the reference area of the canard may be sized simultaneously with the wing position. The definition of relevant geometric parameters and symbols used in the subsequent analysis is shown in Fig. 9.2. The front cross section in this figure represents the canard (left) and the rear one designates the main wing (right). The balance of forces and moments produced by the canard and the main wing is found using Equation (9.1) and Equation (9.2), respectively.

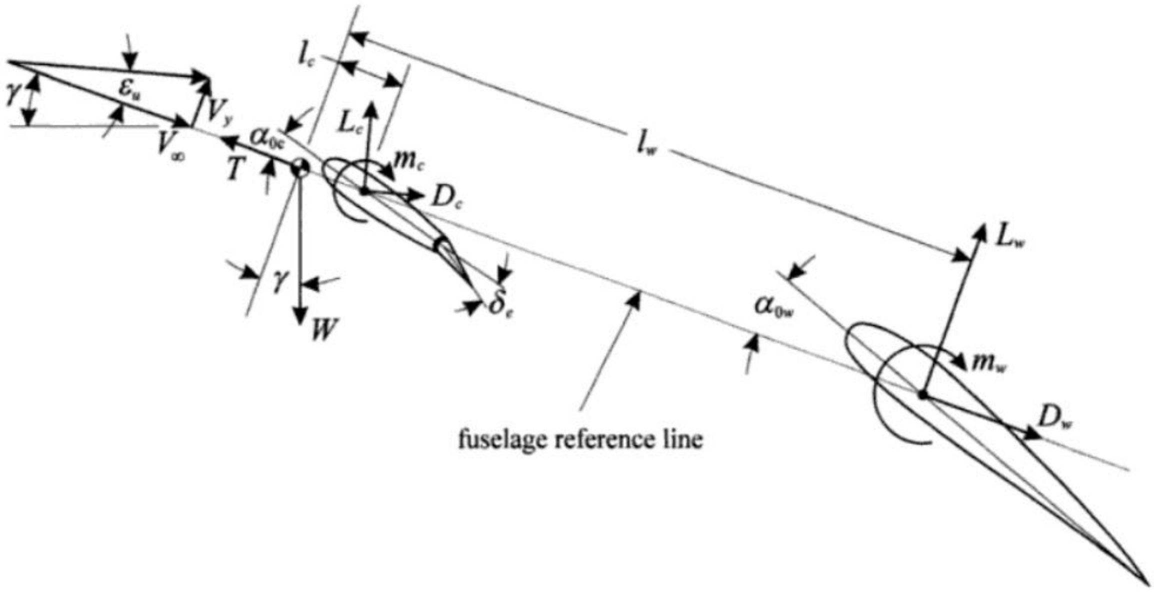

Figure 9.2: Forces and moments acting on a wing combined with a forward canard [35]

$$C_{L_w} + \frac{S_c}{S_w} C_{L_c} = \frac{W \cos\gamma}{\frac{1}{2}\rho V^2 S_w} \tag{9.1}$$

$$C_m = C_{m_w} + \frac{S_c \bar{c}_c}{S_w \bar{c}_w} C_{m_c} - \frac{l_w}{\bar{c}_w} C_{L_w} - \frac{S_c l_c}{S_w \bar{c}_w} C_{L_c} = 0 \tag{9.2}$$

A canard is, by definition, always mounted forward of the main wing and the aircraft c.g. It thus has a negative moment arm $l_c < 0$. As such, a canard produces positive lift at the trim condition. For pitch stability, it is required that the change in the total aircraft pitching moment with respect to a change in angle of attack is negative. That is, if the angle of the aircraft is instantaneously increased by a disturbance, the aerodynamic forces should pitch the aircraft downwards and thus reduce the angle of attack. In essence, the longitudinal stability condition for the wing-canard combination requires that:

$$\frac{\partial C_m}{\partial \alpha} = -\frac{l_w}{\bar{c}_w} \frac{\partial C_{L_w}}{\partial \alpha} - \frac{S_c l_c}{S_w \bar{c}_w} \frac{\partial C_{L_c}}{\partial \alpha} < 0 \tag{9.3}$$

The first term to the right of the equals sign in Equation (9.3) represents the wing contribution to the aircraft longitudinal moment stability derivative and the second term is the canard contribution. Because $l_c < 0$, the canard always has a destabilising effect on the aircraft, as it yields a positive (pitch-up) moment contribution while a negative one is desired. To offset the destabilising effect of the canard, the aerodynamic centre of the main wing should have a positive moment arm, i.e. be behind the c.g. of the aircraft.

Moreover, trim and static stability requirements may be met for a range of c.g. locations. In the design process, changes in c.g. location arise due to the adjustment of the layout of the aircraft subsystems (such as the wing), while during operation the loading of passengers and fuel shifts the c.g. from that of the empty aircraft. Thus, to enable the sizing of the canard and a simultaneous positioning of the wing, a “scissor plot“ is utilised. This combines in a single figure the controllability and stability plot of the aircraft with the aircraft c.g. position plot. The benefit of a scissor plot is that it allows an optimal canard size and wing position to be selected which meet both stability and controllability requirements.To determine aid in sizing of the canard and positioning of the wing, the following definition of the canard volume ratio with negative l_c is to be used:

$$\bar{V}_c = \frac{S_c\,(-l_c)}{S_w \bar{c}_w} \tag{9.4}$$

The first step in creating a scissor plot is calculating a set of loading diagrams for different longitudinal positions of the wing. In this case, the original position was used along with one where the wing is shifted 10% forward and one where the wing is shifted 10% backward. These “potato“ diagrams are shown in Figs. 8.6 to 8.8 and lead to a combined c.g. range diagram shown in Fig. 8.9.
The ensure the aircraft has sufficient stability even for extreme c.g. locations, a stability margin (S.M.) is used in the sizing of the canard. A typical value for the S.M. was found to be 0.02 [45]. The plot of controllability of the wing-canard configuration is defined through Equation (9.5) while the stability curve is computed using Equation (9.6)[39]. The upwash gradient $\frac{\mathrm{d}\varepsilon}{\mathrm{d}\alpha}$ in these two equations is intended to account for the induced flow effect the wing has on the canard. However, it may be neglected [39] as the canard trailing edge is more than 1.5 times the wing root chord ahead of the wing. The lift rate coefficient of the wing and the canard follow the method presented in [39].

By overlapping the stability and control plot with the c.g. range plot, as shown in Fig. 9.3, the optimal area of the canard combine with a wing position is determined. The numerical output of the scissor plots are presented in Table 9.2. The surface area of the canard is 17.7 m^2 which is around 13% of the main wing area. Furthermore, this canard area results in a c.g. travel limit of 16.69 m - 22.7 m. The stability derivative C_{m_α} is calculated from Equation (9.7) and has a value of -0.41 per radian. This lies within the typical range of -0.3 to -1.5 [45] and indicates the Starling 9000 is longitudinally stable.

$$\frac{S_c}{S} = \left(\overline{x}_{cg} - \overline{x}_{ac} + \frac{C_{m_{ac}}}{C_{L_{A-c}}}\right) \cdot \frac{C_{L_{A-c}}}{C_{L_c}} \left(\frac{V}{V_c}\right)^2 \cdot \frac{\overline{c}}{l_c} \tag{9.5}$$

$$\frac{S_c}{S} = \left(\overline{x}_{cg} - \overline{x}_{ac} + S.M.\right) \frac{C_{L_\alpha}}{C_{L_{\alpha_c}}} \frac{1}{1 - \frac{\mathrm{d}\varepsilon}{\mathrm{d}\alpha}} \left(\frac{V}{V_c}\right)^2 \cdot \frac{\overline{c}}{l_c} \tag{9.6}$$

$$C_{m_\alpha} = C_{L_{A-c}} \left(\bar{x}_{ac_{A-c}} - \bar{x}_{cg}\right) - C_{L_{\alpha_c}} \eta_h \frac{Sh}{S} \left(\frac{l}{\bar{c}} - \bar{x}_{ac_{A-c}}\right)\left(1 - \frac{\mathrm{d}\varepsilon}{\mathrm{d}\alpha}\right) \tag{9.7}$$

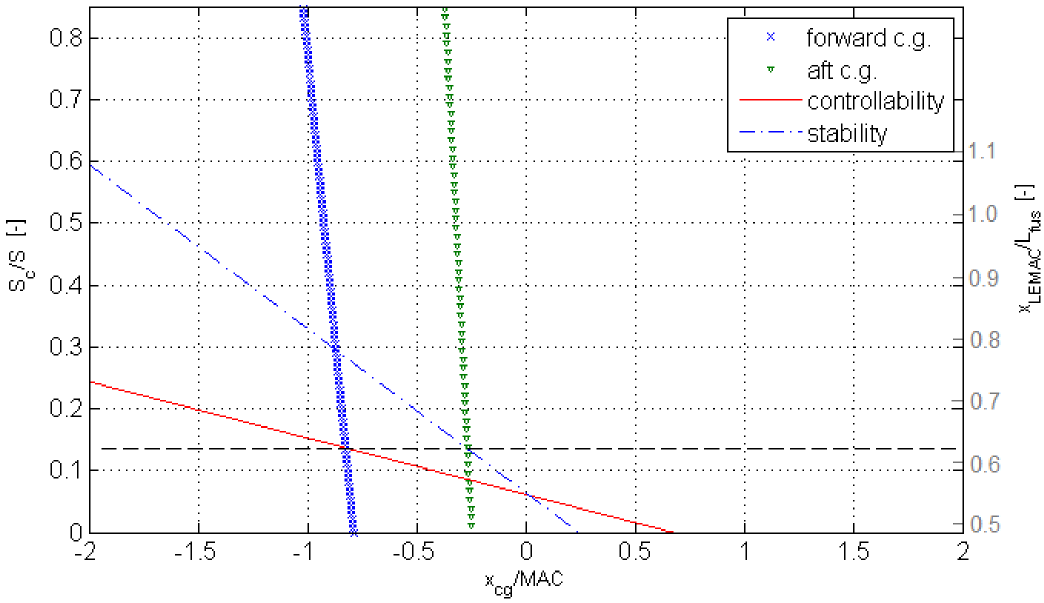

Figure 9.3: Scissor plot and c.g. plot to determine canard surface and wing position

Table 9.2: Output parameters for wing positioning and canard sizing

	Symbol	Value	Unit
Location of LEMAC	x_{LEMAC}	23	[m]
Location of the root of the wing	-	20.4-27.41	[m]
Ratio between canard and wing areas	S_c/S	0.13	-
Canard area	S_c	17.7	$[m^2]$
Canard span	b_c	12.26	[m]
Canard aspect ratio	AR_c	8.5	-
Aerodynamic centre position from nose	x_{ac}	24.02	[m]
Pitching moment coefficient at aerodynamic centre	$C_{m_{ac}}$	-0.1775	-
Pitching moment derivative	C_{m_α}	-0.41	$[\frac{1}{rad}]$
Front c.g. limit	x_{cg_f}	19.7	[m]
Back c.g. limit	x_{cg_b}	22.7	[m]

9.1.2 Winglet Design

The two winglets of the Starling 9000 double as vertical stabilisers and are the most important contributors to maintaining directional stability. Specifically, a balance must be found between the winglet area and moment arm. Since the aircraft is symmetrical in the "xz" plane its directional trim is naturally maintained. Because the winglets are located behind the c.g., the lift on the winglet generates a stabilising yawing moment about the z-axis, helping to maintain directional trim and contribute positively to the directional stability. The preliminary evaluation of the directional stability is applied through the winglet tail volume coefficient $\bar{V}_v$ as outlined in [45].

$$\bar{V}_v = \frac{l_v S_v}{bS} \tag{9.8}$$

where l_v is the distance between the winglet aerodynamic centre and the wing/fuselage aerodynamic centre. The directional stability derivative (C_{n_β}) of the Starling 9000 is approximated by Equation (9.9).

$$C_{n_\beta} \approx C_{n_{\beta_v}} = K_{f1} C_{L_{\alpha v}} \eta_v \frac{l_v S_v}{bS} \tag{9.9}$$

Where $C_{L_{\alpha v}}$ denotes the winglet lift curve slope, and η_v is the dynamic pressure ratio at the winglet. K_{f1} represents the contribution of the fuselage to the aircraft C_{n_β}. For a statically directionally stable aircraft, C_{n_β} should be positive. A higher value of C_{n_β} implies a more directionally stable aircraft. The Starling 9000 has a positive directional derivative of 0.139 (stable) which is within the typical range of 0.05 to 0.4 [45]. The complete results of the winglet design are presented in the Table 9.3.

Table 9.3: Output parameters from winglet sizing

	Symbol	Value	Unit
Volume coefficient of winglet	$\bar{V}_v$	0.03	-
Moment arm	l_v	5.73	[m]
Area of one winglet	S_v	11.034	[m^2]
Height of the winglet	b_v	4.06	[m]
Root chord of the winglet	c_{v_r}	3.3	[m]
Tip chord of the winglet	c_{v_t}	2.135	[m]
Taper ratio of the winglet	λ	0.647	-
MAC of the winglet	$\bar{c}_v$	2.72	[m]
Directional stability derivative	C_{n_β}	0.139	[$\frac{1}{rad}$]

9.1.3 Aileron sizing

The primary function of the ailerons is to provide a rolling moment such that the aircraft can bank. The size and span-wise location of the ailerons determine their effectiveness in creating this moment. Placing the ailerons further outboard increases the control moment arm, but also the added moment experienced by the wing structure. Additionally, placing the ailerons further outboard leads to a decrease in the aileron chord and thus the span-wise extent of the ailerons must be increased to preserve the aileron area. This increase in aileron span may have a negative impact on the space available for trailing edge high-lift devices. To mitigate the increase in bending moment, the Starling 9000 will use split ailerons similar to those on the A380.

The aircraft will also have two sets of ailerons; outboard ailerons for low-speed manoeuvring, and inboard ailerons for cruise, see Fig. 9.4. Spoilers which are used for lift dumping on the tarmac in order to achieve the 2000 m landing distance requirement, may also used as spoilerons during low-speed operation. Deflecting a spoiler disturbs the flow on the top-side of the wing, causing a reduction in lift. As a result the wing drops and the aircraft rolls. On the other hand, ailerons function by increasing or decreasing the effective camber of the local aerofoil. This causes an asymmetric lift distribution and an unbalanced rolling moment.

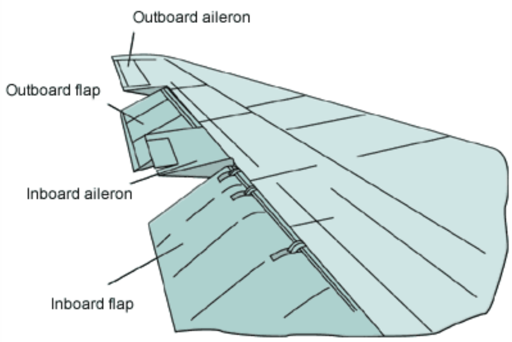

Figure 9.4: Picture indicating the location of the inward (high speed) and outward (low speed) ailerons

The deflection of the ailerons also causes asymmetric drag which leads to adverse yaw. Future design efforts should also consider the risk of control reversal on the ailerons. This may occur when the torsional stiffness of the wing being insufficient and a downward deflection of the ailerons causing the angle of attack of the wing to decrease to the point that it produces less lift, rather than more. Aileron deflection may also cause flutter as it produces a combination of torsional and bending loads. A flutter instability analysis should be carried out both computationally and in a wind-tunnel setting.

9.1.4 Elevator Sizing

Longitudinal control is a fundamental requirement for a safe flight. The Starling 9000 business jet achieves longitudinal through deflection of elevator located on the trailing edge of the canard. The preliminary design of the elevator mainly deals with the following four parameters: elevator planform area, elevator chord, elevator span, and lastly the maximum elevator deflection.

Take-Off Rotation Requirement

The most critical elevator design requirement is sizing for take-off rotation. Specifically, the elevator must increase the camber of the canard enough for the aircraft to rotate about the main gear and the nose to lift at a pre-specified angular pitch acceleration. This requirement should be satisfied for the case where the centre of gravity is at the forward-most limit. A typical value for the pitch acceleration was taken from [45] and is equal to $\ddot{\theta} = 8$ $[deg/s^2]$ at the rotation speed of 1.3 stall speed. Additionally [45] states that a common value for the maximum downward deflection of the elevator to be 25°. Lastly, for ease of calculation as a value of 1 was chosen for the elevator span-to-canard span ratio. This may be further iterated in the more detailed design phases in the future. The diagram in Fig. 9.5 illustrates all forces and moments contributing to the pitch-up moment about the main gear during the take-off rotation. The three corresponding governing equations of motion are given in Equations (9.10) to (9.12).

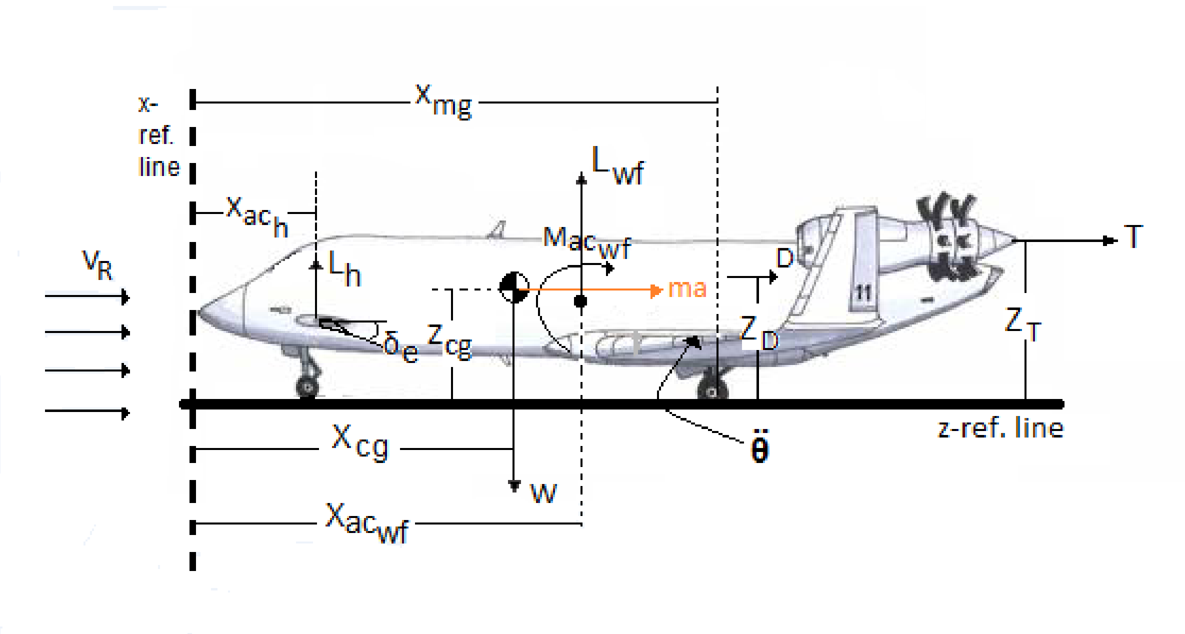

Figure 9.5: Forces and moments during take-off rotation for Starling 9000

$$\sum F_x = T + D + F_f = ma \tag{9.10}$$

$$\sum F_z = L_{wf} + L_c + N = W \tag{9.11}$$

$$\sum M_{cg} = -W(x_{mg} - x_{cg}) + D \cdot z_D + T \cdot z_T + L_{wf}(x_{mg} - x_{ac_{wf}}) + M_{ac_{wf}} + L_h(x_{mg} - x_{ac_c}) + ma \cdot z_{cg} = I_{yy}\ddot{\theta} \tag{9.12}$$

The elevator-to-canard chord ratio C_E/C_H is determined by the corresponding angle of attack effectiveness of the elevator which is calculated from:

$$\tau_e = \frac{\alpha_h + \frac{C_{L_c}}{C_{L\alpha_c}}}{\delta_{E_{max}}} \tag{9.13}$$

This results in C_E/C_H of 0.400. The most relevant input and output of the calculations for take-off rotation are presented in Table 9.4:

Table 9.4: Parameters for the sizing of the elevator during take-off rotation

	Symbol	Value	Unit
Take-off pitch angular acceleration	$\ddot{\theta}$	8.00	$[deg/s^2]$
Desired maximum down-deflection of the elevator	$\delta_{e_{max}}$	25.0	degree
Aircraft linear acceleration at the time of take-off rotation	a	3.62	$[m/s^2]$
Thrust of the operative engine	T	79704	[N]
Angle of attack effectiveness of the elevator	τ_e	0.605	[-]
Elevator-to-canard span ratio	b_E/b_h	1.00	[-]
Elevator-to-canard chord ratio	c_E/c_h	0.400	[-]

Longitudinal trim requirement

The elevator and elevator tabs enable the Starling 9000 to be longitudinally trimmed at various flight conditions. The governing longitudinal trim equations for the aircraft while cruising with a constant speed can be written as functions of stability derivatives:

$$C_{L_0} + C_{L_\alpha}\alpha + C_{L_{\delta_E}} = \frac{W}{\bar{q}\cdot S} = C_{L_1} \tag{9.14}$$

$$C_{m_0} + C_{m_\alpha}\alpha + C_{m_{\delta_E}} = \frac{T\cdot z_T}{\bar{q}\cdot S\cdot\bar{c}} \tag{9.15}$$

C_{L_1} is the steady-state aircraft lift coefficient at the cruising flight. The elevator deflection to maintain the aircraft longitudinal trim can be obtained directly from Equation (9.17). For the calculation, both the most aft aircraft centre of gravity and the most forward centre of gravity are considered. Fig. 9.6 shows the elevator deflection needed to maintain longitudinal trim with respect to aircraft speed in clean configuration. The maximum upward elevator deflection is found to be -7.7°. Therefore:

$$\delta_{E_{max_{down}}} = +25deg \qquad \delta_{E_{max_{up}}} = -7.7deg \tag{9.16}$$

$$\delta_E = \frac{\left(\frac{T\cdot z_T}{\bar{q}\cdot S\cdot\bar{c}} + C_{m_0}\right)C_{L_\alpha} + \left(C_{L_1} - C_{L_0}\right)C_{m_\alpha}}{C_{L_\alpha}C_{m_{\delta_E}} - C_{m_\alpha}C_{L_{\delta_E}}} \tag{9.17}$$

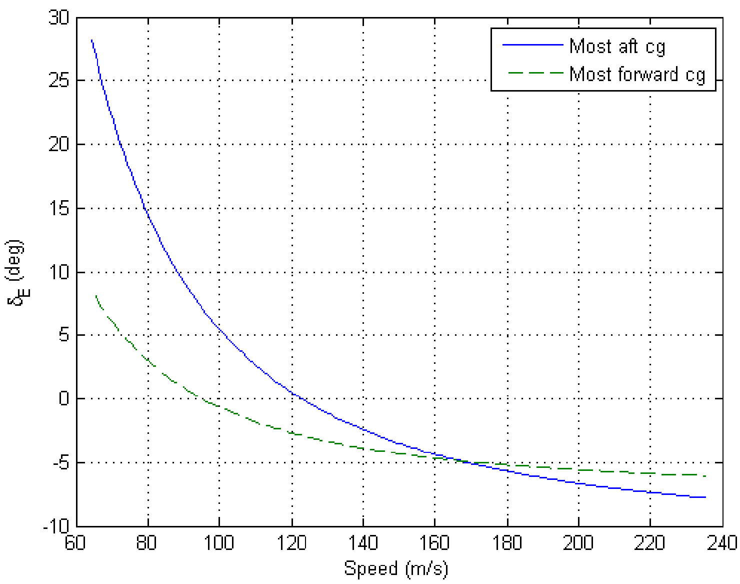

Figure 9.6: Variations of elevator deflection with respect to aircraft speed

9.1.5 Rudder sizing

The design requirements of the rudder are mainly driven by directional control and directional trim. The most critical case for the rudder sizing has been identified as a cross-wind landing. However, the situation of single engine inoperative case is considered. The main rudder parameters to be designed are the rudder chord (C_R), rudder span (b_R), and rudder area (S_R). These are defined in Fig. 9.7. The maximum rudder deflection is set to 30°. This is a typical value found for similar aircraft in [45]. To maintain the aircraft directional stability, the static directional derivative C_{n_β} must be positive.

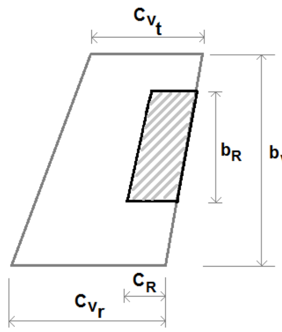

Figure 9.7: Parameters of the rudder geometry for the Starling 9000

Cross-Wind Landing

The most critical directionaly stability case for an aircraft with fuselage mounted engines is the cross-wind landing [45]. Furthermore, every general aviation aircraft must be able to carry out a successful landing for up to 25 knots of cross-wind at 90-deg to the approach path [45]. During an approach in cross-wind the rudders are used to counteract the destabilising yawing moment created by the wind acting on the fuselage, wing, and canard. The deflection of the rudder produces both a yawing moment and side force. The equilibrium of forces and moments governing the flight path during a crabbed landing are [45]:

$$\frac{1}{2}\rho {V_T}^2 Sb\left(C_{n_0} + C_{n_\beta}(\beta-\sigma) + C_{n_{\delta R}}\delta_R\right) + F_w \cdot d_c \cos\sigma = 0 \tag{9.18}$$

$$\frac{1}{2}\rho {V_W}^2 S_s C_{D_y} - \frac{1}{2}\rho {V_T}^2 S\left(C_{y_0} + C_{y_\beta}(\beta-\sigma) + C_{y_{\delta R}}\delta_R\right) = 0 \tag{9.19}$$

Aircraft sideslip derivatives C_{n_β} and C_{y_β} are calculated by:

$$C_{n_\beta} = K_{f1} C_{L_{\alpha_V}}\left(1 - \frac{\mathrm{d}\sigma}{\mathrm{d}\beta}\right)\eta_V \frac{l_{V_t} S_V}{bS} \tag{9.20}$$

$$C_{y_\beta} = K_{f2} C_{L_{\alpha_V}}\left(1 - \frac{\mathrm{d}\sigma}{\mathrm{d}\beta}\right)\eta_V \frac{S_V}{S} \tag{9.21}$$

The two rudder control derivatives $C_{y_{\delta R}}$ and $C_{n_{\delta R}}$ are calculated from Equation (9.22).

$$C_{y_{\delta R}} = C_{L_{\alpha_V}} \eta_V \tau_r \frac{b_R}{b_V}\frac{S_V}{S} \qquad C_{n_{\delta R}} = -C_{L_{\alpha_V}} V_V \eta_V \tau_r \frac{b_R}{b_V} \tag{9.22}$$

Table 9.5 presents the results of the rudder sizing. Most importantly, it should be noticed that the maximum rudder deflection needed in the cross wind loading is lower than the maximum allowable deflection of 30° found in [45]. As such, the Starling 9000 is able to land safely in 25 knots of cross-wind.

Table 9.5: Output parameters from the sizing of the rudders for cross-wind landing

	Symbol	Value	Unit
Chord length of the rudder	C_R	0.92	[m]
Height of the rudder	b_R	3.25	[m]
Area per rudder	S_R	3.00	$[m^2]$
Side-slip angle during cross wing landing	β	9.32	degree
Aircraft side force produced by the cross-wind	F_w	7230	[N]
Static directional derivative	C_{n_β}	0.186	$[\frac{1}{rad}]$
Side-slip derivative	C_{y_β}	-0.920	$[\frac{1}{rad}]$
Rudder control derivative	$C_{y_{\delta_R}}$	0.326	$[\frac{1}{rad}]$
Rudder control derivative	$C_{n_{\delta_R}}$	-0.0621	$[\frac{1}{rad}]$
Rudder deflection angle	δ_R	28.7	degree

Asymmetric thrust

The Starling 9000 should be able to achieve directional trim in the case of failure of one of the open rotor engines, i.e. if one of the engines is inoperative. The rudders must have enough authority to overcome the yawing moment produced by the asymmetric thrust arrangement. Since the engines of the Starling 9000 are mounted close to the centre-line, this operational condition is less critical than for conventional airliners with wing-podded engines, or cross-wind landing. In order to comply with FAR regulations, a multi-engine aircraft should be directionally controllable at a critical speed referred to as the minimum controllable speed V_{MC}. This speed may not exceed 1.13 [sic] stall speed [45] at the most unfavourable c.g. position. Assuming the ailerons are not deflected and the side-slip angle is zero, the required rudder deflection for directional trim is found using the Equation (9.23). The input and output values are summarised in the Table 9.6. It is again found that the rudder deflection is less than the maximum allowable deflection of 30°. Therefore the rudder size is sufficient to trim the aircraft in case of asymmetric thrust caused by a single engine being in-operative.

$$\delta_R = \frac{T_L y_T}{-qSbC_{n_{\delta_R}}} \tag{9.23}$$

Table 9.6: Parameters for rudder deflection during asymmetric thrust

	Symbol	Value	Unit
Thrust of the operative engine	T_L	7420	[kN]
Engine location form the fuselage center line	y_L	3.90	[m]
Minimum controllable speed	V_{mc}	50.7	[m/s]
Rudder control derivative	$C_{n_{\delta_R}}$	-0.0621	$[\frac{1}{rad}]$
Rudder deflection to balance the asymmetric thrust	δ_R	20.07	degree

9.2 Dynamic Stability

For a canard aircraft such as the Starling 9000, the dynamic and static stability is critical during the approach phase of the mission. To validate the performance during this critical phase, the aerodynamic stability derivatives of the wing-body-tail configuration were evaluated using USAF DATCOM [11] and XFLR5 software. For the DATCOM assessment the basic geometry of the aircraft, including the selected aerofoil, was used as an input in the form of a text file. However, during the time of development of the DATCOM method in the 1970s [11] winglets were not yet a common design feature and are not present in the implementation of the software. Instead, an equivalent vertical tail had to be used. This tail was defined to have the same tail volume as the winglets, allowing it to mimic the performance of the winglets as best as possible. Additionally, the surface area and aspect ratio of the winglets was preserved in order to maintain accuracy of the friction and induced drag components due to the winglets. The equivalent tail is shown in Fig. 9.8 along with the rest of the simulation geometry. DATCOM has allowed the estimation of the following aerodynamic and stability coefficients/derivatives for the approach phase:

- C_L Lift coefficient
- C_D Drag coefficient

- C_m Pitching moment coefficient
- C_N Normal force coefficient
- C_A Axial force coefficient
- $C_{L\alpha}$ Lift curve slope
- $C_{m\alpha}$ Pitching moment curve slope
- $C_{Y\beta}$ Derivative of side-force coefficient with respect to sideslip angle
- $C_{n\beta}$ Derivative of yawing-moment coefficient with respect to sideslip angle
- $C_{l\beta}$ Derivative of rolling-moment coefficient with respect to sideslip angle

The values of the Starling 9000 stability coefficients from the DATCOM simulation are listed in Fig. 9.9. In order to verify that the values produced by the DATCOM method for the Starling 9000 are realistic, these were compared against stability coefficients of the B737 as obtained using DATCOM. The input parameters defining the B737 were copied from the user manual [11], and the results of the analysis are shown in Fig. 9.10. Fig. 9.9 and Fig. 9.10 show that the Starling 9000 and the Boeing 737 have quite comparable stability derivatives. All stability derivatives except for the $C_{m\alpha}$ have the same order of magnitude. This, however, is to be expected given the fact that the Starling 9000 has a canard configuration, which is typically less stable in pitch compared to traditional configurations. The simulated value of $C_{m\alpha}$ for the Starling 9000 is nonetheless negative, indicating a statically stable aircraft. To evaluate the longitudinal dynamic stability of the aircraft as well, a time-series simulation and modal analysis were performed in Section 9.2.1. Moreover, in the lateral stability direction the DOTCOM simulation showed the stability of the Starling 9000 to be comparabale to a 737 as well. Specifically, the C_{N_β} represents the weather vane stability moment generated by the winglets under an impulse of side-slip. While Fig. 9.9 shows the conventional tail of the 737 outperforming the Starling winglets by 18% in terms of static yaw stability, the dynamic behaviour of the aircraft is not only dependent on the value of the moment coefficients but also on the mass moments of inertia of the aircraft. The placement of the engines on the Starling 9000 is closer to the aircraft centre of gravity than on the 737. This means that the lower yawing moment coefficient produced by the winglets may be compensated for by a lower mass moment of inertia about the yawing axis due to the favourable placement of the engines. In order to better understand the stability behaviour of the Starling 9000 on a qualitative level, a dynamic time-series simulation is highly beneficial and therefore presented in Section 9.2.1.

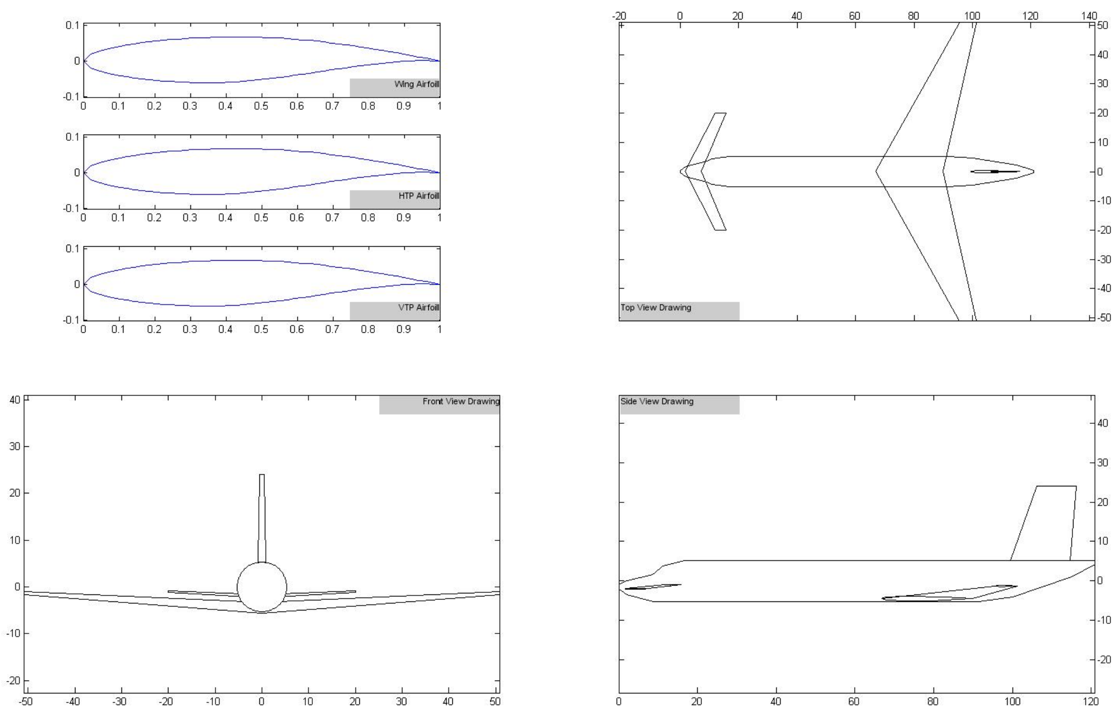

Figure 9.8: DATCOM geometry with vertical tail instead of winglets

AUTOMATED STABILITY AND CONTROL METHODS PER APRIL 1976 VERSION OF DATCOM
CHARACTERISTICS AT ANGLE OF ATTACK AND IN SIDESLIP
WING-BODY-VERTICAL TAIL-HORIZONTAL TAIL CONFIGURATION
----- STARLING -----

FLIGHT CONDITIONS						REFERENCE DIMENSIONS				
MACH NUMBER	ALTITUDE	VELOCITY	PRESSURE	TEMPERATURE	REYNOLDS NUMBER	REF. AREA	REFERENCE LENGTH LONG.	REFERENCE LENGTH LAT.	MOMENT REF. CENTER HORIZ	MOMENT REF. CENTER VERT
	FT	FT/SEC	LB/FT**2	DEG R	1/FT	FT**2	FT	FT	FT	FT
0.180	1500.00	199.90	2.0040E+03	513.321	2.5850E+07	1463.000	121.000	101.800	67.900	0.000

ALPHA	CD	CL	CM	CN	CA	CLA	CMA	CYB	CNB	CLB
						DERIVATIVE (PER DEGREE)				
-3.5	0.014	-0.062	0.0135	-0.063	0.011	8.913E-02	-3.639E-03	-2.002E-02	3.786E-03	-3.314E-03
-3.0	0.014	-0.017	0.0116	-0.018	0.013	9.025E-02	-3.784E-03			-3.330E-03
-2.5	0.013	0.028	0.0097	0.027	0.015	9.000E-02	-3.666E-03			-3.346E-03
-2.0	0.013	0.073	0.0079	0.073	0.016	8.908E-02	-3.442E-03			-3.362E-03
-1.5	0.014	0.117	0.0062	0.117	0.017	8.882E-02	-3.335E-03			-3.379E-03
-1.0	0.015	0.162	0.0046	0.162	0.018	9.119E-02	-3.621E-03			-3.396E-03
-0.5	0.017	0.208	0.0026	0.208	0.019	9.385E-02	-3.940E-03			-3.413E-03
0.0	0.019	0.256	0.0006	0.256	0.019	9.422E-02	-3.919E-03			-3.431E-03
0.5	0.023	0.303	-0.0013	0.303	0.020	9.406E-02	-3.831E-03			-3.448E-03
1.0	0.027	0.350	-0.0032	0.350	0.021	9.478E-02	-3.881E-03			-3.466E-03
1.5	0.031	0.397	-0.0052	0.398	0.021	9.547E-02	-3.933E-03			-3.485E-03
2.0	0.037	0.445	-0.0072	0.446	0.021	9.610E-02	-3.981E-03			-3.503E-03
2.5	0.043	0.493	-0.0092	0.495	0.022	9.667E-02	-4.026E-03			-3.521E-03
3.0	0.050	0.542	-0.0112	0.544	0.022	9.716E-02	-4.069E-03			-3.540E-03
4.0	0.067	0.640	-0.0153	0.643	0.022	9.834E-02	-4.116E-03			-3.577E-03
6.0	0.111	0.839	-0.0235	0.846	0.022	1.012E-01	-4.106E-03			-3.653E-03
8.0	0.166	1.045	-0.0317	1.057	0.019	9.924E-02	-4.006E-03			-3.732E-03
10.0	0.229	1.236	-0.0396	1.257	0.011	8.560E-02	-2.861E-03			-3.786E-03
12.0	0.291	1.387	-0.0432	1.417	-0.004	6.724E-02	-9.672E-04			-3.774E-03
14.0	0.344	1.505	-0.0434	1.544	-0.030	5.080E-02	6.865E-04			-3.711E-03

Figure 9.9: DATCOM results for the Starling jet

AUTOMATED STABILITY AND CONTROL METHODS PER APRIL 1976 VERSION OF DATCOM
CHARACTERISTICS AT ANGLE OF ATTACK AND IN SIDESLIP
WING-BODY-VERTICAL TAIL-HORIZONTAL TAIL CONFIGURATION
----- B737 -----

FLIGHT CONDITIONS						REFERENCE DIMENSIONS				
MACH NUMBER	ALTITUDE	VELOCITY	PRESSURE	TEMPERATURE	REYNOLDS NUMBER	REF. AREA	REFERENCE LENGTH LONG.	REFERENCE LENGTH LAT.	MOMENT REF. CENTER HORIZ	MOMENT REF. CENTER VERT
	FT	FT/SEC	LB/FT**2	DEG R	1/FT	FT**2	FT	FT	FT	FT
0.180	1500.00	199.90	2.0040E+03	513.321	2.5850E+07	1329.900	14.300	93.000	41.300	0.000

ALPHA	CD	CL	CM	CN	CA	CLA	CMA	CYB	CNB	CLB
						DERIVATIVE (PER DEGREE)				
-3.5	0.017	-0.217	0.2205	-0.217	0.004	7.371E-02	-4.256E-02	-1.668E-02	3.016E-03	-2.417E-03
-3.0	0.016	-0.180	0.2000	-0.180	0.006	7.333E-02	-4.092E-02			-2.424E-03
-2.5	0.015	-0.143	0.1796	-0.144	0.009	7.306E-02	-4.056E-02			-2.431E-03
-2.0	0.014	-0.107	0.1594	-0.107	0.011	7.271E-02	-4.017E-02			-2.437E-03
-1.5	0.014	-0.070	0.1394	-0.071	0.012	7.236E-02	-4.255E-02			-2.443E-03
-1.0	0.013	-0.034	0.1169	-0.035	0.013	7.207E-02	-3.946E-02			-2.448E-03
-0.5	0.013	0.002	0.1000	0.001	0.013	7.205E-02	-3.646E-02			-2.453E-03
0.0	0.013	0.038	0.0804	0.038	0.013	7.225E-02	-3.900E-02			-2.458E-03
0.5	0.013	0.074	0.0610	0.074	0.013	7.249E-02	-3.885E-02			-2.462E-03
1.0	0.014	0.110	0.0416	0.110	0.012	7.273E-02	-3.882E-02			-2.467E-03
1.5	0.014	0.147	0.0221	0.147	0.010	7.300E-02	-3.894E-02			-2.472E-03
2.0	0.015	0.183	0.0026	0.184	0.008	7.324E-02	-3.912E-02			-2.477E-03
2.5	0.016	0.220	-0.0170	0.220	0.006	7.343E-02	-3.924E-02			-2.482E-03
3.0	0.017	0.257	-0.0366	0.257	0.003	7.360E-02	-3.938E-02			-2.487E-03
4.0	0.019	0.330	-0.0762	0.331	-0.004	7.379E-02	-3.967E-02			-2.497E-03
6.0	0.026	0.478	-0.1561	0.478	-0.024	7.378E-02	-4.023E-02			-2.516E-03
8.0	0.036	0.625	-0.2371	0.624	-0.052	7.327E-02	-4.083E-02			-2.532E-03
10.0	0.048	0.771	-0.3194	0.768	-0.087	6.778E-02	-3.965E-02			-2.544E-03
12.0	0.061	0.897	-0.3957	0.890	-0.126	5.654E-02	-3.697E-02			-2.524E-03
14.0	0.074	0.997	-0.4672	0.986	-0.169	4.429E-02	-3.460E-02			-2.466E-03

Figure 9.10: DATCOM results for the B737

9.2.1 Verification of Dynamic Stability and Recommendaitons

To verify the results of the DATCOM simulation and to understand the dynamic behaviour of the Starling 9000, a second analysis was performed using XFLR5. Fig. 9.11 shows the longitudinal eigenmotions (short period and phugoid). The short period can be though of as a response of the aircraft to an impulse input on the elevator, while the phugoid is a response to a step input on the elevator. As seen from Fig. 9.11, the short period shows a highly damped response, while the phugoid shows a slow, damped oscillation. As such, both the short-period and the phugoid behave as is typical of general aviation aircraft. From the root-locus plot in Fig. 9.13, the short period eigenvalues remain oscillatory and damped as the angle of attack of the aircraft increased. On the other hand, the phugoid eigenvalues are clustered very closely to the origin of the root-locus argand plane. Thus the phugoid may be classified as stable to marginally (un)stable, and even unstable in some instances. This slight phugoid instability is not considered problematic however, as the phugoid motion may be brought under control by the pilot with a minimum level of input.

The Fig. 9.12 shows the lateral eigenmotions of the Starling 9000. Specifically, the ones shown are the aperiodic roll and the Dutch roll. The results for the spiral motion have not been included in this report. This is due to the large time-scale of the spiral motion, which leads to inaccuracies in the numerical simulation. However, as can be surmised from the root-locus plot in Fig. 9.13, the eigenvalues of the spiral motion are clustered around the origin of the argand plane. The behaviour of the spiral motion is thus best described as marginally (un)stable. The Dutch roll is the response of the aircraft to a impulse in rudder input, while the aperiodic roll is a response to an step aileron input. The Dutch roll can be highly uncomfortable for the passengers and should be hihgly damped in a good design. In the case of the Starling 9000, the oscillation amplitude becomes significantly smaller after only two periods (about 4 seconds), and dies out nearly completely after 9 seconds. This result is quite realistic and may be improved further by the inclusion of a Dutch roll damper. Nowadays this is becoming a standardised piece of equipment on new aircraft. The root-locus plot in Fig. 9.13 shows that the Dutch roll remains oscillatory and damped as the operational angle of attack increases. Lastly, the aperiodic roll is indeed aperiodic as characterised by the eigenvalues in Fig. 9.13. These show that the eigenvalues for aperiodic roll only have a negative real part and are therefore stable and non-oscillatory. This behaviour is reflected in the roll rate almost instantly returning to a constant rate as expected. However, due to the nature of the numerical model the roll rate returns to zero, whereas in reality the value would be finite and non-zero. Additionally, as the angle of attack increases, the aperiodic roll becomes less damped but remains stable and aperiodic.

Overall, it has been verified that the Starling 9000 exhibits the desired dynamic stability characteristic both in the longitudinal and lateral modes. Future design efforts should aim to analyse a greater st of operational points such as cruise, take-off rotation, as well as the effect of flaps. Furthermore, the Dutch roll damper should be investigated and designed so as to minimise passenger discomfort. However, the true verification and validation of the aircraft's handling and stability characteristic should be performed through a comprehensive flight test campaign as well as aerodynamic model testing. The effect of fuel sloshing, and pumping should also be evaluated, and baffles should be installed in the tanks if necessary to prevent adverse effects to controllability and stability. Particularly during final approach, disturbances to the flight path due to fuel movement should be minimised.

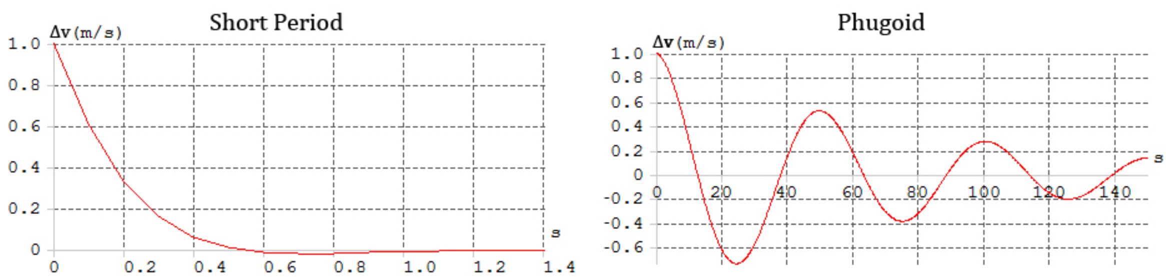

Figure 9.11: Longitudinal eigenmotion response (XFLR5): Short Period and Phugoid

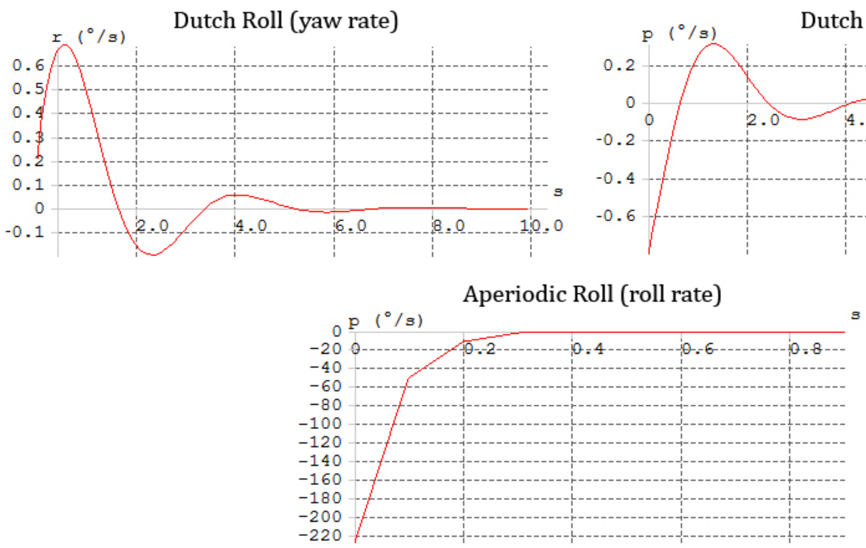

Figure 9.12: Lateral eigenmotion response (XFLR5):Aperiodic and Dutch Roll

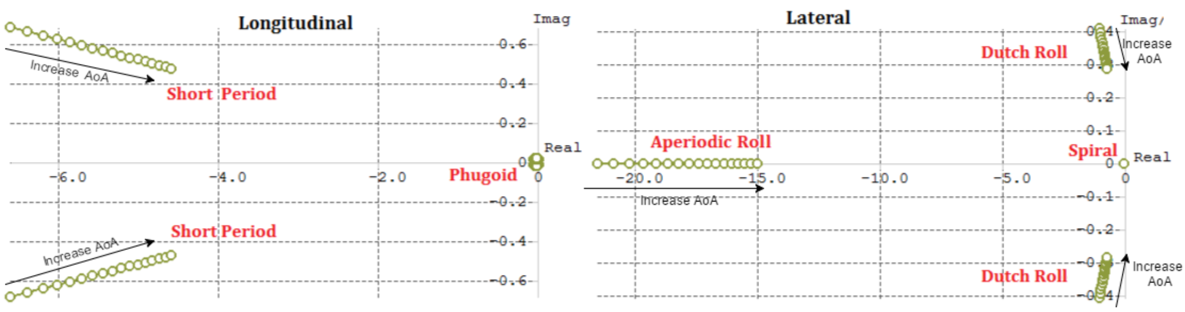

Figure 9.13: Root-locus plot for different longitudinal and lateral modes

10. Material Selection and Trade-off

The following section describes the reasoning behind the selected materials used in the design of the concept aircraft. The materials considered should have the optimal combination of strength, stiffness, density, maintainability, cost and sustainability. Within these parameters aluminium alloys and composites perform well and will thus be the main materials of interest [2]. Table 10.1 shows the materials considered in the trade-off with the properties [10] [1] [2] [3]. Sixty percent of the final composite volume is assumed to be fibres for this chapter and at least fifty percent of these fibres are in the critical stress direction of their respective location. Mainly the wing and the fuselage structures will be considered. These elements consist of skin stiffened with stiffeners which will be examined separately. Therefore different trade-off weights are assigned for stiffeners and skin as shown in Table 10.2. First the trade-off criteria and weights are discussed to aid in the selection of the appropriate materials.

Table 10.1: Material options

	Density ($\frac{g}{cm^3}$)	**Young's modulus** (GPa)	**Yield strength** (MPa)
Aluminium 2024-T851	2,78	72,4	400
Aluminium 6061-T913	2,70	69,0	455
Aluminium 7075-T651	2,81	71,7	503
Aluminium 7475-T651	2,81	71,7	510
Aluminium 2099-T83 (lithium)	2,64	78,6	490
High Modulus (HM) carbon[1]	1.56	118,8	1370
High strength (HS) carbon[1]	1.56	87,0	1680
Aramid[1]	1,34	33,0	880

[1] 50% of the fibres are in 0°direction and a 0.6 fibre volume fraction is assumed

Table 10.2: Trade off criteria and weights

	Stiffener	**Skin**
Specific stiffness	4	4
Specific strength	3	4
Sustainability	2	2
Maintainability	2	3
Cost efficiency	2	3

The specific stiffness and strength allow objective performance to weight analysis for stiffness and strength respectively. For both the stiffener and the skin stiffness is very important. For the stiffeners strength is less important because this will not dominate the design. Sustainability has to be kept in mind for both the skin and the stiffeners, sustainability can give an advantage to a material but should not be critical in the trade-off. The maintainability score represents how well maintenance and repairs can be performed. Because the stringers are hard to reach, they should be more durable and therefore requires less maintenance. Hence the lower weight for the stiffener maintainability compared to the skin. Cost is the final criteria and is as important to the manufacturer as to the costumer. Because of the durability requirement just imposed on the stringers, stringers are allowed to be more expensive than the skin, which is reflected by a lower weight for the cost efficiency criteria. The following section will describe how the materials under consideration perform for the selected trade-off criteria.

[1] URL http://www.aerospacemetals.com/aluminum-distributor.html [cited May 27 2016]
[2] URL http://www.composite-oracle.com/main.asp?q=123 [cited May 27 2016]
[3] URL http://www.alcoa.com/global/en/products/overview.asp?Product=Aerospace&Category=26&Query=&page=0 [cited May 27 2016]

10.1 Material Properties

Specific Material Indices

The factor that is used to minimise the total weight of a component is the specific material index for a given load case. The stiffeners and skin have specific strength and specific stiffness indices for bending.Section 11.4.1 The skin can be considered a plate with the thickness as design variable and the stiffeners can be considered to be beams with the cross sectional area as design variable. For these cases the specific material indices can be found to be as displayed in Table 10.3 [6]. A high value for these indices is preferable to minimise the weight of the respective component. Numerical values of the indices for the materials of interest are shown in Fig. 10.1. In the graph the metals are closely grouped compared to the composites with higher specific values. The specific properties of a composite sheet are determined by the fibre directions as specified above, whereas metals always have isotropic properties. The graph only displays the specific properties for stiffeners, for the skin the ordering of the specific properties is the same.

Table 10.3: Specific material indices

	Specific stiffness	Specific strength
Stiffener	$\frac{E^{\frac{1}{2}}}{\rho}$	$\frac{\sigma^{\frac{2}{3}}}{\rho}$
Skin	$\frac{E^{\frac{1}{3}}}{\rho}$	$\frac{\sigma^{\frac{1}{2}}}{\rho}$

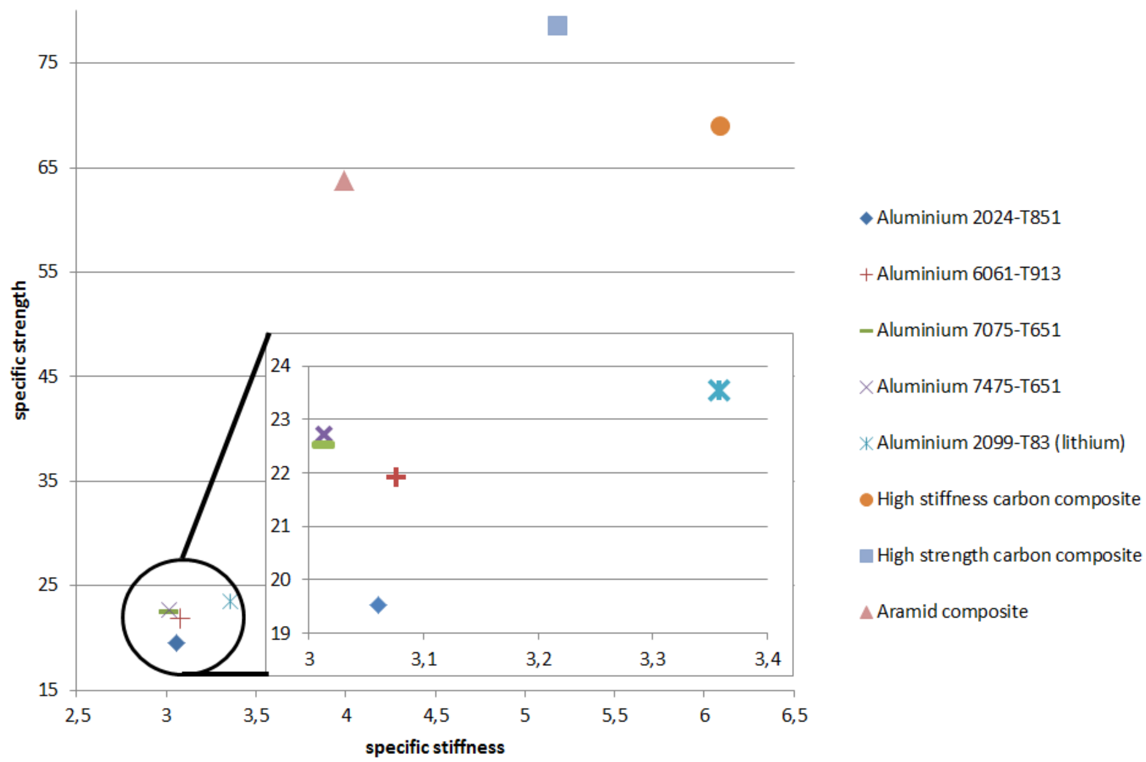

Figure 10.1: Specific strength property $\frac{\sigma^{\frac{2}{3}}}{\rho}$ for stiffeners

Maintainability

Maintenance is approximately 20% of the operational cost, as shown in Section 13.2, minimising this cost is important to the customers. Furthermore simple maintenance and easy to repair materials and components require less expertise and thus improve safety. For metals there exists a wide range of visual methods for inspection, for carbon fibre reinforced plastics (CFRP) inspection extra equipment is often a necessity as damage often occurs internally and is not visible from the outside. The CFRP structures are less prone to fatigue but more susceptible to impact damage compared to metals [4]. If damage is perceived in a metal structure there are methods such as welding and riveting that produce a structure that is as strong as the original or even stronger [5]. These repair methods have been optimised for decades, repair methods for CFRP are more complicated and time consuming [6]. Since extra attention should be paid when removing the damaged part in case of the delamination of the surrounded areas, more time is demanded. Also it is critical to replace each damaged ply with a similar ply and ply orientation thus the process is complicated.

Sustainability
Aluminium is produced from ore and alloyed with other metals to produce the materials appropriate for the aerospace industry, the processing of the ore requiring a lot of energy. At the end of its useful life aluminium alloys can be remelted and refined, a large part of the present aluminium production being based on recycled scrap aluminium with only five percent material loss [7]. The high value of aluminium scarps combined with very low recycle cost compared to processed aluminium, make it a highly recyclable material with a low ecological footprint. Carbon fibres and the resin used for curing are oil based products, with chemical operations being employed in producing the high quality fibres used in the aerospace industry. Unlike metals there is not yet an efficient solution for recovering carbon fibres, most of the high grade composite parts are grind up to produce carbon fibre filler for less demanding applications[8]. Processes to extract the fibres as a whole from the resin exist but are not environment friendly nor very cost efficient [9]. The main sustainability advantages gained from composites are the good fatigue resistance and the reduced fuel consumption during its operational lifespan.

Cost efficiency
Most of the metals have a comparable price point compared to the composite materials, the metals are close to ten US dollar per kilogram with the aluminium 2099 lithium alloy as the most expensive. The composite materials are more expensive, up to ten times the cost of metals, although this has to be put into perspective as less mass of composite material is used to achieve the same properties in constructions and furthermore the fibres are mixed with resin which lowers the price as well. Indicative material pricing is given in Table 10.4. The manufacturing cost for the metals is generally high because of the high tooling and machinery cost, for high volume production this is no problem as the machinery improves automation and thus reduces cost over time with high production volume. Generally the total component cost for metal components is high for low volume. The manufacturing cost of the composites is highly dependent on the production method used and the production volume[10]. For low volume production and out of autoclave production the tooling cost for the carbon composites is low compared to the metals. The low automation level and high material cost dominate the total component cost and make composites more expensive than metals.

Table 10.4: Material cost per kilogram [11]

	Cost ($\frac{USD}{kg}$)
Aluminium 2024	8
Aluminium 6061	10
Aluminium 7075	8
Aluminium 7475	13
Aluminium 2099	40
High modulus carbon composite	70
High strength carbon composite	60
Aramid fibre	40

[4] URL http://www.boeing.com/commercial/aeromagazine/articles/qtr_4_06/AERO_Q406_article4.pdf [cited May 30 2016]
[5] URL https://www.faa.gov/regulations_policies/handbooks_manuals/aircraft/amt_airframe_handbook/media/ama_Ch04.pdf [cited May 30 2016]
[6] URL http://www.faa.gov/regulations_policies/handbooks_manuals/aircraft/amt_airframe_handbook/media/ama_ch07.pdf [cited May 30 2016]
[7] URL http://www.world-aluminium.org/media/filer_public/2013/01/15/fl0000181.pdf [cited May 31 2016]
[8] URL http://www.eucia.eu/userfiles/files/20130207_eucia_brochure_recycling.pdf [cited June 9 2016]
[9] URL http://www.boeingsuppliers.com/environmental/TechNotes/TechNotes2003-11.pdf [cited May 31 2016]
[10] URL https://www.infosys.com/engineering-services/white-papers/Documents/carbon-composites-cost-effective.pdf [cited June 9 2016]
[11] Expert consultation, J. Sinke, May 2016

10.2 Material Trade-off

In Table 10.5 the scores of the different materials are shown, because the scores are relative and for highly varying properties values there is not much distinction within the material categories. The metals show very similar scores and the carbons as well, aramid is in between the low scoring metals and the high scoring carbons. For the skin material the composite materials outperform the metals, because of the low production volume the metals do not provide enough cost advantage to compensate for the strength and stiffness offered by the carbon composites. High strength carbon again takes the lead over high modulus (high stiffness) carbon and high strength carbon will thus be used for the skin composite. The focus on stiffness and strength puts the composite materials forward with high strength carbon and high modulus carbon at the top. For the stiffeners the scores between the two carbon composites is especially close, stiffness is the dominating aspect in choosing the material for stiffener. It would be logical to use high modulus carbon for the stiffeners, but this would imply having different strains in a co-bonded wing. To avoid extra stresses, high stress carbon is used for the stringers.

Table 10.5: Tradeoff table for the stiffener and skin material

	Aluminium alloys					**Fibre reinforced plastics**		
	2024	**6061**	**7075**	**7475**	**2099**	**HM carbon**	**HS carbon**	**Aramid**
Specific stiffness	2	2	2	2	3	8	7	5
Specific strength	2	3	3	3	3	7	8	6
Sustainability	8	8	8	8	8	4	4	4
Maintainability	7	7	7	7	7	4	4	4
Cost efficiency	7	7	7	7	5	4	5	6
Stiffener score	**61**	**61**	**61**	**61**	**61**	**77**	**78**	**66**
Skin score	**78**	**78**	**78**	**78**	**76**	**92**	**95**	**82**

11. Structural Analysis

With safety as one of the main design philophies, the literal backbone supporting this criterion is the structural design of the aircraft. This conceptual design consists of the sizing of the major structural elements comprising the airframe of the Starling 9000. In Section 11.1, three critical load cases will be analysed, from which the most critical one will be chosen for design. In Section 11.2, the structural concept design for the wing and fuselage will be presented, and preliminary estimates for stringer, longeron, frame and rib spacing and spar inertia will be given. Then, in Section 11.3, a fuselage-wing model will be analysed for the chosen load case in the finite element modelling program Abaqus. Additionally, in Section 11.4, a verification of the finite element method will be done by a beam analysis of the wing and fuselage. Finally, Section 15.3.4 will elaborate on recommendations to improve the design and reduce structural weight.

11.1 Load Cases

If the aircraft is to fly its mission safely, it should be designed for the most critical load cases it will encounter on its mission. In the case of the chosen concept, three load cases are considered, listed in the sections below.

11.1.1 Load Case 1: High-g Manoeuvre at Cruise

The first load case under consideration is assumed to be the most critical one during cruise: a manoeuvre resulting in the ultimate load factor the aircraft should be able to sustain. The following assumptions hold for this case:

- The aircraft is flying at the beginning of cruise at cruise altitude
- The aircraft is executing a high-g manoeuvre at its ultimate load factor
- The fuel tanks are full
- The engines are producing maximum thrust
- The rudder is fully deflected
- The elevator is fully deflected
- The cabin is fully pressurised

The aircraft is flying at the beginning of cruise at cruise altitude:
This assumption implies values for density, temperature and pressure at an International Standard Atmospheric altitude of 40000 ft, or 12200 m. This gives an ambient air pressure of 19000 Pa, air density of 0.3 kg/m^3 and temperature of 217 K.
The aircraft is executing a high-g manoeuvre at its ultimate load factor:
This is likely the most critical assumption of this load case. The aircraft should be able to sustain its ultimate load factor, which is defined to be 1.5 times the maximum load factor the aircraft will ever experience in its lifetime. This implies a multiplication of the weight by 4.65 to obtain the lift, which the structure should be able to sustain. The lift in this case will be equal to 4.65 times the MTOW, or $2.42 \cdot 10^6$ N. The drag is determined from calculating the C_L from this lift force, with this the C_D from the drag polar, and then using the drag formula to find a total wing drag force of 64313 N.
The fuel tanks are full:
The load factor is defined as the ratio between lift and weight. For a given load factor, the most critical case is the highest weight, leading to the highest lift. Therefore, if the fuel tanks are assumed to be close to being full, the wing will experience the highest stress, even though this weight causes wing bending relief by acting opposite to the lift. The weight of the wings according to the class II weight estimation is 7730 kg. With a fuel mass of 23300 kg, assuming the fuel tanks in the wing are sufficient to hold all the fuel, the total weight causing wing bending relief is 31030 kg or $3.04 \cdot 10^5$ N. It is assumed that this weight is linearly distributed along the wing (linearly decreasing towards the tip). With the ultimate load factor of 4.65, the wing weight is equal to $1.51 \cdot 10^6$ N.
The engines are producing maximum thrust:
In order to fully envelop the most critical instantaneous but static load case, an additional force to be accounted for is the maximum thrust the engines can deliver, which is $1.48 \cdot 10^5 N$ in total. In addition to the

compressive load this will cause on the fuselage, the force will also cause a bending load due to the assumed offset from the centre line of the fuselage. It is assumed that this force is concentrated away from the fuselage structure.

The rudder is fully deflected:
For the same reason as for the engines, it is assumed that the rudder is fully deflected, leading to an additional bending, torsional and shear load in the wing, since the winglet that incorporates the rudder is placed at the tip of the main wing. Using an assumed maximum lift coefficient with deflected rudder of 2.0, using the winglet surface area of 11.034 m^2 and cruise density and speed, the lift force of each winglet is equal to $1.86 \cdot 10^5$ N.

The elevator is fully deflected:
In addition to the rudder, it is also assumed that the elevator is fully deflected. This will cause the canard to produce maximum lift, leading to a bending and shear load being introduced into the front section of the fuselage. From requirements, the total force the elevator must be able to generate during take-off is $6.99 \cdot 10^4$ N. Using the density at cruise altitude and take-off and the cruise and take-off speed, when scaled with a velocity difference of $(\frac{236}{84})^2$ and a density difference of $\frac{0.30}{0.97}$, the lift force the canard can generate at cruise is determined to be equal to $1.71 \cdot 10^5$ N

The cabin is fully pressurised:
The final assumption to be made is that the cabin is fully pressurised, meaning the internal pressure is equal to the pressure at an International Standard Atmospheric altitude of 4500 ft, or 85896.8 Pa. The pressure difference between the inside and outside of the fuselage causes longitudinal and circumferential normal stresses and is equal to 67143 Pa.

Load	Application	Magnitude	Distribution
Pressurisation	Fuselage skin	$6.71 \cdot 10^4 Pa$	Evenly distributed (conc. near windows)
Wing weight	Wing box	$1.51 \cdot 10^6$ N	Linearly distributed
Fuselage weight	Fuselage	$6.90 \cdot 10^5$ N	Evenly distributed
Wing lift	Wing box	$2.42 \cdot 10^6$ N	Elliptically distributed
Thrust	End of the fuselage	$1.48 \cdot 10^5$ N	Concentrated away from fuselage
Engine weight	End of the fuselage	$1.26 \cdot 10^5$ N	Concentrated away from fuselage
Wing Drag	Wing box	$6.43 \cdot 10^4$ N	Elliptically distributed
Winglet lift	End of the wing box	$1.86 \cdot 10^5$ N	Concentrated away from wing
Winglet weight	End of the wing box	$2.67 \cdot 10^4$ N	Concentrated away from wing
Canard lift	Front of the fuselage	$1.28 \cdot 10^5$ N	Concentrated away from fuselage
Canard weight	Front of the fuselage	$2.49 \cdot 10^4$ N	Concentrated away from fuselage

Table 11.1: Load case for a high-g manoeuvre during cruise

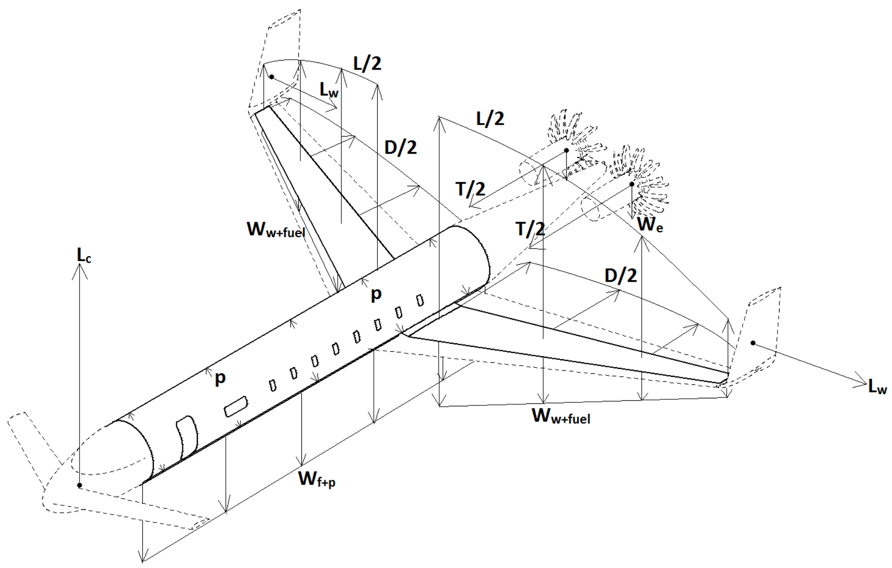

Figure 11.1: Free body diagram of the first load case

11.1.2 Load Case 2: Landing Impact

Another, more dynamic, critical load case that will be considered is the impact during touch-down while landing the aircraft. The following list of assumptions hold for this load case:

- Landing performed at maximum landing weight (MLW):
- The aircraft is touching down on only one main gear strut
- The wings are producing lift at maximum lift coefficient
- The engines are on idle
- The rudder is fully deflected
- The elevator is fully deflected
- Cabin pressure difference is neglected

Landing performed at maximum landing weight (MLW):
CS25 certifications regarding landing come in the form of sink rates which represent limit descent velocities. At the design landing weight, a limit descent velocity of 10 ft/s (3.05 m/s) is required. Based on reference aircraft data, a vertical descent velocity of 10 ft/s on a concrete runway is equivalent to a 2g impact load. The maximum landing weight is set as 0.9 times the the maximum takeoff weight and equals 47671 kg (468 kN). Taking into account the vertical impact load factor, a landing case design load of 935 kN is obtained.
The aircraft is touching down on only one main gear strut:
Due to the difficulty that is involved with landing an aircraft, especially during cross-wind landings, the aircraft will sometimes touch-down on only one strut, and often involve touch-down with a high-g loading on this strut. Additionally, during a cross-wind landing the aircraft is yawing into the direction of the wind in order to stay lined up with the airstrip. Just before touch-down, the pilot will yaw the aircraft back in order to line up the wheels to the flight/roll path. However, sometimes this is not done on time, meaning that the one strut that impacts the ground during landing will experience a significant torsional load that is caused by the wheels trying to line up with their roll path. This load is partly transferred to the wing, which will try to rotate the entire aircraft into the roll direction of the wheels.
The wings are producing lift at maximum lift coefficient:
For an aircraft to land, a pilot will try to maintain flight at low altitude above the runway for as long as possible by increasing angle of attack, while reducing airspeed. This is known as flaring. During touchdown, the flaps are fully deployed and wings are generating lift with maximum landing lift coefficient. This however, is not a critical scenario. The most critical case would be when the pilot does not flare, so when the touchdown speed is the same as the approach speed, given by CS25 specifications as 1.3 times the landing configuration stall speed. With a $C_{L_{max,land}}$ of 2.1, density taken as 1.2 kg/m^3 and lift equal to the maximum landing weight, the landing speed is 67.2 m/s, and the lift is equal to $7.9 \cdot 10^5$ N. Wing drag is neglected in this case.
The engines are on idle:
In order to maintain the required approach speed which is defined as 1.3 times the landing stall speed, it is assumed that the engines are on idle, meaning they do not generate any thrust.
The rudder is fully deflected:
For the aircraft to be able to land during cross-wind conditions, it should be able to withstand a full rudder deflection to yaw into the direction of the wind, or to yaw back just before touch-down to line the aircraft up with the direction of the runway. To analyse the most critical load case, the winglets are producing maximum lift. That lift is in this case equal to $6.1 \cdot 10^4$ N, assuming a maximum rudder deflected lift coefficient of 2.0, air density of 1.23 kg/m^3, landing velocity of 67.19 m/s (1.3 times the stall speed) and winglet surface area of 11.03 m^2.
The elevator is fully deflected:
As previously discussed, the pilot will pitch up the aircraft as far as possible. It is therefore assumed that the canard is also producing maximum lift, at the speed given as the approach speed previously determined. The lift is in this case equal to a scaling of velocity and density times the lift force the canard should be able to deliver during take-off:

$$L_c = \left(\frac{67.19}{84}\right)^2 \cdot \frac{1.23}{0.97} \cdot 6.99 \cdot 10^4 = 5.62 \cdot 10^4\ N \tag{11.1}$$

Cabin pressure difference is neglected:
As specified by requirements, the aircraft should be able to land at airfields at an altitude of 5000 ft. Since the cabin pressure is also specified to correspond to an altitude of 4500 ft or less, the difference in air pressure

between the outside and inside of the fuselage is neglected because the variance in standard air pressure is in the same order of magnitude as the difference between cabin and ambient air pressure.

Load	Application	Magnitude	Distribution
Wing+fuel weight	Wing box	$5.05 \cdot 10^5\ N$	Linearly distributed
Fuselage+payload weight	Fuselage	$2.46 \cdot 10^5\ N$	Evenly distributed
Wing lift	Wing box	$7.90 \cdot 10^5\ N$	Eliptically distributed
Canard lift	Front of fuselage	$5.62 \cdot 10^4\ N$	Concentrated away from fuselage
Canard weight	Front of fuselage	$1.07 \cdot 10^4\ N$	Concentrated away from fuselage
Engine weight	End of the fuselage	$7.17 \cdot 10^4\ N$	Concentrated away from fuselage
Winglet lift	End of the wing box	$6.10 \cdot 10^4\ N$	Concentrated away from wing
Winglet weight	End of the wing box	$1.15 \cdot 10^4\ N$	Concentrated away from wing
Landing gear reaction force	Wing box	T.B.D.	Concentrated behind wing box

Table 11.2: Load case during landing

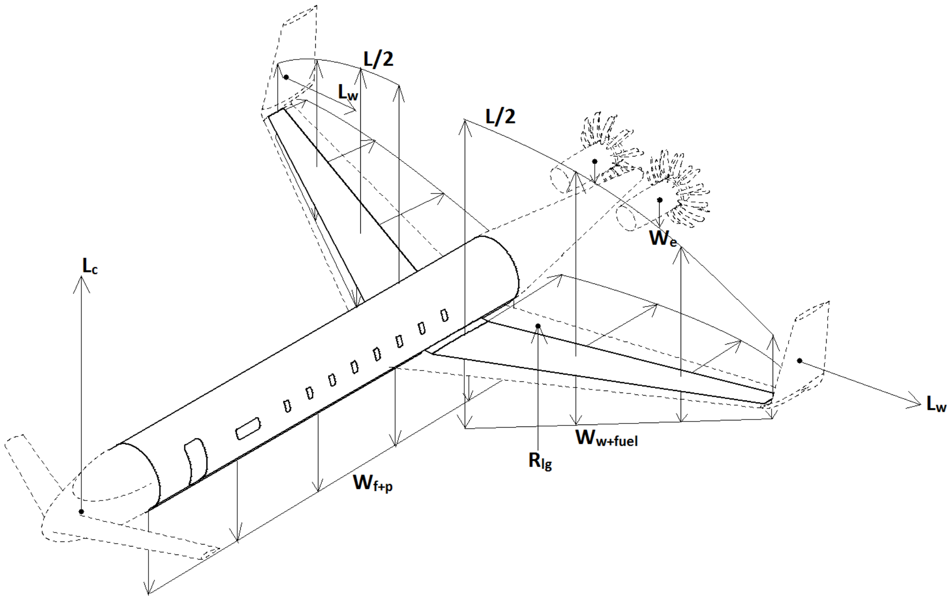

Figure 11.2: Free body diagram of the second load case

11.1.3 Load Case 3: Fatigue Life

In addition to obviously heavy load cases, the aircraft might fail well below the stresses induced by these cases. Fatigue stress is the maximum amplitude stress for a given material, loading frequency and load life.

- The aircraft experiences 1000 flight hours per year over a period of 25 years (Section 13.2)
- The main cyclic load on the fuselage is the pressurisation of the cabin
- The main cyclic load on the wing is lift at cruise

1000 flights per year over a period of 25 years:
The aircraft is estimated to fly for a period of 25 years. Using an estimated 1000 flight hours per year, and assuming the minimum average flight to take about 5 hours as a safety factor (an 8500 nm flight is around 20), the total number of loading cycles over the lifetime of the aircraft is 5000.
Pressurisation is main cyclic load on the fuselage:
The main cyclic load acting on the fuselage during flight is the pressurisation of the cabin. The maximum stress of all fuselage components should be lower than the fatigue stress of the material given the total number of cycles. The pressurisation load is the same as the value determined in Load Case 1.
Lift at cruise is main cyclic load on the wing:
While not as high as the above considered load cases, the maximum stress in the wing during normal cruise operation should be lower than the fatigue stress for the given number of cycles. The lift is calculated using the lift formula, a cruise C_L of 0.3944, cruise density of 0.302 kg/m^3 and a cruise speed of 236 m/s.

Load	Application	Magnitude	Distribution
Pressurisation	Fuselage skin	67143 Pa	Evenly distributed (conc. near windows)
Lift force (wing)	Wing box	$4.51 \cdot 10^5$ N	Elliptically distributed

Table 11.3: Load case for fatigue loading

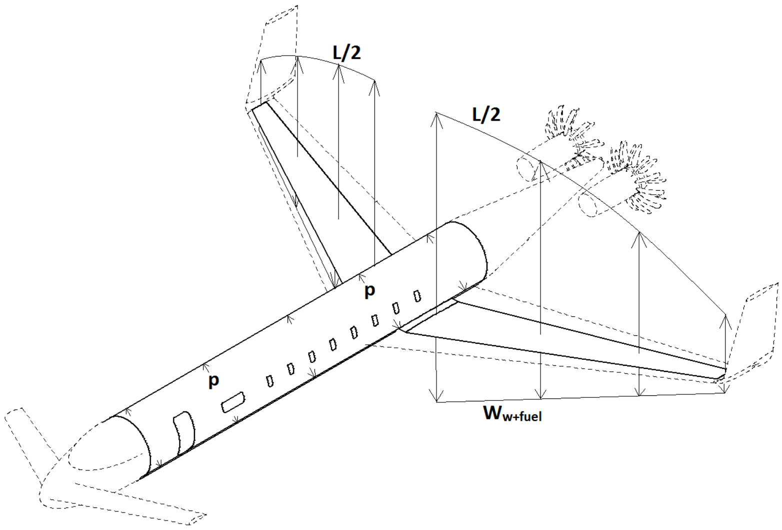

Figure 11.3: Free body diagram of the third load case

In most metals, fatigue failure is mostly dictated by crack growth due to cyclic loading. Composites however, exhibit many other fatigue failure modes like delamination and resin fracture, which are not yet well understood. As an initial fractured fibre 'crack initiation' does not affect the fibres close to it, propagation of cracks from fibre to fibre is a lot slower, if not non-existent. Because of this, composite laminates are usually more resistant to fatigue than their metal counterparts. This, combined with the fact that the number of cycles is relatively low (10^4) in comparison to the usual number of cycles a metal airliner sustains (10^5), it is assumed that fatigue loading will not be critical for this aircraft.

11.2 Structural Concept Design

In this section, the conceptual structural design of the wing and the fuselage will be presented. These concepts were chosen on the basis of reference aircraft and aircraft sections available in the aerospace material laboratory. To limit the scope of the structural analysis to be realistically time-bound, a semi-monocoque structure for both the fuselage and the wing is chosen due to the familiarity with the layout.

11.2.1 Wing Structural Design

With the materials that were determined for certain elements of the wing and some restrictions like high-lift devices limiting the space for structural components, a preliminary wing box structure was developed. It was assumed that this structure will carry all loads acting on the wing, and transfer them to several fuselage frames. The wing box consists of a typical configuration: Two spars limit the width of the box and will mainly sustain the shear loads introduced by the lift force. The height of the box is dictated by the wing profile which, together with longitudinally placed stringers, will carry the normal stresses caused by the bending moment introduced by the lift force. The skin and spars together will carry the shear loads introduced by the torsion that is caused by the lift. Furthermore, by adding stringers to the wing panels, the wing box is stiffened due to increased inertia, and the stringers carrying a significant portion of the normal stresses. Finally, ribs are added to the structure for several reasons: First, ribs with certain spacing with respect to each other will limit buckling by acting as buckling nodes. Secondly, ribs provide attachment points for external components like movable wing surfaces and the landing gear, and help to distribute the introduced shear load throughout the structure. Additionally, ribs may be used to seal separate fuel tank sections from each other. As an initial

design based on reference aircraft in the aircraft hall, the parameters specified in Table 11.4 were used as input for shape specific characteristics. Finally, there is a rib at the spanwise position of the angle discontinuity of the spars. This serves to distribute out of plane stresses that are introduced by the angle change.
The wing is integrated into the fuselage by means of a wing carry through structure. This structure features the same elements as the wing box, but its spars are positioned parallel to the fuselage frames. From an ergonomics point of view, it was important that the wing box would not be higher than the floor of the cabin. With a cabin height of 2.1 m, the available height for the wing carry through structure in the fuselage was 80 cm. To further strengthen the wing carry through structure, horizontal members were added to the fuselage frames directly supporting the wing. An illustration of this layout can be found in Fig. 11.4. Stringers are not yet included in this figure. Since it is assumed that the wing box carries all the loads, the sections of the chord in front and behind it are excluded from the analysis. Additionally, the winglet is not included in the structural analysis as it is not expected to be a critical area, implying the generated winglet lift can be represented as a concentrated force acting at the centre of pressure of the winglet.

Parameter	Value	Unit
Front spar x/c	0.15	-
Rear spar x/c	0.7	-
Wing box nr. of ribs	15	-
Wing root nr. of stringers top	15	-
Wing root nr. of stringers bottom	13	-
Wing carrythrough nr. of ribs	6	-
Stringer height	75	mm
Wing carrythrough nr. of frames	6	-
Frame height	150	mm

Table 11.4: Wing box shape parameters

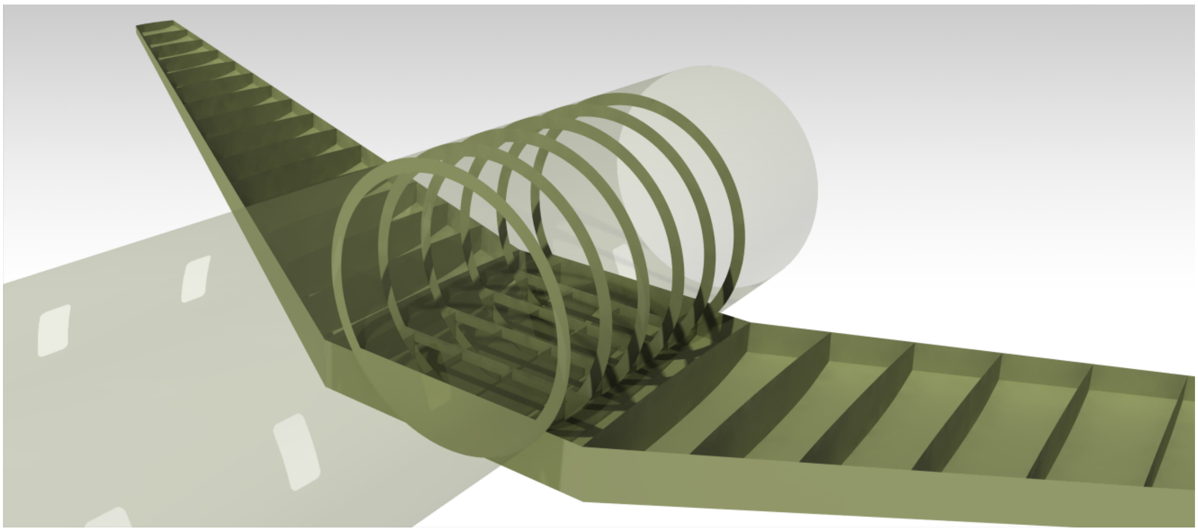

Figure 11.4: Chosen structural layout for the wing box

11.2.2 Fuselage Structural Design

The concept chosen for the fuselage structural layout is similar to the wing box layout. It is a semi-monocoque consisting of a load carrying outer skin, with supporting frame members which are longitudinally spaced. Stringers, or longerons, are spaced in circumferential direction and run along the entire length of the aircraft, except for areas where a cutout is present. These cutouts come in two variants: load carrying and non load carrying. The load carrying elements are the main door and the two emergency exits at the rear of the aircraft above the wing (two type III emergency exits specified by CS-25 regulations). The non load carrying cutouts are the windows. Since the aircraft design incorporates the large Skyview windows, special strengthening elements have to be added around the windows not only to reduce stress concentrations, but also to transfer the load acting through the frame intersecting the window to other frame members around it. Also, even though the fuselage door is load carrying, it intersects a fuselage frame as well, implying an additional structure around the door is required to transfer loads from the frames to other elements. The smaller windows were spaced with the same dimension as the fuselage frames, resulting that the windows were always in the middle of two fuselage frames. Detail views of all cutouts and their reinforcements are shown in Fig. 11.5 and Fig. 11.6. The fuselage structural analysis was limited to only the constant cross-section area, because it was expected that the most critical areas would be in this section due to the wing and large windows both being present here. This implied that the structural design of frames and longerons was greatly simplified, and that loads acting outside of these areas could be modelled as concentrated forces. The full structural layout is shown in Fig. 11.7, where also the partition of the aircraft that was analysed is shown.

Parameter	**Value**	**Unit**
Frame spacing	700	mm
Frame height	150	mm
Nr. of longerons	72	-
Longeron height	50	mm

Table 11.5: Fuselage structural shape parameters

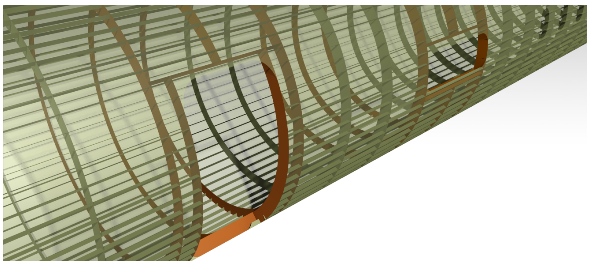

Figure 11.5: Detail view of the door and large window cutouts

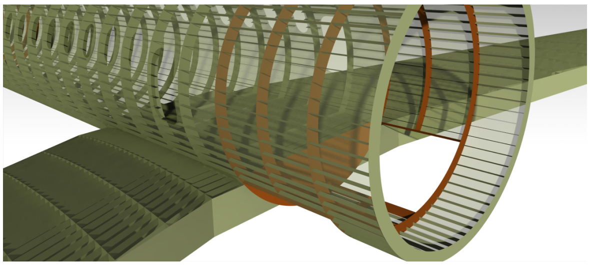

Figure 11.6: Detail view of the emergency exit and small window cutouts

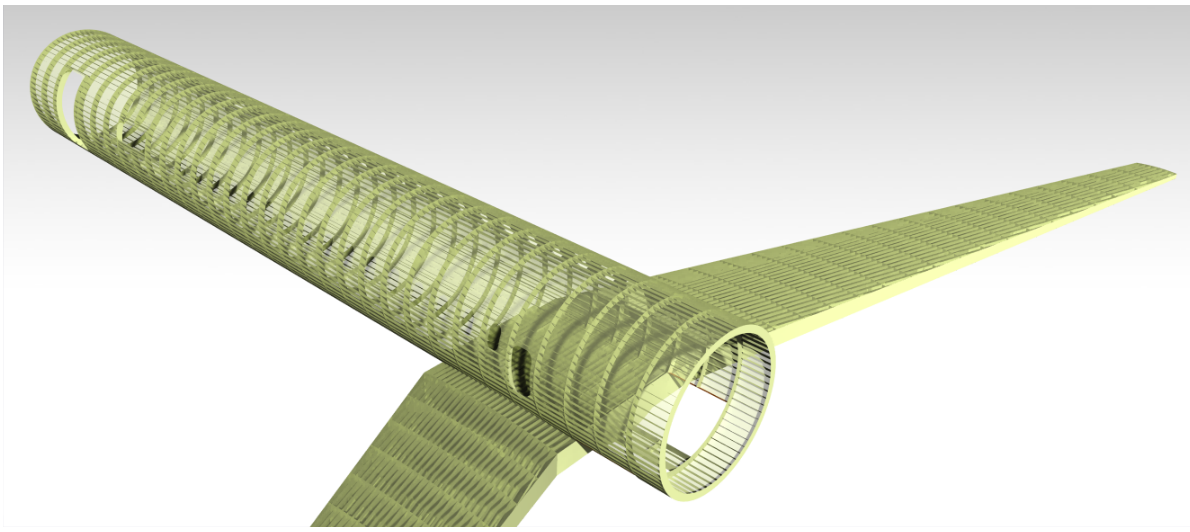

Figure 11.7: Chosen structural layout

11.3 Stress Analysis

Safety is the most important design criterion of a structural design. If For the analysis of the conceptual wing-fuselage structure, the dedicated Finite Element Method (FEM) program Abaqus from Dassault Systemes was used. This program takes into account geometrical properties, part connections, separate stiffness properties, boundary conditions and the given load case. If performed correctly, the program will output stresses and deformations, and will serve as an accurate method to determine critical areas in the structure, as well as whether the structure will fail (yield) for the given load case. As the results are highly sensitive to the inputs given, this section will elaborate on the process that was followed, and will discuss the results of this analysis.

11.3.1 Method

In Abaqus, a specified order in the form of workbenches is always followed to ensure all parameters are specified. This order consists of creating the parts, assigning properties to these parts, assembling them, creating a step input file, defining interaction between parts, loading the model and applying boundary conditions, meshing all the parts, optimizing the program and creating a job file to be executed, after which the results can be visualised.

Part

With the part workbench, Abaqus allows parts to be created in the program itself. However, the part design feature in this program pales in comparison to the design freedom offered by CATIA (also from Dassault Systemes), which is why the program also allows for interfacing with this program. As a first step, the CATIA model shown in Section 11.2 was imported into the program, creating separate parts like skins, stringers, spars, ribs, frames and load-carrying cutouts like the fuselage door.

Property

The second step involves assigning material properties to the newly created parts. In this case, properties approximating an isotropic composite material with a Young's modules of $83 \cdot 10^9$ GPa, Poisson's ratio of 0.33 and a certain thickness were specified. This was done by creating one isotropic material, and assigning shell sections this material with a certain thickness for each part. All input parameters for these properties are specified in Table 11.6.

Part	Material	Thickness [mm]
Fuselage door	HS CFRP	5
Emergency exit	HS CFRP	5
Fuselage door rib	HS CFRP	20
Wing top skin	HS CFRP	10
Wing bottom skin	HS CFRP	10
Front spar	HS CFRP	20
Rear spar	HS CFRP	20
Fuselage skin	HS CFRP	5
Spar frame	HS CFRP	20
Wing ribs	HS CFRP	10
Wing carrythrough ribs	HS CFRP	10
Wing carrythrough frames	HS CFRP	15
Normal fuselage frames	HS CFRP	10
Window reinforcements	HS CFRP	10
Door reinforcements	HS CFRP	10
Wing stringers	HS CFRP	10
Fuselage stringers	HS CFRP	10

Table 11.6: Property specific input parameters

Assembly

With all parts possessing properties, they could be assembled into a single product. As the parts already had the correct position with respect to each other from CATIA, no further dimensional constraints between parts were necessary.

Step

In the step module, the input to and output from the model can be specified. In this case, for the input general static properties were used with default settings, which implied a direct solver and full Newton solution technique.

Interaction

Next, the interaction between parts had to be specified. These interactions are the first assumptions made that significantly impact the results of the analysis. Here, it was assumed that the nodes of parts were tied together at their edges, simulating an infinitely strong adhesive bond. This assumption is justified if the adhesive fails later than the parts themselves. To connect the edge nodes between parts, a tie constraint was used. This constraint requires the specification of a relatively stiff master surface, and slave surfaces to connect to it. Coupling constraints were used to specify a transmission of loads between reference points where certain external loads were acting and surfaces where these loads were introduced into the structure. All specified constraints are specified in Table 11.7.

Interaction	**Master Part(s)**	**Slave Part(s)**
Tie constraint	Fuselage and wing skins, wing spars, spar frames	All stringers, frames, doors and wing ribs
Coupling constraint	Canard reference point	Front frame
Coupling constraint	Engine reference point	Rear frame
Coupling constraint	Left winglet reference point	Outer rib
Coupling constraint	Right winglet reference point	Outer rib
Coupling constraint	Landing gear reference point	Closest rib rear edge

Table 11.7: Interaction specific input parameters

Load

Next, the assembly could be assigned the load cases specified in Section 11.1. For these load cases, points were specified as the application point of loads that were acting away from the analysed structure. These points were coupled to move together with the structure they were attached to. Distributed loads were specified as pressures acting on their respective surfaces. For the lift, this pressure was distributed elliptically along the span, while assumed to be constant over the chord. In reality, lift is produced by a high surface pressure below the wing and a low surface pressure above the wing. While intuitively one could say that most of the lift is produced by the high pressure below pushing the wing upwards, the largest contribution is in fact by the wing being sucked into the low pressure area above the wing. The ratio between these two pressures could be obtained from the pressure coefficient of the aerofoil, leading to the two pressure components acting on the bottom and top of the wing. Wing drag was assumed to act in a similar way with a spanwise elliptical distribution, but was assumed to act as a pressure on the front and rear spar, for this analysis with a 1 on 1 ratio between these two components. Finally, wing weight was assumed to be acting as a spanwise linearly distributed pressure on the lower panel of the wing, and a longitudinally evenly distributed pressure on the lower side of the fuselage.

Other than the interaction between parts, boundary conditions also have a very significant impact on the results of the analysis. These boundary conditions impose limitations on translation or rotation, and if not enough or improper boundary conditions are used, the solution will not converge. For the first load case, imposing boundary conditions proved to be a serious challenge. Since the aircraft is simply suspended in the air, the sum of the forces is not necessarily equal to zero. In this case however, it is assumed that all forces are (nearly) balanced, with the centre of gravity being constrained from displacing to absorb the sum of the forces. For the second load case, boundary conditions were a lot more straight-forward. By assuming the landing gear to be infinitely stiff (an over-estimation of the problem), the point where the landing gear reaction force acted through was constrained from translating in x,y and z direction.

Load	Magnitude	Direction (x,y,z)	Application ((x,y,z)/equation) [m]
Load case 1			
Wing lift	$2.42 \cdot 10^6\ N$	z	$\frac{L^2}{49986.6^2} + \frac{y^2}{13.725^2} = 1$
Wing drag	$64313\ N$	-x	$\frac{D^2}{7567.57^2} + \frac{y^2}{13.725^2} = 1$
Wing+fuel weight	$1.51 \cdot 10^6\ N$	-z	$W = -2797.13y + 43355.515$
Fuselage+payload weight	$6.90 \cdot 10^5\ N$	-z	Evenly distributed
Fuselage pressure	$67143\ Pa$	-	Evenly distributed
Winglet lift	$1.86 \cdot 10^5\ N$	y: -sin(85), z: ± cos(85)	-13,16,1.7
Canard lift	$1.28 \cdot 10^5\ N$	z	15.8,0,-0.3
Engine thrust	$1.48 \cdot 10^5\ N$	x	-17.5,0,1.5
Engine weight	$1.26 \cdot 10^5\ N$	-z	-17.5,0,1.5
Load case 2			
Wing lift	$7.90 \cdot 10^5\ N$	z	$\frac{L^2}{16343.6^2} + \frac{y^2}{13.725^2} = 1$
Wing+fuel weight	$5.05 \cdot 10^5\ N$	-z	$W = -936.816y + 14520.7$
Fuselage+payload weight	$2.46 \cdot 10^5\ N$	-z	Evenly distributed
Winglet lift	$6.10 \cdot 10^4\ N$	y: -sin(85), z: ± cos(85)	-13,16,1.7
Canard lift	$4.55 \cdot 10^4\ N$	z	15.8,0,-0.3
Engine weight	$7.17 \cdot 10^4\ N$	-z	-17.5,0,1.5
Landing gear	-	z	-8.1,3.3,-1.2

Table 11.8: Input parameters for given load cases

Mesh
One of the key elements of finite element modelling is the division of the analysis space into separate small sections, for which the governing equations are solved. This process is called meshing, and the more elements are used, the more accurate the analysis will be. Normally, a mesh should contain elements of roughly the same size, and many methods are available to make the mesh as uniform as possible. However, to limit the scope of this project, the meshing of parts was kept relatively simple for this analysis. In Abaqus, a mesh is created by dividing the edges into different sections in a process called seeding. Using a global size of 50 mm for most parts and a mostly structured mesh control, meshes on all parts could be generated from these edges.
Optimization
The optimization workbench is used in order to optimise the design by varying parameters. As for the case of this model, only one iteration would be performed to further limit the scope of this analysis to a more realistic time-scale, so this workbench was not used.
Job
In the job workbench, a job file can be created to submit for analysis. This file acts as the execution platform for the analysis, and here one can specify the resources to be used for the analysis, like the number of processor cores. It is also the platform where errors may surface, which implies changes in previous steps of the analysis have to be made. After the analysis has been submitted and completed in this workbench, one can view the results in the visualization workbench.
Visualization
The visualization workbench is used to display the results of the analysis. After the job has completed, one can easily review the deformations and von Mises stresses in the entire model, and visualise areas of critical stress. If the stress is too high, the thickness of the specific element is increased in the property workbench, and the job is submitted again. This process is repeated until the structure does not fail for the considered load cases.

11.3.2 Results

Load Case 1:
For the first load case under consideration, the resulting deformation of the wing is displayed in Fig. 11.8, combined with a table specifying the magnitude of the stresses in the structure (deformation is exaggerated by a factor 5.5). In order to reduce the stresses below the yield stress of the material, the parameters that were changed are listed in Table 11.9. The maximum stress in the figure can be observed to be 505 MPa. Even though this stress is still below the yield stress of the material, due to the fact that the location of this

stress was around one of the clamping points of the model, this value is unrealistic. Excluding this point lead to a maximum stress of 210 MPa in the tip of the left wing skin due to the compression caused by the rudder deflection. On the other side, the wing flexes back at the tip because of the tension that is caused by the rudder deflection on that side. The second highest stress occurs at the root, with a value of around 180 MPa. It is interesting to observe that the stresses near the corners of the large windows were not as high as expected: only around 42 MPa. This can be attributed to the reinforcements around the windows, combined with the choice that there are no cutouts in a circumference of roughly 1.5 m around the window. This has been made possible by interfacing with the seating arrangement in the cabin. It can be observed that the ribs and frames where external loads are introduced on, had to be made significantly thicker. In reality, these loads are introduced through the skin and stringers into the analysed structure, implying the frames are not loaded as highly as they currently are.

Parameter	Old value	New value	Unit
Thickness			
Fuselage door	5	3	mm
Emergency exit	5	3	mm
Fuselage door rib	20	15	mm
Wing top skin	10	10 (root), 4 (tip)	mm
Wing bottom skin	10	10 (root), 4 (tip)	mm
Fuselage skin	5	3	mm
Wing ribs	10	5	mm
Front fuselage frame	10	50	mm
Rear fuselage frame	10	50	mm
Wing outer rib	10	50	mm
Amount			
Wing stringers top	15	25	-
Wing stringers bottom	13	21	-
Wing ribs	15	20	-
Wing carry through ribs	6	8	-

Table 11.9: Parameters that were changed to size for the first load case

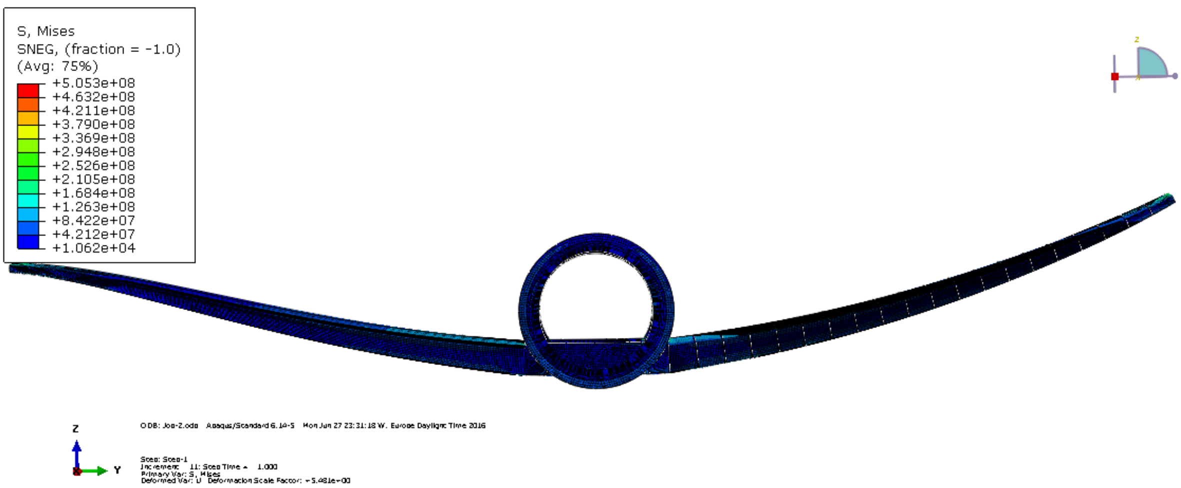

Figure 11.8: FEM deformation and stress results for the first load case

Load Case 2:
After adapting the model for the second load case, it was observed that the stresses within most structural elements were lower than the ones for the first load case. This was the case for all elements except for the rib closest to the landing gear, where the gear strut would be attached to. This rib, which is the same rib that provides a load path for out of plane stresses that are introduced by the angle discontuity in the spars, had to be reinforced in order to lower the stress. The new value for this rib can be found in Table 11.10.

Parameter	Old value	New value	Unit
Thickness			
Wing carry through outer rib	10	20	mm

Table 11.10: Parameters that were changed to size for the second load case

Weight Estimation:
With the structural design parameters fixed, the total structural weight could be obtained. It was found that the total structural volume was 4.61 m^3. Using the density of HS carbon reinforced epoxy of 1560 kg/m^3, the structural weight was found to be 7200 kg in total. The total weight of the wings and fuselage was estimated to be $7700+11100 = 18800$ kg. Assuming the structural weight is only half of the airframe component weight, which is a very conservative assumption, the total weight obtained from the analysis is 14400 kg, well below the estimated value.

11.4 Verification

The results presented above rely on intricate calculations and computer optimisations. To check whether this is all in line with reality or not, the calculations are repeated independent of the previous results and more simplified. This method will mitigate the chance for mistakes. Because simplified methods are used input parameters are always chosen such that the real life stresses are smaller than the ones calculated.

11.4.1 Wing Calculations

With the critical case lift distribution given in Table 11.8 it is possible to find the position of where the lift force applies as a point force on one wing. This lift force will be the main contributor to the stresses in the wing box at the root connection. The lift force will generate a moment making the wing bend upwards, a torque is generated because of the sweep angle and furthermore a shear stress is present in the spars.
By integration the location of the equivalent point force of the lift is found. This location allows for the calculation of the upward moment and the torsion that the wing box experiences at the root. The moment of inertia of the wing box is calculated in a simplified manner without taking into account the shape of the top and bottom skin which are defined by the aerofoil. The moment of inertia of the wing box will be larger in real life and thus more resistant to bending. With the moment and moment of inertia known the stresses in the top and bottom of the wing box can be calculated. The stringers take most of the stresses caused by bending. The spars are calculated as if they take all the shear force generated by the lift and the torsion. Varying certain parameters changes the stresses at specific locations. To optimise the result a combination of parameters should result with the stresses in the structure as close as possible to the allowable stresses. Multiple combinations of parameters may lead to the same result for stresses, but different results for wing weights. A possible combination is presented in Table 11.11 for carbon composite and a different combination is shown in Table 11.12 for 2024 aluminium, both have been preliminarily optimised for weight reduction. The comparison shows how the safety factor influences the design, whereas the aluminium has a safety factor of two, the carbon composite has a safety factor of four applied. Table 11.13 and Table 11.14 show the stresses to be just allowable at the wing root for the carbon composite and the aluminium design respectively. From the analysis it is clear that designing the wing box revolves around avoiding buckling failure, the buckling is caused by the upward bending of the wing.

Table 11.11: Carbon composite wing box parameters at the wing root

Parameter	Value	Unit
Number of top stringers	26	-
Number of bottom stringers	20	-
Number of ribs	20	-
Stringer height	0.065	m
Stringer thickness	0.006	m
Spar thickness	0.027	m
Skin thickness	0.013	m
Wing total weight	7340	kg

Table 11.12: Aluminium 2024 wing box parameters at the wing root

Parameter	Value	Unit
Number of top stringers	25	-
Number of bottom stringers	15	-
Number of ribs	20	-
Stringer height	0.065	m
Stringer thickness	0.003	m
Spar thickness	0.019	m
Skin thickness	0.008	m
Wing total weight	7500	kg

Table 11.13: Carbon composite wing box maximum allowable stresses and applied stresses for the critical load case

Failure mode	Allowable stress (GPa)	Applied stress (GPa)
shear	0.100[1]	0.098
buckling	0.204	0.204

[1] 60% of fibres in + and - 45° direction, and 20% in 0° and 90° direction. This results in 25% strength of the tensile strength.

Table 11.14: Aluminium 2024 wing box maximum allowable stresses and applied stresses for the critical load case

Failure mode	Allowable stress (GPa)	Applied stress (GPa)
shear	0.140	0.139
buckling	0.340	0.337

For this verification chapter the skin was assumed equal in thickness on both the bottom and top side, by allowing different thickness on top and bottom the wing weight can be reduced. The torsion in the wing box causes more shear stress in one spar and a reduction of shear stress in the other. It was assumed that the front and rear spar have an equal thickness, for ease of calculation. Allowing the spars to have a different thickness will again have a weight reducing effect. For the purpose of verification weight reduction is no priority, but validates the calculations by being close to the wing weight estimate in Section 8.4. The tables presented above (Table 11.13 and Table 11.14) prove the order of magnitude of stresses at the wing root for the critical load case from Table 11.8.

12. Production Plan

In order to successfully build and deliver a certain number of airframes within a fixed time span, a production plan must be set up. This describes how manufacturing, assembly and integration are organised. Moreover it specifies which components are to be internally manufactured and which are to be externally outsourced. A production rate analysis is performed with the aim of obtaining the throughput time needed to complete one airframe, as well as the time needed to reach the desired production output.

12.1 Manufacturing, Assembly and Integration

The factory layout is presented in Fig. 12.1. The internally manufactured components are produced in batches. This takes place in the aerostructures, electronics and hydraulics workshops. Batches of parts are then sent to the storage facility which act as a buffer. Components production can start up to two years in advance of the first aircraft delivery. Once the batches are ready, the sub-assembly is performed in three different facilities namely the wing, the fuselage and the empennage assembly. This is followed by the final assembly, the paint station and the production flight where pre-flight checks are performed.

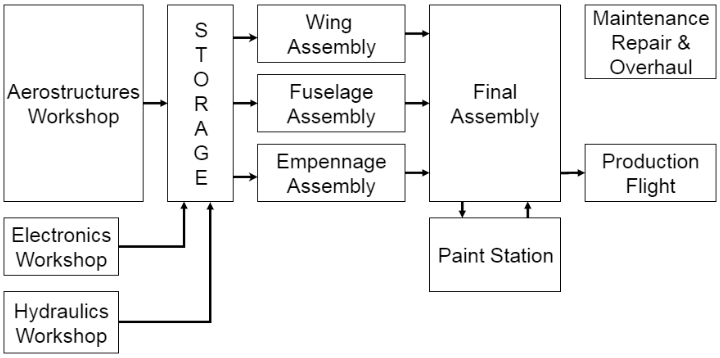

Figure 12.1: Factory layout

The production chart is depicted in Fig. 12.2 and presents the manufacturing and assembly activities as a function of throughput time. While most parts are manufactured using the batch production principles long before the assembly starts, there are also components that are manufactured at later stages. These are mainly large composite components such as the wing lower panel that are to be manufactured as one piece. This is achieved by preparing the mould, tape laying, stringer integration, vacuum bagging, curing and milling. This reduces the number of joints needed, thus reducing the overall weight of the structure. There are in total 15 stations, each assigned equal work packages of 6 days. The assembly process is based on the principle of line production where aircraft sections at different completeness level are assembled at different stations.
In order to maximise efficiency, certain production and assembly activities are to be performed in parallel. In the beginning of the production cycle, work is performed concurrently on the fuselage panels, the cockpit section, the forward pressure bulkhead and the front fuselage fairings. The time needed to perform certain assembly activities may take up to two stations working time. In these cases, two stations working in parallel are employed. After the fuselage panels are produced, assembly of the front, middle and aft fuselage sections takes place, followed by the joining of these three major fuselage sections. During the fuselage joining phase, the activities related to wingbox and outer wing production commence in a separate station. At this point work also starts on the canard, winglet and rudder. Before entering the final assembly line, the empennage components are joined together in a sub-assembly station. Since this is one of the stations to which a workpackage of double the station time is assigned, there are two empennage assembly stations working in parallel. Concurrent with the empennage assembly, the centre wingbox, followed by the landing gears are integrated into the fuselage in order to increase the airframe's mobility. Once the aircraft is moving on its own wheels, the wings, the engine pylons and the empennage are integrated. The last assembly activities consist of painting, integration of hydraulics, electronics, avionics and finally the engines.

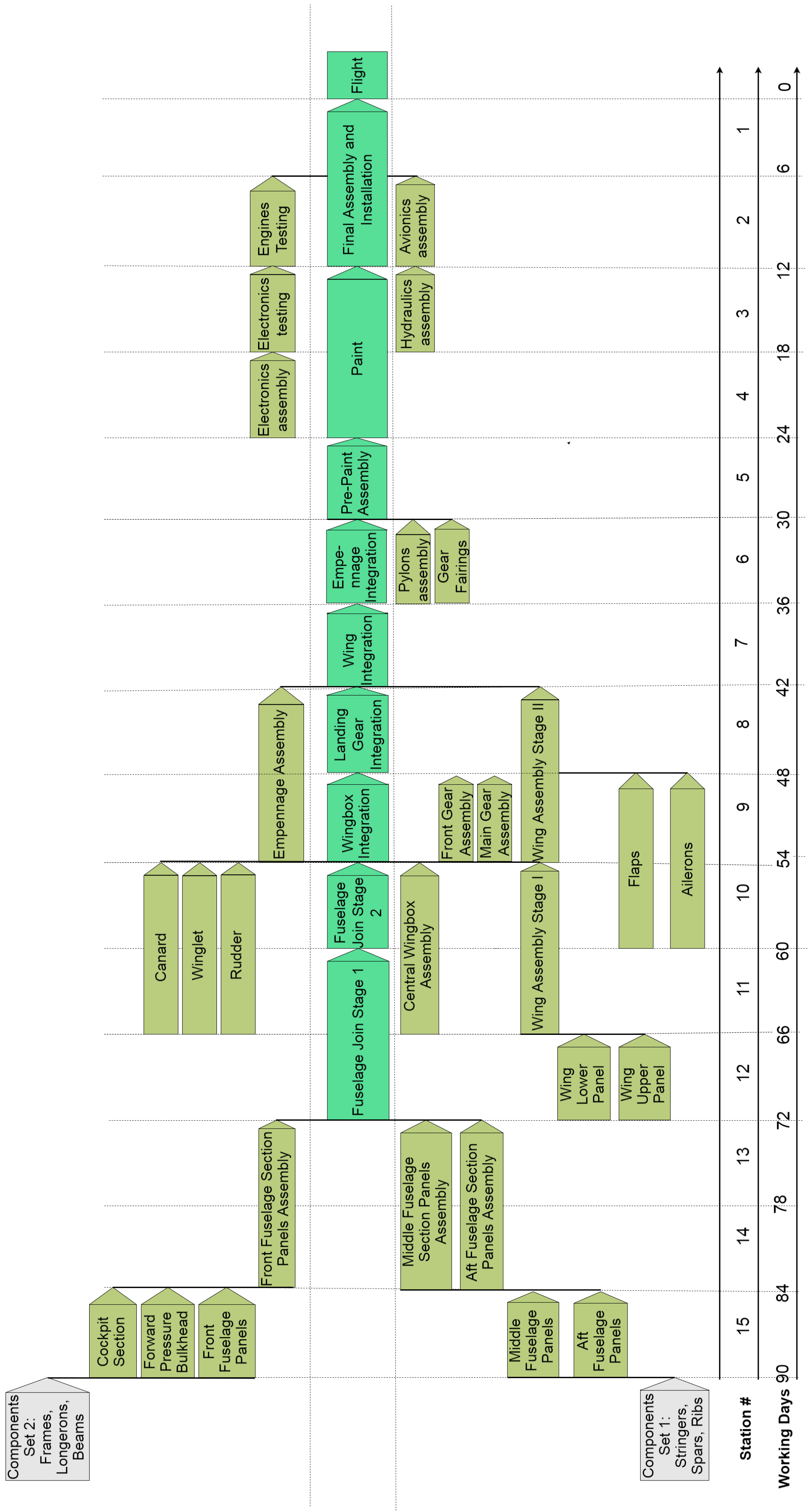

Figure 12.2: Production chart

12.1.1 Internal production and external out-sourcing

Parts can be internally manufactured. A company can decide to manufacture the parts at one facility or at multiple facilities at different sites. The former requires the entire manufacturing line and the required knowledge to be in one place, which is often not possible. The latter is more often used and is called internal out-sourcing [21]. The main advantage of internal out-sourcing is the displacement of non-core activities and overheads from the main organisation while keeping the knowledge and control within the company[1]. The issue with internal out-sourcing is the work share: what and how much work should be assigned to each facility. The cost and the time of the manufacturing could increase even more when the design of the aircraft is not compatible with the work-share locations [21]. In order to avoid these problems, internal outsourcing is kept to a minimum and the majority of internal production is to be performed at a single location.

Internally produced components

The main aircraft components are to be internally produced. These include the fuselage, the wingbox together with the wings, the empennage and several structural components of the landing gear.

The opposite of internal out-sourcing is external out-sourcing. With external out-sourcing, activities of a company are assigned to third parties. External out-sourcing is done to get access to facilities you do not have yourself, lowering operational and labour cost and use the knowledge of different experts.[2]. Next to the benefits of out-sourcing, it also comes with several risks. The quality can differ between the different suppliers. This risk can be minimised by quality contracts within the supply chain and on-site quality and technical support from the contractor[2].

Next to the risk of quality, there is also the out-sourcing risk itself. Some components needs to be out-sourced because of the lack in expertise, such as the engines. However, outsourcing many components can increase costs [21]. Out-sourcing on a large scale will result in profit and knowledge for the supplier and increases cost for the contractor[2].

Outsourcing performed through other countries is referred to as offshoring and comes with further risks that need to be considered. Cultural and physical distance between different countries create a large supply chain. The communication and on-site involvement needed for this supply chain lead to additional cost.

Externally produced components

Expensive parts such as engines, auxiliary power units and avionics are added to the airframe at a later stage in the assembly process and are externally procured.

12.2 Production Rate Analysis

For the production rate analysis, first the manufacturing throughput time is calculated which represents the total time needed for manufacturing and assembling a complete aircraft. There are in total 15 main and sub assembly stations to which equal work packages are assigned. A station time of 6 days is set. In order to make the production profitable and reach the break even point at an early stage, a seven days per week work schedule is chosen. This can be implemented by increasing the number of working shifts as compared to the more conventional five days per week schedule. To calculate the throughput time, Equation (12.1) is used, resulting in a throughput time of 90 days.

$$T_{throughput} = T_{station} \cdot N_{stations} \tag{12.1}$$

The production run represents the time needed to produce 600 aircraft. With 11 months of working time per year, a production run of approximately 11 years is estimated. The results are summarised in Table 12.1.

Table 12.1: Summary production rate analysis for 7 days work week

Parameter	Value
Number of stations (-)	15
Station time (days/aircraft)	6
Throughput time (days)	90
Aircraft per month delivered (-)	5
Production run (years)	11

[1]URL http://www.elevationlearning.co.uk/ourthinking/articles/our_thinking_article4.htm[cited June 1 2016]
[2]URL http://www.forbes.com/sites/stevedenning/2013/01/21/what-went-wrong-at-boeing[cited June 1 2016]

12.3 Parts Batches Production

Lean manufacturing is regarded as a philosophy and way of thinking where the manufacturer strives to manufacture without (or limits) waste which is a dynamic, knowledge driven and customer-focused process [48]. One form of waste encountered during production is waiting time. This may be caused by the production line of the parts or when parts run out before a new batch is produced. Another source of waste could occur when more part are produced than needed (over production). Overproduction results in more required storage space for parts and this type of waste may be caused by long process set-up time, unbalanced workload and unleveled scheduling. Therefore, careful consideration should be placed on the batch production rate, timing and size. [48].

As mentioned previously, the parts that are required during production of the aircraft are produced in batches, unlike assemblies in production lines. A batch is a group of parts produced as one group. These parts will be produced in dedicated workshops where all required equipment is present to produce the parts. The workshops will be located away from the assembly lines, and supply the parts to the assembly line through the warehouse which will act as a buffer [49].

For the production of the batches of parts, the ideal lean manufacturing system for batch production and delivery would be the Just-In-Time (JIT) system. This is where the right items, in time and amount are produced and delivered which would result in no stock or buffers. However, for the production of the aircraft as a whole, the JIT system cannot be achieved but getting as close possible to the ideal JIT system will be strived for to reduce costs and waste [48]. This will be achieved by storing the batches in local warehouses near the assembly line, from which the parts are retrieved from stock one by one to be used in the assembly lines. At a certain point when the batch decreases below a critical amount, N_{crit}, there will be a new production order submitted to start producing the new batch of parts. The size of the production order for the new batch is such that the warehouse is filled with N_{max} parts again. This process is illustrated in Fig. 12.3 [49].

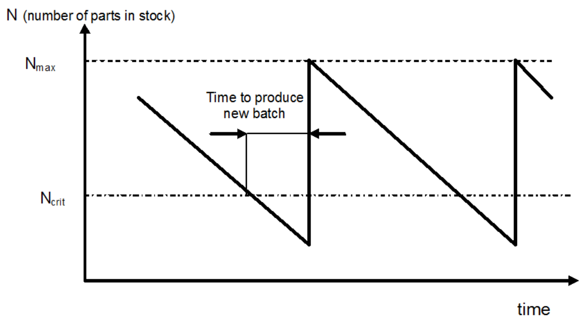

Figure 12.3: Batch production principles

This procedure is intended for the warehouse to never run out of parts and for the overall production to be able to continue undisturbed with limited waiting times. The size of the batch will depend on several parameters such as delivery time of the aircraft.

The longer the delivery time the larger the batch size should be. Second parameter is the size of the part. The larger the part size, the more storage area required, which will cost more money for storage space. Thirdly, the ratio of manufacturing time to change-over time because if this is decreased it becomes more advantageous to further increase the batch size [49].

Since the batch size for different parts are different as they depend on several parameter, an inventory management software will be used to submit new production orders once the parts decreases below N_{crit} in the warehouse. This is to ensure that enough, but not too many, parts are present at all time in the warehouse. The inventory management software that will be used for the production will be Inventory Manager developed by Aircraft Maintenance Systems [3].

12.4 Quality

Quality is considered a relative standard, therefore the quality that is strived for with regard to the parts and the aircraft as a whole will depend on the parties involved. Some of the main parties are the customer, manufacturer and authority. The appropriate quality is said to be achieved when: “the totality of characteristic

[3] URL http://www.aircraftms.com/inventory-manager.html [cited June 3 2016]

of an entity that bear on its ability to satisfy stated needs and implied needs" [47]. One of the methods to ensure that a certain quality standard is met for the stakeholders is by setting requirements that should be complied with. This therefore requires to have knowledge on the stakeholders needs to be able to specify the appropriate requirements, which were specified in Chapter 1 [47]. Secondly, quality can be achieved through careful planning and reliable purchase of equipment and tools. Throughout the production process a Quality Management System will be used. The system serves as the organisational structure, procedures, processes, responsibilities and resources used for implementing the Quality Management [47].

The Quality Management (QM) serves as the overall top function and is the responsibility of all levels of management. The main purpose of the QM is to accomplish business success and an continuous improvement of the overall performance of the organisation/production to satisfy the customers[47] . The management that will be appointed therefore does not require to have a purely technical background but a variety of proven skills to ensure the QM. The techniques that will be employed in the QM are Cost of Quality analysis to investigate whether the improvement of quality by comparing the increase cost compared to profit generated. Together with Quality Planning and with regular set QM meetings to establish current status and next course of action. The staff to be appointed for the QM shall be either hired or trained by a firm such as Delpha Quality Consulting and/or SAI Global due to their experience in quality management in the aerospace industry.

Secondly, Quality Assurance (QA) shall be implemented on the the levels bellow QM. The main purpose of the QA is to accomplish and demonstrate that all the planned implementation with in the quality system are met, to provide sufficient confidence in the product (aircraft) to fulfil the set quality requirements. The quality requirements that are to be implemented by the QA are established either by the ISO or FAR. QA can be separated into internal and external. Internal QA is conducted within the company and production plan, which provides confidence to management. External QA is conducted to provide confidence to customers[47]. QA will be achieved through means of appropriate checklist depending the element or product produced of requirements and standards that needed to be met. Secondly by having a project audits, which are detailed reviews of the processes used in the production of the required elements and produta [4].

Finally, Quality Control (QC) lies at the core of the quality management system. The purpose of QC is to achieve awareness of quality in all the layers of production and ensuring that all operational techniques and activities fulfill the requirements for quality and are maintained through out inspection. QC and QA actions are usually interrelated[47]. QC will be carried out by means of having statistical sampling of different parts and elements which will be analysed in more detailed. During the detailed analyses the part will be investigated whether it meets the quality requirements set in QA and meet the set benchmark as well as go through a complete load analysis. Other QC methods that will be employed are regular quality tool checking and using assembly line checking stations.

Having a well functioning Quality Management System has several benefits. Firstly, the marketing benefits are greater as a quality aircraft delivered by a company with known high quality standards is easier to sell. Secondly, internal benefits in improvement in efficiency and productivity and potential improved profitability. Improvement in quality should be continued as long as there is an increase in profit by at least the same amount.
A appropriate Quality Management System is therefore essential for the production of the aircraft.

12.5 Carbon Composite Production

Aircraft have been produced with metal for decades. Now, the transition starts towards composite materials and more specifically towards carbon composite. New materials require new production methods, some of the production methods for composites resemble metal processing methods. The main difference is that metals are processed in either molten or solid state and carbon fibres are always processed solid. The flexible nature of the carbon fibres allows easy tailoring to a preferred shape, it is the resin which gives the composite its desired transverse stiffness after curing. On one hand, metals always require heavy tools and machines to be processed, on the other hand, carbon composites can be formed by hand. This makes the tools and machinery needed for carbon composite production generally cheaper because of the lower forces needed for shaping the composite.

[4]URL http://www.iia.nl/sitefiles/project-auditing.pdf [cited June 27 2016]

Stringers

The stringer's cross sections will be constant in axial direction for both the wing and the fuselage. For this reason the process of making the stringers can be easily automated. The stringers will consist of a mixture of long fibres and carbon fibre fabric impregnated with epoxy. The most economical and easiest processing option is pultrusion, the fibres and the woven fabric are pulled through resin and through a die that shapes the material and that is able to apply pressure and heat. A schematic drawing is shown in Fig. 12.4. The use of the die allows for easy curing of many resin materials by applying pressure and heat. Because the carbon sheets and fibres are pulled straight from a reel into shape they are very straight. In this case it can improve structural properties and also there is nearly no wasted carbon material or epoxy [5]. The process of pultrusion is relatively fast when compared to other composite production methods. Two different dies will be necessary to make the different stringers for the fuselage and for the wing. Two separate stations can be set up, resulting in a station for each stringer cross section. The stringers are pulled as one long piece which can then be cut to the preferred length.

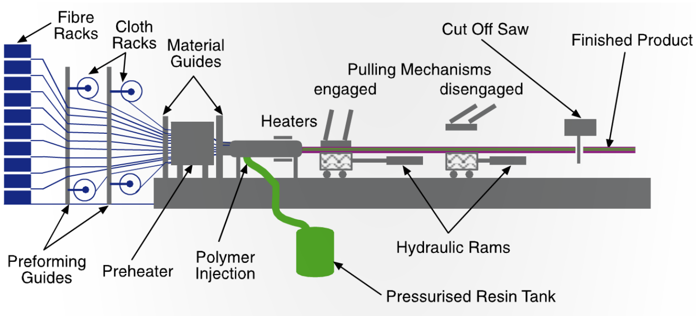

Figure 12.4: Pultrusion schematic [6]

Fuselage Skin

It is decided to use automated layup with prepreg fibres to guaranty the quality of the final product. The main advantage of tape laying is that the fuselage skin will be one big part with as few connections as possible. The fibres are close together to form as a strip, referred to as 'tape' and then laid upon the mould. The tape laying system consists of a rotating tube, a mandrel, on which the fuselage is taped by a moving printer-head, this process is also known as filament winding. The tape can be laid on the fuselage at almost any angle except parallel to the longitudinal axis. Fortunately this is no requirement as stringers provide the main support in the longitudinal direction of the fuselage. The whole mandrel with the tape laid upon it on the outside can be put in to the autoclave. Three different parts will be produced separately: the tail cone, the centre fuselage and the cockpit (excluding the nosecone). The drawback is the high equipment cost, the lay up installations, the mandrels and the autoclaves. After this initial investment the costs are mainly raw material and energy for curing. The initial investment for the tape laying machine can be kept down by selecting a machine with limited axes of freedom as the rotating mould eliminates the need for several axes of freedom.

Fuselage Frames

The mid fuselage has a constant diameter and the fuselage frames can be made constant as well. Because of the large quantities of a single part required, it is worth investing in an automated process. With the use of prepreg carbon composite sheets a press can be used to shape and cure the composite into a mould. This process will require only minimal manual labor. Tooling cost will be dependent on the pressure and temperature needed for curing, which will be determined by the prepreg sheets used.

Ribs, Spars and Wing Box Skin

The wing box will be stiffened with stringers as mentioned before and ribs. These ribs have a different size at different points along the span of the wing. This means only small batches of the same rib should be made, this eliminates press forming as a production method. To keep the production speed up to par with the wing assembly requires a fast and tailored production method. Prepreg carbon fibre fabric is already saturated with an optimal amount of resin, which comes at an increased cost. The prepreg fabrics negate the need for any infusion method. This simplifies the process for hand layup in a mould. The relative small size for ribs

[5] URL https://issuu.com/gurit/docs/guide_to_composites_2011 [cited June 3 2016]
[6] URL https://issuu.com/gurit/docs/guide_to_composites_2011 [Cited June 24 2016]

requires only a small autoclave. A bigger autoclave to cure multiple pieces at once would be a bigger intial investment, but this would reduce the amount of curing cycles and thus energy consumption. The tooling cost is low but the need for manual labour and autoclaves for the spars and wing skin will add to the total component cost. Fig. 12.5 shows the necessary components for the layup and the order in which they should be applied, in the end only the cured prepreg makes up the aircraft component. For the composite structure it is required to implement a metal mesh for electric conductivity in case of a lighting strike, this is most easily done right before curing. Because the spars and skin are made in low production volume they can be made by hand layup. If there are funds available it would be preferred to use tape laying to tailor the fibre direction and skin thickness for optimal component performance.

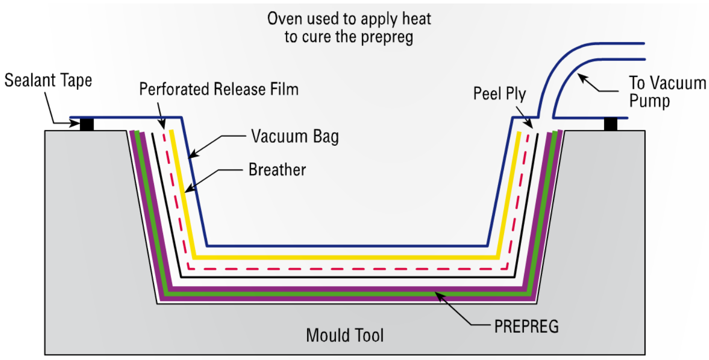

Figure 12.5: Layup schematic[7]

Assembly
With all parts for the wing box available they can be assembled and coated. The wing box parts can be co-bonded together or joined by adhesives in non critical locations to save weight. Critical connections should be bolted together because of safety considerations. Bolted connections are easy to check, whereas the adhesive connecting two parts might have spots where the attachment is not ideal and that are hard to check[33]. The fuselage sections are connected by butt joints and a stiffening lap over the connection, and the wing to fuselage connection should be bolted.

Composite Variations
As mentioned in Chapter 10 different smaller components can be optimised with different composites. The nose cone, or random, of the aircraft should be impact resistant, metals are known for good impact resistance but are heavy weight compared to composites. Glare is aluminium reinforced with glass fibres, this combines the good impact resistance capabilities of metals with the weight reduction of the glass fibres. The leading edge of the wing should also be impact resistant and is thus also constructed from glare. The trailing edge, including movable surfaces carry loads over a fraction of the span and are loaded in bending. To cope with the moments induced by manoeuvring the trailing edge parts are constructed from carbon composite sandwich panels. Furthermore the gear doors, the cabin floor panel and the wingtips benefit from the low weight bending resistance that the sandwich panels offer.

Many of the carbon fibre composite parts require either a big initial investment for production equipment or intricate manual labour. It is kept in mind that not all production speeds are equal, the only requirement is that the slowest station produces enough parts to deliver five aircraft a month. Production of certain components can be outsourced if the speed or quality required can not be achieved internally. The production process internally will be optimised while it is ongoing by using the input from workers and gaining experience in relatively unknown disciplines of manufacturing. To optimise assembly, aircraft components should be manufactured as one part, the stringers could be cured with the wing box skin to form one strong integral part. A second optimisation could be to divide components that take long to produce in more parts, as these can be produced at the same time. Splitting components comes at the cost of added weight because of the increased number of connections.

[7]URL https://issuu.com/gurit/docs/guide_to_composites_2011 [Cited June 24 2016]

13. Operations & Logistics

An important aspect of designing an aircraft is optimizing the design for smooth daily operation. A smart design results in short turnaround times, leading to increased customer satisfaction and decreased operational costs. Fig. 13.1 shows typical ground activities while the new business jet is on the ramp. Fig. 13.2 depicts the timeline of different activities during a typical 30 minute turnaround time, as stated by Boeing [9]. This schedule applies for a normal daily operation, e.g. no abnormal weather conditions and a fully functional aircraft.

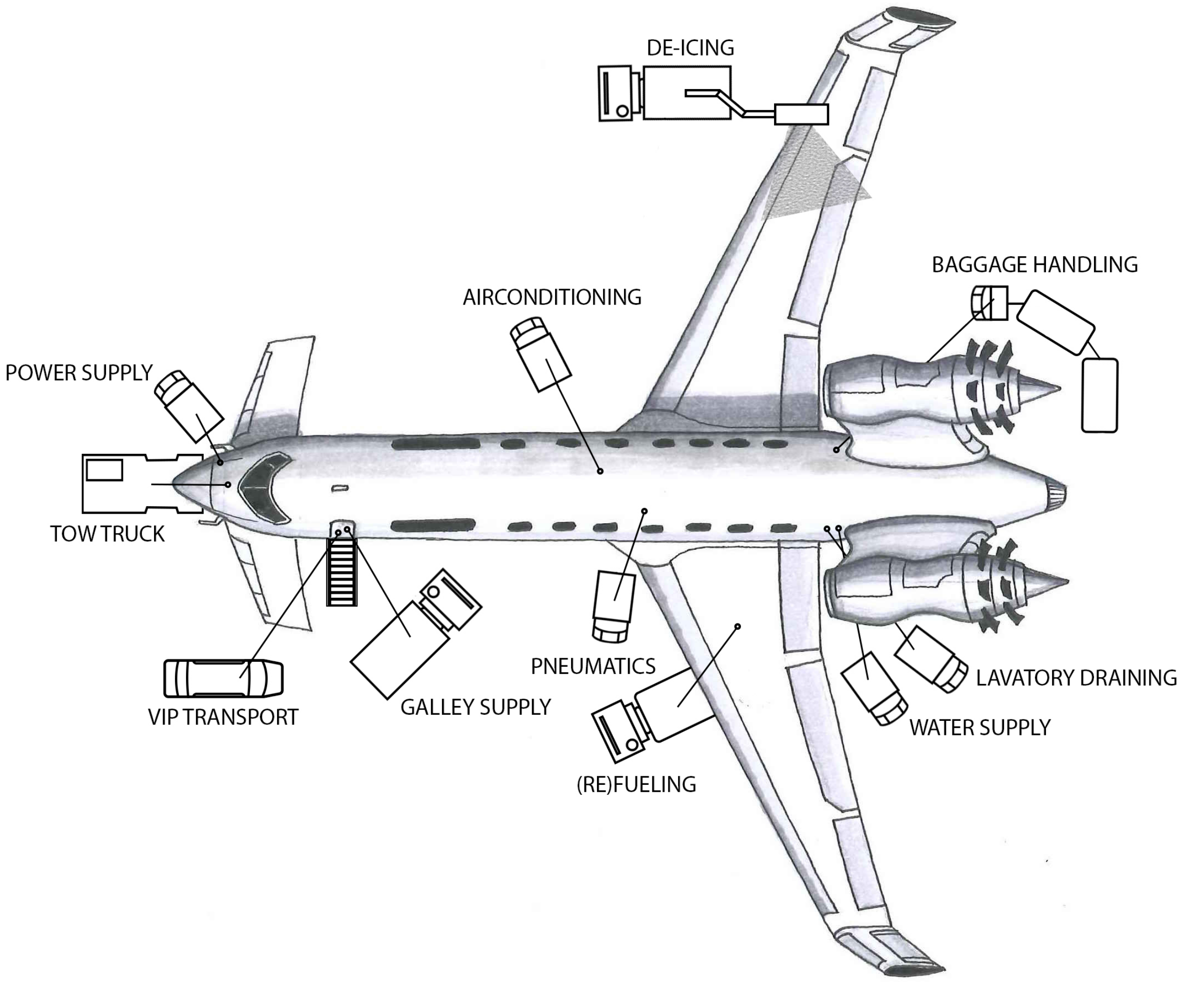

Figure 13.1: Typical ground handling activities

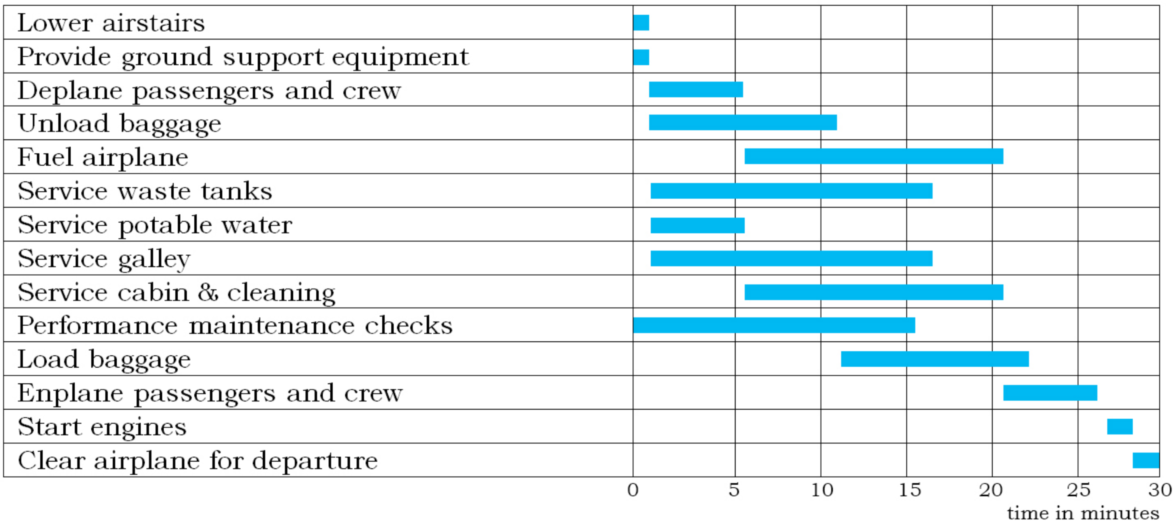

Figure 13.2: Typical turnaround time, based on Boeing statistics [9]

13.1 Design Choices

According to a research by the Hamburg University of Applied Sciences [30], a convenient aircraft design can reduce the Direct Operating Cost (DOC) by 1.3-4% per seat-kilometer. The business jet will therefore make use of the following smart design choices:

Operational Design Choices

- Short landing gear (no engines underneath the wings) for easy access
- Convenient fuel, septic tank and power access points at ground level
- Continuous cargo hold instead of separate sections
- Ground level cargo doors, opening outwards

Apart from daily operations, aircraft also need support in the form of maintenance. Most models have a large amount of parts that need to be maintained or replaced once in a while. Also, because of their long life cycle, aircraft are often retrofitted with new technology during their operational time. Manufacturers can implement different strategies in order to make maintenance as easy and convenient as possible [26]. Design choices for the business jet include:

Maintenance Design Choices

- Podded engines instead of for example wing rooted engines
- Hatches and panels for easy maintenance access
- Transparent panels for visual inspection
- Modular design that allows for easy subsystem replacement (wings, tail, etcetera)

When acquiring a new aircraft, operators require support in the form of technical and operational manuals, (ground) crew training and technician training. For general aviation this support is usually limited to manuals, while for commercial airliners it extends up to full-flight simulators. Furthermore, manufacturers can offer technical support such as maintenance programs or even own maintenance facilities and service centers. For example, Bombardier has nine fully-owned service centers and more than fifty third-party authorised maintenance facilities [1]. Service centers run by the manufacturer usually offer replacement aircraft to customers for the duration of the maintenance. In order to provide the best service possible, our customers will be offered the following support services:

[1] URL http://www.bombardier.com/en/aerospace/business-aircraft/customer-services.html [cited June 3 2016]

Included Support Design Choices

- Technical and operational manuals
- Maintenance programs

Optional Support Design Choices (annual fee applies)

- Ground, cabin and cockpit crew training
- Flight simulators
- Test flight facilities
- Service centers
- Replacement aircraft during maintenance

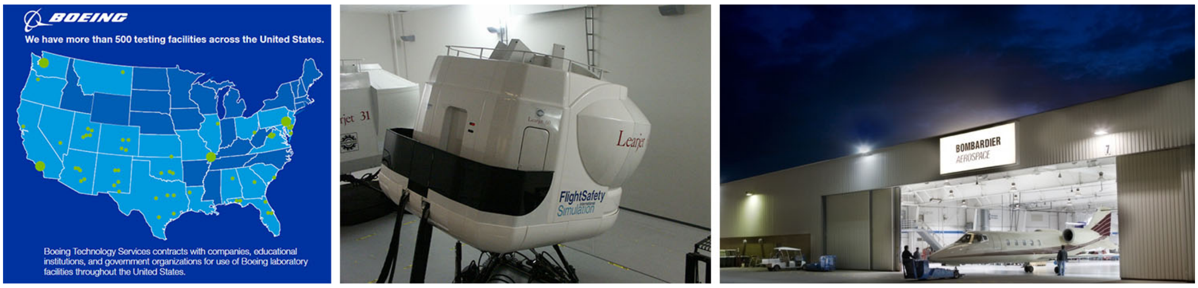

Figure 13.3: Boeing has over 500 testing facilities in the US alone. Bombardier offers full flight simulators for Learjet models while also operating 7 service centers across the globe.[2]

13.2 Operational Costs

The operational costs of any aircraft are of great importance to the customer. As aircraft usually have a life span of around 25 years, even a small decrease in the hourly operational costs can have a large influence on the total operational costs during the entire life span. Since business jets are operated by corporations or individuals, there are no indirect operational costs and no program operating costs. The operational cost therefore only consists of the direct operating cost.

Roskam [43] provides a method to determine the direct operational costs of a commercial aircraft. This method was used to produce the results below. Similar to the resource allocation, the operational costs were also calculated in dollars.

$$DOC = DOC_{flt} + DOC_{main} + DOC_{depr} + DOC_{lnr} + DOC_{fin} \tag{13.1}$$

where:

DOC_{flt} = Flying DOC in USD/nm
DOC_{main} = Maintenance DOC in USD/nm
DOC_{depr} = Depreciation DOC in USD/nm
DOC_{lnr} = Landing fees, navigation fees, etc. in USD/nm
DOC_{fin} = Financing DOC in USD/nm

Direct Operating Cost of Flying

The direct operating cost of flying (per nautical mile) can be estimated using:

$$DOC_{flt} = C_{crew} + C_{pol} + C_{ins} = \$6.46/nm \tag{13.2}$$

where:

C_{crew} = Crew cost
C_{pol} = Fuel and oil cost
C_{ins} = Insurance cost

[2] URL http://customerservices.aero.bombardier.com/Service-and-Maintenance-Network [cited June 24 2016]

$$C_{crew} = \sum_{j=1}^{2} n_{c_j} \cdot (1+K)/V_{bl} \cdot (SAL_j/AH) + (TEF/V_{bl}) = \$0.99/nm \tag{13.3}$$

where:

j	= Type of pilot, where 1 = captain, 2 = co-pilot	
n_{c_j}	= Number of pilots of type j	= 2 captains & 1 co-pilot
K	= Vacation pay, training costs, tax and crew insurance factor	= 0.26
V_{bl}	= Airplane block speed	= 425 kts (8,500 nm/20 hrs)
SAL_j	= Annual salary for type j crew (inflation corrected)	= \$84,000 (captain) or \$60,667 (co-pilot)[43]
AH	= Annual number of flight hours	= 750 hrs for every crew member
TEF	= Travel expense factor for crew	= \$12.8/blockhr

$$C_{pol} = 1.05(W_{F_{bl}}/R_{bl}) \cdot (FP/FD) = \$1.23/nm \tag{13.4}$$

where:

$W_{F_{bl}}$	= Fuel used	= 51,332 lbs (23,284 kg)
$R_b l$	= Block distance	= 8,500 nm
FP	= Fuel price	= \$1.31/gal [3]
FD	= Fuel density	= 6.74 lbs/gallon (A-1)

$$C_{ins} = (f_{ins} \cdot AMP)/(U_{ann_{bl}} \cdot V_{bl}) = \$4.24/nm \tag{13.5}$$

where:

f_{ins}	= Annual insurance rate per USD airplane price	= \$0.03/USD/airplane/year
AMP	= Airplane market price	= \$60,000,000
$U_{ann_{bl}}$	= Annual block hours	= 1,000 hrs [4]

Direction Operating Cost of Maintenance

Apart from the direct operating cost of flying, operators also need to account for maintenance cost. The DOC of maintenance can be approximated using:

$$DOC_{main} = C_{lab/ap} + C_{lab/eng} + C_{mat/ap} + C_{mat/eng} + C_{amb} = \$9.13/nm \tag{13.6}$$

where:

$C_{lab/ap}$	= Airframe and systems labor cost
$C_{lab/eng}$	= Engine labor cost
$C_{mat/ap}$	= Airframe and systems material cost
$C_{mat/eng}$	= Engine material cost
C_{amb}	= Applied maintenance burden

$$C_{lab/ap} = 1.03 \cdot \left[3.0 + \frac{0.067 W_A}{1000}\right] \cdot R_l / V_{bl} = \$0.85/nm \tag{13.7}$$

where:

W_A	= Airframe weight	= 59,785 lbs (27,100 kg)
R_l	= Airplane maintenance hourly labor rate	= \$50

$$C_{lab/eng} = 1.03 \cdot 1.3 \cdot N_e \cdot \left[(0.718 + 0.0317 \cdot \frac{T_{TO}/N_e}{1000}) \frac{1100}{H_{em}} + 0.10\right] \cdot R_l / V_{bl} = \$0.18/nm \tag{13.8}$$

where:

N_e	= Number of engines	= 2
T_{TO}	= Takeoff thrust	= 33,339 lbs (148 kN)
H_{em}	= Hours between engine overhauls	= 3,000 hours (relatively low due to experimental engine)

$$C_{mat/ap} = 1.03 \cdot \left[30.0 \cdot \frac{CEF}{CEF_{1989}} \cdot ATF + 0.79 \cdot 10^{-5} \cdot AFP\right] / V_{bl} = \$0.32/nm \tag{13.9}$$

[3]URL http://www.iata.org/publications/economics/fuel-monitor/Pages/price-analysis.aspx [cited May 31 2016]
[4]URL http://av-info.faa.gov/data/utilization/2007QUARTER%20BYAIRCRAFT.PDF [cited May 31 2016]

where:
CEF = Cost Escalation Factor = 3.5
CEF_{1989} = Cost Escalation Factor (1989) = 3.0
ATF = Airplane Type Factor = 1.0
AFP = Airframe Price = $12,337,307 (Chapter 3)

$$C_{mat/eng} = 1.03 \cdot 1.3 \cdot N_e \cdot \left[(5.43 \cdot 10^{-5} \cdot EP \cdot ESPPF - 0.47) \frac{1}{K_{H_{em}}} \right] / V_{bl} = \$3.66/nm \tag{13.10}$$

where:
EP = Engine Price = $10,000,000
$ESPPF$ = Engine Spare Parts Price Factor = 1.5
$K_{H_{em}}$ = Attained Period between Engine Overhaul Factor = 1.40

$$C_{amb} = 1.03 \cdot [f_{amb/lab} \cdot (MHR_{map_{bl}} \cdot R_l + N_e \cdot MHR_{meng_{bl}} \cdot R_l) + f_{amb/mat} \cdot (C_{mat/apblhr} + N_e \cdot C_{mat/engblhr})]/V_{bl} = \$4.12/nm \tag{13.11}$$

where:
$f_{amb/lab}$ = Labor overhead distribution factor = 1.0 (Roskam)
$MHR_{map_{bl}}$ = Airframe maint. man hours per block hour = 7.01 (Equation (13.7), bracketed part)
$MHR_{eng_{bl}}$ = Engine maint. man hours per block hour = 0.56 (Equation (13.8), bracketed part)
$f_{amb/mat}$ = Material overhead distribution factor = 0.4 (Roskam)
$C_{mat/apblhr}$ = Airframe maint. material cost per block hour = $132.46/hr (Equation (13.9), bracketed part)
$C_{mat/engblhr}$ = Engine maint. material cost per block hour = $581.45/hr (Equation (13.10), bracketed part)

Direct Operating Cost of Depreciation

The direct operating cost of depreciation of the aircraft (per nautical mile) is broken down into the components shown in Equation (13.12). Since the jet will be operated by corporations and private owners, depreciation of spare parts is not taken into account since it is assumed that maintenance is outsourced.

$$DOC_{depr} = C_{dap} + C_{deng} + C_{dav} = \$5.41/nm \tag{13.12}$$

where:
C_{dap} = Cost of airplane depreciation (without engines and avionics)
C_{deng} = Cost of engine depreciation
C_{dav} = Cost of avionics depreciation

$$C_{dap} = \frac{F_{dap}(AEP - N_e \cdot EP - ASP)}{DP_{ap} \cdot U_{ann_{bl}} \cdot V_{bl}} = \$2.56/nm \tag{13.13}$$

where:
F_{dap} = Airframe depreciation factor = 0.85
AEP = Aircraft Estimated Price = $60,000,000
ASP = Avionics Systems Price = $8,000,000
DP_{ap} = Airplane depreciation period = 25 years

$$C_{deng} = \frac{F_{deng} \cdot N_e \cdot EP}{DP_{eng} \cdot U_{ann_{bl}} \cdot V_{bl}} = \$1.60/nm \tag{13.14}$$

where:
F_{deng} = Engine depreciation factor = 0.85
DP_{eng} = Engine depreciation period = 25 years

$$C_{dav} = \frac{F_{dav} \cdot ASP}{DP_{av} \cdot U_{ann_{bl}} \cdot V_{bl}} = \$1.25/nm \tag{13.15}$$

where:
F_{dav} = Avionics depreciation factor = 1.0
DP_{av} = Avionics depreciation period = 15 years

Direct Operating Cost of Landing Fees, Navigation Fees and Registry Taxes

Apart from flying, maintenance and depreciation costs, aircraft owners also need to take landing and navigation fees as well as taxes into account. These costs can be estimated using:

$$DOC_{lnr} = 0.002W_{TO}/(V_{bl} \cdot t_{bl}) + C_{apnf}/(V_{bl} \cdot t_{bl}) + (0.001 + 10^{-8} \cdot W_{TO}) \cdot DOC = \$0.03/nm + 2.17 \cdot 10^{-3} \cdot DOC \tag{13.16}$$

where:

W_{TO}	= Maximum takeoff weight	= 116,772 lbs
t_{bl}	= Block time	= 20 hrs
C_{apnf}	= Navigation fee per flight	= \$10 (Roskam, international flights)

Direct Operating Cost of Financing

The thumbrule for calculating the financing cost is shown below:

$$DOC_{fin} = 0.07 \cdot DOC = \$/nm \tag{13.17}$$

Total Direct Operating Cost

Now the total direct operating cost can be calculated. Filling in Equation (13.1), the following results are obtained:

$$DOC = \$6.46 + \$9.13 + \$5.41 + \$0.03 + 2.17 \cdot 10^{-3} \cdot DOC + 0.07 \cdot DOC \tag{13.18}$$

$$DOC = \$22.67/nm \tag{13.19}$$

Converting this to the hourly operating cost can be done by multiplying the DOC by the block speed.

$$DOC_{hr} = \$16.78/nm \cdot 425kts = \$9,633/hr \tag{13.20}$$

This shows that the new business jet will be more expensive than its main competitors, being the Dassault Falcon 7X ($7,865/hr), Bombardier Global Express ($8,045) or Gulfstream G550 ($8,640)[5]. However, opposed to its competitors the Starling business jet will carry twice the passengers and fly up to 1.6 times further (Global Express). Table 13.1 shows a comparison of these four similar aircraft.

Table 13.1: Comparison to other aircraft

	DOC (/hr)		Range (nm)		Pax @ Stated Range	
Starling 9000	$9,633		8,500		18	
G650	$8,640	-10%	7,000	-18%	8	-56%
Falcon 7X	$7,865	-18%	5,950	-30%	8	-56%
Global Exp.	$8,045	-16%	5,200	-39%	8	-56%

[5]URL http://www.forbes.com/sites/davidewalt/2013/02/13/thirty-amazing-facts-about-private-jets/#42f4bb872730[cited June 1 2016]

14. Sustainable Development

14.1 Aircraft Noise

Noise generated by aircraft is one of the most annoying noise sources to people [7]. The noise is also almost not subjected to noise attenuation from passive protection, like walls or trees. Therefore community noise annoyance from aircraft noise is a significant problem around airports [7]. This section discusses the main contributions to aircraft noise and the noise footprint.

14.1.1 Airframe Noise

Airframe noise is the noise generated by the structure of the aircraft. It can be split into several components. One of the components is the noise resulting from the wing, especially the aerofoil. The noise is caused by the interaction of the aerofoil and its boundary layer and wake [7]. A turbulent boundary layer causes pressure changes at the trailing edge, generating noise. A laminar boundary layer creates vortices at the trailing edge that cause tonal noise. The aerofoil can also generate noise if the angle of attack is increased, because of flow separation. This can lead to additional noise up to 10 dB [7]. Next to two dimensional effects, there is also the tip vortex noise generated by the interaction of the vortex with a free edge of the wing, such as the edge of the airfoil or flap. Compared to the other noise sources mentioned above, this is the most dominant source of noise[7]. The amount of noise generation depends strongly on operating conditions and geometry. To reduce the noise, the wing should be designed for a low angle of attack and the aerofoil should be designed for low boundary layer separation.

The landing gear is also a dominant source of noise. The airframe noise is dominated by the contribution of the landing gear [7], if extended. The interaction of airflow with an object generates broadband noise on any component. The landing gear components also have flow separation and vortex shedding [7]. The noise generated by the landing gear can be reduced by adding fairings to the struts and wheels, which can result in a noise reduction of up to 5 dB [24].

14.1.2 Propulsion Noise

The noise from the engine follows from turbulent air that is causing pressure fluctuations. In case of an open rotor engine, the noise is generated by the rotors and by the jet core, as depicted by the high bypass ratio engine in Fig. 14.1.

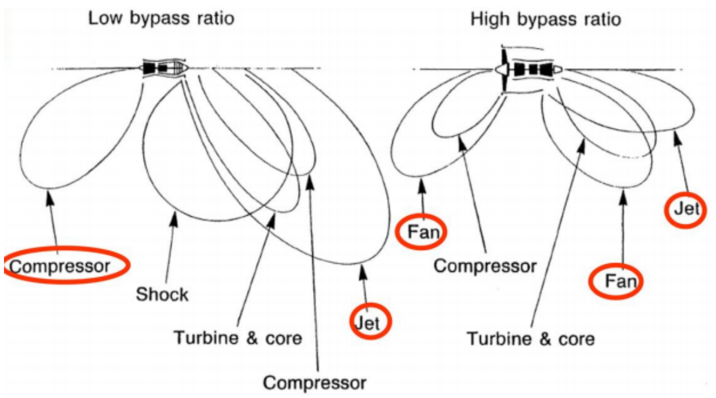

Figure 14.1: Distribution of noise generated by a low bypass ratio and high bypass ratio engine [7]

The jet noise is mainly generated along the shear layer, the region between different air streams. The hot core flow from the engine mixes with cold bypass flow and the free stream airflow. This leads to turbulent flow that generates pressure fluctuations and therefore noise [7]. The jet noise can be reduced by using chevron nozzles. They change how the different airflows are mixed resulting in less low frequency mixing noise from turbulent flow [22], therefore resulting in less noise.

The propeller noise is generated by the interaction of the blades with the airflow. The boundary layer and the wake of the front propeller blades generate turbulent flow which interacts with the aft blades causing the noise. Also the edges of the blades cause vortexes that contribute to the noise [7]. The propeller noise can be reduced by several noise abatement measures that can be taken during the design process that will positively influence the noise level. These are presented in the following section.

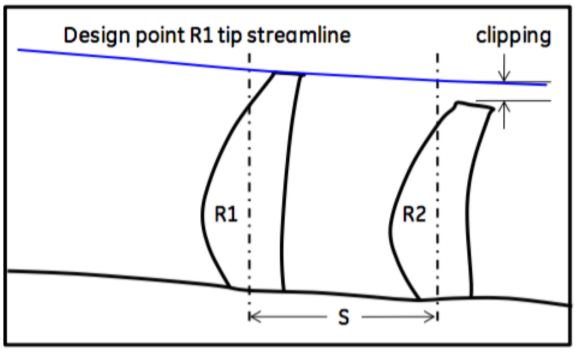

Figure 14.2: Illustration of open rotor aft clipping and the rotor spacing

- **Aft Clipping** The interaction of the front tip vortex on aft rotors represents an important noise source, particularly at high thrust and low flight speed conditions such as takeoff in which the propeller streamtube contracts more than at the high flight speed design point [44]. Clipping is the distance between the aft rotor tip and the streamline. This is illustrated in Fig. 14.2. The research conducted by General Electric uses the clipping optimisation of 5% span reduction of the aft blade which resulted in lower noise level. This was taken as a start point for the rotor design for the Starling 9000.

- **Blade count** Ideally, it is desirable to increase the blade count as it reduces the loading per blade, which reduces induced losses and rotor-rotor interaction noise. Rotor-rotor noise is affected in two ways: the front blade loading directly affects the strength of its shed wakes and vortices, and the aft blade loading affects its unsteady response to the incoming front blade gusts [44]. This makes the blade count selection an important parameter to have a good acoustic behaviour. They are primarily limited by pitch change mechanism, blade solidity for reverse thrust and engine weight. The Starling 9000 has 12 forward and 10 aft blades configuration based on most of the modern open rotor blade count.

- **Diameter** An increase in propeller diameter was evidently positive to the strong relationship between the disk loading and noise. The increased diameter improves net efficiency (by 2 to 3 %) via increased propulsive efficiency [44]. The acoustic benefits for lower disk loading is very significant. The GE research increased the rotor diameter from roughly 3.25 m for 1980's UDF designs to 4.27 m. The historical 1980's design that was tested in the program has a max disk loading of 803kW/m^2, whereas for the modern adapted design, disk loading is 474kW/m^2 [44].

- **Spacing** Generally, increasing spacing reduces noise by mixing the wakes and vortices prior to their impingement on the aft rotors. The GE research yielded a spacing to diameter ratio, S/D, of 0.27, where S refers to the distance between rotor pitch change axes (see Fig. 14.2) [44]. This will serve as a reference for the rotor design of the Starling 9000.

- **Pitch setting** The pitch settings or equivalently tip speed, of both front and aft rotors can be used to optimise both performance and acoustics [44]. [15] showed that increasing the front rotor tip speed at low flight speed resulted in quieter operation. Same front and aft rotor RPM was used for the experimental data which is not necessarily best for either acoustics or performance.

- **Blade design** This is one of the most important factors to improve the acoustic behaviour of the engine. The Starling 9000 uses *Gen2A* which is designed for lower disk loading with larger diameter than historical blade designs. It also incorporates features to further improve takeoff acoustics, particularly controlling the front rotor leading edge and tip vortex compared to *Gen1A* [44]. These features to reduce interaction noise associated with the front rotor vorticity interaction with aft rotor are incorporated into the design.

14.1.3 Combined Noise Footprint

For the perceived noise, the airframe noise is combined with the propulsion noise. However, the distribution of the airframe noise and the propulsion noise in the combined noise footprint is not constant. The distribution is different for different flight phases. The most critical flight phases, regarding noise generation, are take-off and approach. During take-off the main source is the propulsion noise, due to the high thrust setting. The propulsion noise is approximately twice as high as the airframe noise. Therefore the total aircraft noise is basically equal to the propulsion noise [7]. The distribution of the noise during take-off is depicted in Fig. 14.3.

During approach, the jet noise is negligible, but propeller noise is still significant. Also the contribution of the airframe noise is increased [7]. This is due to the use of flaps and the deployed landing gear. In this case, the propulsion noise and airframe noise are approximately equal [7]. The distribution of the noise during approach is depicted in Fig. 14.4.

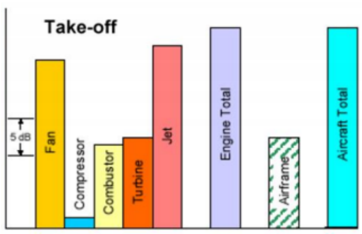

Figure 14.3: Distribution of noise sources during take-off [7]

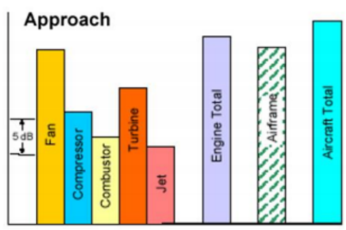

Figure 14.4: Distribution of noise sources during approach [7]

The combined noise of the Starling 9000 is compared to the noise of reference aircraft. The reference aircraft that are used in the comparison are the Boeing 737-600 and the Embraer E190-100. These aircraft have a similar take-off weight and external dimensions. For these aircraft, an approximation of the airframe noise is made using the contributions of the wing, the horizontal stabilisers and vertical stabilisers. The noise is calculated and it is measured at 1 metre from the source [7]. The parameters used in the calculations are the span, the MAC, the trailing edge sweep angle and the dihedral angle of the wing, horizontal and vertical stabilisers. The inputs and the results are presented in Table 14.1.

Table 14.1: Approximations of airframe noise of the Starling 9000, Boeing 737-600 and Embraer E190-100

Aircraft	**Starling 9000**			**Boeing 737-600**			**Embraer E190-100**		
Parameters	Wing	Canard	Winglet	Wing	HTP	VTP	Wing	HTP	VTP
Span [m]	31.05	12.26	4.06	34.32	14.35	7.16	28.72	12.08	5.45
MAC [m]	4.91	1.44	2.72	3.65	2.33	3.72	3.68	1.8	3.49
TE Sweep [°]	12.7	22.74	3.44	12.0	25.0	30.0	10.0	30.0	35.0
Dihedral angle [°]	3.63	3	85	6	7	0 5	7	0	
Noise [dB]	**97.77**			**98.53**			**97.57**		

As can be seen from the table, there is not a significant difference between these aircraft, even though the Starling 9000 has a very different configuration. Therefore, it can be concluded that the airframe noise of the Starling 9000 is similar to the noise level of the reference aircraft.

During approach, the noise is increased due to the use of slats. However, the Starling 9000 does not use slats and will therefore be quieter during approach. Also, the landing gear generates significant noise during approach. which is related to the size of the landing gear. The landing gear of the Starling 9000 is discussed and sized in Section 5.7. The size of the nose and main landing gear tires, 66 cm and 97 cm respectively is compared to the nose and main landing gear of the Boeing 737-600 with a tire diameter of 68 cm and 113 cm, respectively[1]. It can be seen that the tires of the main landing gear of the Starling 9000 are smaller than the tires of the Boeing 737-600. Therefore it can be concluded that the noise generated during approach is lower than the noise generated by the 737-600, hence it is quieter.

As mentioned above, during take-off, the noise is dominated by the engine noise and not the airframe noise. It is assumed the open rotor engines are noisier than conventional turbofan. According to a study of NASA,

[1] URL http://www.b737.org.uk/techspecsdetailed.htm[cited June 15 2016]

turbofans are 10 to 12 dB quieter than open rotor engines[2]. But the open rotor engines are still 10 to 13 dB below the regulations [2], defined by [28].
Taking everything into account, it is assumed that the noise generated during the approach phase is lower than reference aircraft and that the noise generated during take-off is higher than reference aircraft, but still below regulatory limits. Therefore, it is concluded that the aircraft is within the noise limits set by the ICAO [28].

14.2 Structural Health Monitoring and Prognosis

In order to ensure that future owners of the Starling 9000 may benefit from maintenance advancements, the aircraft will be fitted with Structural Health Monitoring (SHM) systems, and complementary data collection software. SHM is a nondestructive testing (NDT) methodology which aims to reduce maintenance costs, optimise aircraft operations, scheduling efficiency, and facilitate the transition to smart structures[3]. SHM uses sensors integrated into the structure to collect, analyse, localise and possibly predict the loads acting on the structure and damage that might be present [17]. The levels of SHM are discussed in Section 14.2.1. The system of the SHM sensors is discussed in Section 14.2.2 and its application in Section 14.2.3. The key advantage of modern structural health monitoring coupled with digital systems is the ability to monitor the structure continuously during service, rather than performing inspections on the ground at discrete time intervals. As such, the system downtime and interruption to normal operations may be reduced. This means that Starling 9000 owners will be able to enjoy their aircraft a greater percentage of the time.

14.2.1 Levels of SHM: From Loads to Prediction

Within industry, SHM is typically divided into different levels depending on the complexity of the use of the gathered sensor data. For the Starling 9000 a continuously improving SHM program is planned which will increase in complexity the more airplanes are delivered, and the more fleet data is collected. Specifically, all SHM data will pass through Starling Corporate Aircraft and be processed on the fleet level to help determine performance trends, improve damage, fatigue growth models, and in extreme cases may lead to a redesign of a component or part.
The zeroth level of SHM address quality control of the manufacturing process and the aircraft life prior to operation [17]. Starling Corporate Aircraft will also implement SHM methods to detect damage that may occur after the inspections but prior to customer delivery. Potential damage of components during transport will be detected using accelerometers and prevented using padding of components. Components arriving at the factory from external suppliers will be visually inspected and tested against a certified benchmark component. During manufacturing all incidents and SHM events will be recorded electronically and the data will be used to further improve the manufacturing process.
The first level of SHM comprises of online monitoring of the loads experienced by different aircraft components. This is the most basic level of SHM and is the foundation for all subsequent levels. This level requires a relatively low number of sensors strategically positioned at locations where high loads are anticipated. The main role of first level SHM sensing is to detect whether the structure is performing within it's designed operational limits [17]. However, at this level, there are no implemented checks for damage. The Starling 9000 will incorporate a comprehensive set of load monitoring equipment on the main wing spar, the wing-winglet junction, the open-rotor blades, the panoramic windows, and the landing gear. The system will also monitor the thermal loads (temperature), and the humidity in the structure.
The second level of SHM builds upon the first level of SHM by detecting and localising structural damage. The suite of aircraft load and impact sensors will be extended into arrays of sensors along a structural component. The data from the sensor array will then be processed to detect and triangulate the location of the damage. This level of SHM is mainly used to verify that a structural damage exists and to schedule a maintenance check. The localisation of damage increases the efficiency of the maintenance check and decreases the time needed for the check [17], because the maintenance crew already knows approximately where to check.
The third level of SHM generates substantial value for the operator. In addition to the damage localisation and detection of level two, the third level is able to quantify the extent of the damage as well as its impact on structural integrity [17]. The need for comprehensive and validated damage models and will be tackled by

[2] URL https://www.flightglobal.com/news/articles/open-rotor-noise-not-a-barrier-to-entry-ge-373817/[cited June 15 2016]

[3] URL http://www.compositesworld.com/articles/structural-health-monitoring-ndt-integrated-aerostructures-enter-service[cited June 2 2016]

monitoring the entire fleet of Staring 9000 aircraft to establish trends and models. As such, it is expected that it will not be possible to have level three SHM available at the roll-out of the first aircraft. However, once reliable models have been build, the information about the extent and severity of the structural damage will be used to determine the urgency of the maintenance check [17], thus improves the efficiency of the condition based preventive maintenance.
The fourth level of SHM is the most advanced level and extends the models of level three such that they are able to predict the rate of growth of the damage area. Damage growth models may utilise approximations of system damage tolerances based on historical data [17]. Such data will be collected continuously throughout the operational fleet life of the Starling 9000 life. With an accurate prognosis the maintenance needed can be even more efficiently planned and the availability of the structure can be increased. However, at the moment, this level of SHM is the least developed and use of it is still unrealistic.

14.2.2 SHM Sensing System: Hardware and Software

For SHM to be used effectively in monitoring of a structure; both sensors and a complementary suite of software are paramount. The added weight of the SHM system should be traded against the benefits and cost savings it provides throughout the operational life of the aircraft. For this reason, the sensor arrays shall not be distributed evenly throughout the system. Instead dense sensor clusters will be located near positions of high stress, poor respectability, and large impact of failure. Elsewhere in the structure, lower levels of SHM will be applied in order to record the load state of the aircraft and provide a more complete (but not detailed) structural health picture. Including all critical locations may nonetheless lead to a large sensing system where the weight and size become important aspects. Additionally, the reliability, connectivity, durability and embeddability of the system are critical aspects [19].
Online load monitoring of the structure most often employs load cells, pressure sensors and fibre bragg gratings (FBG). These are directly used to measure the forces and loads experienced by the structure and the resulting strain changes. For the online load monitoring of the engine blades, accelerometers are used to measure vibrations of the blades. A change in vibration may indicate an unbalance, fault, or failure of the engine.
To detect damage the most often used sensors are acoustic emission sensors, which listen for fibre breakage and delamination[3]; FBG sensors, which measure vibrations and acoustic and ultrasonic signals[3]; acousto-ultrasonics, which consists of a grid of sensors that analyse changes in wave patterns[3], and temperature sensors to monitor overheating of electrics.
If the load data is combined with a finite element model and a damage growth model it can be used to quantify the damage to the structure and to predict the damage growth [17]. This may require considerable computational power and the calculations are typically performed on the ground.
The number of sensors per area is a critical consideration. Using a single sensor per critical area would be most efficient. However, a single sensor is not able to localise damage and is not redundant in a way that sensor fault may be detected or readings verified. To localise damage through triangulation, at least three sensors are needed. The accuracy of the sensing system increases with the number of sensors, and is benefited form the damaged area being encircled by the sensing array rather than lying outside it. However, after approximately 20 sensors it becomes difficult to process the data and the system of sensors become relatively expensive. Usually a cluster of 10 sensors, 100 to 200 mm apart, shall be used to monitor a certain area [17].

14.2.3 Aircraft Application

The current state-of-the art SHM systems in aviation are mainly used during load and fatigue tests of aircraft structures. During the operational phase the use of SHM systems is essentially limited to the first level of SHM, i.e. monitoring of applied loads. Critical stress locations on the structure are monitored and the data is used as “additional information” during the maintenance checks. Another application is the monitoring of the gas path of the engine. Pressures and temperatures inside the engine are monitored during operation and transmitted wirelessly back to the engine manufacturer after the flight. By collecting performance data from the entire fleet of its engines, the manufacturers are starting to be able to recognise fault and failure trends.

The Starling 9000 will be equipped to exceed the current industry standards both in terms of sensors and software, as well as the ability to synchronise data between different RAMS stakeholders. Nonetheless, only a limited selection of critical areas will be actively monitored. Despite the advancements in semiconductor technology and miniaturisation of digital sensors, SHM system weight still represents a critical consideration. Ultimately, a trade-off should be performed between the extent to which a sensor array leads to a decrease in maintenance cost and the additional cost of the SHM system and the life-time fuel cost due to the additional weight of sensors, wires, and processing hardware.

The first category of critical areas covers those components which are at risk of being impacted during high-speed ground operations or flight. The radome on the nose of the aircraft is one such area. Protecting the expensive internal Doppler radar from impact from objects such as hail is critical to the safety of the aircraft and navigation in adverse weather. A pair of acoustic sensors placed on the inside of the nose structure will be used to continuously monitor for impact noise. Additionally, a pressure sensor will be used to detect whether the radome has been breached. As the nose is not structurally critical in terms of its load bearing abilities, there is no need for damage quantification. In addition to the nose other impact critical areas are the leading edges of the canard, the wing, the engines, and the engine pylons. Each leading edge will be equipped with an array of acoustic and force sensors. These will measure loads, acoustic emissions, vibrations, and impact events. The use of an array is recommended as it allows for damage localisation. This gives the maintenance crew a good idea of where to start looking for damage and whether multiple damage areas are present. As such, the repair duration is substantially decreased. The landing gear also needs to be monitored rigorously, due to it experiencing brutally high impacts forces during landing. Particularly, after a crosswind landing, load monitoring can decrease the necessary turn-around time. The sensors on the landing gear of the Starling 9000 will mainly serve to measure loads and strain resulting from the landing impact. Finally, the gearbox of the open rotor engines should be monitored as it is both a highly-stress, unique, and safety critical component. Predictive maintenance of gearboxes is typically possible through counting of particles in gearbox oil. Once the number of particles exceeds a certain level, the extent of faults on the gearbox teeth is considered to be too extensive for continued operation and the gearbox must be scheduled for replacement.
It is important to monitor for impact not only during flight but also during ground operations when airport logistics vehicles may accidentally impact with the jet and either not notice or not disclose the collision to the pilot.
Besides critical areas regarding impact, there are also critical areas regarding the structure. One of those is the connection between the winglet and the wing, due to large size of the winglets and the stresses that act on the connection. Additionally, the uniqueness of the design further increases the need and benefit of monitoring. These sensors are placed in a cluster around the connection to measure loads and strain.

The data from the sensors is used in two ways. On board, data indicating critical damage is processed in real time, and an informative signal is sent to the pilot. On the ground, structural health data indicating impact or other damage are downloaded wirelessly from the Starling 9000 and processed. The wireless transmission of data also allows the maintenance crew to be notified of faults while the aeroplane is still in flight. This allows any necessary parts to be ordered in advance, and the maintenance space reserved.

14.3 End-of-life Solutions

The aircraft end-of-life (EOL) management concerns how aircraft will be handled after useful lifespan. Environmental concerns are stimuli for finding a systematic, complete and qualitative framework for a safe and environmentally responsible management of end-of-life aircraft. The four EOL decisions are reuse, remanufacture, recycling and disposal. According to Airbus's report[4], around 85% of weight of a civil aircraft can be recovered (15% for reuse and 70% through recycling). Recycling includes collecting and sorting recyclable materials that would otherwise be considered as waste and then processing them into raw materials for future aircraft or other industrial applications. Recycling the aircraft can reduce environmental impact while increasing the value of recyclable materials, which is beneficial for the customers of Starling 9000. Parts that can not be recycled are be disposed conventionally.

14.3.1 Approach of Handing EOL Business Jet

There are generally three main steps for handling EOL Starling 9000. During the first step of decommissioning process, all operating liquids could be removed or re-sold for direct re-use e.g. fuel, or disposed in specific a recovery channel according to existing regulations. After this, if the owner of the aircraft decides not to re-enter the business jet into service, a disassembly process could be applied. One technique that could be practical is to dismantle Starling 9000 into certain logical component groups. For example, landing gears,

[4]URL http://ec.europa.eu/environment/life/project/Projects/index.cfm?fuseaction=search.dspPage&n_proj_id=2859&docType=pdf [June 14 2016]

canard sections, leading edge sections and the wing separated from the fuselage. Re-usable and re-sellable parts and equipment, on the basis of the demand in the parts market, will be selected. Re-usable and disassembled parts in Starling 9000 are the two open rotor engines, the landing gears, avionics, auxiliary power unit (APU), parts of the cabin equipment as well as movable parts and structural parts, which can be re-used upon the conditions[5] for the manufacturing of new Starling 9000.
Possible disassembly sequences could be determined by the type of the part, its location in the business jet, disassembly effort, the connection types and relations among disassembly tasks. For the case of a certain number of aircraft to be disassembled in an area, a long-term disassembly planning, which is the capacity planning, could be employed. Several aircraft could be disassembled at the same time. Among the strategies of disassembly, systematic disassembly, which can separate and sort all the components based on material composition, is recommended to be under consideration for minimising the environmental risk. In this case, identification of the material can be performed by using Niton detection. Another strategy smart disassembly is preferred if the time and effort to remove the attachments are limited. The goal is to alleviate the excessive time needed to remove the attachments,by not removing rivets that are shared between components with similar material composition. Although the quality of recovered material by smart disassembly is compromised compared to systematic strategy. [6] [7]

Disassembly will be followed by a dismantling process. In this stage, a dismantle plan will be set up in order to optimise the material recovery. The dismantling could start with the stripping of interiors and will be followed by a cutting phase. In this phase, specific parts or sections like doors, windows can be extracted and certain valuable metal parts and some composite parts can be recovered. The plastic, others composites and wastes can be disposed. The aircraft could be dismantled with different tools, for example plasma torches, high pressure water jet, chainsaw and hydraulic scissors. As the next step, the materials will be grouped e.g. aluminium alloys substrates, wiring, harness, thermoplastics, foams, textiles, carpets and tissues. Finally these materials will be prepared for shredding and sorting and are sent to recovery channels. The recycled metal will return to the appropriate markets like automotive. All the steps will be performed considering the regulatory compliance and the life cycle design to promote and improve the design performance[6].

14.3.2 End-of-life Aircraft Material Recycling

Recycling of the business jet could be divided into two levels: the product recycling level and the material recycling level. Product recycling will focus on the direct re-use or manufacturing of an end-of-life part or assembly, e.g. engines and avionics. End-of-life aircraft will contain a lot of materials that can be recycled, which is the motivation for recycling.

Many parts of the airframe are chosen to be made of composites. End-of-life problems concerned with recycling composites are an vital issue to be taken into account during the design phases. Composites recycling in industry still is under development. One potential way is thermal pyrolysis, which can be considered on a large scale. Also the the quality of the recovered carbon fibre residue is considered high enough, therefore the fibres could be considered for re-use. This technique has been developed in Nottingham University and can continuously recycle cured and uncured carbon fibre composite parts[8]. Also, Airbus is working with CFK-Valley Stade Recycling GmbH & Co kG on the development of a pyrolysis-based recycling plant for the recovery of carbon fibres from decommissioned Airbus aircraft, which is a good indication that thermal pyrolysis is a promising way to recycle the composites[9].
Because the Starling 9000 will be launched into market in 2020, this method is possible to be used for recycling composites parts. Apart from that, an alternative progress for the recovery of carbon fibre from composites uses a low temperature liquid process that digests the organic resin leaving the fibres intact, and is being developed by Adherent Technologies Inc (ATI) in the USA. The company claims that a reasonable profit can be made for recyclate, which could interest the customers[9]. The recycling of the composites in Starling 9000 will be mainly focused on the recovery of reinforcement fibres, since the matrix has much less value and is

[5] URL http://ac.els-cdn.com/S2212827114005009/1-s2.0-S2212827114005009-main.pdf?_tid=6b898842-323a-11e6-a8cf-00000aab0f27&acdnat=1465913897_ed73b2d8aa0f8287f0683c012aa7df20[June 14 2016]
[6] URL http://ac.els-cdn.com/S2212827114008610/1-s2.0-S2212827114008610-main.pdf?_tid=a62e60ee-323a-11e6-9bab-00000aab0f01&acdnat=1465913995_0710a72123cc34d21bcd67b46c2700e7[June 14 2016]
[7] URL http://www.sciencedirect.com/science/article/pii/S2212827116001037[June 14 2016]
[8] URL http://users.ox.ac.uk/~pgrant/Airplane%20end%20of%20life.pdf[cited June 14 2016]
[9] URL http://www.sciencedirect.com/science/article/pii/S0034361710700631[cited June 14 2016]

difficult to recover. In general, the potential uses of recovered fibres can be in the automotive, construction and marine sectors.

Another major material used in the Starling 9000 is metal alloys, especially aluminium alloys. Since aluminium recycling is less expensive than the production of new aluminium from ore, recycling of aluminium could generally results in significant cost savings. The planning of recycling aluminium will start with pre-treatment and alloy recipe preparation. This will be followed by melting and refining and finally to be put for alloying and casting. This industry is under quick development, which will bring efficient ways for better recycling metals in Starling 9000[9].

14.4 LEED Certification of Factory

LEED or Leadership in Energy and Environmental Design is an organisation that works on the verification for green buildings [10]. A LEED certified building addresses several points regarding sustainability. It uses less water and energy, therefore reducing cost and greenhouse gas emissions[10].
The construction of a new factory facility belongs to the 'Building Design and Construction' category of the LEED program. This provides a framework for building a sustainable and green building, resulting in a resource-efficient and cost-effective building[11].

With the constructions of the factory several aspects have to be taken into account, regarding LEED certification. This first aspect is about the location of the factory. To avoid construction on environmentally friendly lands and reduce the environmental impact, the factory will only be build on previously developed land or on land that is not qualified as sensitive land, such as farmland or floodplains [12]. The second is to improve transportation efficiency. The factory will be build on a site that is within 16 km of a main logistic hub and within 1.6 km of an on-off ramp to a highway [12].
The next aspect is about a sustainable site, specifically rainwater management. The intent is to reduce the runoff volume and improve the water quality[12]. Water will be collected and can be used as cooling water for production, water to flush toilets and to clean. Otherwise the water needs to be dispersed evenly over the surrounding environment to reduce the environmental impact.
Also energy saving is taken into account. Energy meters will be installed, at building-level and sub-level, that are aggregated to provide total building energy consumption [12]. This is to support energy management as well as showing possibilities for extra energy savings. Next to the energy saving there is also renewable energy production. The factory could include solar gardens or it could use community renewable energy systems to reduce the building energy cost and reduce the environmental harms regarding fossil fuel energy [12].

Beside the applications within the building, the construction of the building itself should also be taken into account. During construction there will be waste, therefore a construction waste management plan is needed. The plan includes waste diversion goals and diversion strategies about separating or commingling materials. Also the material used to build the factory should be selected from materials with available life cycle information and environmentally and economically friendly impacts [12].

If the building is LEED-certified the building improves its energy performance by at least 10.5% compared to non-LEED-certified projects[11].

14.5 Environmentally Friendly Production

To improve the overall environmental performance, eco-efficient production technologies are also part of the consideration of the design. Several aspects could be covered to minimise the environmental impact during the production. The goals of the production of the business jet are energy saving, water saving, waste reduction and emissions minimisation.

Energy
Improving the energy efficiency is one of the best ways to reduce energy costs and carbon emissions to meet the environmental goals. Conduct an energy audit to find where improvements are necessary. Low-energy

[10] URL http://www.usgbc.org/LEED/ [cited June 14 2016]
[11] URL http://leed.usgbc.org/bd-c.html [cited June 16 2016]

lighting, improved insulation, voltage management and energy efficient heating and cooling are the key practises that could be employed[12]. For example, replacing high bay lighting by LED technology and replacing HVAC (Heating, Ventilation and Air Conditioning) filters in the factories can bring significant energy savings. Another alternative way could be the use of renewable energy that is available[13]. What's more, layout of the factory is strongly related to the energy consumption. The integration of energy efficiency criteria into production system planning could substantially contributes to resource productivity and thus increasing the energy efficiency of production processes.

Water
Processed water could support a wide variety of activities during the production. Emphasis should be put on recycling and reusing water. Conserve water using the best available technology such as water-saving equipment utilities. Also, installing rainwater tanks could be on choice to reduce water consumption. By recycling water for instance the coolant water used for cooling process during material production can result in a more water efficient procedure[12].

Waste
For environmentally friendly manufacturing, it is demanded to implement more efficient waste management. Manufacturing involves raw materials that are not used completely. Part of the raw material is usually discarded, which can harm the environment. It is important to make use of leftovers or dispose them properly. One possible way could be waste segregation that is encouraging employees in the shops to better secrete their waste. Better segregation can increase the possibility of recycling waste. Also to reduce the amount of discarded raw material, production and assembly plan should be carefully designed.

Emissions
Emissions generated during manufacturing is an important issue to be focused on towards a more environmentally friendly production. The application of innovative solutions could be chosen from optimised ventilation systems, solar panels, pipes for geothermal heating, air-sourced heat pumps and more. For example, implementation of a biomass boiler at the Clement Ader site of Airbus reported that up to 15 percent of the CO_2 emissions was avoided, which is a success and could be referenced for our production planning[12].

[12] URL http://www.airbus.com/company/eco-efficiency/eco-initiatives/ [cited June 14 2016]
[13] URL http://smallbusiness.chron.com/making-manufacturing-processes-ecofriendly-38937.html [cited June 14 2016]

15. Compliance Matrix and Recommendations

Accrediting confidence to a design entails validation. This chapter provides a compliance matrix to validate the requirements including lists of requirements including system requirements and stakeholder requirements. Those are determined and defined in the beginning of the project. Recommendations of main elements are summarised for further analysis. Also the parameters of the business jet is presented in the end of this chapter.

15.1 List of Requirements

In this section, requirements that identified in the baseline report are listed. These are used for the validation procedure to ensure agreement between the designed business jet and requirements.

15.1.1 Top Level System Requirements

- URBJ-RNG-01 The business jet shall have a range of at least 8500 nautical miles
- URBJ-RNG-02 The business jet shall hold 18 passengers for a range specified in URBJ-RNG-01
- URBJ-SFT-01 The business jet shall comply with CS-25 safety regulations
- URBJ-MCH-01 The business jet shall have a cruise mach number greater than 0.8 Mach
- URBJ-TKO-01 The business jet shall have a take-off distance of less than 2000 meter (at MTOW and sea level, ISA)
- URBJ-SUS-01 The business jet shall go through a life cycle analysis to optimise for sustainability (materials, manufacturing, end-of-life)
- URBJ-CST-01 The business jet shall cost less than 60 million dollar for a production series of 600 aircraft
- URBJ-DET-01 The first business jet shall be delivered by the end of 2020
- URBJ-ENV-01 The business jet shall comply with Clean Sky 2 environmental targets
- URBJ-ENV-02 The business jet shall comply with Clean Sky 2 noise targets
- URBJ-FLC-01 The business jet shall be able to fly on Jet A-1 fuel
- URBJ-FLC-02 The business jet shall be able to fly on biofuels such as Honeywell Green Jet Fuel

15.1.2 Stakeholder Requirements

Operator requirements:

- URBJ-OPR-RNG-01 The business jet shall have a range of more than 8,500 nm (15,742 km) for 18 passengers
- URBJ-OPR-CRA-01 The business jet shall have a cruising altitude above 40000 ft
- URBJ-OPR-STS-01 The business jet shall be statically stable
- URBJ-OPR-BCL-01 The business jet shall have a business class interior and configuration
- URBJ-OPR-FCA-01 The business jet shall travel faster than 850 km/hour
- URBJ-OPR-LTO-01 The business jet shall be able to land and take-off from most municipal, medium and large airports
- URBJ-OPR-SFL-01 The business jet shall be 80% safer to fly than aircraft made in year 2000
- URBJ-OPR-RLB-01 The business jet shall be reliable with an average availability of 22 hrs per day
- URBJ-OPR-FLC-01 The business jet shall have a fuel consumption of at least 0.15 miles/lb
- URBJ-OPR-FLC-02 The business jet shall be able to fly on Jet A-1 fuel
- URBJ-OPR-FLC-03 The business jet shall be able to fly on biofuels
- URBJ-OPR-BLC-01 The business jet shall cost less than 60 million dollar for a production series of 600 aircraft
- URBJ-OPR-AWC-01 The business jet shall comply with the latest airworthiness and certification regulations
- URBJ-OPR-DET-01 The first business jet shall be delivered by the end of 2020
- URBJ-OPR-CNT-01 The first business jet shall be laterally controllable

- URBJ-OPR-CNT-02 The first business jet shall be longitudinally controllable

Passenger requirements:

- URBJ-PSG-CD-01 The business jet shall have a minimum cabin width of 2.50 m
- URBJ-PSG-CD-02 The business jet shall have a minimum cabin height of 1.90 m
- URBJ-PSG-CP-01 The business jet shall have a maximum cabin pressure altitude of 4,500 ft
- URBJ-PSG-CH-01 The business jet shall have a minimum humidity level of 15 percent
- URBJ-PSG-CT-01 The business jet shall have maximum cabin temperature of 30 degrees Celsius
- URBJ-PSG-CT-02 The business jet shall have a minimum cabin temperature of 15 degrees Celsius
- URBJ-PSG-SC-01 The business jet shall have a seat comfort level comparable to business class
- URBJ-PSG-SC-02 The business jet shall have a seat pitch of 45 inches or more
- URBJ-PSG-SC-03 The business jet shall feature reclining seats
- URBJ-PSG-CF-01 The business jet shall have sanitary facilities
- URBJ-PSG-CF-02 The business jet shall have power outlets at the seats
- URBJ-PSG-CF-03 The business jet shall provide an on-board Wi-Fi network
- URBJ-PSG-CF-04 The business jet shall feature an in-flight entertainment
- URBJ-PSG-CF-05 The business jet shall have catering facilities
- URBJ-PSG-CF-06 The business jet shall have refrigerated storage compartments
- URBJ-PSG-LG-01 The business jet shall be able to accommodate at least 20 kg of luggage per passenger
- URBJ-PSG-CN-01 The business jet shall have maximum cabin noise level of 50 dB
- URBJ-PSG-CW-01 The business jet shall feature windows of at least 27 x 47 cm

Cockpit crew requirements:

- URBJ-CPC-PB-01 The business jet shall have a crew compartment with at least one bed for pilots to rest
- URBJ-CPC-GC-01 The business jet shall feature a glass cockpit
- URBJ-CPC-ER-01 The business jet shall comply with 2020 ergonomic regulations

Cabin crew requirements:

- URBJ-CBC-CS-01 The business jet shall accommodate seating for the crew
- URBJ-CBC-ER-01 The business jet shall comply with 2020 ergonomic regulations

Airport residents requirements:

- URBJ-APR-NR-01 The business jet shall comply with the 2020 noise targets
- URBJ-APR-ER-01 The business jet shall comply with the 2020 emission targets

Governmental aircraft regulators:

- URBJ-GAR-AC-01 The business jet shall comply with airworthiness and certification regulations
- URBJ-GAR-NR-01 The business jet shall comply with the Clean Sky 2 (2020) noise regulations
- URBJ-GAR-ER-01 The business jet shall comply with the Clean Sky 2 (2020) emission regulations
- URBJ-GAR-HT-01 The business jet shall comply with ACARE 2020 targets

15.2 Compliance Matrix

The compliance matrix which follows from the requirements presented in Section 15.1 is presented in table Table 15.1 to indicate whether each requirement is met. It shows the required and achieved values of the requirements. The Compliance columns are ticked as “Fulfilled” if the requirements were met; “Not” is the requirement was not met. As can be seen, most requirements are met. Requirements from aircraft residents and government aircraft regulations are not possible to check at this stage due to the uncertainty of the regulations coming in 2020.

Table 15.1: Compliance matrix

Requirement ID	Required Value	Achieved Value	Compliance	
			Yes	No
Top level system requirements				
URBJ-RNG-01 (URBJ-OPR-RNG-01)	≥ 8500 nm (15,742 km)	maximum 9229 nm (Section 8.1)	✈	
URBJ-RNG-02	18 passengers over 8500 nm	18	✈	
URBJ-SFT-01			✈	
URBJ-MCH-01	≥ 0.8 Mach	0.8 Mach	✈	
URBJ-TKO-01	≤ 2000 m	2000 m	✈	
URBJ-SUS-01			✈	
URBJ-CST-01 (URBJ-OPR-BLC-01)	<60 million	57.5 million (Chapter 3)	✈	
URBJ-DET-01 (URBJ-OPR-DET-01)	End of 2020	Dec 2020 (Section 1.3)	✈	
URBJ-ENV-01			✈	
URBJ-ENV-02 (URBJ-GAR-NR-01)			✈	
URBJ-FLC-01 (URBJ-OPR-FLC-02)			✈ [d]	
URBJ-FLC-02 (URBJ-OPR-FLC-03)			✈ [d]	
Operator requirements				
URBJ-OPR-CRA-01	Above 40000 ft (12192 km)	12192 km	✈	
URBJ-OPR-STS-01			✈	
URBJ-OPR-BCL-01			✈	
URBJ-OPR-FCA-01	>850 km/hour (236 m/s)	236 m/s	✈	
URBJ-OPR-LTO-01			✈	
URBJ-OPR-SFL-01	80%	(Section 4.5)	✈	
URBJ-OPR-RLB-01	22 hrs per day	(Section 4.5)	✈	
URBJ-OPR-FLC-01	≥ 0.15 miles/lb (532.2 m/kg)	712.7 m/kg	✈	
URBJ-OPR-CNT-01			✈	
URBJ-OPR-CNT-02			✈	
Passenger requirements				
URBJ-PSG-CD-01	>2.5 m	3.2 m [b]	✈	
URBJ-PSG-CD-02	>1.9 m	2.4 m [b]	✈	
URBJ-PSG-CP-01			✈ (Section 11.3)	
URBJ-PSG-CH-01	>15%		✈ [a]	
URBJ-PSG-CT-01	<30 degrees Celsius		✈ [a]	
URBJ-PSG-CT-02	>15 degrees Celsius		✈ [a]	
URBJ-PSG-SC-01			✈	
URBJ-PSG-SC-02	>45 inches (1.143 m)	2 m (Table 5.3)	✈	
URBJ-PSG-SC-03			✈ [a]	
URBJ-PSG-CF-01			✈ [a]	
URBJ-PSG-CF-02			✈ [a]	
URBJ-PSG-CF-03			✈ [a]	
URBJ-PSG-CF-04			✈ [a]	
URBJ-PSG-CF-05			✈ [a]	
URBJ-PSG-CF-06			✈ [a]	
URBJ-PSG-LG-01	>20 kg	20 kg [2]	✈	
URBJ-PSG-CN-01	<50 dB			[c]
URBJ-PSG-CW-01	≥ 27 x 47 cm	27 x 47 cm	✈	

[a] See Chapter 5
[b] See mid-term report [2]
[c] Not quantifiable at this stage
[d] See Section 5.3.1

Table 15.2: Compliance matrix (continued)

Requirement ID	Required Value	Achieved Value	Compliance	
			Fulfilled	Not
Cockpit crew requirements				
URBJ-CPC-PB-01			✈	
URBJ-CPC-GC-01			✈	
URBJ-CPC-ER-01			✈	
Cabin crew requirements				
URBJ-CBC-CS-01			✈	
URBJ-CBC-ER-01			✈	
Airport residents requirements				
URBJ-APR-NR-01				[a]
URBJ-APR-ER-01				[a]
Governmental aircraft regulators				
URBJ-GAR-AC-01			✈	
URBJ-GAR-ER-01				[a]
URBJ-GAR-HT-01				[a]

[a] Not quantifiable at this stage

15.3 Recommendations

Due to the time limitation of the project, complete coverage of the design for this ultra-long range business jet is not possible. In this section the recommendations covering aerodynamics, propulsion, structures, stability and control and material selection are summarised in terms of further investigations and the feasibility of the long-term vision.

15.3.1 Propulsion

Starling 9000 makes use of the CROR engine for its added benefits of fuel efficiency and cut back in emissions. This is primarily achieved because of the increase in propulsive efficiency through ultra high bypass ratio. However, at this moment the CROR engines are still under development, making it difficult to analyse the engines needed for the propulsion. From tests, it can already be concluded that the open rotor engines are capable of flying at a Mach number of 0.8 with reduced fuel consumption. Also, from the reduced fuel consumption the emissions are approximated. The challenge was mainly concerned with noise modelling of the open rotors. Additional modelling and experiments should be performed regarding the noise analysis of the open rotor. A jet core and the open rotors needs to be analysed together to determine the combined noise generation. Next to the performance of the CROR engine is the safety aspect of the engines. There has been ample experimental research conducted on the reinforcement of the fuselage regarding engine failure from blade-off event. The design choice was the floating panel made of GLARE. However, there is not much tests conducted on cross-engine debris scenario. The Starling 9000 uses high performance composite panel as a shield to protect the core and blades from the debris.

15.3.2 Aerodynamics

The verification and validation of the aerofoil has been implemented by 4 aerofoil analysis tools are discussed in Section 7.1.2. Still wind tunnel tests should be complied to gain accurate and reliable results. In particular, extra attention should be paid to the performance at higher angles of attack where transition and turbulence effects become more dominant and the appropriateness of the SA viscosity model may diminish. What is more, computational estimation of drag is considerably less accurate than that for lift, and should be given additional attention. Further more, the validation of the aerofoil itself against stakeholder requirements must be conducted. This includes a comprehensive analysis of the effect on fuel volume, structural weight, landing gear, flaps, and winglet integration. The off-design point performance of the aerofoil must also be considered through analysis and multi-point optimisation. Validation of the design through testing is possible for the three dimensional wing but is not as applicable to the 2D aerofoil. Nonetheless, it is recommended to perform further 3D RANS analysis of the wing so as to avoid the high expenses of physically testing a wing design.

15.3.3 Weight estimation

For the weight estimation, with reference to the regular airliners, it is assumed that each passenger and crew member weighs 80 kg and is bringing 20 kg luggage on board. Some stakeholders may expect to carry more luggage to the business jet. Thus refinement of the weight estimation could be conducted in the future. For this refinement a passenger weight including luggage of approximately 150 kg would be a more realistic design choice. Also with more detailed design of interior and choices of equipment on board, weight estimation with improved accuracy could be achieved in the future development. However, it could be conceived that altering the weight estimation will exert effect on the design choices of other subsystems.

15.3.4 Structures

From the fuselage-wing model constructed in Chapter 11, the combined weight of the wing and fuselage structure was determined to be 14400 kg. Compared to the Class II weight estimate of 18800 kg, the structure meets the weight requirement. Still, there is room for improvement. An area that was considered to be too complex within the given time frame and not critical was the tail cone. The significant loads originating from the engine thrust and weight cause significant shear stresses due to the weight, and normal (compressive) stresses due to the thrust and the bending load. This, combined with the locally small cross-sectional area of the cone near the engines, might result in significant local stresses that should be analysed in detail. Another area that should be considered is the winglet structure, and its connection to the wing box. Due to the high curvature, a complex solution will need to be implemented to the structural layout and production of the box structure, and a detailed Finite Element Method model should be constructed to realistically analyse the stresses in this section. Furthermore, the material properties used for the calculations were not realistic. Composite materials are rarely fully isotropic, since the benefit of these materials lies in the specific strength and stiffness they provide in a certain direction. Composite materials can be tailored to accurately fit strength and stiffness for the very specific load case. For a more detailed analysis, the optimum layup should be determined.

15.3.5 Stability and control

As presented in the stability and control chapter, although starling 9000 proved to be stable, certain areas could be investigated to study the exact behaviour of the aircraft in various flight phases. During the design for the canard, upwash induced from the wing and sidewash from the fuselage were neglected because of relative long distance between wing and canard. Also there exists sidewash generated by fuselage exerted on the winglets. Those effects may influence the trim and stability of the aircraft. In the later phases, it is recommended to estimate accurately the interactions between main wing and the canard, fuselage and winglets by employing wind tunnel tests. There are interferences between rudder and ailerons as well thus the lateral and directional dynamics could be frequently couped and should be looked into for the future detailed design for rudders and ailerons. In addition, in the situation of one engine operating, although the rudders are sized to trim this situation, the influence of drag forces created by inoperative open rotor should be considered and quantified. Moreover, yaw dampers could be applied to augment lateral-directional dynamic stability. Aside from take-off, cruise and landing, for example the transition phase and hover phase should also be analysed. Since transition phase is complicated, the analysis of the phase is beyond the scope of the project and additional research will be needed for the design.

15.3.6 Material selection

The resin used to bond the layers of carbon fibres should have good shear characteristics and prevent delamination as much as possible. Epoxy resin offers average properties for a low price and it is often offered as standard resin in preimpregnated (prepreg) composite sheets. The wing and fuselage are decided to be made entirely out of high strength carbon composites. Using composites for both the skin and the stiffeners provides the advantage of co-bonding these components together, this negates the need for adhesive bonding or fasteners to reduce the structures weight. Furthermore adhesive bonding is hard to check for integrity and fasteners can induce corrosion or delamination. If more stiffness is required to complete the design high modulus carbon can be used and if more sustainability or maintainability is required metals should be used. Apart from the major aircraft parts some smaller parts can be made out of different materials tailored to fit a specific purpose. Composite sandwich panels will be used for the floor panels, control surfaces, doors and engine covers. These composite sandwich panels have high bending resistance with a low density. For the radome and leading edge parts it is decided to use an impact resistant material, materials that are a combination of metal and composite fibre provide good impact resistance while having a lower density than pure metals. GLARE, which is a layup of aluminium and glass fibre, is the preferred composite for the highest impact probability areas.

15.4 Summary of Critical Aircraft Parameters

Table 15.3: Some of the Most Important Aircraft Parameters

Parameter	Unit	Rounded value
Take-off weight	[kg]	53000
Empty weight	[kg]	27100
Maximum zero-fuel mass (MZFW)	[kg]	35300
Fuel weight	[kg]	23300
Maximum landing weight	[kg]	47700
Mass fraction Cruise	-	0.980
Cruise weight start	[kg]	51650
Mach cruise start 3D	-	0.8
Velocity cruise start	[m/s]	236.03
Cruise viscosity	[kg/(m · s)]	$1.42{\cdot}10^{-5}$
Cruise Reynolds Number (Based on MAC)	-	24681900
Specific fuel consumption	[kg/Ns]	$1.262{\cdot}10^{-5}$
Approach stall speed deployed	[m/s]	54.5
Approach speed sea level	[m/s]	64.6
Stall speed clean sea level	[m/s]	62.4
Ultimate load factor gust	-	4.65
Ultimate load factor manoeuvre	-	3.75
Aircraft c.g. Min -actual wing position	[m]	19.69
Aircraft c.g. Max -actual wing position	[m]	22.7
Landing distance	[m]	2000
Fuselage length	[m]	36.9
Cabin length	[m]	22.8
Cabin width	[m]	2.9
Cabin height	[m]	2
Seat width	[m]	0.6
Seat pitch	[m]	2
Wing area	[m^2]	136.1
Wing span(Geometric)	[m]	31.05
Wing root chord	[m]	7.01
Wing tip chord	[m]	1.75
Wing MAC	[m]	4.91
Wing sweep angle	[deg]	25.6
Wing taper ratio	-	0.25
Wing dihedral angle	[deg]	3.63
Wing aerofoil 2D maximum thickness [t/c]	-	0.128
Wing aerofoil maximum camber [t/c]	-	0.0136
Wing 3D (C_L/C_D) optimum	-	24.2
Wing 3D C_{L_α}	1/rad	4.92
Wing fuel volume	[m^3]	29.8
Skin thickness	[mm]	6.0
Canard area	[m^2]	17.7
Canard geometric span	[m]	12.3
Canard sweep angle (0.5 chord)	[deg]	25
Area per winglet	[m^2]	11
Height of the winglet	[m]	4.06
Winglet dihedral angle	[deg]	85

Conclusion

With the global economy steadily increasing around the globe, the demand for private long distance travel is rising. Starling Corporate Aircraft identified this new and emerging market potential and proposes the Starling 9000 to enter this market and offer clients the best it has to offer. In comparison to the competition, the Starling 9000 offers customers the benefit of flying 8.500nm non-stop. This enables city pairs currently only connected non-stop by commercial airlines. With the Starling 9000, which seats 18, the passengers can enjoy the added benefits of travelling by private jet. The raised comfort level and Skyview Panoramic Windows provides an office space with unparallelled views over the skies.

For the design, Starling is striving to incorporate the latest technologies on the market, in order to offer the customers the cutting edge and cost efficient plane they are looking for. The most apparent design characteristics are the open rotor engines on the back, the absence of the tail, a large panoramic window on both sides of the fuselage and the lifting canard surface at the nose of the aircraft. During the design phase, the focus lay on providing a quiet cabin and a low drag such that the aircraft is able to achieve its class leading range. As a result, the the wings are configured in a canard configuration, where both the main wing and the canard surface generate a positive lift during the cruise. Furthermore, the tail has been omitted from the design, reducing the airframe drag. The rudder function of the tail has been integrated in the winglets, hereby increasing the efficiency of the wing. The canard enables the aircraft to generate lift in a more efficient manner, paired with the 26% less fuel consuming open rotor engines results in the lowest fuel consuming aircraft of its class. Reducing the weight of the aircraft has been a huge drive during the aircraft design, as lower weight equals less fuel required. To achieve this goal, the entire fuselage and wings will be made from carbon composites, offering lower empty weight and better fatigue resistance than a, traditional, aluminium aircraft.

To complement the cutting edge design, Starling Corporate Aircraft is striving to minimise the environmental impact of the aircraft by presenting an end of life solution for when the aircraft enters retirement. Even before the aircraft is retired, the environmental impact is minimised by employing lean manufacturing, reducing the waste during production.

A. Task Division & Communication

Table A.1: The task division for the Final Report

Member	Contributed Sections	Checked Sections	Additional Task
J. Borghart	Summary, Chapter 1 and Sections 7.5 and 9.1.3, Conclusion	Chapter 6 and Section 15.3	
F. De Voogt	Sections 1.3, 11.4 and 12.5 and Chapters 4 and 10	Chapters 5 and 7	
M. Kosec	Sections 3.3, 7.1, 7.4, 8.2, 9.2 and 14.2, Chapter 6, and Table A.2	Section 8.2 and Chapters 2, 7 and 9, Preface, Summary	Dividing technical and non-technical tasks, managing design process
J. Liu	Sections 8.1, 9.1, 14.3 and 14.5 and Chapter 15	Chapters 1, 3 and 10 and Section 8.4	
S. van Middelaar	Introduction, Summary, Chapters 2, 3 and 13 and Sections 5.1 and 9.2	Chapters 3, 9, 12 and 13	LaTeX manager, layout, Photoshop and DATCOM
M. Moussa	Chapter 4 and Sections 5.5, 5.7, 7.1 to 7.3, 9.2, 12.3 and 12.4	Chapters 1, 2, 10 and 11 and Sections 5.3 and 9.1.1	
A. Pandey	Sections 2.3, 5.2, 5.3.1 to 5.3.4, 5.6, 8.2 and 14.1.2 and Chapter 6	Introduction, Sections 12.1.1, 12.2, 12.3, 12.5 and 14.1, Conclusion	3D modeling, Keyshot rendering and Illustrations
M. Popescu	Sections 5.4, 6.2.2, 6.5, 7.4, 8.3, 9.1.1, 11.1.2, 12.1 and 12.2	Chapters 1, 6 and 10 and Sections 9.1 and 14.2	
N. Weij	Chapter 11 Section 15.3.4		CATIA, Abaqus
C. van Woensel	Sections 4.3, 5.3.1, 8.4, 12.1.1, 14.1, 14.2 and 14.4, Chapter 6, and Table A.1	Chapters 2 to 4 and 7 and Sections 5.2, 11.1, 14.3 and 14.5	

Table A.2: An overview of the personal communication with internal and external experts

Team member	Contact	Affiliation	Topics	Date
J. Borghart	Henk Bulte	Fokker Services	SkyView Panoramic Window	20160614
	Caroline Wepierre	Jet Aviation	Cabin interior design [1]	20160608
F. De Voogt	Jos Sinke	TU Delft	Materials, composite cost	20160531
M. Kosec	Roger Groves	TU Delft	Struct. Health Monitoring	20160608
	Roeland de Breuker	TU Delft	Flutter	20160607
J. Liu	Derk-Jan van Heerden	AELS B.V.	end-of-life solutions [1]	20160616
S. van Middelaar	Ronald Deerenberg	Blackshape S.p.A.	Stability & Control	20160610
M. Moussa	Roeland de Breuker	TU Delft	Flutter	20160607
	Mostafa Abdalla	TU Delft	Flutter	20160602
A. Pandey	Joris Melkert	TU Delft	Open Rotor Performance	20160603
	Eric Roth	Int. Jet Interiors	Cabin interior[1]	20160603
M. Popescu	Joris Melkert	TU Delft	Open Rotor Performance	20160603
N. Weij	Dirk Benade	Dassault Systemes	Abaqus course	20151109
	Berend Jonkers	Dassault Systemes	Abaqus course	20151109
C. van Woensel	Joris Melkert	TU Delft	Open Rotor Performance	20160603
	Roger Groves	TU Delft	Struct. Health Monitoring	20160608
	Mirjam Snellen	TU Delft	Aircraft noise footprint [1]	20160614
	Dick Simons	TU Delft	Aircraft noise footprint [1]	20160615

[1] No response as of time of writing (June 28, 2016)

Bibliography

[1] DSE Group 11. DID-2 Baseline Report: Ultra-Long Range Business Jet. Technical report, Delft University of Technology, April 2016.

[2] DSE Group 11. DID-3 Mid Term Review: Ultra-Long Range Business Jet. Technical report, Delft University of Technology, May 2016.

[3] Federal Aviation Administration. *Aviation Maintenance Technician Handbook - General*. U.S Department of Transportation, 2008. URL https://www.faa.gov/regulations_policies/handbooks_manuals/aircraft/amt_airframe_handbook/media/ama_Ch13.pdf.

[4] European Aviation Safety Agency. Certification Specifications and Acceptable Means of Compliance for Large Aeroplanes CS-25 (Amendment 17). Technical report, European Aviation Safety Agency, 2015.

[5] Bombardier Business Aircraft. Market Forecast 2015-2024. [online], 2015. URL https://www.google.nl/url?sa=t&rct=j&q=&esrc=s&source=web&cd=1&ved=0ahUKEwiwpeba2bjNAhWJF8AKHZsSA8MQFggeMAA&url=http%3A%2F%2Fwww.bombardier.com%2Fcontent%2Fdam%2FWebsites%2Fbombardiercom%2Fsupporting-documents%2FBA%2FBombardier-Business-Aircraft-2015-2024-Market-Forecast-en.pdf&usg=AFQjCNHcsYdaxN3E58xGlvX6OyJWcQYKAw&sig2=Rgb0cTazRcJPkT96D-QXcA&cad=rja.

[6] M. F. Ashby. *Materials Selection in Mechanical Design*. Elsevier, third edition, 2005. ISBN 0750661682.

[7] L. Bertsch. Noise prediction within Conceptual Aircraft Design. Technical report, Institute of Aerodynamics and Flow Technology Braunschweig, 2013.

[8] A. Birolini. *Reliability Engineering*. Springer, ETH Zurich, seventh edition, 2014. ISBN 9783642395345.

[9] Boeing. *737 Airplane Characteristics for Airport Planning*, September 2013.

[10] R. J. Rioja C. Giummarra, B. Thomas, editor. *New Aluminum Lithium Alloys for Aerospace Applications*, 2007.

[11] McDonnell Douglas Astronautics Company. *The USAF Stability and Control DATCOM - Volume I, Users Manual*. USAF, April 1979. URL https://www.google.nl/url?sa=t&rct=j&q=&esrc=s&source=web&cd=1&cad=rja&uact=8&ved=0ahUKEwjbtZOo_qvNAhVDLhoKHa5tCroQFggeMAA&url=http%3A%2F%2Fwpage.unina.it%2Fagodemar%2FDSV-DQV%2FDigital_Datcom_Users_Manual_1.2.pdf&usg=AFQjCNFr-NIHSLjqS-hQQRugCoWRW02dlg&sig2=3k7EQD04ITvDjAbdw2urMg.

[12] U.S. Green Building Council. LEED v4 for Building and Construction. Technical report, LEED U.S. Green Building Council, 2016.

[13] M. Tong E. Hendriks. Performance and Weight Estimates for an Advanced Open Roter Engine. Technical report, NASA, September 2012.

[14] EASA. Open Rotor Engine and Installation. Technical report, EASA, 2015.

[15] P. C. Brown F. B. Metzger. Results of Acoustic Tests of a Prop-Fan Model. Technical report, AIAA/SAE/ASME/ASEE 23rd Joint Propulsion Conference, AIAA-87-1894, July 1988.

[16] P. Fernberg. High performance composites for demanding high temperature. Technical report, Swerea SICOMP, 2013.

[17] R. Groves. Asset Management Lecture - Structural Health Monitoring. TU Delft lecture slides, 2015.

[18] S Gudmundsson. *General Aviation Aircraft Design*. Butterworth-Heinemann, 2013. ISBN 9780123973290. URL http://store.elsevier.com/General-Aviation-Aircraft-Design/Snorri-Gudmundsson/isbn-9780123973290/.

[19] A. Güemes. SHM Technologies and Applications in Aircraft Structures. Technical report, Department of Aeronautics, University Politechnica de Madrid, November 2013.

[20] M. Hans-Reichel. Subsonic versus Supersonic Business Jets: Full Concept Comparison considering Technical, Environmental and Economic Aspects. Master's thesis, Technische Fachhochschule Wildau, 2011.

[21] L. Hart-Smith. Out-sourced Profits - The Cornerstone of Succesful Subcontracting. Technical report, Boeing, February 2001.

[22] D. Huff. Noise Reduction Technologies for Turbofan Engines. Technical report, NASA Glenn Research Center, 2007.

[23] R.B. Cork J.H. Klein. An approach to technical risk assessment. Technical report, Centre for Risk Research, University of Southampton, 1998.

[24] H. Remy L. Chow, K. Mau. Landing Gear and High Lift Devices Airframe Noise Research. Technical report, AIAA, 2002.

[25] E. Hendricks M. Guynn, J. Berton. Initial Assessment of Open Rotor Propulsion Applied to an Advanced Single-Aisle Aircraft. Technical report, American Institute of Aeronautics and Astronautics, September 2011.

[26] E.E. Modic. Design for Testing and Maintenance. *Aerospace Manufacturing and Design*, July 2012. URL http://www.aerospacemanufacturinganddesign.com/article/amd0712-oams-aircraft-maintenance/.

[27] H. E. Bloomer N. E. Samanach, D. C. Reemsnyder. Reverse thrust performance of the qcsee variable pitch turbofan engine. Technical report, Lewis Research Center, 1980.

[28] International Civil Aviation Organization. *Environmental Protection - Volume I - Aircraft Noise*. ICAO, fifth edition, 2008. ISBN 978-92-9231-108-7.

[29] International Civil Aviation Organization. *Environmental Protection - Volume II - Aircraft Engine Emissions*. ICAO, third edition, 2008. ISBN 978-92-9231-123-0.

[30] D. Scholz P. Krammer, O. Junker. Aircraft Design for Low Cost Ground Handling - the Final Results of the Aloha Project. Technical report, Aero - Aircraft Design and Systems Group, Hamburg University of Applied Sciences. Airport Research Center GmbH Aachen, 2010.

[31] Francisco Palacios and Economon et al. Stanford University Unstructured (SU2): Open-source Analysis and Design Technology for Turbulent Flows. *AIAA SciTech*, 24(3), 2014.

[32] D.J. Peery. *Aircraft Structures*. Dover Publications, 2011. ISBN 978-0486485805.

[33] S.T. Peters. *Handbook Of Composites*. Chapman and Hall, second edition, 1998. ISBN 0412540207.

[34] M.C.P. Firmin P.H. Cook, M.A. McDonald. Aerofoil RAE 2822 - Pressure Distributions, and Boundary Layer and Wake Measurements. *AGARD*, 138, 1979. [Accessed Online: June 2016] http://www.grc.nasa.gov/WWW/wind/valid/raetaf/raetaf01/cp.exp.gen.

[35] Warren F. Phillips. *Mechanics of Flight*. John Wiley & Sons, Inc, first edition, 2004. ISBN 0471334588.

[36] B.T.C. Zandbergen R. Vos, J.A. Melkert. Aerospace Design and Systems Engineering Elements I – AE1222-II. TU Delft Lecture Slides, April 2016.

[37] Daniel P. Raymer. *Aircraft Design: A Conceptual Approach*. Aircraft Design. American Institute of Aeronautics and Astronautics, Inc., 1992. ISBN 0-9-30403-51-7.

[38] D. C. Reemsnyder. Effects of forward velocity and cross-wind on reverse thrust performance. Technical report, AIAA, 1979.

[39] G. La Rocca. AE3221-I Systems Engineering and Aerospace Design. TU Delft Lecture Slides, April 2016.

[40] J. Roskam. *Airplane Design Part I: Preliminary Sizing of Airplanes*. Airplane Design. DARcorporation, 1985. ISBN 9781884885426. URL https://books.google.nl/books?id=usXVaf8Qu0cC.

[41] J. Roskam. *Airplane Design Part II: Preliminary Configuration Design and Integration of the Propulsion System*. Airplane Design. DARcorporation, 1985. ISBN 1-884885-43-8. URL https://books.google.nl/books?id=bJlZ4mKf1EkC&hl=nl&source=gbs_similarbooks.

[42] J. Roskam. *Airplane Design Part IV: Layout of Landing Gear and Systems*. Airplane Design. DARcorporation, 2000. ISBN 1-884885-43-8. URL https://books.google.nl/books?id=bJlZ4mKf1EkC&hl=nl&source=gbs_similarbooks.

[43] J. Roskam. *Airplane Design Part VIII: Airplane Cost Estimation: Design, Development, Manufacturing and Operating*. Airplane Design. DARcorporation, 2002. ISBN 9781884885556.

[44] A. Breeze-Stringfellow T. Wood S. Arif Khalid, D. Lurie. Open Rotor Engine Aeroacoustic Technology Final Report. Technical report, FAA, May 2013.

[45] M.H. Sadreay. *Aircraft Design: A Systems Engineering Approach*. John Wiley & Sons Ltd, 2013. ISBN 978-1-119-95340-1.

[46] J. W. Schaefer. Dynamics of high-bypass engine thrust reversal using a variable-pitch fan. Technical report, NASA, 1977.

[47] J. Sinke. AE3211-II Production of Aerospace Systems - Chapter 9 Quality. TU Delft Lecture Reader, April 2016.

[48] J. Sinke. AE3211-II Production of Aerospace Systems - Chapter 10 Lean Manufacturing. TU Delft Lecture Reader, April 2016.

[49] J. Sinke. AE3211-II Production of Aerospace Systems - Chapter 11 Organization. TU Delft Lecture Reader, April 2016.

[50] J. Sinke. Project Guide Design Synthesis Exercise, Ultra-Long Range Business Jet. Technical report, Delft University of Technology, 2016.

[51] R. Snyder. Impact Protection in Air Transport Passenger Seat Design. *SAE Technical Paper*, 4271(821391), 1982.

[52] R. F. Stapelberg. *Handbook of reliability, availability, maintainability and safety in engineering design*. Springer, first edition, 2009. ISBN 9781848001749.

[53] D. Steenhuizen. Aerospace Design and Systems Engineering Elements II - AE2101 - Wing Design Part 4. TU Delft Lecture Slides, 2014.

[54] X.F. Sun. Chinese Journal Of Aeronautics. Technical report, Chinese Society of Aeronautics And Astronautics, January 1988.

[55] P. Ganesan T. Karthik, R. Rathinamoorthy. Sustainable Luxury Natural Fibers—Production, Properties, and Prospects. Technical report, PSG College of Technology, 2015.

[56] J. Thorpe. Fatalities and Destroyed Civil Aircraft due to Bird Strikes, 1912 – 2002. Technical report, International Bird Strike Committee, May 2003.

[57] E. Torenbeek. *Synthesis of Subsonic Airplane Design*. Delft University Press and Kluwer Academic Publishers, 1982. ISBN 90-247-2724-3.

[58] C. Kassapoglou W.A. Timmer, R. De Breuker. AE2111-I Systems Design Project Reader - Aircraft. Technical report, Faculty of Aeropsace Engineering TU Delft, 2014.

[59] R.T. Whitcomb. A Design Approach And Selected Wind Tunnel Results at High Subsonic Speeds For Wing Tip Mounted Winglets. Technical report, Langley Research Centre, July 1976.

[60] A. Seyed Yaghoubi and B. Liaw. Influences of thickness and stacking sequence on ballistic impact behaviors of GLARE 5 FML plates. Technical report, Journal of Composite Materials, 2013.

[61] G. Zdobyslaw. An overview of the deicing and antiicing technologies with prospects for the future. Technical report, Warsaw University of Technology, 2013.